UNIVERSITY OF SOUTHAMPTON

a Thesis

on

Drag Reduction of Bluff Bodies Using Shielding Devices

by

N.H.C. Bromfield

Submitted to the University of Southampton for the degree of M.Phil by research in the Department of Aeronautics and Astronautics, Faculty of Engineering and Applied Science.

September 1987

UNIVERSITY OF SOUTHAMPTON

ABSTRACT

FACULTY OF ENGINEERING AND APPLIED SCIENCE

DEPARTMENT OF AERONAUTICS AND ASTRONAUTICS

Master of Philosophy

DRAG REDUCTION OF BLUFF BODIES USING SHIELDING DEVICES

by Norman Harold Cailes Bromfield

This research is a particular study of bluff body aerodynamics.

The main objective was to determine the least drag geometry of a gauze and solid disc in tandem when placed in uniform incompressible fluid flow. Limited similar experiments were conducted with the solid disc replaced by a cylinder and a brief investigation was made into the effect of adding gauze shields on the drag of a motor car model.

In establishing that the optimum disc configuration has a drag 32% below that of the solid disc alone, for a gauze solidity of 0.4, the work initiates a whole new branch of research into drag reduction. Additionally, the work showed that it is a reasonable proposition to replace the gauze disc by an equivalent windmill and to use the power produced for propulsion.

As well as describing a mainly experimental investigation of drag carried out in a wind tunnel, this thesis propounds for the discs in tandem an explanation of the drag reducing mechanism and provides a simple theory for obtaining a first estimate of the drag reduction.

It is concluded that porous shielding produces more than a reduction in effective approach velocity and since the mechanism is not dependent on mutual interference or flow development, the advantage is not critically dependent on geometry. Larger reductions may be anticipated with shapes other than discs and 50% was achieved with cylinders. There are a number of beneficial side effects.

ACKNOWLEDGEMENTS

The author is extremely indebted to Dr. A.L. Buchan, Department of Mechanical Engineering, Portsmouth Polytechnic, for introducing him to the possibility of reducing the drag of a bluff body by replacing it between, and in tandem with, a windmill driving a propeller. Following these early discussions, experiments were carried out by the author to confirm the feasibility of the proposal.

Under the Link arrangements with the University of Southampton, the author was permitted to register (part-time) for a postgraduate degree on this subject of drag reduction. Professor Lilley agreed to act as supervisor and the author is very grateful to Professor Lilley for agreeing to supervise the research and for his guidance throughout.

All the experimental work connected with the research was carried out in the Department of Mechanical Engineering, Portsmouth Polytechnic, and the author would like to express his gratitude to the President, Portsmouth Polytechnic, and to the Head of the above Department, for providing the necessary facilities.

DECLARATION

None of the material contained in this thesis has been used before by the author.

PERMISSION TO COPY

Permission is granted for this thesis to be copied in whole or in part without further reference to the author subject to normal conditions of acknowledgement.

LIST OF CONTENTS

LIST OF FIGURES

LIST OF TABLES

LIST OF PHOTOGRAPHS

NOTATION

A_B	area of body on which $(C_D)_B$ is based
A_{CAR}	frontal area of car model
$(A)_{D1}$	area of gauze disc = $\pi D_1^2/4$
$(A)_{D1W}$	cross-sectional area of wake from gauze disc
$(A)_{D2}$	area of solid disc = $\pi D_2^2/4$
A_G	gauze area
$(A_G)_{CAR}$	area of gauze shielding car model
A_S	largest cross-sectional area of separated region
$A_S/(A)_{D2}$	separated region maximum area ratio
A_W	cross-sectional area of wake from gauze and solid discs in tandem
b	blockage of solid disc = $(A)_{D2}$/cross-sectional area of working section of wind tunnel
C_D	drag coefficient of a given configuration of gauze and solid discs in tandem as described by its value of D_1/D_2 and g/D_2 corrected for sword and sting drag but not for blockage = drag of gauze and solid discs in tandem/$0.5\rho(A)_{D2} V_\infty^2$
$(C_D)_{CORR}$	C_D corrected for blockage
$(C_D)_B$	drag coefficient of body
$(C_D)_{LEAST}$	least $(C_D)_{MIN}$
$(C_D)_{LEASTCORR}$	$(C_D)_{LEAST}$ corrected for blockage
$(C_D)_{MIN}$	minimum C_D for a given D_1/D_2
$(C_D)_{MINCORR}$	$(C_D)_{MIN}$ corrected for blockage
$(C_D)_{SS}$	calculated C_D using simple shielding theory
$(C_D)_C$	drag coefficient of a given configuration of gauze disc and solid cylinder in tandem as described by its value of D_1/D_C, ℓ/D_C and w/D_C corrected for sword and sting drag but not for blockage = drag of gauze disc and solid cylinder in tandem/ $0.5\rho(0.25\ \pi D_C^2)V_\infty^2$

$(C_D)_{CALONE}$ drag coefficient of unshielded cylinder corrected for sword drag but not for blockage
= drag of cylinder alone/$0.5\rho(0.25\ \pi D_C^2)V_\infty^2$

$(C_D)_{CALONECORR}$ $(C_D)_{CALONE}$ corrected for blockage

$(C_D)_{CCORR}$ $(C_D)_C$ corrected for blockage

$(C_D)_{CLEAST}$ least $(C_D)_{CMINCORR}$ for a given D_1/D_C

$(C_D)_{CMINCORR}$ minimum $(C_D)_{CCORR}$ for a given D_1/D_C and ℓ/D_C

$(C_D)_{CAR}$ measured drag coefficient of car model configuration uncorrected for stimulator, sword drag and blockage
= drag/$0.5\rho\ A_{CAR}\ V_\infty^2$

$(C_D)_{CARCALC}$ calculated $(C_D)_{CAR}$

$(C_D)_{D1ALONE}$ drag coefficient of gauze disc alone
= $0.650\ (D_1/D_2)^2$

$(C_D)_{D1CALC}$ drag coefficient of gauze disc when in tandem with solid disc
= drag of gauze disc in tandem/$0.5\rho(A)_{D2}\ V_\infty^2$
= $(C_D)_{D1ALONE} - (C_D)_I$

$(C_D)_{D2}$ drag coefficient of solid disc when shielded by gauze disc
= drag of shielded solid disc/$0.5\rho(A)_{D2}\ V_\infty^2$
= $(\overline{C_P})_F + (\overline{C_P})_S$

$(C_D)_{D2ALONE}$ unshielded value of $(C_D)_{D2}$

$(C_D)_{D2CALC}$ calculated $(C_D)_{D2}$
= $C_D - (C_D)_{D1ALONE} + (C_D)_{ICALC}$

$(C_D)_{D2CORR}$ $(C_D)_{D2CALC}$ corrected for blockage

$(C_D)_{D2SS}$ calculated $(C_D)_{D2}$ using simple shielding theory

$(C_D)_{FBCALC}$ calculated fore body drag coefficient
= $(\overline{C_P})_{FCALC} + (C_D)_{D1CALC}$

$(C_D)_{GALONE}$ drag coefficient of gauze area alone

$(C_D)_{GB}$ drag coefficient of gauze and body

$(C_D)_I$ mutual interference force coefficient
= mutual interference force between gauze and solid discs/$0.5\rho(A)_{D2}\ V_\infty^2$

$(C_D)_{ICALC}$	calculated $(C_D)_I$
$(C_D)_W$	drag coefficient of windmill = windmill drag/$0.5\rho\ V^2\ \pi R^2$
C_ℓ	Iwasaki's windmill power coefficient = power/$0.5\rho\ \pi R^2\ V^3$
$(C_\ell)_{MAX}$	maximum value of C_ℓ for a given $\beta_{0.75}$
$(C_P)_F$	$p_F/0.5\rho\ V_\infty^2$ when shielded by gauze disc
$(C_P)_{FALONE}$	unshielded value of $(C_P)_F$
$(C_P)_{FCALC}$	calculated value of $(C_P)_F$
$(C_P)_{FALONECALC}$	calculated value of $(C_P)_{FALONE}$
$(\overline{C_P})_F$	$\overline{p_F}/0.5\rho\ V_\infty^2$ when shielded by gauze disc
$(\overline{C_P})_{FALONE}$	unshielded value of $(\overline{C_P})_F$
$(\overline{C_P})_{FCALC}$	calculated $(\overline{C_P})_F$
$(C_P)_S$	$p_S/0.5\rho\ V_\infty^2$ when shielded by gauze disc
$(C_P)_{SALONE}$	unshielded value of $(C_P)_S$
$(\overline{C_P})_S$	$\overline{p_S}/0.5\rho\ V_\infty^2$ when shielded by gauze disc
$(\overline{C_P})_{SALONE}$	unshielded value of $(\overline{C_P})_S$
$(C_P)_W$	power coefficient of windmill = developed power/$0.5\rho\ V^3\ \pi R^2$
$(C_Q)_P$	torque coefficient of propeller = torque/$0.5\rho\ V_\infty^2\ \pi R^3$
$(C_T)_P$	thrust coefficient of propeller = thrust/$0.5\rho\ V_\infty^2\ \pi R^2$
C_W	Iwasaki's windmill drag coefficient = drag/$0.5\rho\ \pi R^2\ V^2$
c	blockage of cylinder = $(\pi D_C^2/4)$ ÷ cross-sectional area of working section of wind tunnel
c/R	chord to radius ratio
D_C	diameter of cylinder
D_S	diameter of A_S

D_1	diameter of gauze disc = 2.00 in (constant)
D_{10}	D_1 at which complete shielding effectively occurs
D_1/D_2	disc diameter ratio
D_2	diameter of solid disc
D_1/D_C	cylinder diameter ratio
F	force, generally
g	gap between gauze and solid discs
g/D_2	disc gap ratio
ℓ	length of cylinder
ℓ/D_C	cylinder length ratio
m	sink or source strength
p	pressure, generally
p_F	pressure at a given position on face of solid disc relative to p_∞
p_S	pressure at a given position on back of solid disc relative to p_∞
p_0	upstream static pressure of flow through windmill
p_1	downstream static pressure of flow through windmill
p_∞	free stream static pressure
$\overline{p_F}$	mean pressure on face of solid disc relative to p_∞
$\overline{p_S}$	mean pressure on back of solid disc relative to p_∞
R	tip radius of windmill or propeller radius of disc or cylinder
r	radius
$(Re)_{DC}$	cylinder Reynolds number = $V_\infty D_C/\nu$
$(Re)_{D2}$	solid disc Reynolds number = $V_\infty D_2/\nu$
S_0	upstream cross-sectional area of flow through windmill
S_1	area of flow at windmill

S_∞	downstream cross-sectional area of flow through windmill
u	velocity defect
u_1, v_1, w_1	downstream velocities in x, y and z directions
V	velocity, generally velocity of advance of propeller
V_{EFF}	calculated effective speed of advance of solid disc in wake of gauze disc $= V_\infty/\sqrt{[\{(\overline{C_P})_S + (\overline{C_P})_{FCALC}\}/(C_D)_{D2ALONE}]}$
V_x	axial component of velocity
V_o	upstream velocity of flow through windmill
V_∞	free stream velocity
V_{EFF}/V_∞	calculated effective velocity ratio
W	velocity of flow relative to propeller blade at radius r
W_o	$\sqrt{(V^2 + \Omega^2 r^2)}$
w	gap between gauze disc and front face of cylinder
w_1	induced propeller velocity at radius r
w/D_C	cylinder gap ratio
X	force in x direction on surface containing flow through windmill
x	radius ratio $= r/R$
α	axial velocity interference factor geometric angle of attack
α_i	induced angle of attack
β	windmill blade pitch angle
$\beta_{0.75}$	value of β at $x = 0.75$
Δ	car shield effectiveness parameter
$\delta(C_D)$	reduction in drag coefficient of windmill, disc and propeller combination due to propeller thrust
ε	blockage factor

κ	circulation function
μ	$\Omega r/R$
ν	kinematic viscosity of air
Ω	angular velocity of windmill or propeller
ϕ	hydrodynamic angle of flow for propeller angle measured in transverse plane, normal to flow, relative to the horizontal starboard direction
ψ	stream function
Θ	angle which flow makes with centre line
$(\Theta)_{D2}$	Θ for shear layer at edge of solid disc

Unless otherwise defined in the text.

1. INTRODUCTION

The drag of two solid discs of equal diameters held in tandem was studied by Eiffel(5) over 70 years ago. More recently Morel and Bohn(15) showed that placing a properly sized solid disc at an optimum distance ahead of a single reference solid disc resulted in a configuration with a drag of 81% lower than that of the reference disc alone. They also detected a number of different flow regimes depending on the diameter ratio of the two discs.

Morel and Bohn's work was a particular case of the more general problem of discs with varying solidities or porosities held in tandem with varying gaps. In the present investigation the forward disc of Morel and Bohn's particular case was replaced by a gauze disc of solidity 0.4 simulating a windmill and producing a further flow regime. As was anticipated from simple considerations of shielding, it was found that a porous disc was less effective than a solid one in reducing drag. A maximum reduction of 32% was achieved.

Similar experiments to Morel and Bohn were conducted at well above the critical Reynolds number to establish the configuration with the lowest drag coefficient and likewise pressure measurements were made to determine the forebody and base drags. With the optimum configuration, shielding was approximately twice as effective in reducing the drag of the forebody than that of the aftbody. The results also showed that the gauze evened out, as well as reduced, the pressures across the face of the solid disc.

Flow patterns around various configurations were found although cotton streamers were employed for this purpose instead of the more normal smoke technique. A smoke technique was used, however, to determine the size of the separated region behind the solid disc and an attempt was made to correlate the edge of the region with turbulence measurements.

Other related experiments were those of Roshko and Koenig(16) and Saunders(17) who investigated the effect of diameter ratio and gap length on the drag of a flat-faced circular cylinder preceded by a concentric circular solid disc and found remarkable reductions were achievable in drag. Limited parallel experiments with the solid disc replaced by a gauze disc confirmed that percentage drag reductions better than that for discs may be obtained with cylinders.

As the references indicate the investigations have relevance to the problem of reducing the drag of road vehicles, especially of lorries with separate cab and trailer(s). Thus they belong to the study of bluff body aerodynamics where the majority of the research has been conducted on either two-dimensional or axisymmetric shapes with the objective of identifying drag mechanisms and understanding the conditions which lead to drag reduction. In view of this connection with road vehicles it was decided to extend the present investigations to a 1:24 scale model motor car and to try and reduce its drag by shielding it with gauze of the same solidity having various shapes and gaps. Although the results were considered to be encouraging no attempt was made to establish the necessary parameters and technique to give reduced drag because the required work would amount to a major departure from the main theme of the research. However it was appreciated throughout that drag reductions are unlikely to be achieved with streamline bodies using gauze shields with such a low solidity and calculations were carried out to demonstrate the importance of solidity.

The present work, as with Morel and Bohn and Roshko and Koenig, concentrated on the interaction between bluff bodies and its effect on the forebody and base drags. Air deflectors to reduce the resistance of lorries work on this principle and demonstrate that beneficial interference between otherwise high drag bodies can be obtained. Lilley(10) provides another example of beneficial interference in his note on the speed gain and acceleration which can be achieved by a racing car travelling in the slip-stream of another. But it may be anticipated that the employment of a gauze disc or windmill for the same purpose would have the extra benefit of cleaning up the flow and therefore moderating the influence of the wind in any actual application by reducing the intensity and scale of natural and artificially induced turbulence and perhaps also the effects of small angles of yaw.

Some confirmation of the above was obtained with the tests on cylinders where it was found that wind tunnel turbulence was sufficient to excite severe vibrations on a number of unshielded cylinders. The gauze extinguished the vibration which otherwise needed a large change in speed to bring down to acceptable levels.

The immediate applications of the present research are not directly obvious although there may well be future applications. The use of

gauze or windmill shielding on bluff road vehicles could be impracticable because of the resulting danger to other road users but situations may arise with other forms of transport or with small or stationary bluff bodies where shielding of the type investigated could be used safely to reduce drag and take advantage of the benefits of cleaner approaching flow. Gauze shielding suffers from blocking in flow containing large foreign matter and windmill shielding may be superior in such cases.

It should be noted that originally the investigation of the effects of gauze shielding was not a primary objective and that its advantages did not come to light until the research was well underway. With the results of the present fundamental work available, future programmes will undoubtedly be of a more ad hoc nature.

It was concluded from a study of Bearman's(1) review of numerical methods for predicting flow patterns and pressure distributions that a wind tunnel study was essential before any complex physical and mathematical modelling, particularly of the wake, was attempted. Consequently this dissertation describes a mainly experimental investigation. Although a suitable prediction method does not exist which can determine the flow pattern and pressure distribution of the problem being studied to a high degree of accuracy, classical actuator-disc theory was applied to the simulated windmill and the solid disc along the lines described by Bramwell(3) and used in conjunction with the recommended treatment of shear flows in Engineering Sciences Data item number 70015(6) to derive a simple shielding theory against which the experimental results on the discs in tandem were compared. As was expected, such a simple theory could not account quantitatively for the reduction in drag caused by the shielding, which was more effective than that predicted, but the theory was able to explain a few of the trends observed.

An important aspect of the work was the mutual reaction due to interference between the gauze and solid discs and experiments were undertaken to measure the interactive force. The proposal by Glauert(7), based on a study of experimental results, that the interference experienced may be accounted for by an effective decrease in speed of advance, varying with radius because of the closeness of the discs, was then adopted as the basis of a predictive theory which gave good agreement with measured data. A number of velocity distributions were tried in the theory for the decrease in speed which were evaluated using Milne Thomson's(14)

work on theoretical hydrodynamics and the best agreement was obtained with a Rankine ovoid having major and minor axes based on Morel and Bohn's observations of the flow around a solid disc. Fortunately, the mutual interference force between discs was found to be small in the case of the optimum configuration so that interference would have little effect on the power developed by a windmill, simulated by the gauze disc, from that available in a free stream. Equally, a propeller driven by the windmill would produce little drag augmentation through interference if positioned to take advantage of the low wake velocities.

Although a considerable number of investigations have been made into the performance of windmills taking into account their interference when placed in arrays, it appears not to have been appreciated previously that the same shielding and interference effect may be used with advantage in reducing body drag. Thus the present work initiates a whole new branch of research into the drag reduction which can be achieved with various body shapes when placed at different positions in relation to arrays of discs of different porosity, or their equivalent windmills, and subjected to winds of different strengths, directions, turbulence levels and scales. Additionally, the porous discs themselves may take on different shapes and need not be simply circular.

As an extension to the above unique line of investigation the present study also showed that it is a reasonable proposition to use the power developed to propel the body and thereby obtain a further reduction in drag. It adds another dimension to this branch of research but since the further reduction obtained in the present work was relatively small (9%) the extent of the propulsive aspect seems to be small and of less importance than originally thought.

Applications of this approach to energy transfer for reducing drag viz a shielding windmill driving a propeller are also not directly obvious although the author did have in mind when constructing his programme initially that the concept might be used generally as a substitute for physical streamlining with the irregular body sandwiched tandem fashion between a forward windmill and an aft propeller.

In determining the thrust of the propeller driven by the windmill power it was necessary to find experimentally the distribution of velocity in the wake of the solid disc at the propeller position and to derive a

function of radius describing the distribution. The asymptotic mean velocity profile of turbulent wakes far downstream, deduced essentially by dimensional analysis and using Prandtl's dimensionless mixing length theory has been calculated by Schlichting and is quoted by Birchoff and Zarantonello(2). Good agreement between theory and experiment was found when account was taken of the turbulence not being initiated by a concentrated source.

Preliminary tests(4) on a windmill, disc and propeller combination gave no indication of instability although the windmill was designed to provide a high axial interference factor well in excess of the limiting condition suggested by Lilley and Rainbird(12). There is a possibility that the propeller provided a stabilising effect. An early decision was taken not to risk instability occurring in the present investigations and for this reason they concentrated on an experimentally derived Iwasaki(8) recommendation for a fast running windmill. Although instability may be a limiting condition if only one windmill is used it is possible that the limitation may be removed or reduced by employing a number of windmills in tandem.

It is important to note that the experimental work carried out for the purpose of this thesis was confined essentially to a gauze disc and a solid disc in tandem and that the propeller thrust was calculated assuming that the recommended windmill and a gauze disc of the same diameter and drag coefficient were completely interchangeable. Thus it was possible to estimate the power supplied to the propeller by the recommended windmill using the performance data given by Iwasaki and, because he obtained good agreement between experiment and theory, a similar vortex theory approach to his was used in the design of the propeller. The design calculations showed that the positioning of the propeller was not of great importance and that there was little point in making the propeller diameter greater than one and a half times the diameter of the windmill.

In examining the differences between a windmill and its gauze disc simulator, the description and comments on the actuator disc, generalised momentum and vortex theory of windmills as given by Lilley and Rainbird (12) and by Lilley(11), together with a similar discussion on rotor aerodynamics by Bramwell(3), were found extremely helpful. The conclusion drawn from the comparison was that the differences would require

only a small modification to the measured drag of the optimum configuration. The design of a windmill to give the most favourable distribution of pressure over the solid disc warrants a separate investigation.

The wind tunnel, in which all the experimental work was conducted, had a relatively small working cross-sectional area. Consequently some of the configurations tested had high blockages whose effect on drag was corrected using Maskell's(13) approach and his recommended correction factor was experimentally confirmed to be applicable. The tunnel was in constant use by students and researchers which meant accepting the then current level of uncertainty interval which was estimated by means of the method of Kline and McClintock(9) at ± 0.02 for the drag coefficient (20 to 1). Normally the accuracy with which drag was measured was better than ± 1%, although some configurations appeared to be liable to random errors which made precision difficult to assess. It was not considered that the experimental errors affected the conclusions drawn.

Substantial shielding was obtained with diameter ratios considerably less than unity and in view, therefore, of the relatively small volumetric flow rate slowed by the gauze disc in such cases its effectiveness in reducing drag was remarkable. The slowed flow eased the encircling fast flow around the solid disc or cylinder and exercised a shielding effect more than commensurate with the area of the gauze disc. Consequently at high diameter ratios approaching that giving complete shielding (approximately 1.2 for the solid disc) the configurations suffered from a drag penalty due to the excessive size of the gauze disc, while at low diameter ratios the lack of shielding more than outweighed the benefit of reducing the gauze disc area.

2. THEORY

2.1 Simple Shielding Theory of an Isolated Body

In the following simple shielding theory the object experiencing drag is considered to be a gauze and solid disc in tandem as illustrated in Figure 1. The discs are assumed to be acted upon by a mutual interference force F_I (see Section 5 of Appendix 5) in addition to drags caused purely by changes in momentum.

Because of the largeness of the gaps (g) in the configurations giving minimum drag, it is further assumed that the wake of the gauze disc is not prevented from developing by the solid disc so that from Section 2.2,

$$\text{momentum drag of gauze disc} = w\,\rho u(V_\infty - u) \text{ for gauze disc}$$

$$= (A)_{D1W}\,\rho\,V_\infty^2\,(1-2\alpha)(2\alpha)$$

where α is the axial velocity interference factor whose value depends on the drag coefficient of the gauze disc (see Section 1 of Appendix 5) and $(A)_{D1W}$ is the wake area of the flow through the gauze disc which from continuity is given by:

$$\rho(A)_{D1W}\,V_\infty(1-2\alpha) = \rho(A)_{D1}\,V_\infty(1-\alpha)$$

or

$$(A)_{D1W} = (A)_{D1}\,\frac{(1-\alpha)}{(1-2\alpha)}$$

Hence the drag coefficient of the gauze disc according to simple shielding theory

$$= (\text{momentum drag} - F_I)/\tfrac{1}{2}\rho(A)_{D2}\,V_\infty^2$$

$$= \{(A)_{D1}\,\frac{(1-\alpha)}{(1-2\alpha)}\,\rho\,V_\infty^2(1-2\alpha)(2\alpha) - F_I\}/\tfrac{1}{2}\,(A)_{D2}\,V_\infty^2$$

$$= 4\alpha(1-\alpha)\,\left(\frac{D_1}{D_2}\right)^2 - (C_D)_I$$

In determining the drag of the solid disc the treatment of shear flow in Engineering Sciences Data 70015(6) is used.

$$\text{Drag of solid disc} = \tfrac{1}{2}\rho(A)_{D2}\,V_{EFF}^2\,(C_D)_{D2ALONE} + F_I$$

where,

$$(C_D)_{D2ALONE} = 1.14$$

and,

$$(A)_{D2}\ V_{EFF}^{\ 2} = \int_{(A)_{D2}} V^2\, d(A)_{D2}$$

in which V is the velocity approaching the differential area and is taken to be $V_\infty(1-2\alpha)$ over $(A)_{D1W}$, that is, inside the wake of the gauze disc, and V_∞ outside the wake.

Thus the drag of the solid disc depends on whether $(A)_{D1W}$ is larger or smaller than $(A)_{D2}$. For:

(i) $(A)_{D1W} \geq (A)_{D2}$

$$\frac{\pi D_1^{\ 2}}{4}\ \frac{(1-\alpha)}{(1-2\alpha)} \geq \frac{\pi D_2^{\ 2}}{4}$$

or,

$$\frac{D_1}{D_2} \geq \sqrt{\frac{(1-2\alpha)}{(1-\alpha)}}$$

and,

$$\text{drag of solid disc} = \tfrac{1}{2}\rho\ \frac{\pi D_2^{\ 2}}{4}\ V_\infty^{\ 2}\ (1-2\alpha)^2\ 1.14 + F_I$$

from which,

$$\text{drag coefficient} = 1.14\ (1-2\alpha)^2 + (C_D)_I$$

(ii) $0 \leq (A)_{D1W} \leq (A)_{D2}$

or,

$$0 \leq \frac{D_1}{D_2} \leq \sqrt{\frac{(1-2\alpha)}{(1-\alpha)}}$$

and,

$$\text{drag of solid disc} = \tfrac{1}{2}\rho\ \frac{\pi D_1^{\ 2}}{4}\ \frac{(1-\alpha)}{(1-2\alpha)}\ V_\infty^{\ 2}\ (1-2\alpha)^2\ 1.14 + \tfrac{1}{2}\rho\left\{\frac{\pi D_2^{\ 2}}{4} - \frac{\pi D_1^{\ 2}}{4}\ \frac{(1-\alpha)}{(1-2\alpha)}\right\}V_\infty^{\ 2}\ 1.14 + F_I$$

from which,

$$(C_D)_{D2SS} = 1.14[1 + (\frac{D_1}{D_2})^2 \{(1-2\alpha)(1-\alpha) - (\frac{1-\alpha}{1-2\alpha})\}] + (C_D)_I$$

Adding the drag coefficient of the solid disc to that of the gauze disc to give the drag coefficient of the gauze and solid discs in tandem results in

$$\frac{D_1}{D_2} \geq \sqrt{\frac{(1-2\alpha)}{(1-\alpha)}} \qquad (C_D)_{SS} = 4\alpha(1-\alpha)(\frac{D_1}{D_2})^2 + 1.14(1-2\alpha)^2$$

$$0 \leq \frac{D_1}{D_2} \leq \sqrt{\frac{(1-2\alpha)}{(1-\alpha)}} \qquad (C_D)_{SS} = 4\alpha(1-\alpha)(\frac{D_1}{D_2})^2 + 1.14[1 + (\frac{D_1}{D_2})^2 \{(1-2\alpha)(1-\alpha) - (\frac{1-\alpha}{1-2\alpha})\}]$$

2.2 Simple Momentum Box Theory

Consider an object experiencing a drag D when placed in a prismatic frictionless tunnel of sectional area h and subjected to a free stream velocity, pressure and density of V_∞, p_∞ and ρ_∞ as shown in Figure 1. The core flow has a sectional area a upstream of the body and an area w downstream where the velocity and density are u and ρ. Outside of the core downstream the velocity and density are V_1 and ρ_1. The downstream pressure is p_1.

Mass flow rate: $V_\infty \rho_\infty h = V_1 \rho_1 (h-w) + u\rho w$

Momentum: $p_\infty h - D - p_1 h = \rho_1 V_1^2 (h-w) + \rho u^2 w - \rho_\infty h V_\infty^2$

giving,

$$-D = w(\rho u^2 - \rho_1 V_1^2) - h(p_\infty - p_1 + \rho_\infty V^2 - \rho_1 V_1^2)$$

When $h \to \infty$, from Bernoulli, $p_1 \to p_\infty$, $\rho_1 \to \rho_\infty$ and $V_1 \to V_\infty$ making the second term indeterminate.

Irrotational mass flow rate $(h-a)\rho_\infty V_\infty = (h-w)\rho_1 V_1$

giving,

$$h = \frac{a \rho_\infty V_\infty - w \rho_1 V_1}{\rho_\infty V_\infty - \rho_1 V_1}$$

$\therefore$ second term $-h(p_\infty - p_1 + \rho_\infty V_\infty^2 - \rho_1 V_1^2)$

$$= -\left(\frac{a\,\rho_\infty V_\infty - w\,\rho_1 V_1}{\rho_\infty V_\infty - \rho_1 V_1}\right)(p_\infty - p_1 + \rho_\infty V_\infty^2 - \rho_1 V_1^2)$$

$$= -(a\,\rho_\infty V_\infty - w\,\rho_1 V_1)\left(\frac{p_\infty - p_1 + \rho_\infty V_\infty^2 - \rho_1 V_1^2}{\rho_\infty V_\infty - \rho_1 V_1}\right)$$

$$= -(a\,\rho_\infty V_\infty - w\,\rho_1 V_1)\left\{\frac{\delta p + \delta(\rho V^2)}{\delta(\rho V)}\right\}$$

where,

$$\delta p = p_\infty - p_1 \text{ etc.}$$

For irrotational flow:

$$\delta p + \rho V\,\delta V = 0$$

so that,

$$\delta p + \delta(\rho V^2) = \delta p + \delta(\rho V^2) - \delta p - \rho V\,\delta V = \delta(\rho V^2) - \rho V\,\delta V$$

$$= V^2\,\delta\rho + 2\rho V\,\delta V - \rho V\,\delta V$$

$$= V^2\,\delta\rho + \rho V\,\delta V = V(V\delta\rho + \rho\delta V) = V\delta(\rho V)$$

giving,

$$-(a\,\rho_\infty V_\infty - w\,\rho_1 V_1)\left\{\frac{\delta p + \delta(\rho V^2)}{\delta(\rho V)}\right\} = -(a\,\rho_\infty V_\infty - w\,\rho_1 V_1)\,\frac{V\delta(\rho V)}{\delta(\rho V)}$$

$$= -(a\,\rho_\infty V_\infty^2 - w\,\rho_1 V_1^2)$$

Hence,

$$-D = w(\rho u^2 - \rho_1 V_1^2) - (a\,\rho_\infty V_\infty^2 - w\,\rho_1 V_1^2) = w\,\rho u^2 - a\,\rho_\infty V_\infty^2$$

or,

$$D = a\,\rho_\infty V_\infty^2 - w\,\rho u^2 = \underline{w\,\rho u(V_\infty - u)}$$

It can easily be shown that for incompressible flow and where the velocity u varies across the area w

$$D = \int_w \rho_\infty u(V_\infty - u)dw$$

2.3 Roshko and Koenig Semi-Infinite Half Body Theory

The theory which is given in Appendix 1 is included for ease of reference and is taken from(16). If applicable, the theory could form the basis of a semi-empirical solution to the drag of a gauze and solid disc in tandem.

2.4 Velocities in Way of a Circular Disc in Irrotational Flow

The velocity distribution derived in Appendix 2 was found by the theoretical approach of Milne-Thomson(14) and was used to provide a comparative theoretical estimate of the mutual interference force between gauze and solid discs in tandem.

2.5 Variation of Pressure with Radius Over a Circular Disc

Appendix 2 also gives the theoretical variation of pressure over a circular disc in irrotational flow which was derived to permit a comparison to be made with the measured pressure variation.

2.6 Over-Pressurisation of Windmill Wake

One of the differences between a windmill and a gauze disc simulator is the wake pressure, the derivation of which for a windmill is given in Appendix 3.

2.7 Vortex Theory for Propeller

The propeller in the simulated windmill, solid disc and propeller combination was designed, using the theory given in Appendix 4, to produce the greatest thrust from the power delivered.

3. EXPERIMENTAL PROGRAMME

As already stated, this dissertation covers a mainly experimental investigation. Consequently, in line with its importance, three sections (Sections 3, 4 and 5) are devoted to the experimental work.

Considerable time went into planning the experiments which are justified in this section. Section 4 indicates the technique employed with the apparatus described in Section 5.

3.1 Drag of Gauze and Solid Discs in Tandem

3.1.1 Model Size

The diameter of the gauze disc was maintained at 2.00 in in all experiments. Although a larger diameter was desirable to give higher drags and consequently greater accuracy in drag measurement, it was decided to limit the size of the gauze disc so as not to exceed a blockage of 1.1%. This was the blockage adopted by Morel and Bohn in their experiments on two circular solid discs in tandem(15).

3.1.2 Wind Tunnel Speed

The lower of the two air speeds at which the experiments of Morel and Bohn(15) were run, was 22 m/s. In order to give approximately the same Reynolds number in the present tests a tunnel speed of 20 m/s was chosen.

Later, an investigation was made into the Reynolds number sensitivity of the experiments (see 3.1.8).

3.1.3 Solidity of Gauze Disc

As stated in the Introduction, an early decision was taken not to risk instability occurring in the main programme of work undertaken, and for this reason the investigations concentrated on a windmill/gauze disc simulator having a drag coefficient of 0.650 and a corresponding axial interference factor of 0.204. The choice was based on an Iwasaki(8) recommendation of 3 blades for fast running windmills with a maximum power coefficient of 0.35.

In accordance with Engineering Sciences Data Item No. 70015(6) the 2.00 in diameter gauze disc was, therefore, cut from sheet having an open area to total area ratio as near to 0.6 as was available.

The drag of the gauze disc was confirmed experimentally.

It should be noted that all the gauze shields referred to in this thesis were cut from the same sheet and thus had the same solidity (0.4).

3.1.4 Velocity Distribution Across Wind Tunnel Working Station in Way of Model

In view of the date of the last speed calibration of the wind tunnel used and bearing in mind the size of the model employed, a check was made on the velocity distribution across the central area of the tunnel enclosed by a square of 3 in side.

Using a good pitot-static tube it was found that the existing calibration gave the wind speed, at any point contained by the 3 in square, accurately to within ± 0.2%.

3.1.5 Diameter Ratios (D_1/D_2) Tested

The selected diameter ratios (D_1/D_2) were obtained by using solid discs of different diameters, namely:

D_2 in	1.709	1.815	1.994	2.402	2.755	3.200	3.601	4.534	6.016
D_1/D_2	1.170	1.102	1.003	0.833	0.726	0.625	0.555	0.441	0.332

Table 1. Diameters of Solid Discs Tested.

The drags were experimentally determined in two phases. In the first phase, tests were conducted on the central five ratios in Table 1 and in the second phase the tests were extended to the lower and higher diameter ratios in order to establish the optimum configuration of least drag and the diameter ratio at which complete shielding of the solid disc effectively occurred, respectively.

3.1.6 Gap Ratios (g/D_2) Tested

Gap ratios of 0.25, 0.5, 0.75, 1, 2, 3 and 4 were examined, generally, in the first phase (see 3.1.5 above). A more pragmatic approach to the choice of gap ratio was employed in the second phase where minimisation was being sought.

3.1.7 Corrections Applied to Measured Drags

The discs were mounted in the wind tunnel on a sting supported by a sword attached to a dynamometer. Corrections were made for the drag of the sting and sword.

In the final analysis, the drag coefficients of the solid discs ($(C_D)_{D2}$) of the minimum drag coefficient configurations were corrected for blockage.

3.1.8 Effect of Reynolds Number

A smoke technique was used to determine the maximum cross-sectional area of the separated region behind the solid disc, which required a very much reduced wind tunnel speed of approximately one-half normal. To confirm the validity of the area found in this manner and the sensitivity of the flow to variations in Reynolds number, the drag of the $D_1/D_2 = 0.625$, $g/D_2 = 2.00$ configuration was measured over a range of speeds from normal to approximately one-third normal ($106\,000 \geqslant$ Re based on $D_2 \geqslant 36\,000$). No change in drag coefficient (C_D) was discovered and only a slight falling off in C_D occurred at speeds below this range (see Table 11).

3.1.9 Check Tests

The work carried out to determine the effect of Reynolds number on C_D suggested a check on previous results and some further 45 tests were made.

Generally the new measured drag coefficients were slightly higher than those previously recorded. It is not suggested that these differences affected the major conclusions drawn from the experiments but the satisfaction of numerical repeatability was not achieved.

The check tests were helpful in establishing the uncertainty interval (see Section 4.4).

3.1.10 Vibration

In the check tests referred to above (3.1.9) the solid disc was positioned as close to the supporting sword as the holding arrangements would permit and this was successful in preventing vibration from occurring which was noticeable with certain configurations in the first phase on the gauze disc at high gaps (g).

With the smaller diameter ratios in the second phase it was necessary to provide further support to limit the vibration of the sting in way of the gauze disc to an acceptable level.

3.2 Drag of Motor Car Model

3.2.1 Choice of Vehicle

The vehicle chosen on which the experiments were carried out was a 1:24 scale model of a Fiat 124 Sport Arbarth. Choice was limited by the small range of models available of suitable size for the wind tunnel, but the selection of a well streamlined car was deliberate to see if reductions in drag might be achieved with such shapes if placed behind a gauze shield.

Calculations (see Section 4 of Appendix 5) indicated that for a car having a drag coefficient of the order of 0.7 (found by measuring the drag of the model), the gauze to be successful must produce a significant effect in addition to simply slowing down the speed of the approaching air (simple shielding) if it has the same solidity (0.4) as that used in the tests on the gauze and solid discs in tandem.

Thus in cutting the car shields from the same sheet as the gauze disc the experiments were directed towards an investigation into the change in flow pattern over the car, brought about by the shields, as detected by a reduction in drag more than commensurate with that of simple shielding.

As stated in the Introduction no attempt was made to establish the necessary parameters to give reduced drag but the calculations of Section 4 of Appendix 5 referred to above were carried out to confirm the importance of solidity and that it would feature prominently in any planned investigations. The calculations which assumed simple shielding demonstrated that high solidities are required to give reduced drag with streamline bodies.

3.2.2 Wind Tunnel Speed

As with the tests on the gauze and solid discs in tandem, the wind tunnel speed was normally 20 m/s.

Similarly, a check was made on the Reynolds number sensitivity of the experiments. The model alone was also run at speeds approximately 30% above and 15% below normal. Only small differences in drag were measured of about 1% (see Table 15).

3.2.3 Corrections Applied to Measured Drags

The model was fitted with sand strip stimulators on the leading edges of the bonnet and roof and held by a sword, attached to a dynamometer, on the centre line of the wind tunnel just above a short false floor representing the ground.

Since the experiments were aimed at determining the difference in drag of the model with and without gauze shield, no corrections for stimulators, sword or blockage were applied.

3.2.4 Flow Tests

After measuring the drag of each configuration of model car and gauze shield, cotton streamers were attached to the gauze to obtain an indication of the streamlines with a view to improving the favourable interference effect.

Smoke was also tried, instead of the cotton streamers, but without success.

3.2.5 First Configuration Tested

The shape and dimensions of the gauze shields employed are shown in Figure 5.

In early studies on the gauze and solid discs in tandem the smallest drag coefficient was predicted to occur with g/D_2 and D_1/D_2 of approximately 2.0 and 0.6, respectively. These ratios were used to decide upon the position and extent of the gauze shield but a compromise was necessary because of the various heights and widths which the model car presented to the oncoming flow.

For practical reasons it was considered prudent to position the gauze relatively close to the front of the car. Consequently, the smallest of the relevant dimensions was assumed for the value of D_2, namely, the height of the bonnet above the lower edge of the mud flaps. Thus the gauze was held twice this height forward of the position of measurement. Also, in the belief that the shielding of the main car body could be separated from that for the cab, 0.6 of the bonnet height above the bottom of the sills was adopted for one of the vertical dimensions of the gauze (16 mm).

The other dimension of the lower part of the gauze area (57 mm) was

obtained by assuming that the width of the wake, and thus the shielded area produced by the gauze, increased linearly with distance behind the gauze at a rate of 0.2, given by:

$$(D_2 - D_1)/2D_2 = (D_2 - 0.6\ D_2)/2D_2 = 0.2$$

Thus the 57 mm was that distance necessary to shield the overall width of the car at the front in accordance with this assumption.

The width of the upper part of the gauze (30 mm) was found by taking 0.6 of the roof width, while the upper edge of the gauze was located so as to shield the leading edge of the roof, using the rate of increase of 0.2, from a position forward of the leading edge equal to twice its height above the bottom of the sills. Fortunately, the longitudinal position chosen for the shield also satisfied reasonably well the $g/D_2 = 2.0$ criterion when applied to the upper part of the gauze.

3.2.6 Second Configuration Tested

The flow visualisation of the first configuration found by attaching cotton streamers to the edges of the gauze shield led to a rectangular shield 57 mm x 18 mm for the second configuration, held at the same longitudinal position as the first with a minimum clearance above the ground.

In the flow tests on the first configuration the widths of the shield at the upper and lower edges were found to be about right, since the corner streamers passed close to the sides of the body and the sides of the roof, but both edges were too high because streamers from the lower edge were touching the underside of the car and coming out from underneath, while streamers from the middle of the upper edge were passing well above the roof of the car. Furthermore, the remaining streamers were touching the bonnet and twisting over its sides, suggesting that the cut-outs were too large.

3.2.7 Third Configuration Tested

The shield was basically the same as in the second configuration but the height dimension was increased to 25 mm.

Streamers from the shield of the second configuration indicated that the width of the gauze was adequate, or perhaps a little larger than necessary, but the action of the streamers from the upper edge showed

that the gauze was not high enough.

It appeared from the flow tests on the third configuration that the gauze was not providing sufficient shielding in way of the sides above wheel arch level.

3.2.8 Fourth Configuration Tested

Again the longitudinal position of the shield was the same as in previous configurations.

Having maintained at 57 mm the bottom edge width of the shields in the first three configurations, it was decided for the fourth configuration to try a rectangular shield with the first configuration's upper edge width and height, the intention being to minimise eventually the shield area.

3.2.9 Fifth Configuration Tested

The idea in this case was to bring together the co-ordinates of the satisfactory streamer attachment positions observed with the previous configurations, namely, the side points of the lower edge and the centre point of the upper edge of the shield used in the third configuration and the side points of the upper edge of the shield in the first configuration.

3.2.10 Sixth Configuration Tested

Perhaps the main conclusion drawn from the flow tests on the fifth configuration was that it was not possible to shield the car effectively with just one piece of gauze.

Thus the sixth configuration consisted of the second configuration, which gave the lowest drag coefficient of the five configurations tried so far, with a gauze shield attached to the bonnet (see Photograph 1).

The height and position of the bonnet shield were based on the ratios given earlier; 0.6 of the height of the cab roof above bonnet level was taken for the height of the shield (9 mm) which was positioned twice this distance forward of the leading edge of the roof (30 mm). The width of the shield (51 mm) was fixed by the bonnet size as constrained by the car wings and by the need for a suitable landing on which to connect the gauze.

3.2.11 Seventh Configuration Tested

This was the bonnet shield by itself which was tested to determine its individual performance.

3.2.12 Eighth Configuration Tested

This was the final configuration tested. It had the shield a considerably greater distance ahead of the car than in the previous configurations in an attempt to heighten and widen the shielding per unit area of gauze.

Considering the ground as a plane of symmetry, "D_2" was assumed to be twice the height of the cab roof above the ground and the shield was positioned $2D_2$ forward of the leading edge of the roof with a height of $0.6D_2/2$. The width of the shield was made 0.6 of the overall width of the car at the front and again, fortunately, the position chosen for the shield also approximately satisfied the $2D_2$ requirement for this dimension.

3.3 Drag of Gauze Disc and Solid Cylinders in Tandem

3.3.1 Parallel Nature of Experiments

Except for the use of a gauze instead of a solid disc, the present investigations and the work of Morel and Bohn(15), Roshko and Koenig(16) and Saunders(17) have a number of similarities and with a view to continuing the parallel nature of the study it was decided to determine the reduction in drag obtainable with solid cylinders held with their axes parallel to the direction of flow.

3.3.2 Wind Tunnel Speed

Generally the wind tunnel speed was varied to maintain a Reynolds number of approximately 67 000, based on the diameter of the solid cylinder. Thus in the experiments with cylinders the wind speeds were very much lower than 20 m/s; they were adopted in order to avoid excessive transverse vibration.

Vibration was first noticed on the 3.000 in diameter cylinder (D_1/D_C = 0.667, ℓ/D_C = 0.338) without gauze shield when run at 20 m/s and was cured by using a thicker holding sword. Experiments were carried out on this non-vibrating configuration to determine the effect of Reynolds number on drag coefficient. Reynolds number appeared to have little

effect (see Table 17).

Even with the lower Reynolds number, vibration again became noticeable, although perhaps not invalidating, with an increase in cylinder diameter to above 3.000 in. The effect of shielding and gap ratio (w/D_C) on the severity of vibration were noted (see Table 24).

3.3.3 Configurations Tested

Guided by the results of the experiments with gauze and solid discs in tandem, where the lowest drag coefficient was achieved with approximately $D_1/D_2 = 0.6$, cylinders were chosen with diameters giving ratios of about this order based on a gauze disc diameter (D_1) of 2.00 in. The alternative of maintaining the cylinder diameter D_C and varying D_1 was discarded because of difficulties with cutting and manufacturing the gauze discs. Thus the gauze disc used in the experiments with discs in tandem was employed again. The actual diameters of the cylinders were fixed by the sizes of available material and tubing.

Details of the cylinders chosen, initially, are given below:-

Diameter (D_C) in	Lengths (ℓ) in		
2.366	1.068	2.113	3.130
3.000	1.013	2.006	3.006
3.503	1.075	2.101	3.139

The corresponding diameter and length ratios were:-

D_1/D_C	ℓ/D_C		
0.845	0.451	0.893	1.323
0.667	0.338	0.669	1.002
0.571	0.307	0.600	0.896

Each of these cylinders was tested alone and with gaps (w) of 2.0 in to 10.0 in by steps of 2.0 in giving the following gap ratios (w/D_C).

D_1/D_C	w/D_C				
0.845	0.845	1.691	2.536	3.381	4.227
0.667	0.667	1.333	2.000	2.667	3.333
0.571	0.571	1.142	1.713	2.284	2.855

Table 2. Diameters, Lengths and Gaps of Cylinders Tested Initially.

Thus initially the series consisted of 9 cylinders, alone and with 5 gaps, a total of 54 configurations, and in the light of the results of the experiments conducted on them which indicated the possibility of even smaller drag coefficients with lower diameter ratios, the series was extended to include 15 further configurations, details of which are given below.

Diameter (D_C) in		Lengths (ℓ) in	
4.506	2.072	3.125	4.164

The corresponding diameter and length ratios were:

D_1/D_C		ℓ/D_C	
0.444	0.460	0.694	0.924

and the cylinders were tested alone and with gaps of 6, 8, 10 and 12 in giving the following gap ratios (w/D_C).

D_1/D_C	w/D_C			
0.444	1.332	1.775	2.219	2.663

Table 3. Diameter, Lengths and Gaps of Further Cylinders Tested.

3.3.4 Corrections Applied to Measured Drags

The cylinders were supported in the wind tunnel by a sword connected to a dynamometer. A centre line sting attached to each cylinder in turn carried the gauze disc. Corrections were made for blockage and for the drag of the sword, but the interference between the sword and cylinder, the shielding effect of the gauze on the sword drag and the drag of the sting were neglected.

3.4 Mutual Interference/Interactive Force Between Gauze and Solid Discs

The mutual force due to interference was measured for the largest, smallest and near optimum disc diameter ratios over a range of gaps as given below.

D_1/D_2	g/D_2				
0.332		1.00		1.50	1.99	2.50
0.555		0.99	1.25	1.49	2.01	2.50
1.17	0.80	1.00		1.50	2.00	2.50

Table 4. Diameter and Gap Ratios Measured for Mutual Interference Force.

This was carried out by measuring at 20 m/s the drag of the gauze disc alone and in the presence of the solid disc, the difference being taken as the force. No corrections were applied.

3.5 Flow Visualisation Tests and Turbulence Measurements

The investigations of the flow around the gauze and solid discs in tandem were carried out in an attempt to explain the mechanism of the reduction in drag with solid disc areas considerably in excess of the fully developed wake area produced by the gauze.

It was originally intended to employ a photographic smoke technique to determine the flow lines but despite development the technique suffered from a lack of photographic definition brought about by the rapid diffusion of the smoke over a distance smaller than that of the length of the combination. Consequently, it was necessary to complement the smoke technique for sketching the flow lines by attaching streamers to the gauze disc and by holding them in the flow.

The configuration on which the development work took place was that predicted by early studies to give the lowest C_D, i.e. $D_1/D_2 = 0.6$, $g/D_2 = 2.0$. Later as the results of further drag tests became available it was realised that a closer configuration to the optimum was $D_1/D_2 = 0.555$, $g/D_2 = 1.79$ and the flow lines for this configuration were also established by streamer and smoke tests. The latter was used to determine the maximum cross-sectional area of the separated region and were carried out at a very much reduced wind speed, approximately half normal, to improve the density and hence the sighting of the smoke. In this respect drag tests to ascertain the effect of Reynolds number (see 3.1.8) confirmed the validity of the flow patterns registered. Even with the reduced speed, difficulties were still found with the smoke technique in determining precisely the diameter of the cross-sectional area of the separated region behind the solid disc and, with a view to obtaining confirmation of the position of the shear layer, measurements were taken of the turbulence in the wake. Figure 6 shows that the peaks of the RMS values (from Table 26) correlated well with the outer edge of the shear layer as determined by smoke tests. The agreement is sufficient to confirm the validity of the smoke tests as a means of finding the extent of the shear layer. The figure also supports the observation, made during the smoke tests, of considerable diffusion occurring aft of 2.909 in. It might be anticipated that diffusion would be reflected by a fall-off

in RMS value.

The final verifying tests concentrated on the main themes of the effects of changes in diameter ratio at constant gap and the effects of changes in gap ratios at constant diameter and thus D_1/D_2. The gap (g) and diameter (D_2) chosen was that of the approximately optimum configuration, $D_1/D_2 = 0.555$ and $g/D_2 = 1.79$. Thus $A_S/(A)_{D2}$ was measured on the following configurations.

D_2 in	g in	D_1/D_2	g/D_2
6.016	6.46	0.332	1.07
4.534	6.44	0.441	1.42
3.601	6.46	0.555	1.79
2.755	6.46	0.726	2.34
1.944	6.45	1.003	3.23
3.601	10.06	0.555	2.79
3.601	7.92	0.555	2.20
3.601	5.04	0.555	1.40
3.601	2.71	0.555	0.75
3.601	0.90	0.555	0.25

Table 5. Configurations On Which $A_S/(A)_{D2}$ and $(\overline{C_P})_S$ Were Measured.

A feature of the flow pattern associated with $A_S/(A)_{D2}$ and having a bearing on C_D was the angle which the flow of the shear layer made at the edge of the solid disc ($(\Theta)_{D2}$). Consequently $(\Theta)_{D2}$ was also measured on most of the configurations listed in Table 5. Additionally because D_1 was fixed at 2.0 in in all experiments, $(\Theta)_{D2}$ was also measured on four further diameter ratios with the gap ratio of the approximately optimum configuration referred to above.

Flow patterns were also determined for three configurations at $D_1/D_2 = 0.726$ of $g/D_2 = 2.34$, 1.80 and 1.27 in order to confirm visually some conclusions drawn on the effect of changes in gap ratio and diameter ratio.

3.6 Velocity Measurements

3.6.1 Behind Gauze Disc

The interference between the gauze and solid discs in tandem was looked upon as being made up of two components. Essentially it was considered

that the first component was caused by the gauze disc slowing down the flow approaching the solid disc while the second was caused by the solid disc slowing down the flow approaching the gauze disc.

With respect to the first component the development of velocity with distance in the wake of the gauze disc was important to the investigation of the effect of gap ratio. For this reason the variation of velocity with radius was measured at D_1, $2D_1$, $3D_1$ and $4D_1$ behind the gauze disc when held alone in the free stream.

3.6.2 In Wake of the Approximately Optimum Configuration of Gauze and Solid Discs in Tandem

As indicated in the Introduction the distribution of velocity was measured in the wake of the solid disc when held in tandem with a gauze disc simulating a windmill. The distribution was used to design a propeller driven by the windmill and thus to estimate the thrust developed.

More precisely, the variation of velocity with radius ($0 \leqslant r \leqslant 3D_1$) was measured in the wake of the approximately optimum configuration at $3D_2$ and $4D_2$ downstream of the solid disc.

3.7 Pressure Measurements

These were confined to the backs and faces of the solid discs.

Drag tests on the gauze and solid discs in tandem showed that in the region of least drag the gap between the discs (g) was sufficiently large as to cause little mutual interference. Consequently, it was the drag of the solid discs and, therefore, the pressures acting on them which very largely determined the optimum configuration. The pressures and their relationship with other parameters also provided an insight into the mechanism of drag reduction.

Back and face pressures were first measured on the solid disc of the approximately optimum configuration, $D_1/D_2 = 0.555$, $g/D_2 = 1.79$, at three radii, $0.1D_2$, $0.2D_2$ and $0.3D_2$, for a number of angular positions over one half of the disc. The results indicated that the near uniformity of pressure found on the back of the disc was not repeated on the face.

It was, therefore, possible to determine the position of the end of one pressure tube giving a reading representative of the back pressure and

the pressure so found was recorded for all the configurations given in Table 5.

In the case of the face pressure, the mean value was estimated from measurements made at 15 different positions and was found for the above approximately optimum configuration and for three other gap ratios, 1.40, 0.75 and 0.25, at the same diameter ratio, 0.555. The same measurements were also taken on the solid disc alone, that is, when unshielded.

4. EXPERIMENTAL TECHNIQUE

4.1 Calibration and Measurement of Drag

The usual preliminaries of allowing the wind tunnel instrumentation a warm-up period were performed and the air supply pressure to the drag dynamometer was adjusted to its operating value.

Except for minor final adjustments, the configuration to be tested was prepared prior to being set up in the tunnel. In the case of the gauze and solid discs in tandem the length of sting was adjusted to suit the gap length and to position the solid disc close to the holding sword as a preventative measure against vibration. With the cylinder configurations the base length attached to the sword held the sting in centralising holes with a push fit. The length of the sting could be adjusted for gap distance by sliding the sting through the centralising holes. The gauze disc and any required extension pieces of cylinder were carried concentrically by the sting.

In the case of the measurement of the interactive force between gauze and solid discs in tandem, the positions of the two holding swords were maintained (see Figure 16) and the required gap between the discs achieved by modifying the length of the sting on the forward sword carrying the gauze disc. Final adjustments for gap were made by sliding the solid disc along the sting on the aft sword.

Only the car model was stimulated for turbulence. 6 mm sand strips were stuck to the leading edges of the bonnet and roof. Care was exercised when fitting the car model to ensure that the false floor simulating the road surface was held level and as close as possible to the wheels of the car without actually touching them.

The sword holding the configuration to be measured for drag was bolted to the central housing of the dynamometer. This housing could be rotated in direction and was used to align the configuration with the centre line of the tunnel. Light cotton sighting pendulums were fitted temporarily to the configuration to facilitate the alignment. Similarly, adjustments for zero elevation were made, using the distances of the configuration from the tunnel walls.

A well balanced calibration pulley with very low friction was attached to the open end of the wind tunnel and a cotton thread run over it to

the sword holding the configuration. The position of the pulley was adjusted to align the thread with the centre line of the tunnel, siting along the thread for direction and measuring to the tunnel walls for elevation. Weights were suspended by the thread to tension it to a value slightly in excess of the drag to be measured and the controls of the Signatrol Measuring Unit set to give approximately full-scale deflection on the Unit's meter. The weights were progressively subtracted and added and corresponding meter readings taken to provide a drag calibration which was checked for linearity.

On completing the calibration, the calibrating equipment was removed and the access side panels to the tunnel were replaced. Initial readings of air temperature, air pressure and drag meter were noted and the wind speed micromanometer zeroed. The tunnel was started and brought up to the required speed as indicated by the micromanometer. Normally, four simultaneous readings of drag meter and speed micromanometer were taken around and close to the required speed before finishing the run and taking final readings of air temperature and pressure. The time at which each reading was taken was also recorded so that the air pressure and temperature corresponding to the drag readings could be estimated by linear interpolation and the wind speed evaluated. In long runs exceeding a few minutes, intermediate readings of air pressure and temperature were taken to improve the accuracy of the interpolation.

Air density was found from tables using the temperature and pressure and wind speed from the empirically derived formula:

$$V \text{ m/s} = \sqrt{(0.9449 \times 2g \times \frac{h}{\rho_{AIR}})}$$

where,

g = acceleration due to gravity

= 9.81 m/s^2

h = micromanometer reading in mm of water

4.2 Correction for Sword and Sting Drag

In the case of the gauze and solid discs in tandem a deduction was made from the drag coefficients for the drag of the holding sword and sting. This drag was found by simply removing the discs by sliding them off the

sting and repeating the runs. Thus no account was taken of the interference and shielding effects of the discs on the sword and sting but they were estimated to be secondary effects well within the uncertainty interval. As might be expected, the sting length had a negligible influence on the results.

Similarly the drag coefficients of the gauze disc and cylinders in tandem were corrected for sword drag. The correction was derived from the experimental results mentioned in the previous paragraph assuming that the drag correction was proportional to the length of the sword. It follows that no account was taken of the interference and shielding effects of the gauze disc and cylinders on the sword drag.

The drags of the car model were not corrected for sword drag.

4.3 Correction for Blockage

4.3.1 Gauze and Solid Discs in Tandem

Flow visualisation tests indicated that the gauze disc made a negligible contribution to blockage because of its small diameter and solidity. Thus it was decided to apply a correction for blockage to the drag of the solid disc only and with this in mind the correction was not made to all results but was confined to the analysis of the minimum drag coefficients for the various diameter ratios tested. By then measurements of the mutual interference force permitted an estimate to be made of the drag component due to each disc.

The blockage corrections were derived using the approach of Maskell(13) which is particularly well suited to the present work because it was developed for thin plates perpendicular to the flow, a fact recognised by Morel and Bohn(15) in deciding to use the approach in the analysis of their experiments. Thus:

$$\frac{1}{(C_D)_{D2CALC}} = \frac{1}{(C_D)_{D2CORR}} - \varepsilon b$$

where ε, the blockage factor, was taken as having a value of 2.75 as recommended by Maskell. Its value was confirmed by measuring the drags of the 9 unshielded solid discs $(C_D)_{D2ALONE}$ and plotting the variation of $1/(C_D)_{D2ALONE}$ with the blockage b, as shown in Figure 7,

and $(C_D)_{D2CALC} = C_D - (C_D)_{D1ALONE} + (C_D)_{ICALC}$

giving

$$(C_D)_{MINCORR} = (C_D)_{D2CORR} + (C_D)_{D1ALONE} - (C_D)_{ICALC}$$

when C_D is the minimum value for a given D_1/D_2 i.e.,

$$C_D = (C_D)_{MIN}$$

4.3.2 Gauze Discs and Solid Cylinders in Tandem

The blockage corrections were also derived using the approach of Maskell (13) and were applied to the measured configuration drags, after deducting sword drag, because in these experiments no attempt was made to isolate the cylinder drag from that of the gauze disc.

$$\frac{1}{(C_D)_C} = \frac{1}{(C_D)_{CCORR}} - \varepsilon c$$

ε, the blockage factor was again taken as 2.75. Its validity was confirmed by plotting the variation of $1/(C_D)_{CALONE}$, interpolated at a ℓ/D_C of 0.9 for the four different diameters D_C employed, with the blockage c (Figure 8 taken from Table 19).

4.3.3 Car Model

No corrections were made for blockage. The same model was used in all experiments which were aimed at observing relative differences in drag.

4.3.4 Mutual Interference/Interactive Force Between Gauze and Solid Discs in Tandem

Again no corrections were made for blockage. The force was taken as the difference in drag of the gauze disc with and without the solid disc present so that the correction if made would have been for a second order effect due to the change in interference of the solid disc with the flow through the gauze disc caused by the former's blockage.

4.4 Estimation of Uncertainty Interval for Drag Tests

The method used to determine the uncertainty interval was that of Kline and McClintock(9).

Drag: arising from calibration of dynamometer and difficulty in reading drag meter due to fluctuations

$100g \pm 2g$(20 to 1)

Dynamic pressure: difficulty in reading dynamic pressure due to fluctuations

25 mm ± 0.25 mm (20 to 1)

Hence uncertainty interval

$$= \left[\left(\frac{2}{100}\right)^2 + \left(\frac{0.25}{25}\right)^2\right] = 0.022$$

an uncertainty interval of ± 0.02 for C_D(20 to 1).

4.5 Determination of Flow Lines

To determine the flow lines around the car model and initially for the gauze and solid discs in tandem (D_1/D_2 = 0.600, g/D_2 = 2.00, Figure 9), light cotton streamers slightly longer than the configuration being examined were attached to the gauze shield. Photographs taken of the streamers assisted in the production of Figure 9.

With the remaining gauze and solid disc configurations, a 3 in long light cotton streamer was attached to the end of the horizontal arm of the sliding unipod and base shown in Photograph 2. The metre rule shown in the photograph guided the base so that the leading end of the streamer moved in the vertical centre line plane at a height determined by the length of the interchangeable vertical leg.

Observations were taken of the angles made with the centre line of the leading and trailing ends of the streamer from which the position of the trailing end was estimated. The estimated positions and angles of the trailing ends found in this manner are shown in Figures 10 to 13.

Behind the solid disc the above observations were limited to areas outside of the separated region bordered by the shear layers due to heavy turbulence causing excessive oscillation of the streamer inside this region.

4.6 Determination of Back and Face Pressures

The manometer bank shown in Photograph 3 was employed at its greatest slope (sensitivity) position of about 18°. It was calibrated using a good quality manometer and in the formula:

pressure = $\rho g \sin(\text{slope angle})\{\text{difference in reading}\}$

the product ρ x sin(slope angle) was found to have a value of 253 kg/m^3.

All pressures were found relative to the upstream static pressure and one manometer of the bank was devoted to the measurement of this pressure which was found to be slightly different from ambient when the tunnel was running.

Measurements were kept to below the centre line to avoid the effects of the holding sword and the 2 mm outside diameter plastic tubing connecting the pressure tappings to the manometer bank.

Figure 14 shows the polar co-ordinates of the 15 positions at which measurements were taken to find the mean face pressure on the solid disc of diameter 3.601 in (see Section 3.7). The co-ordinates conformed to a 5 ordinate Tchebycheff numerical integration rule radially and a 3 ordinate rule angularly. Each measurement was, consequently, weighted by its radial distance before summing and factorising by 2/15R, where R = 3.601/2 in. A correction was again made for a slight difference from ambient of the upstream static pressure.

4.7 Determination of $A_S/(A)_{D2}$ and $(\Theta)_{D2}$ by Smoke Technique

The smoke probe shown in Photograph 4 was inserted into the tunnel working section through a small access hole in the side inspection panel and the tip of the probe was positioned to bleed smoke into the centre line flow over the face of the solid disc of the configuration being investigated at a point close to the periphery of the disc at bottom dead centre. To minimise interference with the centre line flow the "hook" of the probe was led away sideways and upwards and slightly forward.

As stated in Section 3.5, the wind tunnel speed was reduced to approximately half normal to improve the density and hence the sighting of the smoke. Previous investigations into the effect of Reynolds number established the validity of this approach.

$(\Theta)_{D2}$ was estimated from a short length of smoke in the flow extending aft from the edge of the solid disc for approximately 3/16 in, which was necessary because of the considerable curvature in the flow at this position. It made the accurate measurement of $(\Theta)_{D2}$ difficult.

$A_S/(A)_{D2}$ was found by measuring D_S. The tip of the horizontal arm of the sliding unipod shown in Photograph 2 was used to probe the smoke and the height of the tip was adjusted until it just kissed the outer edge of the smoke at the greatest diameter position. Some diffusion of smoke occurred within the separated region so that the true thickness of the smoke band at this position was not readily discernible but it was assumed to be 2 mm. In accordance with Morel and Bohn(15) the shear layer was considered to lie at the middle of the smoke band so that:

$$D_S = (\text{Distance of tangent point from } \mathbb{Q} \times 2) - 2 \text{ mm}$$

At the position of measurement of D_S it was not possible to distinguish between the shear layers springing from the edges of the gauze and solid discs.

4.8 Determination of Turbulence

The horizontal arm of the sliding unipod referred to in Sections 4.5 and 4.7 was replaced by the hot-wire probe of the constant temperature anemometer (Photographs 2 and 5) and the hot-wire was aligned with its axis vertical so that it detected horizontal perturbations of velocity. The metre rule guided the base of the unipod so that the hot-wire moved in the vertical centre line plane at a height determined by the length of the interchangeable vertical leg. Measurements were confined to below the centre line to avoid the wake of the holding sword.

The anemometer was set up in accordance with the maker's instructions. No calibration for turbulence was carried out but the anemometer was calibrated for velocity and found to be reasonably constant over a period of days. Since the position at which the root mean square value peaked was being sought, rather than its absolute value, at one height of the probe in an experiment itself lasting normally no longer than 30 minutes, a technique not involving a calibration was considered acceptable.

4.9 Determination of Velocity Distributions

4.9.1 Behind Gauze Disc

In order to obtain greater definition of the velocity ratio (V_x/V_∞) distribution behind the gauze disc than that possible with the pitot rake shown in Photograph 6, the good double tube device diagrammatically sketched in Figure 15 was used mounted on a lathe's crosshead which

allowed the device to be located accurately relative to the disc.

Initial measurements indicated that in any one transverse the static pressures were nearly independent of radius; generally the difference in static pressure over a difference in radius of 0.25 in was less than 0.1 mm H_2O. The wind speed at the stagnation tube position was, therefore, determined by deducting the static pressure measured simultaneously 0.25 in to port.

As stated in Section 3.6.1, the object of the experiments was to investigate the development of velocity with distance in the wake of the gauze disc and it was considered that the velocity ratio found from the following equation was a sufficiently accurate indicator without the need to calibrate the device:

$$\frac{V_x}{V} = \sqrt{\frac{h_T}{0.9449h}}$$

where,

h_T = difference between stagnation and static tube heads in mm water

h = micromanometer reading in mm of water

4.9.2 In the Wake of the Approximately Optimum Configuration of Gauze and Solid Discs in Tandem

The ratio of the velocities with and without the configuration present in the wind tunnel were found at points along horizontal transverse radii $3D_2$ and $4D_2$ downstream of the plane containing the solid disc by means of the pitot-static rake shown in Photograph 6, extending from the centre line to 6 inches to port.

The static pressure at the stagnation tube position was found by linearly interpolating between the static pressures measured 0.25 in to port and to starboard except for the zero and 6 in positions where the static pressures were taken at 0.25 in and 5.75 in, respectively.

Velocity ratios were determined to take into account that the velocity distribution across the tunnel was not uniform and this necessitated the measured velocities being corrected for tunnel speed. It was assumed that the dynamic pressure heads were proportional to the micromanometer

(Photograph 7) readings.

At r = 4 in the velocity ratios became substantially constant and the further assumption was made that the edge of the wake occurred at this radius and without blockage the free stream velocity. In presenting the distributions as decimal fractions of the velocity ratio at r = 4 in, the blockage effect was proportionally applied.

The pitot-static rake was not calibrated and the calibration coefficient was taken as not varying over the range of speeds measured. Thus the percentages given in Table 29 were calculated by finding V_x/V, using the above equation, at each radius (r) and dividing by V_x/V at r = 4.0 in.

5. APPARATUS

5.1 Wind Tunnel

Particulars of the wind tunnel in which the work was conducted are given below and general views are shown in Photographs 8 to 12.

Builder: Plint and Partners Limited, Engineers, Wargrave, Berks. Tunnel No. WT338.

Fan: The Airscrew Company and Jigwood Limited. Diameter of fan 24 in. Serial No. 70360.

Drive: Electric Construction Company Limited, Wolverhampton. Motor No. 281615. 20 hp. 1500/1440 rev/min. 3 phase. 50 c/s. 27.8 amps. 400 volts.

Inlet Control Motor: Normand Electrical Company Limited, London and Portsmouth. Serial No. 10547A. Frame W5. 0.25 hp. 180 rev/min. 3 phase. 50 c/s. 0.6 amps. 400 volts. Type SC.

Cross-sectional Area at Test Section = 0.20219 m^2.

5.2 Tunnel Wind Speed Measuring Apparatus

Wind speed was determined from the static pressure drop across the tunnel convergence and the air density. A micromanometer was employed for the former, namely, Micromanometer MDC FC001, Furness Controls Limited, Bexhill, shown in Photograph 7, and the latter was found from measurements of the barometric pressure and temperature. The barometer used was:

Precision Aneroid Barometer Mk2,
Type No. M2236, Range 900-1050 mb,
Serial No. A078,
by Negretti and Zambra, Croydon,

shown in Photograph 13.

A check was made on the speed calibration using a good pitot-static tube (see Section 3.1.4).

5.3 Drag Dynamometer

Photographs 14 to 17 show views of the drag dynamometer with holding sword and sting. The dynamometer which is of the air bearing type was designed and manufactured by the Department of Mechanical Engineering, Portsmouth Polytechnic.

The drag force deflects a strain-gauged cantilever whose strain was indicated by a Signatrol Transducer Excitation and Measuring Unit. Type No. GPL-100-02. Ancoms Limited, Devonshire Street, Cheltenham, Glos. GL50 3LT. Series TBSC. SN S81-2908, which is shown in Photograph 18.

A drag force calibration was carried out prior to each run using a pulley and hanging weight system.

All stings were made from decoated 1/8 in diameter brazing bar soldered to the holding swords which were cut and shaped from 1 in wide 1/8 in thick steel plate to give sharp leading and trailing edges.

5.4 Gauze and Solid Discs

The gauze disc and the nine solid discs on which the drag tests were conducted are shown in Photograph 19.

As stated in Section 3.1.3, the gauze disc had an open area to total face area of approximately 0.6. It was cut from an oil filter woven from steel wire of 28 s.w.g.

24 s.w.g. aluminium alloy plate was used for the solid discs which were bossed, to fit tightly the holding sting, and turned to size with square edges. The largest thickness to diameter ratio was 0.013 which was close to the ratio of 0.011 for the square edge disc used by Morel and Bohn(15). Engineering Sciences Data Item No. 70015(6) states that thickness has no effect on normal force coefficient up to a ratio of 0.2.

Photograph 20 shows a configuration of the gauze and solid discs in tandem close to the optimum, that is, the configuration giving $(C_D)_{LEAST}$.

5.5 Motor Car Model

The 1:24 scale model, in the sixth configuration mode, is shown in Photograph 1. It was made in Italy by Durago and had a cast metal body with plastic chassis, wheels, cabin roof, windows, and engine and boot lids.

As the photograph indicates, the cabin roof was slotted to take a holding sword, similar to that used for the tests on the gauze and solid discs, which was secured by brackets bolted to the cabin roof.

Two 2 mm diameter light alloy rods were tapped into the forward edge of the chassis to carry the leading gauze shields. The lower edge of the bonnet gauze was flanged and glued in position.

A 1/4 in thick sheet of plywood with sharpened leading edge, extending forward of the model as far as the leading gauze shields and fitted across the width of the tunnel at mid height, acted as the false floor (see Photograph 21).

5.6 Solid Cylinders

The solid cylinders on which the drag tests were conducted are shown in Photograph 22. They were made from plastic Durapipe with light alloy plate facings except for the 3 in diameter cylinder which was made in perspex. The various lengths of cylinder tested at a given diameter were produced by adding similarly constructed extension pieces to the smallest length which was slotted to take, and cemented to, the holding sword.

A central 1/8 in diameter hole was drilled in each length of cylinder to take the sting which was utilised to carry the gauze shielding disc at various gaps and to hold the lengths of cylinder concentrically together.

Photograph 23 shows a configuration of the gauze disc and solid cylinder in tandem close to the optimum, that is, the configuration giving $(C_D)_{CLEAST}$.

5.7 Mutual Interference/Interactive Force

The interactive force was determined by measuring the drag of the gauze disc alone and in the presence of the solid disc. The apparatus is shown diagrammatically in Figure 16 in which it is seen that the solid disc, when present, was held in tandem by a second sword and sting fastened to the tunnel floor.

5.8 Smoke Apparatus

A diagrammatic sketch of the smoke apparatus used to investigate origi-

nally the flow around the gauze and solid discs in tandem is shown in Figure 17. In spite of development it did not prove to be very successful and cotton streamers were used instead.

The apparatus was discarded for that shown in Photograph 4 which was employed to determine only the maximum cross-sectional area of the separated region behind the solid disc (see Section 3.1.8). T.E.M. Engineering Limited manufactured the smoke probe which burnt Shell Vitrea Oil from a bottle reservoir through a heating element connected to a control box designed and made by Portsmouth Polytechnic.

5.9 Hot Wire Anemometer

Turbulence was measured by the constant temperature anemometer specified below and shown in Photograph 5.

DISA Electronik Type 55A01 Code 9055 A 0018
Serial No. 643 Herley, Denmark.

The hot-wire probe was positioned in the wake of the near optimum gauze and solid discs in tandem configuration by means of the sliding unipod and base shown in Photograph 2. A metre rule guided the base so that the hot-wire moved in the vertical centre line plane of the configuration at a fixed height determined by the length of the interchangeable vertical leg. Two weighted lines were passed through small holes in the floor of the wind tunnel and connected to the ends of the sliding base which produced sufficient static friction to prevent movement of the probe by the air stream. Readings of the scale on the metre rule as given by the leading edge of the sliding base were used to determine the longitudinal position of the probe relative to the aft face of the solid disc. The probe was held with the axis of the hot-wire vertical.

5.10 Velocity Measurement Rake and Manometer Bank

These are shown in Photographs 6 and 3, respectively. The former, constructed by Portsmouth Polytechnic, consisted of a pitot-static arrangement of 25 tubes spaced 0.25 in apart connected by polythene tubing to the manometer bank (Serial No. 9545) which was obtained from T.E.M. Instruments Limited, Crawley, Sussex. The manometric liquid had a relative density of 0.787 and the bank could be sloped to increase sensitivity.

Measurements of velocity were taken with the above apparatus in the wake

of the approximately optimum configuration of gauze and solid discs in tandem (see Section 3.6.2).

5.11 Solid Discs' Pressure Tappings

Pressures were taken on the face and back of the solid disc of the approximately optimum configuration of gauze and solid discs in tandem. Photograph 24 shows the arrangement of tappings for measuring the face pressures at 15 different positions (see Section 3.7). At each position a hole was drilled to take a short length of hypodermic tubing which was secured by Araldite so that the inserted end of the tube was flush with the face. Small bore polythene tubing connected the tappings to the manometer bank shown in Photograph 3. A similar arrangement was used in the initial experiments with only 9 tapping positions and the simple expedient was employed of reversing the faces of the disc to determine the 9 back pressures.

Figure 18 shows diagrammatically the positioning of the pressure tube to give a single representative reading of the back pressure. Small bore polythene tubing was run down the holding sword and taped to the rear face of the solid disc with the open end at centre line height and as close to the centre as was allowed by the boss.

6. CALCULATIONS

Calculations using the simple shielding theory of Section 2.1 were carried out to allow a comparison to be made with the experimental results and the calculations were extended to assess the effectiveness of the shields on the drags of the car configurations and the importance of gauze solidity in drag reduction.

Calculations were also made to estimate the mutual interference force between a simulated windmill and solid disc in tandem and the reduction in drag obtainable with a propeller driven by the windmill power.

A number of parameters were calculated in support of the discussion.

Details of the calculations are given in Appendix 5.

7. RESULTS

7.1 Experimental Results

7.1.1 Drag Coefficient of Gauze Disc Alone

$(C_D)_{GALONE}$ was measured on eight occasions throughout the experiments and the following results were obtained.

0.64, 0.68, 0.65, 0.65, 0.65, 0.65, 0.68, 0.66

$(C_D)_{GALONE}$ was therefore taken as 0.65.

7.1.2 Drag Coefficients of Gauze and Solid Discs in Tandem. First Phase.

D_1/D_2 = 1.003

g/D_2	0.25	0.50	0.75	1.00	1.00	1.00	2.01	2.01
C_D	1.16	1.11	1.09	1.05	1.08	1.05	1.04	1.04
g/D_2	3.01	3.01	4.01	4.01				
C_D	1.06	1.04	1.07	1.05				

D_1/D_2 = 0.833

g/D_2	0.25	0.50	0.75	1.00	2.00	3.00	4.00
C_D	1.09	1.02	0.97	0.93	0.90	0.91	0.94

D_1/D_2 = 0.726

g/D_2	0.25	0.50	0.75	1.00	2.00	2.99
C_D	1.09	0.98	0.93	0.88	0.83	0.85

D_1/D_2 = 0.625

g/D_2	0.25	0.50	0.75	1.00	2.00	2.50
C_D	1.13	1.02	0.91	0.86	0.78	0.80

D_1/D_2 = 0.555

g/D_2	1.00	1.50	2.00
C_D	0.86	0.80	0.79

Table 9. C_D for Gauze and Solid Discs in Tandem. First Phase.

7.1.3 Drag Coefficients of Gauze and Solid Discs in Tandem. Second Phase.

D_1/D_2 = 0.322

g/D_2	1.00	1.41	1.81	2.21	2.60
C_D	1.18	1.11	1.15	1.20	1.21

D_1/D_2 = 0.441

g/D_2	1.35	1.41	1.80	2.00	2.20
C_D	0.88	0.88	0.86	0.87	0.89

D_1/D_2 = 1.102

g/D_2	0.99	1.38	1.76	2.20
C_D	1.17	1.15	1.19	1.22

D_1/D_2 = 1.170

g/D_2	0.60	0.80	1.00	1.40
C_D	1.25	1.24	1.25	1.29

Table 10. C_D for Gauze and Solid Discs in Tandem. Second Phase.

7.1.4 Effect of Reynolds Number on Drag Coefficient of Gauze and Solid Discs in Tandem

D_1/D_2 = 0.625 g/D_2 = 2.00

$(Re)_{D2}$	105700	94700	80600	67400	47400	36300	25800
C_D	0.84	0.84	0.83	0.84	0.84	0.84	0.81

Table 11. Effect of Reynolds Number on C_D for Gauze and Solid Discs in Tandem.

7.1.5 Check Tests on Drag Coefficients of Gauze and Solid Discs in Tandem

$D_1/D_2 = 1.003$

g/D_2	1.29	1.67	2.05	2.47	3.04
C_D	1.10	1.13	1.11	1.12	1.14

$D_1/D_2 = 0.833$

g/D_2	1.39	1.70	1.71	2.04	2.53	3.01
C_D	0.95	0.97	0.96	0.96	0.98	0.99

$D_1/D_2 = 0.726$

g/D_2	1.45	1.75	2.18	2.59
C_D	0.89	0.89	0.90	0.89

$D_1/D_2 = 0.625$

g/D_2	0.25	0.50	0.75	1.00	1.30	1.50	2.00	2.49
C_D	1.16	1.02	0.97	0.91	0.88	0.90	0.83	0.85

$D_1/D_2 = 0.555$

g/D_2	0.25	0.51	0.75	1.00	1.40	1.50	1.59	1.74	1.79	
C_D	1.22	1.07	0.97	0.91	0.80	0.88	0.79	0.83	0.82	
g/D_2	1.79	1.79	1.79	1.79	1.80	1.98	2.00	2.09	2.19	2.20
C_D	0.82	0.84	0.82	0.82	0.79	0.79	0.82	0.80	0.80	0.78
g/D_2	2.28	2.45	2.50							
C_D	0.80	0.82	0.83							

Table 12. C_D for Gauze and Solid Discs in Tandem. Check Tests.

7.1.6 Blockage and Drag Coefficients of Solid Discs Alone

D_2 in	1.709	1.815	1.994	1.994	1.994	2.402	2.402
b	0.0073	0.0083	0.0100	0.0100	0.0100	0.0145	0.0145
$(C_D)_{D2ALONE}$	1.12	1.13	1.12	1.10	1.23	1.16	1.23
D_2 in	2.755	2.755	3.200	3.200	3.601	3.601	4.534
b	0.0190	0.0190	0.0257	0.0257	0.0325	0.0325	0.0515
$(C_D)_{D2ALONE}$	1.16	1.23	1.18	1.28	1.24	1.30	1.30
D_2 in	6.016						
b	0.0907						
$(C_D)_{D2ALONE}$	1.55						

Table 13. b and $(C_D)_{D2ALONE}$ for Solid Discs.

7.1.7 Minimum Drag Coefficients of Gauze and Solid Discs in Tandem for Each D_1/D_2 and Corresponding Gap Ratios (from Figures 26, 27, 28 and 29)

D_1/D_2	1.170	1.102	1.003	0.833	0.726	0.625	0.555	0.441	0.332
g/D_1 for $(C_D)_{MIN}$	0.70	1.15	1.50	2.35	2.80	3.10	3.40	3.95	4.35
g/D_2 for $(C_D)_{MIN}$	0.80	1.25	1.50	1.95	2.05	1.95	1.90	1.75	1.45
$(C_D)_{MIN}$	1.24	1.15	1.06	0.93	0.86	0.83	0.81	0.86	1.12
corresponding values of									
$(C_D)_{ICALC}$ (Table 39)	0.24	0.11	0.07	0.03	0.02	0.02	0.01	0.01	0.01
$(C_D)_{D1ALONE}$	0.89	0.79	0.65	0.45	0.34	0.25	0.20	0.13	0.07
$(C_D)_{D2CALC}$	0.59	0.47	0.48	0.51	0.54	0.60	0.62	0.74	1.06
$(C_D)_{D2CORR}$	0.58	0.47	0.47	0.50	0.53	0.58	0.59	0.67	0.84
$(C_D)_{MINCORR}$	1.23	1.15	1.05	0.92	0.85	0.81	0.78	0.79	0.90

Table 14. $(C_D)_{MINCORR}$ for Each D_1/D_2 and Corresponding Gap Ratios and Drag Coefficients.

7.1.8 Effect of Speed on Drag of Car Model

Model Speed m/s	17.3	20.7	25.6
$(C_D)_{CAR} \times A_{CAR} \times 10^3$ m^2	1.77	1.76	1.77

Table 15. Effect of V_∞ on $(C_D)_{CAR} \times A_{CAR}$.

7.1.9 Drag of Car Configurations

Configuration	1	2	3	4	5	6	7	8
$(C_D)_{CAR} \times A_{CAR} \times 10^3$ m^2	2.04	1.86	1.91	1.94	2.06	1.95	1.85	1.89

Table 16. Drag of Car Configurations/$0.5\rho V_\infty^2$.

7.1.10 Effect of Reynolds Number on Cylinder Drag Coefficient

D_1/D_C = 0.667 $\quad \ell/D_C$ = 0.338 $\quad$ Cylinder Unshielded

V_∞ m/s	$(Re)_{DC}$	$(C_D)_{CALONE}$
13.4	67000	1.36
19.8	99000	1.35
23.1	116600	1.37

Table 17. Effect of $(Re)_{DC}$ on $(C_D)_{CALONE}$.

7.1.11 Drag Coefficients of Cylinders Alone

D_C = 2.366 in

ℓ in	1.068	2.113	3.130
ℓ/D_C	0.451	0.893	1.323
$(C_D)_{CALONE}$	1.21	1.12	0.87
$(C_D)_{CALONECORR}$	1.16	1.07	0.84

D_C = 3.000 in

ℓ in	1.013	2.006	3.006
ℓ/D_C	0.338	0.669	1.002
$(C_D)_{CALONE}$	1.29	1.25	1.16
$(C_D)_{CALONECORR}$	1.19	1.16	1.08

D_C = 3.503 in

ℓ in	1.075	2.101	3.139
ℓ/D_C	0.307	0.600	0.896
$(C_D)_{CALONE}$	1.29	1.35	1.22
$(C_D)_{CALONECORR}$	1.16	1.21	1.11

D_C = 4.506 in

ℓ in	2.072	3.125	4.164
ℓ/D_C	0.460	0.694	0.924
$(C_D)_{CALONE}$	1.42	1.40	1.28
$(C_D)_{CALONECORR}$	1.18	1.17	1.09

Table 18. $(C_D)_{CALONE}$ for Cylinders.

7.1.12 Blockage and Drag Coefficients of Cylinders Alone at ℓ/D_C = 0.9

D_C in	2.366	3.000	3.503	4.506
c	0.01403	0.02205	0.03075	0.05088
$(C_D)_{CALONE}$	1.12	1.20	1.22	1.29
$(C_D)_{CALONECORR}$	1.07	1.12	1.11	1.09

Table 19. c and $(C_D)_{CALONE}$ for Cylinders at ℓ/D_C = 0.9.

7.1.13 Drag Coefficients of Gauze Discs and Cylinders in Tandem. Corrected for Blockage.

					$(C_D)_{CCORR}$		
D_1/D_C	ℓ/D_C	w/D_C =	0.845	1.691	2.536	3.381	4.227
0.845	0.451		0.94	0.87	0.85	0.82	0.81
0.845	0.893		0.75	0.73	0.74	0.73	0.74
0.845	1.323		0.72	0.71	0.71	0.73	0.74
		w/D_C =	0.667	1.333	2.000	2.667	3.333
0.667	0.338		0.94	0.86	0.82	0.80	0.80
0.667	0.669		0.89	0.74	0.66	0.66	0.67
0.667	1.002		0.72	0.64	0.64	0.64	0.65
		w/D_C =	0.571	1.142	1.713	2.284	2.855
0.571	0.307		0.99	0.82	0.75	0.73	0.72
0.571	0.600		0.91	0.71	0.61	0.60	0.58
0.571	0.896		0.73	0.60	0.57	0.56	0.58

		w/D_C =	1.332	1.775	2.219	2.663
0.444	0.460		0.72	0.64	0.64	0.69
0.444	0.694		0.57	0.56	0.56	0.57
0.444	0.924		0.55	0.55	0.56	0.59

Table 20. $(C_D)_{CCORR}$ for Gauze Discs and Cylinders in Tandem.

7.1.14 Minimum Drag Coefficients of Gauze Discs and Cylinders in Tandem for Each D_1/D_C and ℓ/D_C (from Table 20)

D_1/D_C	0.845	0.845	0.845	0.667	0.667	0.667
ℓ/D_C	0.451	0.893	1.323	0.338	0.669	1.002
$(C_D)_{CMINCORR}$	0.81	0.73	0.71	0.80	0.66	0.64
D_1/D_C	0.571	0.571	0.571	0.444	0.444	0.444
ℓ/D_C	0.307	0.600	0.896	0.460	0.694	0.924
$(C_D)_{CMINCORR}$	0.72	0.58	0.56	0.64	0.56	0.55

Table 21. $(C_D)_{CMIN}$ for Gauze Discs and Cylinders in Tandem.

7.1.15 Least Drag Coefficients of Gauze Discs and Cylinders in Tandem for Each D_1/D_C (from Table 21)

D_1/D_C	0.845	0.667	0.571	0.444
$(C_D)_{CLEAST}$	0.71	0.64	0.56	0.55

Table 22. $(C_D)_{CLEAST}$ for Gauze Discs and Cylinders in Tandem.

7.1.16 Effect of Speed on Vibration of Unshielded Cylinders

D_1/D_C	ℓ/D_C	V_∞ m/s	$(Re)_{DC}$	Vibration
0.444	0.460	8.9	71400	Noticeable
0.444	0.460	12.4	97200	Little
0.444	0.460	14.91	118700	Less Disappearing Occasionally

Table 23. Effect of Speed on Vibration of Unshielded Cylinders.

7.1.17 Effect of Shielding and Gap Ratio on Cylinder Vibration

D_1/D_C	ℓ/D_C	w/D_C	V_∞ m/s	$(Re)_{DC}$	Vibration
0.571	0.307	0.571	11.6	66100	Noticeable
0.571	0.307	1.142	11.6	66900	Less
0.571	0.307	1.713	11.6	66500	Very Little

0.571	0.600	Unshielded	11.5	66700	Noticeable
0.571	0.600	0.571	11.5	66600	Much Less
0.571	0.600	1.142	11.5	66600	Very Little
0.571	0.600	2.855	11.7	67500	Some Vibration of Gauze Shield
0.444	0.460	Unshielded	8.9	71400	Noticeable
0.444	0.460	1.332	8.4	66400	Little
0.444	0.460	1.775	8.7	68400	Little or None
0.444	0.460	2.219	8.8	69000	Little
0.444	0.460	2.663	8.6	67600	Some Vibration of Gauze Shield

Table 24. Effect of Shielding and Gap Ratio on Cylinder Vibration at Approximately Constant $(Re)_{DC}$.

7.1.18 Mutual Interference Force Coefficient of Gauze and Solid Discs in Tandem

D_1/D_2	0.332	0.332	0.332	0.332	
g/D_2	1.00	1.50	1.99	2.50	
$(C_D)_I$	0.019	0.009	0.004	0.002	
D_1/D_2	0.555	0.555	0.555	0.555	0.555
g/D_2	0.99	1.25	1.49	2.01	2.50
$(C_D)_I$	0.053	0.035	0.023	0.015	0.009
D_1/D_2	1.17	1.17	1.17	1.17	1.17
g/D_2	0.80	1.00	1.50	2.00	2.50
$(C_D)_I$	0.189	0.135	0.088	0.061	0.034

Table 25. $(C_D)_I$ for Gauze and Solid Discs in Tandem.

7.1.19 Flow Line Diagrams

The flow line diagrams for gauze and solid discs in tandem for the following configurations are shown in Figures 9 to 13, respectively.

D_1/D_2	g/D_2	Figure Number
0.600	2.00	9
0.555	1.79	10
0.726	2.34	11
0.726	1.80	12
0.726	1.27	13

7.1.20 Turbulence in Way of Solid Disc for Near Optimum Gauze and Solid Discs in Tandem. $D_1/D_2 = 0.555$, $g/D_2 = 1.79$.

$\frac{\text{Radius}}{\text{Radius of Solid Disc}} = \frac{2r}{D_2}$	$(Re)_{D2}$	Distance aft of Solid Disc/D_2	Turbulence Volts RMS
1.11	121000	- 0.372	1.16
		- 0.132	2.08
		- 0.040	2.52
		0	2.63
		0.015	2.66
		0.025	2.69
		0.061	2.76
		0.092	2.76
		0.124	2.75
		0.165	2.73
		0.195	2.71
		0.237	2.70
		0.286	2.70
		0.337	2.69
		0.385	2.69
1.25	118000	0	1.90
		0.165	2.75
		0.247	2.78
		0.380	2.76
		0.462	2.76
		0.506	2.75
		0.589	2.74
		0.647	2.74
		0.765	2.73
		0.860	2.73
		0.963	2.74
1.39	122000	0	1.32
		0.139	1.92
		0.237	2.31
		0.298	2.46
		0.340	2.53
		0.430	2.65

		0.572	2.75
		0.656	2.75
		0.747	2.76
		0.856	2.75
1.46	117000	0	1.17
		0.154	1.59
		0.258	1.84
		0.305	1.90
		0.423	2.22
		0.477	2.42
		0.532	2.59
		0.599	2.67
		0.636	2.69
		0.750	2.72
		0.812	2.72
		0.857	2.71
		0.911	2.72
		1.019	2.70
		1.134	2.66
		1.238	2.62
		1.337	2.54
1.53	118000	0	1.08
		0.214	1.62
		0.331	1.96
		0.464	2.10
		0.586	2.23
		0.694	2.45
		0.844	2.61
		0.954	2.63
	121000	0.681	2.42
		0.786	2.56
		0.909	2.63
		1.008	2.65
		1.138	2.63
		1.321	2.52
1.67	121000	0	1.23

			0.386	1.53
			0.724	2.11
			0.784	2.20
			0.848	2.28
			0.914	2.33
			0.980	2.36
			1.086	2.35
			1.195	2.30
			1.346	2.22
	1.94	118000	0	1.06
			0.415	1.20
			0.727	1.32
			0.892	1.50
			1.104	1.63
			1.176	1.68
			1.233	1.65
			1.360	1.63
			1.430	1.61
			1.589	1.55

Table 26. Turbulence in Way of Near Optimum Configuration. D_1/D_2 = 0.555, g/D_2 = 1.79.

7.1.21 Flow Characteristics for Gauze and Solid Discs in Tandem. A_S and $(\Theta)_{D2}$.

D_1/D_2	g in	g/D_2	$A_S/(A)_{D2}$	$(\Theta)_{D2}^{\circ}$
0.332	6.46	1.07	2.22 ($2^{+}16$)	50.2
0.441	6.44	1.42	2.11	43.7
0.555	6.46	1.79	2.14	38.8
0.726	6.46	2.34	2.17	32.9
1.003	6.45	3.23	2.20	22.3
				+ repeat values given in brackets
0.555	10.06	2.79	2.20	
0.555	7.92	2.20	2.11	
0.555	5.04	1.40	2.16	38.8
0.555	2.71	0.75	2.40	40.2
0.555	0.90	0.25	2.81	50.3

0.332	10.83	1.80		39.5
0.441	8.16	1.80		35.0
0.726	4.96	1.80		32.3
1.003	3.59	1.80		29.3
0.726	3.50	1.27		23.5

Table 27. $A_S/(A)_{D2}$ and $(\Theta)_{D2}$ for Gauze and Solid Discs in Tandem.

7.1.22 Velocities in Wake of Gauze Disc

The velocities were measured across a diameter, port (P) and starboard (S), at centre line height.

		V_x/V_∞ at			
$\frac{2r}{D_1}$	$(x)_{D1}/D_1$	1.00	2.00	3.00	4.00
	$(Re)_{D1}$	66600	66700	66400	66900
1.625 P					1.000
1.5				0.995	0.995
1.4375			1.007	0.992	0.988
1.375		1.015	1.006	0.988	0.968
1.3125		1.012	0.998	0.964	0.935
1.25		1.014	0.965	0.913	0.879
1.1875		0.995	0.888	0.852	0.818
1.125		0.879	0.775	0.765	0.753
1.0625		0.727	0.688	0.685	0.699
1.000		0.641	0.611	0.619	0.635
0.9375		0.616	0.580	0.576	0.605
0.875		0.596	0.566	0.558	0.575
0.75		0.601	0.580	0.568	0.580
0.625		0.623	0.609	0.588	0.586
0.5		0.641	0.603	0.580	0.571
0.375		0.616	0.588	0.568	0.557
0.25		0.597	0.567	0.548	0.527
0.125 P		0.592	0.535	0.517	0.517
0		0.534	0.519	0.502	0.509
0.125 S		0.515	0.528	0.507	0.511
0.25		0.546	0.515	0.500	0.505
0.375		0.550	0.516	0.506	0.512
0.5		0.549	0.525	0.511	0.528
0.625		0.566	0.557	0.546	0.572

0.75	0.616	0.569	0.567	0.640
0.875	0.547	0.573	0.647	0.743
0.9375	0.543	0.642	0.703	0.809
1.000	0.637	0.732	0.783	0.856
1.0625	0.792	0.835	0.834	0.898
1.125	0.956	0.921	0.898	0.936
1.1875	1.011	0.977	0.955	0.968
1.25	1.019	1.004	0.987	0.990
1.3125	1.018	1.009	0.998	0.998
1.375	1.018	1.009	1.000	0.998
1.4375		1.009	0.998	0.999
1.5 S			0.996	0.999

Table 28. Velocities in Wake of Gauze Disc.

7.1.23 Velocities in Wake of Near Optimum Gauze and Solid Discs in Tandem. $D_1/D_2 = 0.555$, $g/D_2 = 1.79$.

The variation of velocity with radius was measured with and without the discs present, that is, with and without the configuration in the wind tunnel. The ratio of these two velocities expressed as a percentage of the same ratio at a radius of 4.00 in, where the ratio became substantially constant, is given below.

Velocity Ratio/Velocity Ratio at r = 4.0 in %

Distance downstream of solid disc/D_2		3.00	4.00
r	r/D_2		
0 in	0	63.6	80.3
0.5	0.139	62.8	79.5
1.0	0.278	66.6	80.4
1.5	0.417	73.4	83.0
2.0	0.555	81.7	86.3
2.5	0.695	90.3	91.6
3.0	0.833	95.9	96.2
3.5	0.972	98.7	99.1
4.0	1.111	100	100

Table 29. Velocities in Wake of Gauze and Solid Discs in Tandem. $D_1/D_2 = 0.555$, $g/D_2 = 1.79$.

7.1.24 Variation of Base Pressure Over Solid Disc for Near Optimum Gauze and Solid Discs in Tandem. $D_1/D_2 = 0.555$, $g/D_2 = 1.79$.

$2r/D_2$	$(C_p)_S$		
ϕ° =	0	180	270
0.2	0.365	0.362	0.362
0.4	0.365	0.362	0.362
0.6	0.365	0.362	0.365

Table 30. Variation of $(C_p)_S$ with r and ϕ for Gauze and Solid Discs in Tandem. $D_1/D_2 = 0.555$, $g/D_2 = 1.79$.

7.1.25 Variation of Face Pressure Over Solid Disc for Near Optimum Gauze and Solid Discs in Tandem. $D_1/D_2 = 0.555$, $g/D_2 = 1.79$.

$2r/D_2$	$(C_p)_F$		
ϕ° =	0	225	270
0.2	0.315	0.305	0.321
0.4	0.326	0.313	0.339
0.6	0.331	0.315	0.352

Table 31. Variation of $(C_p)_F$ with r and ϕ for Gauze and Solid Discs in Tandem. $D_1/D_2 = 0.555$, $g/D_2 = 1.79$.

7.1.26 Base Pressures for Gauze and Solid Discs in Tandem

D_1/D_2	g in	g/D_2	$(\overline{C_p})_S$
0.332	6.46	1.07	0.690
0.441	6.44	1.42	0.454
0.555	6.46	1.79	0.352 (0.363)
0.726	6.46	2.34	0.252
1.003	6.45	3.23	0.201
0.555	10.06	2.79	0.341
0.555	7.92	2.20	0.349
0.555	5.04	1.40	0.355
0.555	2.71	0.75	0.406
0.555	0.90	0.25	0.460

Table 32. $(\overline{C_p})_S$ for Gauze and Solid Discs in Tandem.

7.1.27 Variation of Face Pressure with Radius for Unshielded Solid Disc

D_2 in	$2r/D_2$	$(C_P)_{FALONE}$
3.601	0.084	0.810
	0.313	0.846
	0.500	0.931
	0.687	0.957
	0.916	0.661

Table 33. Variation of $(C_P)_{FALONE}$ with r for Unshielded Solid Disc.

7.1.28 Variation of Face Pressure with Radius for Gauze and Solid Discs in Tandem

D_1/D_2	g/D_2	$(C_P)_F$				
$2r/D_2$ =		0.084	0.313	0.500	0.687	0.916
0.555	1.777	0.313	0.327	0.341	0.345	0.303
	1.402	0.347	0.359	0.376	0.386	0.338
	0.753	0.462	0.478	0.492	0.500	0.409
	0.253	0.812	0.838	0.857	0.806	0.576

Table 34. Variation of $(C_P)_F$ with r for Gauze and Solid Discs in Tandem.

7.2 Calculated Results

7.2.1 Drag Coefficients of Gauze and Solid Discs in Tandem According to Simple Shielding Theory

α = 0.204

D_1/D_2	0	0.1	0.2	0.3	0.4	0.5	0.6	0.7	0.8	0.862
$(C_D)_{SS}$	1.14	1.137	1.126	1.109	1.085	1.053	1.015	0.970	0.918	0.883

D_1/D_2	0.9	1.0	1.1	1.17
$(C_D)_{SS}$	0.926	1.049	1.185	1.289

α = 0.1

D_1/D_2	0	0.1	0.2	0.3	0.4	0.5	0.6	0.7	0.8	0.9	0.943	1.0
$(C_D)_{SS}$	1.14	1.139	1.136	1.131	1.124	1.115	1.103	1.090	1.075	1.058	1.050	1.090

α = 0.2

D_1/D_2	0	0.1	0.2	0.3	0.4	0.5	0.6	0.7	0.8	0.866	0.9	1.0
$(C_D)_{SS}$	1.14	1.137	1.127	1.110	1.087	1.057	1.020	0.977	0.927	0.890	0.929	1.050

α = 0.3

D_1/D_2	0	0.1	0.2	0.3	0.4	0.5	0.6	0.7	0.756	0.8	0.9	1.0
$(C_D)_{SS}$	1.14	1.132	1.107	1.065	1.006	0.931	0.839	0.730	0.662	0.720	0.863	1.022

α = 0.4

D_1/D_2	0	0.1	0.2	0.3	0.4	0.5	0.577	0.6	0.7	0.8	0.9	1.0
$(C_D)_{SS}$	1.14	1.117	1.047	0.931	0.768	0.559	0.366	0.391	0.516	0.660	0.823	1.006

Table 35. Variation of $(C_D)_{SS}$ with D_1/D_2 and α.

7.2.2 Drag Coefficients of Gauze and Solid Discs in Tandem Using Idealised Speed Distribution in Wake of Gauze Disc

D_1/D_2	1.00	0.833	0.727
$(C_D)_{SS}$	1.02	0.93	0.96

Table 36. $(C_D)_{SS}$ Using Idealised Speed Distribution.

7.2.3 Effectiveness Parameter for Car Shields

Configuration	1	2	3	4	5	6	7	8
$\Delta \times 10^3$ m^2	0.55	0.56	0.35	0.59	0.29	0.36	0.94	0.46

Table 37. Δ for Car Shields.

7.2.4 Limiting Solidities (α) for Body Shields

$(C_D)_B$	0.1	0.2	0.3	0.4	0.5	0.6	0.7	0.8	0.9
α	0.474	0.444	0.412	0.375	0.333	0.286	0.231	0.167	0.091

Table 38. Limiting α for Body Shields.

7.2.5 Mutual Interference Force Coefficients of Gauze and Solid Discs in Tandem

D_1/D_2	0.332	0.332	0.332	0.332	0.332	0.332	
g/D_2	1.00	1.07	1.45	1.50	2.00	2.50	
$(C_D)_{ICALC}$	0.017(0.006)	0.016	0.009*	0.008	0.005	0.003(0.0004)	
D_1/D_2	0.441	0.441	0.555	0.555	0.555	0.555	
g/D_2	1.42	1.75	0.25	0.75	1.00	1.40	
$(C_D)_{ICALC}$	0.015	0.010*	0.186	0.070	0.046	0.025	
D_1/D_2	0.555	0.555	0.555	0.555	0.555	0.555	0.555
g/D_2	1.50	1.79	1.90	2.00	2.20	2.50	2.79
$(C_D)_{ICALC}$	0.022	0.015	0.014*	0.013	0.010	0.008	0.006

D_1/D_2	0.625	0.726	0.726	0.833	1.003	1.003	1.102
g/D_2	1.95	2.05	2.34	1.95	1.50	3.23	1.25
$(C_D)_{ICALC}$	0.017*	0.021*	0.016	0.029*	0.069*	0.014	0.113*
D_1/D_2	1.170	1.170	1.170	1.170	1.170		
g/D_2	0.80	1.00	1.50	2.00	2.50		
$(C_D)_{ICALC}$	0.241*	0.178(0.048)	0.092	0.054	0.034(0.0054)		

Note: Figures in brackets are corresponding results given by circular disc theory.

*At g/D_2 giving $(C_D)_{MIN}$.

Table 39. $(C_D)_{ICALC}$ for Gauze and Solid Discs in Tandem.

7.2.6 Theoretical Variation of Pressure with Radius Over a Circular Disc

$2r/D_2$	0	0.1	0.2	0.3	0.4	0.5	0.6	0.7	0.8	0.9	1.0
$(C_p)_{FALONECALC}$	1	0.996	0.983	0.960	0.923	0.865	0.772	0.611	0.286	- 0.728	- ∞

Table 40. Variation of $(C_p)_{FALONECALC}$ with r.

7.2.7 Gauze and Solid Discs in Tandem. Other Parameters.

Note for ease of comparison the values of $(\overline{C_p})_F$, $1 + \{(\overline{C_p})_F/(\overline{C_p})_S\}$ and $(C_D)_{D2}$ as measured are also given in the following table.

D_1/D_2	1.003	0.726	0.555		0.441	0.332	
g/D_2	3.23*	2.34*	1.79*	+	1.42*	1.07*	*g constant at 6.46 in
$(\overline{C_p})_{FCALC}$	0.280	0.330	0.316(0.303)		0.353	0.484	
$(\overline{C_p})_F$			0.325(0.324)				
V_{EFF}/V_∞	0.647	0.696	0.725(0.724)		0.788	0.873	
$(C_D)_{FBCALC}$	0.920	0.657	0.502(0.489)		0.464	0.540	+ repeat values given in brackets
$1+\{(\overline{C_p})_{FCALC}/(\overline{C_p})_S\}$	2.39	2.31	1.90 (1.83)		1.78	1.70	
$1+\{(\overline{C_p})_F/(\overline{C_p})_S\}$			1.92 (1.89)				
$(C_D)_{D2CALC}$	0.445	0.539	0.627		0.761	1.111	
$(C_D)_{D2}=(\overline{C_p})_F+(\overline{C_p})_S$			0.677(0.687)				

D_1/D_2	0.555	0.555	0.555	0.555	0.555	0.555
g/D_2	2.79	2.20	1.79*	1.40	0.75	0.25
$(\overline{C_p})_{FCALC}$	0.337	0.316	0.316(0.303)	0.346	0.489	0.792
$(\overline{C_p})_F$			0.325(0.324)	0.362	0.461	0.736

V_{EFF}/V_∞	0.731	0.724	0.725(0.724)	0.743	0.844	0.993
$(C_D)_{FBCALC}$	0.532	0.507	0.502(0.489)	0.522	0.629	0.807
$1+\{(\overline{C_P})_{FCALC}/(\overline{C_P})_S\}$	1.99	1.91	1.90 (1.83)	1.97	2.23	2.72
$1+\{(\overline{C_P})_F/(\overline{C_P})_S\}$			1.92 (1.89)	2.02	2.14	2.60
$(C_D)_{D2CALC}$	0.634	0.624	0.627	0.656	0.839	1.149
$(C_D)_{D2}=(\overline{C_P})_F+(\overline{C_P})_S$			0.677(0.687)	0.717	0.867	1.196

Table 41. Variation of $(\overline{C_P})_F$, $(\overline{C_P})_{FCALC}$, V_{EFF}/V_∞, $(C_D)_{FBCALC}$, $1 + \{(\overline{C_P})_{FCALC}/(\overline{C_P})_S\}$ and $(C_D)_{D2CALC}$ with D_1/D_2 and g/D_2.

7.2.8 Drag Coefficients of Solid Disc in Tandem with Gauze Disc According to Simple Shielding Theory

D_1/D_2	0.3	0.4	0.5	0.6	0.7	0.8	0.862	0.9	1.0	1.1	1.17
$(C_D)_{D2SS}$	1.059	0.991	0.903	0.798	0.672	0.530	0.434	0.442	0.468	0.512	0.641

Table 42. Variation of $(C_D)_{D2SS}$ with D_1/D_2.

7.2.9 Reduction in Drag Coefficient Due to Propeller Thrust for Windmill-Disc-Propeller Combination

Propeller Diameter	D_1	$1.5D_1$	$1.962D_1$
$\delta(C_D)$	0.0893	0.0991	0.1002

Table 43. Variation of $\delta(C_D)$ with Propeller Diameter.

8. DISCUSSION OF RESULTS

8.1 Gauze and Solid Discs in Tandem

8.1.1 Variation of C_D with g/D_2 and D_1/D_2

The experimental results given in Tables 9, 10 and 12 are plotted in Figures 26, 27, 28 and 29.

The reason for D_1/D_2 optimising, that is, giving $(C_D)_{LEAST}$, is readily discernible from a consideration of its effects as the ratio tends to its limits. With large D_1/D_2 substantial shielding of the solid disc by the gauze disc is achieved but the penalty is a high combination C_D because of the relatively large size and drag of the gauze disc. Conversely, with small D_1/D_2 the benefits of the gauze disc having a low drag are outweighed by the consequential lack of shielding of the solid disc. Thus a compromise is necessary in order to minimise the drag of the combination.

The anticipated effect of g/D_2 on C_D is clearly perceptible, for D_1/D_2 ratios less than unity, at very low gap ratios. With g/D_2 values close to zero there can be little flow through the gauze disc and its effect would amount to a slight virtual upstream movement of the solid disc. In other words, the gauze disc would not essentially alter the flow approaching the solid disc from that for the solid disc in isolation and the drag of the combination must tend to that of the solid disc alone, namely 1.14(6), except for a slight edge effect.

For D_1/D_2 ratios greater than unity the drag coefficient rises above 1.14 as g/D_2 tends to zero because of the annulus of gauze area surrounding the solid disc. There is experimental evidence for this in Figure 29 where $(C_D)_{MIN}$ for a D_1/D_2 ratio of 1.170 is well in excess of 1.14 at a value of 1.24.

Figure 30 shows that g/D_1 at $(C_D)_{MIN}$ is not independent of D_1/D_2 and gives no grounds for believing that it is necessary to allow the flow through the gauze disc to develop fully in order to minimise the drag of the combination. It is possible that entrainment prevents any such benefit from being obtained. Furthermore, measurements of the velocity distribution behind the gauze disc alone (see Sections 3.6.1, 4.9.1, Table 28 and Figure 20) showed that the flow is essentially fully developed as little as one diameter (D_1) behind the gauze disc, which gives added weight to the suggestion that development does not have a major

influence on the combination drag.

It seems pertinent to suggest that the upper limit of D_1/D_2 relevant to the research is that ratio at which complete shielding effectively takes place. This may be determined from the plot of $(C_D)_{MIN}$ against D_1/D_2 (Figure 31) using the knowledge that at higher ratios any increase in drag coefficient is simply due to the increased drag of the gauze. That is, at higher ratios

$$C_D = \text{constant} + \{1 - (\frac{D_{10}}{D_1})^2\} (C_D)_{D1ALONE}$$

and since

$$(C_D)_{D1ALONE} = 0.650 (D_1/D_2)^2$$

$$C_D = \text{constant} + (\frac{D_1^2 - D_{10}^2}{D_2^2}) 0.650$$

Assuming D_2 to be constant and D_1 to vary, then

$$\frac{d C_D}{d(D_1/D_2)} = 1.30 \frac{D_1}{D_2}$$

and Figure 31 suggests that $D_{10} \cong 1.20$ with a corresponding value of g/D_2 of approximately 0.7.

Equally it is very noticeable from Figure 31 that at D_1/D_2 ratios of unity and below all the benefit of lowering D_1/D_2 is not realised presumably due to the reduced shielding provided by the smaller gauze discs. At D_1/D_2 less than 0.6 this lack of shielding overcomes the drag reducing effects of smaller gauze discs and there is a rapid rise in the drag coefficient of the combination. Since the interference between discs is small for D_1/D_2 less than 0.6 (see Sections 3.4, 4.3.4, 5.7, Section 5 of Appendix 5 and Tables 25 and 39), it must be presumed that the beneficial effects of the tandem arrangement are associated with shielding.

The variation of g/D_2 with D_1/D_2 giving $(C_D)_{MIN}$ is shown in Figure 32. In the region of optimum gap the results indicate that gap has a relatively small effect on the combination drag so that the precise positioning of the discs is not vital to optimisation.

8.1.2 The Effects of the Variation in D_1/D_2 at Constant Gap (g = 6.46 in)

The gap (g) chosen was that of the approximately optimum configuration $D_1/D_2 = 0.555$, $g/D_2 = 1.79$. It has already been mentioned that precise positioning is not vital to optimisation and Figure 19 shows that there is a sizeable range of diameter ratios ($0.44 \leq D_1/D_2 \leq 0.57$) over which C_D is not significantly different from $(C_D)_{LEAST}$. The remarks contained in this section are considered to be relevant to those configurations which would normally be adopted with the objective of achieving drag reduction. The mutual interference between discs at these gaps is low.

Referring to the measured values of $A_S/(A)_{D2}$ in Figure 33, the results show that $A_S/(A)_{D2}$ minimises but there is no evidence, at low and high D_1/D_2, to indicate its upper values. However, it is reasonable to accept that as D_1/D_2 tends to zero, and thus D_1, $A_S/(A)_{D2}$ tends to the unshielded value for a solid disc of 2.72(15).

Figure 33 shows the variation of the measured values of $(\overline{C_p})_S$ with D_1/D_2 and demonstrates the considerable effect which the latter has on the former. It is noticeable that $(\overline{C_p})_S$ does not minimise at a value of 0.147, which is the value which should be achieved if D_1 is large enough to provide complete shielding. This is possibly due to entrainment by the surrounding near irrotational fast flow.

The value of D_1/D_2 at which $(\overline{C_p})_S$ minimises is approximately 1.2, which is in agreement with the conclusion drawn in Section 8.1.1 even though the corresponding g/D_2 is much larger.

The cause of $(\overline{C_p})_S$ increasing to beyond the value of 0.419 for a solid disc alone(15) at low D_1/D_2 values was not investigated, but the regular variation of $(\overline{C_p})_S$ does not suggest large experimental error (see also Section 8.1.4). $(\overline{C_p})_S$ in excess of 0.419 gives added weight to the conclusion that shielding must produce more than a simple reduction in the effective velocity approaching the solid disc.

A further controlling influence on $(\overline{C_p})_S$ appears to be the flow pattern produced by the shielding. The two configurations giving $(\overline{C_p})_S$ in excess of 0.419 had the highest values of $(\Theta)_{D2}$. If these large angles reflect a considerable narrowing of the flow lines in way of the solid disc, and consequently very high velocities since at low D_1/D_2 the shielding is small, then high values of $(\overline{C_p})_S$ must be expected.

Further confirmation of the narrowing of the flow lines in way of the solid disc with decreasing D_1/D_2 is provided by the flow visualisation experiments (Figures 10 and 11). A comparison shows that although $(\Theta)_{D2}$ increases with decreasing D_1/D_2 the slopes in the surrounding fluid decrease.

The difference between the measured and calculated values of $(\overline{C_p})_F$ are considered to be due to p_S not being uniform over the back of the solid disc (see Section 8.1.4).

Despite the error which the use of the constant coefficient k in $(\overline{C_p})_{FCALC}$ may impose, there is sufficient evidence in Figure 33 to suggest that the variation of $(\overline{C_p})_F$ is similar to that of $(\overline{C_p})_S$, that is, $(\overline{C_p})_F$ decreases with increasing D_1/D_2 and reaches a minimum at approximately $D_1/D_2 = 1.2$. The plotted $(\overline{C_p})_F$ are uncorrected for blockage, which apparently has a large effect (Section 8.1.5), so that at low D_1/D_2 where the blockage is high it may be anticipated that the corrected slope of the curve is lower than that drawn. In no case does $(\overline{C_p})_F$ exceed the value for an unshielded disc without blockage of 0.721(15) or fall below the fully shielded value of 0.257.

Guided by the graphs of $(\overline{C_p})_S$ and $(\overline{C_p})_F$ the conclusion must be drawn that it is the ability of the gauze disc to reduce the pressure coefficients on the solid disc which gives the combination its worthwhile low drag coefficients. It appears that both $(\overline{C_p})_S$ and $(\overline{C_p})_F$ rise continuously as D_1/D_2 is made smaller which explains why all the benefit of reducing the area of the gauze disc, and thus D_1/D_2, is not realised. Eventually the increasing slopes of the $(\overline{C_p})_S$ and $(\overline{C_p})_F$ curves are sufficient to cancel out completely the reduction in drag brought about by lowering D_1, at which point the $(C_D)_{LEAST}$ configuration is reached. The $(\overline{C_p})_S$ and $(\overline{C_p})_F$ graphs bear out that such slopes occur in the region of $D_1/D_2 = 0.5$.

It is the combined effects of the magnitudes and directions of the slow flow (from the gauze disc) and the near irrotational flow, around the solid disc, which determine the value of $A_S/(A)_{D2}$. Although there may have been considerable variation in individual effects, as indicated by $(\Theta)_{D2}$ for example, the combined effects produced little change in $A_S/(A)_{D2}$.

The experimental evidence, as D_1/D_2 falls below unity, confirms that

$A_S/(A)_{D2}$ decreases. But the decrease is small even though $(\overline{C_P})_S$ increases considerably. Consequently, $(\overline{C_P})_S$ does not have a large influence on $A_S/(A)_{D2}$ and the ability of the suction at the rear of the solid disc to pull the flow inwards appears to be slight. It may also be concluded from the small variation in $A_S/(A)_{D2}$, over a wide range of diameter ratios, that the size of the wake is essentially determined simply by the diameter of the solid disc (D_2). Nevertheless, as D_1/D_2 gets substantially smaller than unity, say below a value of 0.5, it must be anticipated that the streamlines in way of the solid disc of both the slow flow through the gauze disc and the fast flow around it adopt on average large slopes relative to the centre line which oppose the decrease in $A_S/(A)_{D2}$. The effect gets larger as D_1/D_2 decreases and leads to $A_S/(A)_{D2}$ minimising and then increasing to its unshielded value of 2.72.

V_{EFF}/V_∞ is also reduced by increasing D_1/D_2 up to a value of about 1.2 where D_1 is sufficiently large to provide complete shielding. The theoretical least value of 0.592 is not reached again probably because of entrainment.

It appears, by extrapolating the higher values of the effective velocity ratio, that ratios in excess of unity may be achieved at low diameter ratios. The mechanism of this interference which results in a higher solid disc drag than when alone is worthy of investigation but is not particularly relevant to the present work.

8.1.3 The Effects of the Variation of g/D_2 at Constant D_1/D_2 (0.555)

The diameter ratio (D_1/D_2) chosen was that of the approximately optimum configuration and again the remarks contained in this section are considered to be relevant to those configurations which would normally be adopted.

Figure 34 indicates that V_{EFF} decreases and becomes essentially uniform when g/D_2 is increased. It emphasises the need to choose a sufficiently high gap ratio to allow V_{EFF} and consequently the drag of the solid disc to level off. There appears to be no benefit in allowing the gap ratio to exceed the value at which V_{EFF} becomes essentially uniform. As with low diameter ratios, it seems that effective velocity ratios in excess of unity may be achieved with low gap ratios.

It is noticeable that $(C_D)_{FBCALC}$ increases considerably below gap ratios

of approximately 1.2 and if in accordance with mutual interference theory the increase in drag due to interference occurring on the solid disc is offset by the decrease in drag on the gauze disc, it follows that the pressure forces acting on the face of the solid disc are greater at low gap ratios for reasons other than higher interference. Besides the changes in flow pattern over the solid disc caused by the nearness of the gauze disc, the velocities of flow over the solid disc are higher because the gap is not large enough to allow the flow from the gauze disc to develop fully.

The further consequences of the above is that the improvement in drag coefficient of the combination with increasing g/D_2 rests more on the reduction in forebody drag coefficient than on $(\overline{C_p})_S$.

Some confirmation of the foregoing conclusions is given by the flow patterns of Figures 11, 12 and 13. Only relatively small changes in flow angles occurred over the range of gap ratios of the configurations for which the flow patterns were determined (g/D_2 = 2.34, 1.80 and 1.27 at D_1/D_2 = 0.726). This is particularly true of the slopes upstream of the solid disc and accounts for the small variation in $(C_D)_{FBCALC}$ at gap ratios in excess of 1.2. The occurrence of such small changes in slopes over a relatively large range of g/D_2 in way of the optimum gap ratio (2.05) is supported by the measured values of $A_S/(A)_{D2}$ and $(\overline{C_p})_S$ at D_1/D_2 = 0.555 which also show very little variation over corresponding gaps.

The slight rise in $(C_D)_{FBCALC}$ at high gap ratios above its minimum value is possibly due to entrainment between the flow through the gauze disc and the surrounding near irrotational fast flow. This is also the likely reason for a similar rise in $(\overline{C_p})_F$.

A noticeable feature of the variations plotted in Figure 34 is that $(\overline{C_p})_F$ drops away more rapidly than $(\overline{C_p})_S$ with increasing g/D_2 at low gap ratios. The effect of blockage on $(\overline{C_p})_F$ is also shown on the figure. The measured value of $(\overline{C_p})_F$ was 0.824 for an unshielded solid disc with b = 0.0325 which is considerably above the corresponding without blockage value of 0.721. Thus corrected for blockage none of the derived values of $(\overline{C_p})_F$ exceeded that for a solid disc alone. It is assumed that the minimum value of $(\overline{C_p})_F$ lies above that for a fully shielded disc (0.257) partly due to blockage and partly due to lack of shielding.

The pressure distributions across the face of a shielded solid disc at $D_1/D_2 = 0.555$ for four gap ratios $g/D_2 = 0.253$, 0.753, 1.402 and 1.777 of Figure 35 reflect the steep rise in $(\overline{C_p})_F$ with decreasing g/D_2. It appears from the distributions that for gap ratios in excess of about unity, the shielding produces a near uniform variation in pressure over 90% of the disc face. Presumably this result is caused by the slow flow in the wake of the gauze disc not only reducing the effective velocity but also deflecting outwards to larger radii the surrounding fast flow where its influence on the pressure is attenuated by the disc edge effect. At low gap ratios the curves suggest that the face pressures tend to their unshielded values and that probably due to interference, shielding has little influence on the inner radii pressures.

Returning to Figure 34, at the lowest gap ratio at which $(\overline{C_p})_S$ was measured ($g/D_2 = 0.25$) the aft face pressure coefficient is above that for an unshielded solid disc (0.419). It is likely that the effects which produced high $(\overline{C_p})_F$ at low gap ratios, namely changes in flow pattern caused by the nearness of the gauze disc and fast undeveloped flow, are also responsible for this value of $(\overline{C_p})_S$. The figure also shows that the variation in $(\overline{C_p})_S$ with g/D_2 is relatively small and much less than that for $(\overline{C_p})_F$. Consequently, at high gap ratios the measured values are well above $(\overline{C_p})_S$ for a fully shielded disc (0.147).

Further evidence of the change in flow pattern which results from closing the gap between the gauze and solid discs is provided by the curve of $A_S/(A)_{D2}$. There is an increasing rise in $A_S/(A)_{D2}$. A major effect of gap ratio is also shown by the figure, that of reducing the size of the separated region behind the solid disc (from 2.72 for an unshielded disc).

Although it may not be necessary to allow the flow through the gauze disc to develop fully in order to minimise the drag of the combination, the above discussion on the effects of small gap ratios on $(\overline{C_p})_F$ and $(\overline{C_p})_S$ suggests there is a limit to the lack of development which can be tolerated. The figures indicate that the development associated with a g/D_2 of about unity and above is adequate.

It appears that, at constant diameter ratio, gap ratio has a larger effect on $A_S/(A)_{D2}$ than $(\overline{C_p})_S$.

The plots of $(\overline{C_p})_S$ and $A_S/(A)_{D2}$ reveal that $A_S/(A)_{D2}$ rises with g/D_2 at

gap ratios greater than optimum whereas the slight falling off in $(\overline{C_p})_S$ is maintained. This is possibly brought about by entrainment at high gap ratios, leading to greater approach velocities, which was the same reason advanced earlier for the corresponding small increases in $(\overline{C_p})_F$ and $(C_D)_{FBCALC}$.

It is self evident from the results that the drag of the gauze disc benefits from large mutual interference effects at low gap ratios and provided that there is little mutual interference $(C_D)_{MIN}$ is obtained when $(C_D)_{D2}$ minimises.

8.1.4 Applicability of Roshko and Koenig Semi-Infinite Half Body Theory

The theory (see Section 2.3 and Appendix 1) could be of considerable importance to a semi-empirical solution. If the drag of the solid disc can be estimated in this manner then the prediction of the combination drag is simplified. Although the variation of the calculated area ratio, $1 + \{(\overline{C_p})_{FCALC}/(\overline{C_p})_S\}$ with the measured $A_S/(A)_{D2}$ shows good correlation at both constant D_1/D_2 and constant g, the variable nature of the correction required to give equality, shown by the broken line in Figure 36, casts doubt on the applicability of the theory to gauze and solid discs in tandem.

The slight scatter in the values of $1 + \{(\overline{C_p})_F / (\overline{C_p})_S\}$, found using the measured values of $(\overline{C_p})_F$ and $(\overline{C_p})_S$, may be partly attributed to a lack of precision in the measurement of A_S. As a consequence any remarks made in respect of $A_S/(A)_{D2}$ must be looked upon, to some extent, as qualitative.

The lack of certainty with regard to the measured values of $A_S/(A)_{D2}$ is due to the assumption that the centre of the band of smoke locates the shear layer and that the band has a width of 2 mm. As pointed out in Section 4.7, there are two shear layers involved, one from the gauze disc and one from the solid disc, which were not distinguishable at the position of measurement. With such complexity of flow, a simple assumption as the above is unlikely to be adequate.

Confirmation, or otherwise, of the applicability of the Roshko and Koenig theory was also dependent on the uncertainties in the determination of $(\overline{C_p})_F$ and $(\overline{C_p})_S$ and in this respect good repeatability was found for both $(\overline{C_p})_F$ and $(\overline{C_p})_S$ with the approximately optimum configuration, $D_1/D_2 = 0.555$, $g/D_2 = 1.79$, viz

$(\overline{C_p})_F$ 0.325 and 0.324 $(\overline{C_p})_S$ 0.352 and 0.363

Although the use of 15 pressure tappings (see Section 3.7) assured that the values of $(\overline{C_p})_F$ were realistic, $(\overline{C_p})_S$ on the other hand was found from a single centre line measurement on the assumption that the base pressure was uniform (an earlier check on the uniformity of the pressure over the back of the solid disc (Table 30) indicated that between $2r/D_2$ of 0.2 and 0.6 $(\overline{C_p})_S$ varied by only 0.003). An examination of the Roshko and Koenig theory (Appendix 1) suggests that its inapplicability is mainly due to the under-pressure not being sufficiently uniform over the back of the solid disc and at the boundary of the separated region(2). Confirmation that a single centre line base pressure measurement is insufficient to determine $(\overline{C_p})_S$ is provided by Figure 37 which shows the variation of both $(C_D)_{D2} = (\overline{C_p})_F + (\overline{C_p})_S$ and $(C_D)_{D2CALC}$ with g/D_2 at $D_1/D_2 = 0.555$ and indicates that $(\overline{C_p})_S$ given by a single centre line pressure measurement slightly over-estimates the base drag of the solid disc assuming that the difference between $(C_D)_{D2}$ and $(C_D)_{D2CALC}$ is due to $(\overline{C_p})_S$.

8.1.5 Effect of Blockage on $(\overline{C_p})_S$ and $(\overline{C_p})_F$

$(\overline{C_p})_{FALONE}$ was measured on a solid disc having a diameter ratio of 0.555 and was found to be 0.824. Without blockage $(\overline{C_p})_{FALONE} = 0.721$. Hence in Maskell's(13) approach to blockage correction:

$$\frac{1}{0.824} = \frac{1}{0.721} - \varepsilon.0.0325$$

giving blockage factor

$$\varepsilon = 5.33$$

This suggests that blockage had a much larger effect on $(\overline{C_p})_{FALONE}$ than on $(\overline{C_p})_{SALONE}$ and by inference on $(\overline{C_p})_F$ than on $(\overline{C_p})_S$.

If it is assumed that blockage has no effect on $(\overline{C_p})_{SALONE}$, then

$$(C_D)_{D2ALONE} \text{ with blockage} = (\overline{C_p})_{SALONE} \text{ without blockage} + (\overline{C_p})_{FALONE} \text{ with blockage}$$

$$= 0.419 + 0.824 = 1.243$$

and $(C_D)_{D2ALONE}$ with blockage using Maskell's approach and $\varepsilon = 2.75$ (see Section 4.3.1)

$$\frac{1}{(C_D)_{D2ALONE}} = \frac{1}{1.14} - 2.75 \times 0.0325$$

giving

$$(C_D)_{D2ALONE} \text{ with blockage} = 1.269$$

The former is only 2% less than the latter and confirms the suggestion that blockage has little effect on $(\overline{C_p})_{SALONE}$ and by inference on $(\overline{C_p})_S$.

8.1.6 Effects of Shielding. Comparison with Simple Shielding Theory.

Figure 19 gives the variation of $(C_D)_{MINCORR}$ and $(C_D)_{SS}$ with D_1/D_2. Comparison shows that the latter exceeds the former between diameter ratios of approximately 0.3 to 0.8 and in excess of about unity. The figure also indicates that $(C_D)_{LEASTCORR}$ is reached at $D_1/D_2 = 0.505$. Other features of the figure are that simple shielding theory does not predict well $(C_D)_{MINCORR}$ even at high diameter ratios i.e. between 0.8 and 1.2, and in particular the theory exaggerates the rate at which $(C_D)_{MINCORR}$ falls off with decreasing D_1/D_2 in this range. In addition the theory does not provide an accurate guide to $(C_D)_{LEASTCORR}$ or to the value of D_1/D_2 at which $(C_D)_{LEASTCORR}$ occurs; both are over-estimated. It is also apparent that the actual effective shielding of the solid disc by the gauze disc at moderate diameter ratios was considerably greater than that anticipated by theory and it is this beneficial difference which is central to the thesis.

Since complete effective shielding exists at the point where the drag of the solid disc levels off, the value of $(C_D)_{D2CORR}$ is also plotted. The figure suggests a diameter ratio of between 1.0 and 1.1, which is slightly lower than the 1.2 found in Sections 8.1.1 and 8.1.2.

With proper attention to gap ratio as well as diameter ratio, it is possible to achieve a maximum reduction in drag of

$$\frac{1.14 - 0.775}{1.14} \times 100\% = 32\%$$

In this respect it is noticeable from the results of the tests on the near optimum configuration ($D_1/D_2 = 0.555$, $g/D_2 = 1.79$) that whereas the shielding reduces $(\overline{C_p})_S$ from 0.419 (mean base pressure coefficient for an unshielded solid disc) to 0.352 (see Table 32), a reduction of 16%, the corresponding reduction in $(\overline{C_p})_F$ is from 0.721 (mean face pressure coefficient for an unshielded solid disc) to 0.325 (see Table 41),

a fall of 55% and in $(C_D)_{FBCALC}$ to 0.502 (see Table 41), a drop of 30%. Thus the forebody effect is about twice as powerful as the aft body effect in reducing drag by gauze shielding.

Despite the limitations of simple shielding theory stated above, the theory does account for the initial fall in the drag coefficient of the combination as the diameter ratio is reduced, below that at which complete shielding effectively takes place. It also gives a reasonable indication of the order of drag reduction which may be anticipated from shielding.

The considerable underestimation of drag by simple shielding theory over the range $0.3 \leqslant D_1/D_2 \leqslant 0.8$ clearly indicates that there is a further beneficial effect from the presence of the gauze disc which the theory does not take into account. The effect is very likely associated with the radial movement of the slow flow from the gauze disc which eases the fast encircling flow around the solid disc. Thus drag reduction is also obtained by deflecting the free stream velocity by means of a cushion of slow moving air.

The reason for the drag coefficient minimising, given in Section 8.1.1, readily discernible by considering the effect of simple shielding as the diameter ratio tends to its limits, is not radically altered by the existence of the above further drag reducing effect because it falls asymptotically to zero as D_1/D_2 tends to zero and to approximately 1.2 where complete shielding of the solid disc occurs.

It has already been seen that in the region of $(C_D)_{MIN}$, gap (g) has a relatively small effect on drag coefficient. Presumably as the gap is reduced below its optimum value the resulting increase in flow slopes raises the deflecting ability of the slow flow passing through the gauze disc and produces a larger $A_S/(A)_{D2}$ which is coupled with a higher $(\overline{C_P})_S$ through the narrowing of the streamlines in way of the separated region. The converse is true for gaps greater than optimum but it is likely that entrainment has an overriding effect on $A_S/(A)_{D2}$ and $(\overline{C_P})_S$. There is supporting evidence in Figure 34 and in Figures 11, 12 and 13.

8.1.7 Wake Characteristics

The velocities in the wake of the gauze disc alone taken from Table 28 are plotted in Figure 20 which shows that although the lowest velocities

were attained in the region of 3 to 4 diameters (D_1) downstream, even at one diameter downstream the wake was very well developed. At 1 and 2 diameters downstream speeds slightly in excess of the free stream ($\nmid$ 2%) were measured at radii greater than about 1.3 R(= $D_1/2$) associated with the flow around the edges of the disc. The plottings indicated some lack of symmetry but they are not too different from one dimensional theory. A simplified representation of the distribution is a frustrum of a cone with the slope of the side slightly increasing with distance downstream. Such a representation for $x/D_1 = 4$ is shown in Figure 21 which was used to calculate the results of Table 36 which gives $(C_D)_{SS}$ for three diameter ratios and confirm that differences between the actual and uniform (step) velocity distributions cannot account for the greater actual effective shielding.

The asymptotic mean velocity profile of turbulent wakes far downstream, deduced essentially by dimensional analysis and using Prandtl's dimensionless mixing length theory, is given by(2, p. 307):

$$u = \text{constant}\{1-(\frac{r}{R})^{1.5}\}^2$$

However, a preliminary examination of the measured velocity profile in the wake of the approximately optimum configuration of gauze and solid discs in tandem given in Table 29 suggested that it is necessary to take into account that the turbulence is not being generated by a concentrated source and that better agreement would be given by:

$$u/V_\infty = K \qquad \text{for } 0 \leqslant r/R \leqslant a$$

and

$$u/V_\infty = K\{1 - (\frac{r/R - a}{1 - a})^{1.5}\}^2 \qquad a \leqslant r/R \leqslant 1$$

This profile in which it is assumed that at

3 diameters (D_2) downstream of the solid disc K = 0.364, a = 0.15

and

4 diameters (D_2) downstream of the solid disc K = 0.197, a = 0.255

is shown in Figure 38 together with, for comparison purposes, the corresponding measured distributions for the approximately optimum configuration. Very good agreement occurs at 4 diameters downstream.

Although it was noted that the velocity distribution across the tunnel, without the discs present, was slightly non-uniform and that the static pressures recorded by the measuring rake varied with radius and were generally slightly lower than the static upstream pressure, they were not too different from "open" conditions to nullify completely any comparison made between the measured drags and calculated values based only on changes of momentum.

Accepting that the velocity distribution in the ultimate wake is given by the last equation and that the values of 'K' and 'a' are such that the momentum drag is equal to the drag of the optimum configuration then

$$0.775 \times 0.5\rho(A)_{D2} V_\infty^2 = \int_0^R \rho(V_\infty - u)u \, 2\pi r \, dr$$

in which $R = 2D_1 = 1.03D_2$.

As Figure 38 demonstrates, K = 0.364 and a = 0.15 gives reasonably good agreement with the measured velocity profile 3 diameters (D_2) downstream of the solid disc. For these values of 'K' and 'a' it can be shown that (see Appendix 6, Propeller Approach Velocities)

$$\int_0^R \rho(V_\infty - u)u \, 2\pi r \, dr = 0.773 \times 0.5\rho(A)_{D2} V_\infty^2$$

The closeness of this drag coefficient (0.773) to that experimentally derived (0.775) gave added confidence to the use of the wake profile velocity equation in the calculations on the windmill-disc-propeller combination of Appendix 6.

The above agreement also supports the correctness of the measured velocity distributions and gives weight to the argument that they may be used to give an approximate indication of the volumetric flow rate affected by the drag of the approximately optimum gauze and solid disc configuration.

Figure 39 shows the variation of the volumetric flow rates with radius derived from Table 29 expressed as ratios of the flow rate passing through the gauze disc as given by $(A)_{D1} \times V_\infty(1 - \alpha)$ where $\alpha = 0.204$ (see Section 1 of Appendix 5).

Regardless of the inaccuracies caused by the above assumptions, Figure 39 indicates that little of the total volumetric flow rate passed

through the gauze disc (5-6% in figure) which is remarkable in view of the considerable reduction in drag which it produced.

It follows that the cross-sectional area of the flow approaching the approximately optimum configuration, and affected by it, is essentially independent of the size of the gauze disc and this would be true for all configurations except those with relatively large gauze disc diameters.

Support that all of the flow affected does not pass through the gauze disc is readily provided by considerations of momentum and continuity using equations similar to those found in Section 2.1 (Simple Shielding Theory). For the optimum configuration,

$$(C_D)_{LEAST} \times 0.5\rho(A)_{D2} V_\infty^2 = 0.775\ 0.5\rho(A)_{D2} V_\infty^2 = \rho A_W V_\infty^2 \beta(1-\beta)$$

assuming a uniform distribution of velocity across A_W of $V_\infty(1-\beta)$. If all of the flow in the wake passes through the gauze disc then by continuity

$$\rho A_W V_\infty(1-\beta) = \rho(A)_{D1} V_\infty(1-\alpha)$$

Substituting

$$0.775\ 0.5\rho(A)_{D2} V_\infty^2 = \rho(A)_{D1} V_\infty^2 \beta(1-\alpha)$$

$$\therefore \quad \beta = \frac{0.775 \times 0.5}{(1-\alpha) \times (A)_{D1}/(A)_{D2}}$$

But $\alpha = 0.204$ and for $(C_D)_{LEAST}$, $(A)_{D1}/(A)_{D2} = 0.505$. Hence,

$$\beta = \frac{0.775 \times 0.5}{0.796 \times 0.505} = 0.964$$

and wake velocity $V_\infty(1-\alpha) = 0.036\ V_\infty$.

This very low value of wake velocity is inconsistent with the measured value (see Table 29) and leads to the conclusion that the cross-sectional area of the wake is very much larger than that assumed and, consequently, that flow other than that passing through the gauze disc is affected.

8.1.8 Mutual Interference Force Coefficient

The experimental results for diameter ratios D_1/D_2 = 0.332, 0.555 and 1.17 are plotted in Figure 40, together with the calculated values (see Section 5 of Appendix 5) at these diameter ratios taken from Table 39. Figure 40 demonstrates that except for the largest diameter ratio at gap ratios lower than about unity very good agreement between measurement and theory was obtained. It was because of this agreement that the mutual interference force coefficients were determined theoretically rather than experimentally when required in subsequent calculations (see Table 39).

Table 39 also shows the corresponding results for selected configurations of $(C_D)_{ICALC}$ found using axial components of velocity as given by hydrodynamic theory for a circular disc instead of those generated by a Rankine ovoid (see Section 5 of Appendix 5). It is clear that the circular disc theoretical velocities are too high to give agreement with the measured results and even if q_x were doubled the velocities would still be too large. It follows that any prediction based on the total theoretical velocity q would also make the agreement worse.

The significant feature of the mutual interference force coefficient is its relative smallness for the optimum configuration which indicates that the mechanism of drag reduction is not significantly dependent on mutual interference.

8.2 Gauze Discs and Solid Cylinders in Tandem

The variations of minimum drag coefficient with ℓ/D_C for each D_1/D_C on which the experiments were conducted are shown in Figure 41. Although the curves exhibit the characteristic fall-off in drag with increase in cylinder length of unshielded cylinders (Table 18) it should be noted that the curves do not relate to fixed configurations because the gap ratio at which minimum drag coefficient occurred was not constant. Figure 41 indicates that excessive lengths of cylinder are not required in order to minimise drags; length diameter ratios of about unity appear to be adequate for a wide range of diameter ratios. The values of the corresponding gap ratios (w/D_C) near to $(C_D)_{CLEAST}$, from Table 20, are only slightly greater and suggest that these optima may be obtained with practical configurations.

The lowest value of $(C_D)_{CMINCORR}$ for each D_1/D_C, which Figure 41 shows

approximate closely to the drag coefficient of the optima $(C_D)_{CLEAST}$, are plotted in Figure 42 against D_1/D_C. There is evidence to suggest that the smallest diameter ratio (0.444) is near the best for drag.

Assuming that $(C_D)_{CCORR} = 0.55$ cannot be bettered, then this represents from Table 18 a maximum reduction in drag of

$$\frac{1.09 - 0.55}{1.09} \times 100\% = 49.5\%$$

which is very much better than that for gauze and solid discs in tandem (32%) and was achieved with a smaller gauze disc ($D_1/D_C = 0.444$ instead of $D_1/D_2 = 0.505$). It indicates that the technique of using shields with solidities less than unity to reduce drag can be applied to three-dimensional as well as two-dimensional bodies with good effect.

Another interesting feature of the results is the effect of the gauze shield on the vibration of the cylinders. Although, as indicated by Section 3.3.2 and Table 24, a reduction in Reynolds number of approximately one third was able to prevent excessive transverse vibration occurring on the gauze disc and solid cylinders in tandem for $D_C \geq 3.000$ in, Table 23 shows that for an unshielded cylinder, $D_1/D_C = 0.444$ $\ell/D_C = 0.460$, an increase in Reynolds number and thus speed by about 40% was equally effective in reducing vibration. More importantly, Table 24 indicates that at constant Reynolds number the addition of the gauze disc in tandem with the cylinders not only considerably reduced drag but also noticeably reduced vibration. It appears that, generally, increasing gap ratio (w/D_C) also reduced vibration but excessive gaps led to some vibration of the gauze disc depending on the support provided.

8.3 Windmill-Disc-Propeller Combination. Reduction in Drag Coefficient Due to Propeller Thrust.

It is again emphasised that the reduction in drag coefficient was determined purely by calculation as described in Appendix 6.

As Table 43 shows there was little gain in $\delta(C_D)$ above a propeller diameter one and a half times larger than that of the windmill. It must be concluded from the results that the original concept of drag reduction by energy transfer, approximately 0.1 on drag coefficient in this case, is far less effective than shielding. Nevertheless the propulsive force provided a further

$$\frac{0.100}{0.775} \times 100\% = 12.9\%$$

reduction in drag of the windmill and disc, or a further

$$\frac{0.100}{1.14} \times 100\% = 8.8\%$$

reduction in the drag of the disc by itself.

With a propeller having $R = 0.75\ D_1$, working in the free stream (V_∞) and not in the wake, and supplied with the same power at the same rate of revolutions, the corresponding $\delta(C_D)$ was found to be 0.0721. This confirms the increase in $\delta(C_D)$ which can be obtained by siting the propeller in the lower velocities of the wake. Because the difference in $\delta(C_D)$ is relatively small compared with the drag of the combination, it is concluded that the positioning of the propeller is not important.

There is doubt as to the applicability of the concept of a drag reducing propeller driving a windmill and body in tandem when the body has a streamline shape, as distinct from a bluff shape like a disc, and therefore a low drag coefficient of less than say 0.1.

Assuming that a windmill may be simulated by a gauze disc, Table 38 indicates that a windmill with a high drag coefficient would be required in a windmill and streamline body tandem combination in order to give a combination drag lower than that of the streamline body by itself.

It is highly unlikely that such high shielding could be produced by a single windmill without it becoming unstable. Even if, as suggested in the Introduction, this problem could be overcome by having more than one windmill in tandem and a suitable multi-windmill arrangement could be found to drive a propeller, such a requirement would, of course, greatly increase the difficulties and cost of manufacture.

Since no investigations were carried out on shields with high solidity, it must remain pure conjecture that a drag reducing flow mechanism similar to that described in this dissertation would result. For the moment it would appear prudent to consider that the drag reducing benefits described are limited to bluff bodies only.

9. CONCLUSIONS

9.1 Gauze and Solid Discs in Tandem

A study has been made of the possible reduction in drag of a bluff body by the use of shielding devices. In the majority of cases the bluff body is a solid disc and the shielding device an upstream gauze disc of appropriate dimensions.

9.1.1 Mechanism of Drag Reduction

The major conclusion drawn which is central to the thesis is that gauze shielding produces more than a simple reduction in the effective velocity approaching the solid disc. A further benefit is obtainable through the radial movement of the slow flow from the gauze disc which cushions and deflects the encircling faster free stream flow. By a suitable choice of diameter (D_1/D_2) and gap (g/D_2) ratios the resulting reduction in drag of the solid disc more than offsets the increase in drag due to the gauze disc and with a gauze shield of 40% solidity a maximum net reduction in drag of 32% is achievable. There is considerable analytical support that this large benefit is provided by a remarkably small percentage (5 to 6%) of the total volumetric flow rate affected by the configuration and that the area of the gauze disc required is only 18% of that necessary for complete shielding of the solid disc.

It is the ability of the gauze disc to reduce the pressure coefficients on the solid disc which gives the combination its worthwhile low drag coefficient and this may be achieved with a sizeable range of diameter and gap ratios, that is, large drag reductions of the order of 30% are not critically dependent on the precise size and positioning of the gauze shield relative to the solid disc. The forebody effect produced by the gauze shielding is about twice as powerful as the aft body effect in reducing drag.

The mechanism of drag reduction is not dependent on mutual interference between the gauze and solid discs.

There is doubt as to whether the mechanism could be utilised to reduce the drag of streamline bodies.

9.1.2 Variation of D_1/D_2 at Constant Gap

The ability of the suction on the rear of the solid disc to pull the

flow inwards and reduce $A_S/(A)_{D2}$ is slight and is offset, as D_1/D_2 decreases, by larger disc edge flow slopes $(\Theta)_{D2}$ which accompany the higher $(\overline{C_p})_S$ and produce the associated narrowing of the streamlines. There is little change in $A_S/(A)_{D2}$ and essentially A_S is determined by $(A)_{D2}$. The variation of $(\overline{C_p})_F$ is similar to $(\overline{C_p})_S$.

9.1.3 Variation of g/D_2 at Constant D_1/D_2

There is no benefit in allowing the gap ratio to exceed the value at which V_{EFF} becomes essentially uniform. Mutual interference is not the cause of high face pressures on the solid disc at low gap ratios.

The major effect of gap ratio is to reduce the size of the separated region.

9.1.4 Inapplicability of Roshko and Koenig Semi-Infinite Half Body Theory

The Roshko and Koenig theory partly rests on the assumption of uniformity of pressure over the aft face of the solid disc and over the boundary surface of the separated region behind the solid disc. Even taking into account the uncertainties of measurement, there is experimental evidence to suggest that with an actual solid disc in tandem with and shielded by a gauze disc, the pressure over the aft face of the former is not uniform. It is reasonable to assume that the pressure over the surface of the actual separated region behind the solid disc is also not uniform.

Thus the conclusion is drawn that at least one factor in the theory which makes it inapplicable and prevents it from providing reasonable answers for the component of drag due to the solid disc is the lack of pressure uniformity.

9.1.5 Blockage

Tunnel blockage had a much larger effect on $(\overline{C_p})_F$ than $(\overline{C_p})_S$.

9.1.6 Simple Shielding Theory

It is clear that although simple shielding theory is not an accurate predictor of the least drag, it does give a reasonable indication of the order of greatest drag reduction which may be anticipated from shielding, which is all that might be expected of a simple mathematical model. In the other important aspect of the variation of drag with diameter ratio, simple shielding theory is less accurate. Nevertheless, the lack

of agreement highlights the central tenet of the thesis that there is a further beneficial effect from the gauze shield, associated with the deflecting cushion of slow moving air which the shield produces. The simple theory may be used to account for the minimisation of drag and for its initial reduction as the diameter ratio falls to below that effectively giving complete shielding.

9.1.7 Wake Characteristics

Even at one diameter (D_1) downstream of the gauze disc by itself the wake is very well developed and not too different from one-dimensional theory. Thus drag minimisation is not dependent on the full development of the flow from the solid disc.

At 3 and 4 diameters (D_2) downstream of the solid disc in the approximately optimum tandem configuration the measured wake velocities fit well with the deduced asymptotic mean velocity profiles for turbulent wakes when they are modified to take into account that the turbulence is not generated by a concentrated source.

The momentum drag as given by the velocity profile at 3 diameters (D_2) downstream agrees closely with the measured drag of the tandem configuration.

9.1.8 Mutual Interference

Good agreement was obtained between experimentally derived and calculated mutual interference force coefficients when the latter was based on an extension of an assertion by Glauert(7, pp. 273-286) that the interactive force on the gauze disc may be represented by a decrease in effective velocity of advance.

The agreement was obtained over a range of diameter and gap ratios when the effective velocity of advance was taken to be that produced by a Rankine ovoid source-sink system enclosing the solid disc as determined by an examination of reference 15. In contrast, the use of effective velocities of advance using hydrodynamic theory for a circular disc gave poor agreement.

9.2 Gauze Discs and Solid Cylinders in Tandem

The technique of drag reduction by tandem gauze shielding may be applied to circular cylinders, held with their centre lines parallel to the flow, with even greater effect than that obtained with circular solid discs.

A nearly 50% reduction in drag is achievable with the best configuration tested which has practical length-diameter and gap ratios only slightly greater than unity. The diameter ratio required is less than that necessary to minimise the drag of a shielded solid disc.

An equally important effect is the reduction in cylinder transverse vibration which may be achieved with the shield. Changes in speed and increases in gap ratio also reduce vibration but excessive gaps lead to vibration occurring on the gauze disc depending on the support provided.

9.3 Windmill-Disc-Propeller Combination

The original concept of drag reduction by energy transfer is far less effective than gauze shielding, only a further 8.8% reduction in drag, at the most, being possible.

A propeller diameter about one and a half times that of the windmill is required. The further reduction does not depend on the precise positioning of the propeller.

The applicability of the concept to a combination where the disc is replaced by a streamline body appears to rest on whether a suitable windmill arrangement providing very much greater shielding can be found.

10. RECOMMENDATIONS

This work and other work referenced are particular cases of the general problem of reducing the drag of bodies by shields with varying porosities. They represent the initiation of a new branch of investigations which require to be carried out on the reduction in drag which may be achieved with various body shapes when placed at different positions in relation to arrays of shields of varying porosity, shapes and sizes and subjected to winds of different strengths, directions, turbulence levels and scales. A tremendous task.

An understanding of the mechanism of drag reduction and the flow regimes are equally as important as the experimental determination of the drag reduction. Major dynamic effects such as vibration may be uncovered by the work and the benefits of constructing a suitable predictive theory should also not be overlooked.

As a first step there appears a need to demonstrate the applicability of the research and in this respect a continuation of the work described in Sections 3.2 and Section 3 of Appendix 5 on a motor car might be a suitable choice.

Because of the complexities and thus cost of manufacturing and fitting windmill driven propeller propulsion systems the relatively small reduction in drag obtained does not appear to be economically worthwhile and further research is not advocated unless a case can be established which demands the ultimate in least resistance.

Simple mathematical models are very helpful to engineers for providing first estimates of performance and for this reason it would be interesting to see how close simple shielding theory comes to predicting $(C_D)_{LEASTCORR}$ over the complete range of solidities (0 to 1.0).

Although it is not considered that any experimental errors affected the conclusions drawn it might be prudent in the event of further work being carried out for it to be conducted in a larger wind tunnel to reduce the blockage and to increase the order of size of the forces being measured. The author would like to see checks made on the present experimental results in a larger facility. A flow visualisation requirement suggests a closed tunnel with smoke generating and associated photographic facilities.

11. REFERENCES

1. BEARMAN, P.W. Bluff body flows applicable to vehicle aerodynamics. Journal of Fluids Eng. Trans. A.S.M.E. Vol. 102, No. 3, Sep. 1980. pp. 265-274.

2. BIRKHOFF, G. and ZARANTONELLO, E.H. Jets, Wakes and Cavities. Academic Press, New York, 1957. pp 305-307.

3. BRAMELL, A.R.S. Helicopter Dynamics. E. Arnold, 1976. pp 76-123.

4. BROMFIELD, N. Reduction of drag by power transmission. Confidential note to G.M. Lilley, Professor of Aeronautics and Astronautics, University of Southampton, on proposed thesis.

5. EIFFEL, G. The Resistance of the Air and Aviation. Constable and Company, London. 1913.

6. Fluid Forces and Moments on Flat Plates. Engineering Sciences Data Item No. 70015, Oct. 1972.

7. GLAUERT, H. Airplane propellers. In: Durand, W.F. (ed.) Aerodynamic Theory. Vol. 4, Div. L. Springer, Berlin, 1935. pp 269-293.

8. IWASAKI, M. The experimental and theoretical investigations of windmills. Reports of Research Institute for Applied Mechanics (Japan), Vol. 11, No. 8, Dec. 1953. pp 181-229.

9. KLINE, S.J. and McCLINTOCK, F.A. Describing uncertainties in single-sample experiments. Mech. Eng., Vol. 75, No. 1, Jan. 1953. p 38.

10. LILLEY, G.M. A note on the aerodynamics of motor vehicle slipstreaming. Draft paper 1961. Private communication 1982.

11. LILLEY, G.M. The aerodynamic efficiency of windmills. Aeronautical Quarterly. Feb. 1978. pp 1-17.

12. LILLEY, G.M. and RAINBIRD, W.J. A preliminary report on the design and performance of ducted windmills. College of Aeronautics, Cranfield, Rep. No. 102, Apr. 1956.

13. MASKELL, E.C. A theory of blockage effects on bluff bodies and stalled wings in a closed wind tunnel. A.R.C. R & M 3400, Nov. 1963.

14. MILNE-THOMSON, L.M. Theoretical Hydrodynamics. Macmillan, 1968.

15. MOREL, T. and BOHN, M. Flow over two circular discs in tandem. Journal of Fluids Eng. Trans. A.S.M.E. Vol. 102, No. 1, Mar. 1980. pp 104-111.

16. ROSHKO, A. and KOENIG, K. Interaction effects on the drag of bluff bodies in tandem. In: Proceedings of the symposium on Aerodynamic Drag Mechanisms of Bluff Bodies and Road Vehicles. General Motors Research Laboratories, Sept. 1976. Edited by Sovran, G., Morel, T. and Mason. Jr., W.T. Plenum Press, New York, 1978. pp 253-286.

17. SAUNDERS, W.S. Apparatus for reducing linear and lateral wind resistance in a tractor-trailer combination vehicle. U.S. Patent Office 3, 241, 876. 1966.

APPENDIX 1 - ROSHKO AND KOENIG SEMI-INFINITE HALF BODY THEORY

Consider the semi-infinite half body in Figure 2 which has zero drag in potential flow. The half body consists of the leading face of a solid disc and a constant pressure boundary separating the surrounding potential flow from the separated region behind the solid disc. The boundary becomes parallel to the free stream where the maximum cross-sectional area of the separated region (A_S) is reached.

It is assumed that the separated region is one of uniform constant pressure so that p_S acts over the aft face of the disc and on the boundary surface of the separated region. If zero drag, that is from simple shielding theory

$$0 = \int_w \rho_\infty u(V_\infty - u)dw$$

then,

$$0 = \text{force on front face of solid disc + force contributed by constant pressure surface}$$

$$0 = F_D + F_S$$

or,

$$F_D = - F_S$$

Hence, drag of disc

$$= F_D - \{(A)_{D2} \times \bar{p}_S\} \text{ since } \bar{p}_S \text{ is negative}$$

$$= - F_S - \{(A)_{D2} \times \bar{p}_S\}$$

$$= - \{A_S - (A)_{D2}\} \bar{p}_S - \{(A)_{D2} \times \bar{p}_S\}$$

$$= - A_S \bar{p}_S$$

$$= A_S (\overline{C_P})_{SALONE} \tfrac{1}{2}\rho V_\infty^2$$

but,

$$(C_D)_{D2ALONE} = (\overline{C_P})_{SALONE} + (\overline{C_P})_{FALONE}$$

$$= \frac{\text{drag of disc}}{\tfrac{1}{2}\rho (A)_{D2} V_\infty^2}$$

$$= \frac{A_S}{(A)_{D2}} \times (\overline{C_P})_{SALONE}$$

$$\therefore \quad \frac{A_S}{(A)_{D2}} = 1 + \{(\overline{C_P})_{FALONE}/(\overline{C_P})_{SALONE}\}$$

It is further assumed, for the purpose of the present work, that the theory is also applicable to a solid disc in tandem and shielded by a gauze disc then,

$$A_S/(A)_{D2} = 1 + \{(\overline{C_P})_F/(\overline{C_P})_S\}$$

APPENDIX 2 - VELOCITY AND PRESSURE DISTRIBUTIONS OVER A CIRCULAR DISC IN IRROTATIONAL FLOW

Employing cylindrical co-ordinates x, $\bar{\omega}$, where

$$x = c \sinh\varepsilon \cos\eta$$

and

$$\bar{\omega} = c \cosh\varepsilon \sin\eta$$

Let,

$$z_1 = x + i\bar{\omega} = c \sinh\zeta$$

and

$$\overline{z_1} = x - i\bar{\omega} = c \sinh\bar{\zeta}$$

where,

$$\zeta = \varepsilon + i\eta$$

and

$$\bar{\zeta} = \varepsilon - i\eta$$

Hence,

$$f'(\zeta) = \frac{\partial z_1}{\partial \zeta} = \frac{\partial}{\partial \zeta}(c \sinh\zeta) = c \cosh\zeta = c \cosh(\varepsilon+i\eta)$$

$$\overline{f'(\zeta)} = \frac{\partial \overline{z_1}}{\partial \zeta} = \frac{\partial}{\partial \zeta}(c \sinh\bar{\zeta}) = c \cosh\bar{\zeta} = c \cosh(\varepsilon-i\eta)$$

$$\frac{\partial \psi}{\partial \varepsilon} = \frac{\partial}{\partial \varepsilon}\{- k \sin^2\eta(\sinh\varepsilon - \cosh^2\varepsilon \text{ arc cot } \sinh\varepsilon)\}$$

where,

$$k = \tfrac{1}{2}Uc^2/(e\sqrt{1-e} - \text{arc sine}) = -\frac{Uc^2}{\pi}$$

since for a disc,

$$e = 1$$

$$c = \text{radius of disc}$$

$$\therefore \frac{\partial \psi}{\partial \varepsilon} = -k \sin^2\eta\{\cosh\varepsilon - \cosh^2\varepsilon \left(\frac{-1}{1 + \sinh^2\varepsilon}\right)\cosh\varepsilon$$

$$- \text{arc cot } \sinh\varepsilon \; 2 \cosh\varepsilon \sinh\varepsilon\}$$

$$= -k\sin^2\eta \; (\cosh\varepsilon + \cosh\varepsilon - 2 \cosh\varepsilon \sinh\varepsilon \text{ arc cot } \sinh\varepsilon)$$

$$= -k \sin^2\eta \; (2 \cosh\varepsilon - 2 \cosh\varepsilon \sinh\varepsilon \text{ arc cot } \sinh\varepsilon)$$

and,

$$\frac{\partial \psi}{\partial \eta} = -k \; 2 \sin\eta \cos\eta \; (\sinh\varepsilon - \cosh^2\varepsilon \text{ arc cot } \sinh\varepsilon)$$

$$J^2 = f'(\zeta).\overline{f'}(\bar{\zeta}) = c^2 \cosh(\varepsilon+i\eta) \cosh(\varepsilon-i\eta)$$

$$= c^2(\cosh\varepsilon \cosh i\eta + \sinh\varepsilon \sinh i\eta)(\cosh\varepsilon \cosh i\eta - \sinh\varepsilon \sinh i\eta)$$

$$= c^2(\cosh^2\varepsilon \cosh^2 i\eta - \sinh^2\varepsilon \sinh^2 i\eta)$$

$$= c^2(\cosh^2\varepsilon \cos^2\eta + \sinh^2\varepsilon \sin^2\eta)$$

$$q^2 = \frac{1}{\bar{\omega}^2 J^2}\{\left(\frac{\partial \psi}{\partial \varepsilon}\right)^2 + \left(\frac{\partial \psi}{\partial \eta}\right)^2\}$$

$$= \{\;\}/c^2 \cosh^2\varepsilon \sin^2\eta \; c^2(\cosh^2\varepsilon \cos^2\eta + \sinh^2\varepsilon \sin^2\eta)$$

where,

$$\{\;\} = \{k^2 \sin^4\eta \; (2 \cosh\varepsilon - 2 \cosh\varepsilon \sinh\varepsilon \text{ arc cot } \sinh\varepsilon)^2$$

$$+ 4 k^2 \sin^2\eta \cos^2\eta \; (\sinh\varepsilon - \cosh^2\varepsilon \text{ arc cot } \sinh\varepsilon)^2\}$$

$$\therefore q^2 = \frac{1}{c^2 \cosh^2\varepsilon \sin^2\eta} \cdot \frac{1}{c^2(\cosh^2\varepsilon \cos^2\eta + \sinh^2\varepsilon \sin^2\eta)}$$

$$\cdot \frac{4U^2c^4}{\pi^2} \cdot$$

$$\{\sin^4\eta(\cosh\varepsilon - \cosh\varepsilon \sinh\varepsilon \text{ arc cot } \sinh\varepsilon)^2$$

$$+ \sin^2\eta \cos^2\eta(\sinh\varepsilon - \cosh^2\varepsilon \text{ arc cot } \sinh\varepsilon)^2\}$$

$$= \frac{4U^2/\pi^2}{(\cosh^2\varepsilon \cos^2\eta + \sinh^2\varepsilon \sin^2\eta)} \cdot$$

$$\{\sin^2\eta \,(1 - \sinh\varepsilon \operatorname{arc\,cot} \sinh\varepsilon)^2$$

$$+ \cos^2\eta(\tanh\varepsilon - \cosh\varepsilon \operatorname{arc\,cot} \sinh\varepsilon)^2\}$$

when, $\eta = 0$, i.e. on $\not{\mathbb{C}}$

$$q = \frac{2U/\pi}{\cosh\varepsilon} (\tanh\varepsilon - \cosh\varepsilon \operatorname{arc\,cot} \sinh\varepsilon)$$

$$= \frac{2U}{\pi} \left(\frac{\sinh\varepsilon}{\cosh^2\varepsilon} - \operatorname{arc\,cot} \sinh\varepsilon\right)$$

$$= \frac{2U}{\pi} \left(\frac{\sinh\varepsilon}{\cosh^2\varepsilon} - \frac{\pi}{2} + \arctan \sinh\varepsilon\right)$$

$$q_x = I \frac{2}{\bar{\omega}} \frac{\partial\psi}{\partial z_1} \quad \text{and} \quad q_{\bar{\omega}} = R \frac{2}{\bar{\omega}} \frac{\partial\psi}{\partial z_1}$$

$$\frac{2}{\bar{\omega}} \frac{\partial\psi}{\partial z_1} = \frac{2}{c \cosh\varepsilon \sin\eta} \frac{1}{\frac{\partial z_1}{\partial\zeta}} \cdot \frac{\partial\psi}{\partial\zeta} = \frac{2}{c \cosh\varepsilon \sin\eta} \cdot \frac{1}{\frac{\partial z_1}{\partial\zeta}} \cdot \tfrac{1}{2}\left(\frac{\partial\psi}{\partial\varepsilon} - i \frac{\partial\psi}{\partial\eta}\right)$$

$$= \{\}/c \cosh\varepsilon \sin\eta - c \cosh(\varepsilon+i\eta)$$

where,

$$\{\} = -k \sin^2\eta \,(2 \cosh\varepsilon - 2 \cosh\varepsilon \sinh\varepsilon \operatorname{arc\,cot} \sinh\varepsilon)$$

$$+ 2 i k \sin\eta \cos\eta \,(\sinh\varepsilon - \cosh^2\varepsilon \operatorname{arc\,cot} \sinh\varepsilon)$$

But,

$$\frac{1}{c \cosh(\varepsilon+i\eta)} = \frac{1}{c(\cosh\varepsilon \cosh i\eta + \sinh\varepsilon \sinh i\eta)}$$

$$= \frac{1}{c(\cosh\varepsilon \cos\eta + i \sinh\varepsilon \sin\eta)}$$

$$= \frac{\cosh\varepsilon \cos\eta - i \sinh\varepsilon \sin\eta}{c(\cosh^2\varepsilon \cos^2\eta + \sinh^2\varepsilon \sin^2\eta)}$$

$$\therefore \quad q_x = I \frac{2}{\omega} \frac{\partial \psi}{\partial z_1} = \frac{1}{\cosh\varepsilon \sin\eta} \cdot \frac{1}{(\cosh^2\varepsilon \cos^2\eta + \sinh^2\varepsilon \sin^2\eta)} \cdot$$

$$\{- \sinh\varepsilon \sin\eta \frac{U}{\pi} \sin^2\eta \ (2 \cosh\varepsilon - 2 \cosh\varepsilon \sinh\varepsilon \ \text{arc cot} \sinh\varepsilon)$$

$$- \cosh\varepsilon \cos\eta \frac{2U}{\pi} \sin\eta \cos\eta \ (\sinh\varepsilon - \cosh^2\varepsilon \ \text{arc cot} \sinh\varepsilon)\}$$

$$= \frac{1}{(\cosh^2\varepsilon \cos^2\eta + \sinh^2\varepsilon \sin^2\eta)} \cdot \frac{2U}{\pi} \cdot$$

$$\{- \sin^2\eta \ (\sinh\varepsilon - \sinh^2\varepsilon \ \text{arc cot} \sinh\varepsilon)$$

$$- \cos^2\eta \ (\sinh\varepsilon - \cosh^2\varepsilon \ \text{arc cot} \sinh\varepsilon)\}$$

$$= \frac{\frac{2U}{\pi}}{(\cosh^2\varepsilon \cos^2\eta + \sinh^2\varepsilon \sin^2\eta)} \cdot$$

$$\{- \sinh\varepsilon \ (\sin^2\eta + \cos^2\eta) + \text{arc cot} \sinh\varepsilon \ (\cosh^2\varepsilon \cos^2\eta$$

$$+ \sinh^2\varepsilon \sin^2\eta)\}$$

$$= \frac{2U}{\pi} \{\text{arc cot} \sinh\varepsilon - \frac{\sinh\varepsilon}{(\cosh^2\varepsilon \cos^2\eta + \sinh^2\varepsilon \sin^2\eta)}\}$$

$$= \frac{2U}{\pi} \{\frac{\pi}{2} - \text{arc tan} \sinh\varepsilon - \frac{\sinh\varepsilon}{(\cosh^2\varepsilon \cos^2\eta + \sinh^2\varepsilon \sin^2\eta)}\}$$

and when,

$$\varepsilon = 0$$

$$q_x = \frac{2U}{\pi} \frac{\pi}{2} = U$$

i.e. at x = 0

Also,

$$q_{\bar{\omega}} = R\frac{2}{\bar{\omega}}\frac{\partial\psi}{\partial z_1} = \frac{1}{\cosh\varepsilon \sin\eta} \cdot$$

$$\frac{1}{\cosh^2\varepsilon \cos^2\eta + \sinh^2\varepsilon \sin^2\eta)} \cdot$$

$$\{\cosh\varepsilon \cos\eta \frac{U}{\pi} \sin^2\eta \ (2\cosh\varepsilon - 2\cosh\varepsilon \sinh\varepsilon \text{ arc cot } \sinh\varepsilon)$$

$$- \sinh\varepsilon \sin\eta \frac{2U}{\pi} \sin\eta \cos\eta \ (\sinh\varepsilon - \cosh^2\varepsilon \text{ arc cot } \sinh\varepsilon)\}$$

$$= \frac{\frac{2U}{\pi}}{(\cosh^2\varepsilon \cos^2\eta + \sinh^2\varepsilon \sin^2\eta)} \{\cos\eta \sin\eta \ (\cosh\varepsilon$$

$$- \cosh\varepsilon \sinh\varepsilon \text{ arc cot } \sinh\varepsilon) - \frac{\sinh\varepsilon}{\cosh\varepsilon} \sin\eta \cos\eta$$

$$(\sinh\varepsilon - \cosh^2\varepsilon \text{ arc cot } \sinh\varepsilon)\}$$

$$= \frac{\frac{2U}{\pi} \cdot \cos\eta \sin\eta}{(\cosh^2\varepsilon \cos^2\eta + \sinh^2\varepsilon \sin^2\eta)} \cdot \{\cosh\varepsilon - \frac{\sinh^2\varepsilon}{\cosh\varepsilon}\}$$

$$= \frac{2U}{\pi} \cdot \frac{\cos\eta \sin\eta}{\cosh\varepsilon} \cdot \frac{1}{(\cosh^2\varepsilon \cos^2\eta + \sinh^2\varepsilon \sin^2\eta)}$$

and when

$$\varepsilon = 0$$

$$q_{\bar{\omega}} = \frac{2U}{\pi} \tan\eta$$

i.e. at $x = 0$

Using Bernoulli's equation

Upstream		On Disc
$\frac{p_\infty}{\rho} + \frac{V_\infty^2}{2}$	=	$\frac{p_F}{\rho} + \frac{q_{\bar{\omega}}^2}{2}$

$$= \frac{p_F}{\rho} + \tfrac{1}{2} \frac{4V_\infty^{\,2}}{\pi^2} \tan^2\eta$$

where,

$\sin\eta$ = radius r/disc radius c

$$\therefore (C_p)_{FALONECALC} = \{1 - \frac{4}{\pi^2} (\frac{r^2/c^2}{1 - r^2/c^2})\}$$ see Table 40

APPENDIX 3 - OVER PRESSURISATION OF WINDMILL WAKE

Consider the flow through a windmill shown in Figure 3.

Using,

$$\frac{\partial^2\phi}{\partial x\,\partial t} + u\frac{\partial u}{\partial x} + v\frac{\partial v}{\partial x} + w\frac{\partial w}{\partial x} = X - \frac{1}{\rho}\frac{\partial p}{\partial x}$$

Integrating downstream between S_∞ and where the pressure is p_o,

$$\int_1^0 \frac{\partial^2\phi}{\partial t\,\partial x}\,dx + \int_1^0 u\frac{\partial u}{\partial x}\,dx + \int_1^0 v\frac{\partial v}{\partial x}\,dx + \int_1^0 w\frac{\partial w}{\partial x}\,dx = \int_1^0 -\frac{1}{\rho}\frac{\partial p}{\partial x}\,dx$$

since $X = 0$

$$\therefore \int_1^0 \partial\left(\frac{\partial\phi}{\partial t}\right) + \int_1^0 u\,\partial u + \int_1^0 v\,\partial v + \int_1^0 w\,\partial w = -\frac{1}{\rho}\int_1^0 \partial p$$

since ρ = constant

$$\left(\frac{\partial\phi}{\partial t}\right)_0 - \left(\frac{\partial\phi}{\partial t}\right)_1 + \frac{u_o^2 - u_1^2}{2} + \frac{v_o^2 - v_1^2}{2} + \frac{w_o^2 - w_1^2}{2} = -\frac{1}{\rho}(p_o - p_1)$$

At a great distance, both q_o and $\left(\frac{\partial\phi}{\partial t}\right)_0$ tend to zero.

$$\therefore -\left(\frac{\partial\phi}{\partial t}\right)_1 - \frac{u_1^2}{2} - \frac{v_1^2}{2} - \frac{w_1^2}{2} = -\frac{1}{\rho}(p_o - p_1)$$

or,

$$p_o - p_1 = \rho\left(\frac{\partial\phi}{\partial t}\right)_1 + \rho\frac{q_1^2}{2} \quad \text{since} \quad \frac{u_1^2 + v_1^2 + w_1^2}{2} = \frac{q_1^2}{2}$$

The velocity potential at a point is a function of its position relative to the vortex sheets, i.e.

$$\phi = f(x_o, r, \Theta)$$

in cylindrical polar co-ordinates, where x_0 is measured from an axis moving with the vortex sheets.

At infinity the vortex sheets are moving with velocity w_0 in the same direction as that of the windmill. Then x, for fixed axes taken positive in the downstream direction, is given by:

$$x = x_0 - w_0 t \quad \text{or} \quad x_0 = x + w_0 t$$

so that

$$\phi = f(x + w_0 t, r, \Theta)$$

Now,

$$\frac{d\phi}{dx} = \frac{\partial\phi}{\partial t}\frac{dt}{dx} + \frac{\partial\phi}{\partial x}\frac{dx}{dx}$$

and at infinity where ϕ is constant

$$0 = \frac{\partial\phi}{\partial t}\frac{dt}{dx} + \frac{\partial\phi}{\partial x} = \frac{\partial\phi}{\partial t}\left(-\frac{1}{w_0}\right) + u$$

or,

$$\frac{\partial\phi}{\partial t} = w_0 u \quad \text{and substituting}$$

$$p_0 - p_1 = \rho w_0 u + \rho \frac{q_1^2}{2}$$

Integrating with respect to S_∞,

$$\int (p_0 - p_1) dS_\infty = \int \rho w_0 u \, dS_\infty + \int \rho \frac{q_1^2}{2} \, dS_\infty$$

Assuming that $p_0 - p_1$ is uniform across S_∞ and from Lilley and Rainbird (12) Equation 9:

$$(p_0 - p_1)S_\infty = -\rho w_0^2 k S_\infty + \rho \frac{w_0^2 k}{2} S_\infty$$

or,

$$p_1 - p_0 = \tfrac{1}{2}\rho w_0^2 k$$

APPENDIX 4 - VORTEX THEORY FOR PROPELLER

Consider an elementary radius (dr) of the propeller at radius r as shown in Figure 4.

$$\text{Elementary torque } dQ = Br(C_L \sin\phi + C_D \cos\phi)\tfrac{1}{2}\rho c\, dr\, W^2$$

Hence,

$$\text{torque coefficient } C_Q = \text{torque}/\tfrac{1}{2}\rho\pi R^3 V_\infty^2$$

where,

R = propeller radius and ρ = density

or,

$$C_Q = \int_{R_{boss}}^{R} Br(C_L \sin\phi + C_D \cos\phi)\tfrac{1}{2}\rho c\, W^2\, dr/\tfrac{1}{2}\rho\pi R^3 V_\infty^2$$

Letting,

$$\mu_1 = \frac{\Omega r}{V} \text{ and solidity } \sigma = Bc/2\pi r$$

then,

$$C_Q = \int_{R_{boss}}^{R} 2\sigma(1 + \mu_1^2)\cos^2\alpha_1 \left(\frac{r}{R}\right)^2 \left(\frac{V}{V_\infty}\right)^2 (C_L \sin\phi + C_D \cos\phi)\, d\left(\frac{r}{R}\right)$$

Using Lock's equation for w_1:

$$w_1 = \frac{\sigma C_L W}{4\kappa \sin\phi}$$

and from

$$W = W_o \cos\alpha_i$$

and

$$\alpha_i = \frac{w_1}{W_o}$$

$$\sigma = \frac{w_1\, 4\kappa \sin\phi}{C_L W} = \frac{W_o\, \alpha_i\, 4\kappa \sin\phi}{C_L W_o \cos\alpha_i} = \frac{4\alpha_i \kappa \sin\phi}{C_L \cos\alpha_i}$$

$$\therefore \quad C_Q = \int_{R_{boss}}^{R} 2 \cdot \frac{4\,\alpha_i\,\kappa\,\sin\phi}{C_L\,\cos\alpha_i}(1+\mu_1{}^2)\cos^2\alpha_i\left(\frac{r}{R}\right)^2\left(\frac{V}{V_\infty}\right)^2 \cdot$$

$$(C_L\,\sin\phi + C_D\,\cos\phi)\,d\left(\frac{r}{R}\right)$$

or,

$$C_Q = \int_{R_{boss}}^{R} 8\,\alpha_i\,\kappa\,\sin^2\phi\,(1+\mu_1{}^2)\cos\alpha_i\left(\frac{r}{R}\right)^2\left(\frac{V}{V_\infty}\right)^2 \cdot$$

$$\left(1+\frac{\tan\gamma}{\tan\phi}\right)d\left(\frac{r}{R}\right)$$

where,

$$\tan\gamma = C_D/C_L$$

It follows that the corresponding equation for the thrust coefficient

$$C_T = \text{thrust}(T)/\tfrac{1}{2}\,\rho\pi R^2\,V_\infty{}^2$$

is given by

$$C_T = \int_{R_{boss}}^{R} 4\,\alpha_i\,\kappa\,\sin 2\phi\,(1+\mu_1{}^2)\cos\alpha_i\left(\frac{r}{R}\right)\left(\frac{V}{V_\infty}\right)^2 \cdot$$

$$(1-\tan\gamma\,\tan\phi)\,d\left(\frac{r}{R}\right)$$

Iwasaki(8) employs the pitch angle of the vortex sheet at the windmill plane to determine the circulation function κ, the same assumption as Lock in R & M 1377, and obtains very good agreement with experimental results for fast running 3 bladed windmills viz:

Coefficient	Torque	Drag	Power
Calculated	0.119	0.45	0.30
Experimental	0.121	0.43	0.30

Because of this agreement the same procedure for determining κ was used in the present work.

The variation of κ with ϕ and r/R for 3 bladed propellers was taken from R & M 1674. Tables for Use in an Improved Method of Airscrew Strip

Theory Calculation by C.N.H. Lock and D. Yeatman. 3 blades were chosen for the propeller to match the windmill driving it, but the effect of the number of blades on performance is another feature requiring investigation.

If the greatest thrust per unit of power is sought then, at radius r, $dT/(dQ \times \Omega)$ should be made as large as possible and since,

$$\frac{dT}{dQ \times \Omega} = \frac{\frac{1}{2}\rho c\, dr\, W^2 (C_L \cos\phi - C_D \sin\phi)\, B}{\frac{1}{2}\rho c\, dr\, W^2 (C_L \sin\phi + C_D \cos\phi) Br\, \Omega}$$

$$= \frac{C_L \cos\phi - C_D \sin\phi}{C_L \sin\phi + C_D \cos\phi} \cdot \frac{1}{\Omega r}$$

$$= \frac{1 - \tan\gamma \tan\phi}{\tan\phi + \tan\gamma} \cdot \frac{1}{\Omega r} = \frac{1}{\tan(\phi+\gamma)} \cdot \frac{1}{\Omega r}$$

it follows that both ϕ and γ should be made as small as possible.

APPENDIX 5 - CALCULATIONS

1. Drag of Gauze and Solid Discs in Tandem

To allow comparison with experimental results, the drag coefficient of the combination was calculated, using the simple shielding theory (see Section 2.1), over a range of appropriate diameter ratios for a corresponding axial velocity interference factor (α) derived as follows.

$$\text{Drag of gauze disc alone} = 0.65 \times \tfrac{1}{2}\rho A_G \times V_\infty^2$$

$$= \rho A_G V_\infty (1-\alpha) 2\alpha V_\infty$$

from which,

$$\alpha = 0.204$$

The major deficiency with the simple shielding theory was its inability to predict successfully the drag coefficient of the solid disc in tandem with the gauze disc. This was highlighted by the difference between $(C_D)_{D2CORR}$ corresponding to $(C_D)_{MIN}$ (see Section 4.3.1 and Table 14) which was essentially experimentally derived and $(C_D)_{D2SS}$ where

$$(C_D)_{D2SS} = [(D_1/D_2)^2(1-2\alpha)(1-\alpha) + \{1-(D_1/D_2)^2(1-\alpha)/(1-2\alpha)\}] + (C_D)_{ICALC}$$

The difference is shown in Figure 19.

The calculations were repeated for interference factors of α = 0.1, 0.2, 0.3 and 0.4 to demonstrate the relationship between the drag of, and thus the power generated by, the windmill (simulated by the gauze disc) and the combination drag.

2. Effect on Drag Coefficient of Actual Speed Distribution in Wake of Gauze Disc

Examination of the wind speeds measured behind the gauze disc (see Figure 20) indicated that they were not greatly different from those given by one-dimensional theory. As a check that the difference could not account for the measured greater effective shielding of the gauze disc, the idealised speed distribution behind the gauze disc shown in Figure 21 was employed together with simple shielding theory to calculate the drag coefficient of the gauze and solid discs in tandem at three diameter ratios.

3. Effect of Shields on Drags of Car Configurations

The parameter (Δ) by which the effectiveness of the shields was assessed was essentially the difference between the measured and calculated car configuration drags.

The calculated drags assumed that the car body was subjected to a uniform stream of $V_\infty(1-2\alpha)$, where $\alpha = 0.204$, and no mutual interference, that is:

$$\text{Calculated drag}/\tfrac{1}{2}\rho V_\infty^2 = (C_D)_{CARCALC} \times A_{CAR}$$

where,

$$(C_D)_{CARCALC} \times A_{CAR} = (C_D)_{CAR} \times A_{CAR}(1-2\alpha)^2 + (C_D)_{GALONE} \times A_G$$

$$= (1.77 \times 10^{-3} \times 0.592^2) + (0.650\ A_G)$$

$$= (0.62 \times 10^{-3}) + (0.650\ A_G)$$

The measured drag is given by $\{(C_D)_{CAR} \times A_{CAR}\}\tfrac{1}{2}\rho V_\infty^2$.

Thus defining Δ by

$$\Delta = (\text{measured drag} - \text{calculated drag})/\tfrac{1}{2}\rho V_\infty^2$$

then

$$\Delta = \{(C_D)_{CAR} \times A_{CAR}\} - \{(0.62 \times 10^{-3}) + (0.650\ A_G)\}$$

which gave an indication of the favourable interference, other than that ideally due to wind speed reduction over the car body. Measured values of $(C_D)_{CAR} \times A_{CAR}$ are given in Table 16 and were used to derive Δ for each configuration (Table 37).

It can be seen from Table 37 that the fifth configuration had the most favourable interference but the conclusion was drawn that significant reductions in the drag of streamline vehicles are not likely to occur from the application of work on gauze and solid discs in tandem unless the solidity of the gauze disc is greatly increased. Although the results were considered to be encouraging no attempt was made to establish the necessary parameters and technique to give decreased drag because the required work would amount to a major departure from the main theme of the research.

4. Effect of Gauze Solidity on Combination Drag

The calculations referred to in the above sections 1 and 3, led to the conclusion that drag reductions are unlikely to be achieved with bodies having low drag coefficients using gauze shields with low solidity.

Assuming as in 1 that the drag of the gauze shield alone is given by

$$\rho A_G \, V_\infty (1-\alpha) 2\alpha \, V_\infty$$

then

$$(C_D)_{GALONE} = 4\alpha(1-\alpha)$$

and the solidity of the gauze may be related to the axial interference factor α as follows:

at $\alpha = 0.5$,

$$(C_D)_{GALONE} = 1.0$$

and the shield may be assumed completely solid;

at $\alpha = 0$

$$(C_D)_{GALONE} = 0$$

that is zero solidity;

and in between these limits solidity increases with α.

Consider the following simple treatment of the combination drag of a body shielded by a gauze area in tandem. Assuming no mutual interference and that the body is subjected to a uniform stream of speed $V_\infty(1-2\alpha)$ from the shield, then

$$\text{drag of combination} = \text{drag of body} + \text{drag of shield}$$

$$= \{(C_D)_B \, 0.5\rho \, A_B \, V_\infty^2 (1-2\alpha)^2\} + \{2\rho \, A_G \, V_\infty^2 \, \alpha(1-\alpha)\}$$

If the particular case is taken of

$$A_B = A_G \frac{(1-\alpha)}{(1-2\alpha)}$$

that is, the wake area from the shield is the same as the body area,

then

$$\text{drag of combination} = \{(C_D)_B\ 0.5\rho\ A_G(1-\alpha)/(1-2\alpha).V_\infty^2(1-2\alpha)^2\} + \{2\rho\ A_G\ V_\infty^2\ \alpha(1-\alpha)\}$$

and for the shielding to be beneficial this must be less than the drag of the unshielded body which is given by $(C_D)_B \times 0.5\rho\ A_B\ V_\infty^2$

$$= (C_D)_B \times 0.5\rho\ V_\infty^2\ A_G(1-\alpha)/(1-2\alpha)$$

Hence,

$$\{(C_D)_B\ 0.5\rho\ A_G\ V_\infty^2(1-\alpha)(1-2\alpha)\} + \{2\rho\ A_G\ V_\infty^2\ \alpha(1-\alpha)\} \not> (C_D)_B\ 0.5\rho\ V_\infty^2\ A_G(1-\alpha)/(1-2\alpha)\}$$

or,

$$(C_D)_B(1-2\alpha) + 4\alpha \not> (C_D)_B/(1-2\alpha)$$

It follows that for the shielding to be beneficial its solidity, as defined by α, must exceed the level given by the following equation:

$$\alpha = \{1 - (C_D)_B\}/\{2 - (C_D)_B\} \qquad \text{(Table 38)}$$

5. Mutual Interference/Interactive Force Between Gauze and Solid Discs in Tandem

For comparison with experimental results and for use in a semi-empirical account of the mechanism of drag reduction, the interactive force was calculated.

It was assumed that the flow approaching and around the solid disc may be represented by a source-sink system which produces the Rankine ovoid shown in Figure 22. The geometry of the ovoid was decided from an examination of Figure 11 of reference 15 (p. 30) taking into account the comments on a single disc given on page 29 of that reference.

Using;

$$\psi = 0 = -V_\infty \pi Y^2 + \frac{m}{2}\left\{\frac{X+b}{\sqrt{Y^2+(X+b)^2}} - \frac{X-b}{\sqrt{Y^2+(X-b)^2}}\right\}$$

when, $X = 0$, $Y = 0.825\ D_2$ and $X = -X_1$, $Y = D_2/2$; stagnation point when

$$V_\infty - \frac{m}{4\pi(S - b)^2} + \frac{m}{4\pi(S + b)^2} = 0;$$

and,

$$X_1 + S = 3D$$

gives,

$$m = 2.615\ V_\infty\ D_2^{\,2},\ b = 1.172\ D_2,\ X_1 = 1.378\ D_2 \text{ and } S = 1.622\ D_2$$

Thus the axial component of velocity at co-ordinates (x,r) was found from

$$V_x = V_\infty + \frac{2.615\ V_\infty\ D_2^{\,2}(2.550\ D_2 + x)}{4\pi\{r^2 + (2.550\ D_2 + x)^2\}^{3/2}} - \frac{2.615\ V_\infty\ D_2^{\,2}(0.206\ D_2 + x)}{4\pi\{r^2 + (0.206\ D_2 + x)^2\}^{3/2}}$$

and, following the recommendation of Engineering Sciences Data 70015(6), the drag of a gauze disc held in the approaching flow from

$$\text{drag} = \int_0^{r=D_1/2} (C_D)_{GALONE}\ 0.5\rho\ V_x^{\,2}\ 2\pi r\ dr$$

where,

$$(C_D)_{GALONE} = 0.650$$

and x/D_2 is constant, and therefore x, for a given configuration of gauze and solid discs in tandem. The integration was carried out numerically.

Glauert(7, pp. 273-286) suggests that the interference experienced by a propeller at the front of an aeroplane body can be represented approximately as a decrease of the effective velocity of advance of the propeller and outlines a method of estimating the mutual interference force based on an investigation by C.N.H. Lock.

Glauert goes on to state that the mutual interference force, associated with the pressure gradient in the slipstream and causing equal increments of propeller thrust and body drag, is the difference between the free (without body present) and apparent (with body present) thrusts and

may be presumed to be proportional to the apparent thrust. He gives the following formula for calculating the interactive force.

$$\text{Interactive force} = \int h \, dT_a$$

where h, which is a function of radius, is the axial velocity deficiency factor at the plane of the propeller disc, that is,

$$\text{axial velocity} = V_\infty(1-h)$$

The formula was used to determine the mutual interference force for a theoretical windmill and solid disc in tandem driven by a propeller using the windmill power (see Section 8 below and Appendix 6). However, the calculated force was only approximately one-half of the value suggested by experiments on solid discs with a gauze disc simulating the windmill. The disparity casted doubts on the validity of the formula and it was decided to employ in the present work the basic assertion of Glauert that the interactive force is the difference between the free and apparent thrusts due to a decrease in the effective velocity of advance.

In extending the basic assertion of Glauert to the calculation of the mutual interference force between gauze and solid discs in tandem, the drag of the gauze disc in the effective velocity of advance was taken to be that given by the above equation for drag, namely,

$$\text{drag} = \int_0^{r=D_1/2} (C_D)_{GALONE} \, 0.5\rho \, V_x^2 \, 2\pi r \, dr$$

with V_x evaluated at the gauze disc position.

Consequently the mutual interference force coefficient was found from

$$(C_D)_{ICALC} = (D_1/D_2)^2 \{0.650 - (\text{drag}/0.5\rho \, (A)_{D1} \, V_\infty^2)\}$$

In the case of $(C_D)_{D2SS}$ evaluated using the simple shielding theory (see Section 1 above), the value of $(C_D)_{ICALC}$ was taken to be that corresponding to a gap ratio (g/D_2) giving minimum configuration drag coefficient $((C_D)_{MIN})$. These values of $(C_D)_{ICALC}$ are given in Table 39.

For comparison purposes, to see if better agreement could be obtained with experimental results, the interactive force for a selected number

of configurations (see Table 39) was recalculated using $V_\infty - q_x$ in the hydrodynamic theory for a circular disc (see Section 2.4 and Appendix 2) instead of the horizontal component of velocity (V_x) for a Rankine ovoid, that is, using

$$q_x = \frac{2V_\infty}{\pi}\left\{\frac{\pi}{2} - \text{arc tan sinh}\varepsilon - \frac{\sinh\varepsilon}{(\cosh^2\varepsilon\cos^2\eta - \sinh^2\varepsilon\sin^2\varepsilon)}\right\}$$

in which,

$$x = (D_2/2)\sinh\varepsilon\cos\eta,\ \bar{w} = \cosh\varepsilon\sin\eta$$

6. Theoretical Variation of Pressure with Radius Over a Circular Disc

The irrotational theory for the flow over a circular disc employed in the previous section (5) was extended to give the theoretical radial pressure variation (see Section 2.5 and Appendix 2) and thus permit a comparison to be made with the measured variation.

7. Other Parameters Employed in the Discussion on Gauze and Solid Discs in Tandem

7.1 Calculated Mean Face Pressure Coefficient

Mean face pressure coefficient $(\overline{C_p})_F$ was not measured on every configuration and for consistency a calculated coefficient was employed which was determined using the following formula:

$$(\overline{C_p})_{FCALC} = k\{C_D - (\overline{C_p})_S - (C_D)_{D1ALONE} + (C_D)_{ICALC}\}$$

where the constant coefficient k was taken as its average value for those cases where $(\overline{C_p})_F$ was measured (1.149).

Parameters such as the face and back pressures on the solid disc were found useful in evolving a semi-empirical explanation of the cause of drag reduction.

7.2 Calculated Effective Speed of Advance

A parameter closely associated with the face and back pressures was the calculated effective speed of advance:

$$V_{EFF} = V_\infty\sqrt{[\{(\overline{C_p})_S + (\overline{C_p})_{FCALC}\}/(C_D)_{D2ALONE}]}$$

As a velocity ratio (V_{EFF}/V_∞), it provided an indication of the drag

benefit resulting from shielding based on the concept of the solid disc simply operating in a uniform stream of reduced velocity.

7.3 Calculated Fore Body Drag Coefficient

It was found helpful to determine the separate contributions to drag of the fore body (the gauze disc plus the front face of the solid disc) and the aft face of the solid disc.

$$(C_D)_{FBCALC} = (\overline{C_P})_{FCALC} + (C_D)_{D1CALC}$$

7.4 Calculated Area Ratio Parameter

Employing the approach of Roshko and Koenig the drag coefficient of the solid disc is given by $(\overline{C_P})_S \times A_S/(A)_{D2}$. Consequently

$$(C_D)_{D2} = (\overline{C_P})_S + (\overline{C_P})_F = (\overline{C_P})_S \times A_S/(A)_{D2}$$

or

$$A_S/(A)_{D2} = 1 + \{(\overline{C_P})_F/(\overline{C_P})_S\}$$

It was decided to check this approach because, if valid, it could be of considerable importance in a semi-empirical solution. Thus the parameter $[1 + \{(\overline{C_P})_{FCALC}/(\overline{C_P})_S\}]$ was calculated and its variation compared with that of $A_S/(A)_{D2}$.

7.5 Calculated Drag Coefficient of Solid Disc

In examining the applicability of the Roshko and Koenig approach it was instructive to calculate $(C_D)_{D2CALC}$, where

$$(C_D)_{D2CALC} = C_D - (C_D)_{D1ALONE} + (C_D)_{ICALC}$$

8. Windmill-Disc-Propeller Combination. Reduction in Drag Coefficient Due to Propeller Thrust.

In the programme of work initially put forward it was proposed to employ a windmill to shield the solid disc and to use the power developed by the windmill to drive directly a propeller. Thus originally it was the intention to investigate a windmill, disc and propeller combination with the propeller providing through its thrust a further reduction in drag.

Preliminary tests on a windmill, disc and propeller combination(4) gave

no indication of instability although the windmill was designed to provide a high axial interference factor of 1/3. This was well in excess of the limiting condition suggested by Lilley and Rainbird(12).

An early decision was taken not to risk instability occurring in the main programme of work undertaken and for this reason the investigations concentrated on a windmill/gauze disc simulator having a drag coefficient of 0.650 and a corresponding axial interference factor of 0.204. The choice was based on an Iwasaki(8) recommendation of 3 blades for fast running windmills with a maximum power coefficient of 0.35. This was preferred to the above Lilley and Rainbird limit which is, more correctly, the theoretical boundary to the Generalised Momentum Theory.

There are a number of differences between a windmill and a gauze disc simulator. However, in order to make an estimate of the propeller thrust in a windmill, disc and propeller combination, it was assumed that a windmill and a gauze disc of the same area and drag coefficient are completely interchangeable.

The optimum gauze and solid disc configuration was considered, D_1/D_2 = 0.515, g/D_2 = 1.83, with the gauze disc replaced by an equivalent windmill driving a propeller working in the wake.

The calculations that were carried out to determine the propeller thrust are given in Appendix 6 which also summarises the estimates made of the mutual interference drag coefficient of the windmill and solid disc.

APPENDIX 6 - WINDMILL-DISC-PROPELLER COMBINATION. CALCULATION OF REDUCTION IN DRAG COEFFICIENT DUE TO PROPELLER THRUST AND MUTUAL INTERFERENCE FORCE COEFFICIENT OF WINDMILL AND DISC.

This appendix essentially describes the calculations which were made in connection with the determination of the drag reducing propeller thrust of a windmill-disc-propeller combination. As stated in Section 8 of Appendix 5, the optimum gauze and solid disc configuration was considered, $D_1/D_2 = 0.515$, $g/D_2 = 1.83$, with the gauze disc replaced by an equivalent windmill driving a propeller working in the wake of the configuration.

An Iwasaki(8) windmill was selected to drive the propeller and the first calculation described shows how the power developed was found.

In determining the percentage reduction in drag provided by the propeller thrust (see Section 8.3) it was assumed that the gauze disc of the optimum configuration may be replaced by its equivalent windmill without affecting the drag coefficient of the configuration (0.775) and that the mutual interference between the propeller and the configuration is negligible. The major differences between a gauze disc and its equivalent windmill are examined in this appendix.

The propeller, designed in accordance with the theory of Appendix 4, used the same blade sections as were employed for the windmill and were adapted to the wake of the optimum configuration to produce the greatest thrust from the delivered power. The procedure for calculating the thrust is given in detail below.

It was necessary when determining the power available at the propeller to find the mutual interference drag coefficient of the windmill and disc configuration for which Glauert's(7) formula (see Section 5 of Appendix 5) was used initially. It was this exercise which led to the adoption of the difference between the free and apparent drags instead of Glauert's formula for calculating the coefficient.

Power Available at the Propeller

The assumption made was that the gauze disc is replaced by a windmill having the same drag coefficient and the same area as in the optimum configuration. If completely interchangeable and with the further assumption that the reduction in drag, when in tandem with the solid disc, is caused effectively by a decrease in velocity from V_∞ to V,

then

drag of windmill alone = drag of disc alone

and

$$\frac{V}{V_\infty} = \sqrt{\left\{\frac{(C_D)_{D1CALC}}{(C_D)_{D1ALONE}}\right\}}$$

Letting $(C_D)_W$ be the drag coefficient of the windmill, it follows that

$$(C_D)_{WALONE} \times \left(\frac{D_1}{D_2}\right)^2 = (C_D)_{D1ALONE} = 0.650 \times \left(\frac{D_1}{D_2}\right)^2$$

and

$$\text{power developed} = (C_P)_W \times \tfrac{1}{2}\rho\, V^3\, \pi R^2$$

where $R = D_1/2$ and $(C_P)_W$ is the power coefficient of the windmill. Thus

$$\text{power developed} = (C_P)_W \times \tfrac{1}{2}\rho \left\{\frac{(C_D)_{D1CALC}}{(C_D)_{D1ALONE}}\right\}^{3/2} \times (A)_{D1} \times V_\infty^3$$

For the optimum configuration $D_1/D_2 = 0.515$

$$(C_D)_{D1CALC} = (C_D)_{D1ALONE} - (C_D)_I$$

$$= (0.650 \times 0.515)^2 - 0.013 = 0.172 - 0.013$$

$$= 0.159$$

From Iwasaki's data for 3 bladed windmills (see Figure 23) at $(C_D)_W = 0.650$, $(C_P)_W = 0.350$ and $\Omega R/V = 2.776$.

Consequently, assuming a transmission efficiency of 97%,

$$\text{power at propeller} = 0.97 \times 0.350 \times \left(\frac{0.159}{0.172}\right)^{3/2} \times \tfrac{1}{2}\rho\, (A)_{D1}\, V_\infty^3$$

$$= 0.302 \times \tfrac{1}{2}\rho\, (A)_{D1}\, V_\infty^3$$

It should be noted that because the interferences between the solid and gauze discs and the windmill and gauze disc are not precisely the same, then the powers developed are also different. Additionally the effect

of interference is to cause the windmill to operate in a non-uniform stream which is not correctly taken into account by a reduction in uniform velocity from V_∞ to V. The equations also indicate that interference needs to be kept to a minimum because it reduces the power developed.

Propeller Approach Velocities

Earlier work (see Section 8.1.7) showed that a good approximation to the velocity profile in the wake of the approximately optimum gauze and solid disc configuration is given by:

$$u/V_\infty = K \text{ for } 0 \leqslant r/R \leqslant a$$

$$u/V_\infty = K\{1 - (\frac{r/R-a}{1-a})^{1.5}\}^2 \text{ for } a \leqslant r/R \leqslant 1$$

where u is the velocity defect. At 3 diameters (D_2) downstream of the solid disc, K = 0.364 and a = 0.15. At 4 diameters, K = 0.197 and a = 0.25.

Assuming that the velocities approaching the propeller are given by the above equations and that the values of "K" and "a" are such that the momentum drag is equal to the drag of the optimum configuration (0.775 x $\frac{1}{2}\rho$ $(A)_{D2}$ V_∞^2) then,

$$0.775 \times \tfrac{1}{2}\rho\ (A)_{D2}\ V_\infty^2 = \int_0^R \rho(V_\infty - u)u\pi 2\ r\ dr$$

in which,

$$R = 2D_1 = 2 \times 0.515D_2 = 1.03D_2$$

Considering the velocities at $3D_2$ downstream, where K = 0.364 and a = 0.15.

r/R	0	0.075	0.15	0.235	0.320	0.405	0.490	0.575	0.660	0.745
u/V_∞	0.364	0.364	0.364	0.341	0.302	0.254	0.203	0.152	0.104	0.062
r/R	0.830	0.915	1.0							
u/V_∞	0.029	0.008	0							

Table 6. Propeller Approach Velocities.

$$\therefore \int_{1}^{1.03D_2} \left(1 - \frac{u}{V_\infty}\right)\left(\frac{u}{V_\infty}\right)\left(\frac{r}{R}\right) d\left(\frac{r}{R}\right) \times \rho\, 2\pi\, V_\infty^{\,2}\, (1.03D_2)^2$$

$$= 16 \times 1.03^2 \times \tfrac{1}{2}\rho \frac{\pi D_2^{\,2}}{4} V_\infty^{\,2} \int_{0}^{1} \left(1 - \frac{u}{V_\infty}\right)\left(\frac{u}{V_\infty}\right)\left(\frac{r}{R}\right) d\left(\frac{r}{R}\right)$$

$$= 0.773 \times \tfrac{1}{2}\rho\, (A)_{D2}\, V_\infty^{\,2}$$

which gives good agreement with the required value of $0.775 \times \frac{1}{2}\rho\, (A)_{D2}\, V_\infty^{\,2}$ (see Sections 8.1.6 and 8.1.7).

In order to correct for this small difference, "K" was taken as 0.365 (instead of 0.364) and "a" as 0.15 in calculating the approach velocities.

Of course the propeller may be placed at any position in the wake and the best position is yet another matter for investigation, but there is benefit from operating the propeller in as low velocities as possible. If the pressure in the wake has fully recovered by the time the velocities in the wake have fully developed, then the assumed u/V_∞ represent the largest reductions achievable.

Mutual Interference Between Propeller and Solid Disc + Windmill

It was inferred from the work on interference that the velocities and pressures (suctions) induced by the propeller on the solid disc, $3D_2$ upstream, are small. Consequently, the drag due to these suctions on the solid disc was neglected.

This modification of the velocity and pressure distribution around the solid disc, and to a lesser extent around the windmill, leads to a velocity distribution in the wake which is different from that found without the propeller.

The interference requires investigation, but for the purpose of the present work, which is only intended to give a first estimate of the propeller thrust, the nominal approach velocities specified above were assumed to apply in conformity with other similar effects not being taken into account such as those due to the rotational velocities induced by the windmill.

Windmill Induced Rotational Velocities

The windmill induced rotational velocities also modify the velocity and pressure distributions around the combination of windmill and solid disc and lead to changes in the velocities approaching the propeller.

In turn the distribution of induced rotational velocities are considerably modified by the solid disc and its turbulent wake.

These effects were also ignored in the present work.

Over-pressurisation in Windmill Wake

As the theory shows (see Section 2.6 and Appendix 3) the windmill wake is over-pressurised. However, the over-pressurisation is not the same as in the wake of the gauze disc. It is likely that this difference in wake pressure leads to differences in drag between a windmill and solid disc combination and a corresponding gauze and solid disc combination.

Again the effect was not taken into account and requires investigation.

Design of Propeller Using Vortex Theory

The theory is given in Appendix 4.

Three blades were chosen for the propeller to match the windmill driving it, but the effect of the number of blades on performance is another feature requiring investigation.

Again to match the windmill the Gottingen 623 section was assumed for the propeller, but here also an investigation is required to determine which are the best aerofoil sections to use. The characteristics of the Gottingen 623 section, as given by Iwasaki, are shown in Figure 24. γ minimises at $\alpha = 3.45°$ where $C_L = 0.858$ and $C_D = 0.0168$. Any Reynolds number scale effect on the aerofoil data was neglected.

In the design of the propeller as in the case of the windmill, no account was taken of cascade, flow curvature and radial flow effects.

The radius of the propeller's boss was made the same as that of the windmill, namely 0.27R, and it was assumed that the thrust of the boss caused by the rise in pressure across the propeller disc, cancelled out the viscous drag of the boss. It is likely that the former exceeds the latter and results in a small net thrust.

To satisfy the Betz condition for the propeller working in a variable wake

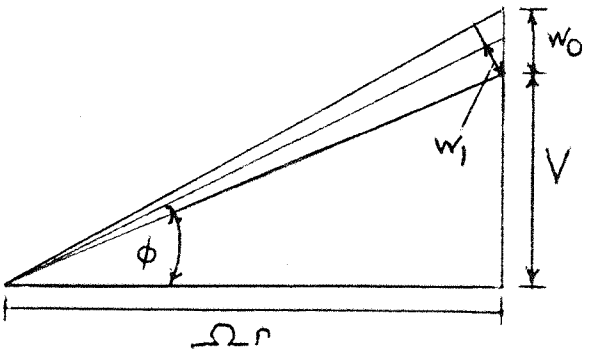

$V + 2(\Omega r \tan\phi - V)$ was made the same at all r.

But,

$$V + 2(\Omega r \tan\phi - V) = 2\Omega r \tan\phi - V = \left(\frac{2\Omega r}{V_\infty} \tan\phi - \frac{V}{V_\infty}\right) V_\infty$$

Since V_∞ is constant for all r and

$$\frac{\Omega D_1}{2 \times (0.159/0.172)^{0.5} V_\infty} = 2.776$$

then,

$$(2 \times 2.669 \times 2) \frac{r}{D_1} \tan\phi - \frac{V}{V_\infty}$$

or,

$$\{10.676 \left(\frac{R}{D_1}\right)\left(\frac{r}{R}\right) \tan\phi - \left(\frac{V}{V_\infty}\right)\}$$

was made constant.

Procedure for Calculating $\delta C_D = T/0.5\rho\left(\frac{\pi D_2}{4}\right)^2 V_\infty^2$

Numerical integration was used and the following quantities were determined at x = r/R values of 1.0, 0.95, 0.9, 0.8, 0.7, 0.6, 0.5, 0.4, 0.3 and 0.27. The Newton-Cotes 3 ordinate rule was applied between x = 1.0 and 0.3, and the trapezoidal rule between x = 0.3 and 0.27.

(i) V/V_∞ (from above Propeller Approach Velocities)

$$V/V_\infty = (V_\infty - u)/V_\infty$$

where

$$u/V_\infty = 0.365 \text{ for } 0 \leq r/2D_1 \leq 0.15$$

and

$$u/V_\infty = 0.365 \left[1 - \left\{ \frac{(r/2D_1) - 0.15}{0.85} \right\}^{1.5} \right]^2 \text{ for } 0.15 \leq r/2D_1 \leq 1.0$$

As the equations suggest, the calculation of V/V_∞ involved an initial step of choosing a radius (R) for the propeller, as a decimal fraction of D_1. The first radius assumed was $R = 0.5D_1$, that is, a propeller having the same diameter as the windmill.

(ii) $1 + \mu_1^2$

where

$$1 + \mu_1^2 = 1 + \left(\frac{\Omega r}{V}\right)^2 = 1 + \left\{\left(\frac{\Omega D_1}{2V_\infty}\right)\left(\frac{2r}{D_1}\right)\left(\frac{V_\infty}{V}\right)\right\}^2$$

$$= 1 + \left\{2.669\left(\frac{2R}{D_1}\right)\left(\frac{r}{R}\right)\left(\frac{V_\infty}{V}\right)\right\}^2 = 1 + \left\{\frac{5.338}{V/V_\infty}\left(\frac{R}{D_1}\right)\left(\frac{r}{R}\right)\right\}^2$$

(iii) Arc tan $V/\Omega r$

where

$$\text{arc tan } V/\Omega r = \text{arc tan } 1/\mu_1$$

(iv) ϕ

ϕ, and thus α_i, were initially unknown and must be such as to satisfy the power delivered to the propeller (see Power Available at the Propeller above).

Consequently a tentative value of α_i was assumed for x = 0.7 giving

$$\phi_{x=0.7} = (\text{arc tan } V/\Omega r + \alpha_i)_{x=0.7}$$

This allowed the constant in the Betz condition equation (see Design of Propeller Using Vortex Theory above) to be determined

$$\text{constant} = \left\{10.676\left(\frac{R}{D_1}\right)\left(\frac{r}{R}\right)\tan\phi\right\} - \left(\frac{V}{V_\infty}\right)$$

and in turn the corresponding values of ϕ for all other values of x.

(v) α_i from

$$\alpha_i = \phi - \arctan (V/\Omega r)$$

(vi) The circulation function κ was taken from R & M 1674.

(vii) $1 + (\tan\gamma/\tan\phi)$

where

$$1 + (\tan\gamma/\tan\phi) = 1 + (0.0168/0.858 \tan\phi)$$

Thus the geometrical angle of attack was maintained at 3.45° for all radii.

(viii) $d(C_Q)_P$ from

$$d(C_Q)_P = 8\alpha_i \kappa \sin^2\phi (1 + \mu_1^2)\cos\alpha_i \left(\frac{r}{R}\right)^2 \left(\frac{V}{V_\infty}\right)^2 \left(1 + \frac{\tan\gamma}{\tan\phi}\right)$$

Integration of the elementary torque coefficient gave $(C_Q)_P$ which was then multiplied by $\{R/(D_1/2)\}^3$. If the product of $(C_Q)_P$ and $\{R/(D_1/2)\}^3$ did not give a value of 0.113, calculations (iv) and onwards were repeated with different assumed values of α_i at x = 0.7 until agreement was obtained. This requirement followed from

$$\text{torque} \times \Omega = \text{power delivered to propeller}$$

$$= 0.302 \times \tfrac{1}{2}\rho (A)_{D1} V_\infty^3 \quad \text{(see Power Available at the Propeller above)}$$

$$\therefore \quad (C_Q)_P \times \tfrac{1}{2}\rho \pi R^3 V_\infty^2 \times 2.669 \times \frac{2V_\infty}{D_1} = 0.302 \times \tfrac{1}{2}\rho\pi \left(\frac{D_1}{2}\right)^2 V_\infty^3$$

or

$$(C_Q)_P\{R/(D_1/2)\}^3 = 0.302/2.669 = 0.113$$

Using the factors giving the required $(C_Q)_P$ the following further calculations were made to determine $\delta(C_D)$.

(ix) $1 - (\tan\gamma \tan\phi)$

where

$$1 - (\tan\gamma \tan\phi) = 1 - \left(\frac{0.0168}{0.858} \tan\phi\right)$$

(x) $d(C_T)_P$ from

$$d(C_T)_P = 4\alpha_i \kappa \sin 2\phi(1 + \mu_1^2)\cos\alpha_i \left(\frac{r}{R}\right) \left(\frac{V}{V_\infty}\right)^2 \{1 - (\tan\gamma \tan\phi)\}$$

Integration of the elementary thrust coefficients gave $(C_T)_P$ from which $\delta(C_D)$ was found as follows:

$$\delta(C_D) = T/\tfrac{1}{2}\rho\pi \frac{D_2^2}{4} V_\infty^2 = (C_T)_P \times \tfrac{1}{2}\rho\pi R^2 V_\infty^2 / \tfrac{1}{2}\rho\pi V_\infty^2 \frac{D_2^2}{4}$$

$$= (C_T)_P \times \{R/(D_2/2)\}^2 = (C_T)_P \left(\frac{2R}{D_1}\right)^2 \left(\frac{D_1}{D_2}\right)^2$$

$$= (C_T)_P \left(\frac{2R}{D_1}\right)^2 (0.515)^2$$

Calculated values of $\delta(C_D)$ for three propeller diameters are given in Table 43.

The largest propeller giving the highest $\delta(C_D)$ was found by making α_i = 0 at x = 1.0.

Glauert Approach to Mutual Interference Force Coefficient. Application to Windmill and Disc.

The Glauert(7, pp. 273-286) formula was used to determine the mutual interference force for the windmill and disc of the windmill-disc-propeller theoretical combination (see Section 5 of Appendix 5).

Geometric details of the equivalent windmill are given below and are also shown in Figure 25.

r/R	0.34	0.40	0.60	0.75	0.85	0.925	0.975	1.000
c/R	0.307	0.308	0.314	0.326	0.340	0.355	0.368	0.378
$\beta°$	32.77	28.97	18.82	13.30	10.42	8.57	7.48	7.00

D_1/D_2 = 0.515 Ω = 5.338 . $V_\infty/2R$ = 2.669 . V_∞/R $R = D_1/2$

Table 7. Geometric Details of Equivalent Windmill.

The windmill was placed at g/D_2 giving $(C_D)_{MIN}$ at D_1/D_2 = 0.515 for gauze and solid discs in tandem, that is, at g/D_2 = 1.83. It may be shown that

the variation of the axial component of velocity (V_x) with radius at the windmill position produced by a source-sink system forming the Rankine body shown in Figure 22, following the approach of Section 5 of Appendix 5, is:

$$\frac{V_x}{V_\infty} = 1 - \frac{2.615\ D_2^2}{4\pi}\left[\frac{2.036}{\{y^2 + (2.036\ D_2)^2\}^{3/2}} - \frac{4.380}{\{y^2 + (4.380\ D_2)^2\}^{3/2}}\right]$$

giving,

r_R	1.0	0.95	0.90	0.80	0.70	0.60	0.50	0.40	0.30
V_x/V_∞	0.9618	0.9617	0.9616	0.9614	0.9612	0.9611	0.9609	0.9608	0.9607
r/R	0.27	0.20	0.10	0					
V_x/V_∞	0.9607	0.9607	0.9607	0.9606					

Table 8. Variation of Axial Component of Velocity with Radius at Windmill Position.

Using Iwasaki's(8) approach and ignoring the small radial flow and the effects of drag ($C_D = 0$), the windmill's drag coefficient is given by

$$C_W = 2\int_{boss}^{1} \frac{B\Gamma}{\pi VR}\sqrt{1+\mu^2}\cos\alpha_i \cos\phi\, d\left(\frac{r}{R}\right)$$

Hence, applying Glauert's formula,

$$(C_D)_{ICALC} = \text{interactive force}/0.5\rho\,(A)_{D2}\,V_\infty^2$$

$$= \int h\, dT_a/0.5\rho\,(A)_{D2}\,V_\infty^2$$

$$= 2\left(\frac{D_1}{D_2}\right)^2 \int_{boss}^{1} \left(1 - \frac{V_x}{V_\infty}\right) \frac{B\Gamma}{\pi VR}\sqrt{1+\mu^2}\cos\alpha_i \cos\phi\, d\left(\frac{r}{R}\right)$$

The above integral for $(C_D)_{ICALC}$ was evaluated employing the Newton-Cotes 3 ordinate numerical integration rule between r/R = 1.0 and 0.3 and the trapezoidal rule between r/R = 0.3 and 0.27 and gave

$$(C_D)_{ICALC} = 0.00653$$

The corresponding value for $(C_D)_{ICALC}$ using, from Section 5 of Appendix 5, the equation for the difference between the free and apparent drags of the equivalent gauze shield

$$(C_D)_{ICALC} = (D_1/D_2)^2 \{0.650 - (\text{drag}/0.5\rho\,(A)_{D1}\,V_\infty{}^2)\}$$

$$= 0.650 \times (0.515)^2 - \int_0^{y=0.515D_2/2} \left(\frac{0.650 \times \tfrac{1}{2}\, 2\pi y\, V_x{}^2\, dy}{\tfrac{1}{2}\rho \frac{\pi D_2{}^2}{4} V_\infty{}^2}\right)$$

$$= 0.172 - 0.159 = 0.013$$

As stated in Section 5 of Appendix 5, it was the disparity between the above values for $(C_D)_{ICALC}$ which led to abandoning the Glauert formula in favour of the latter for calculating the mutual interference force coefficient for gauze and solid discs in tandem.

FIGURE No. 1

SIMPLE SHIELDING THEORY. FLOW OVER A BODY IN A TUNNEL

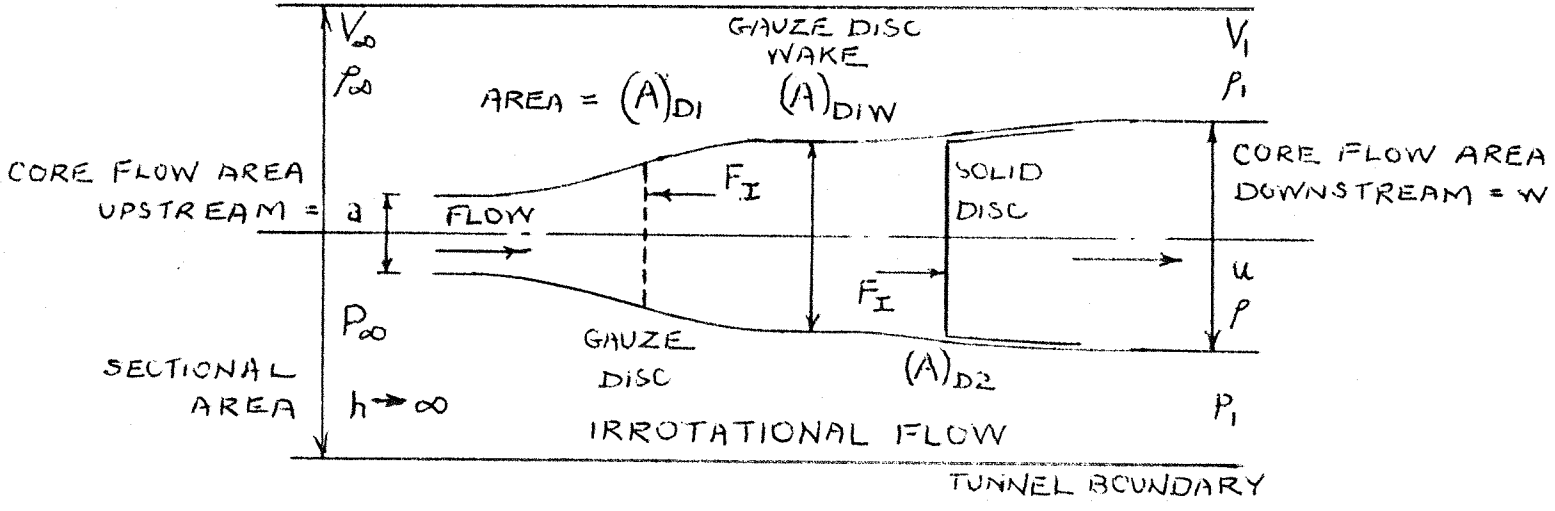

F_I = MUTUAL INTERFERENCE FORCE

FIGURE NO. 2

ROSHKO AND KOENIG SEMI-INFINITE HALFBODY

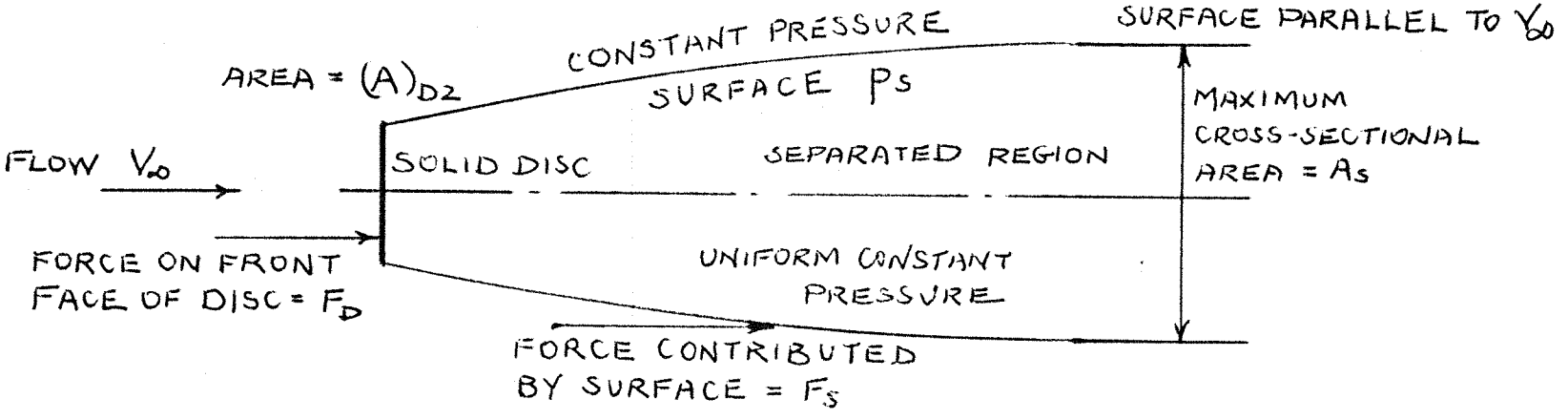

IRROTATIONAL FLOW OVER SURFACES

FIGURE No.3

FLOW THROUGH A WINDMILL

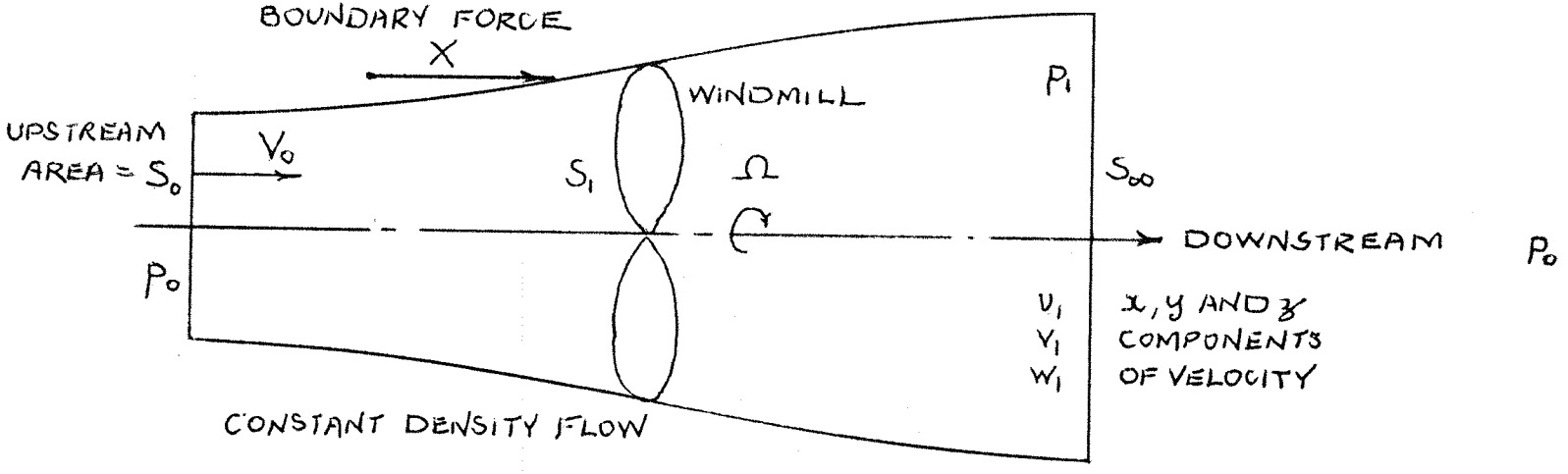

FIGURE No. 4

VORTEX PROPELLER THEORY. FLOW AT AN ELEMENTARY RADIUS

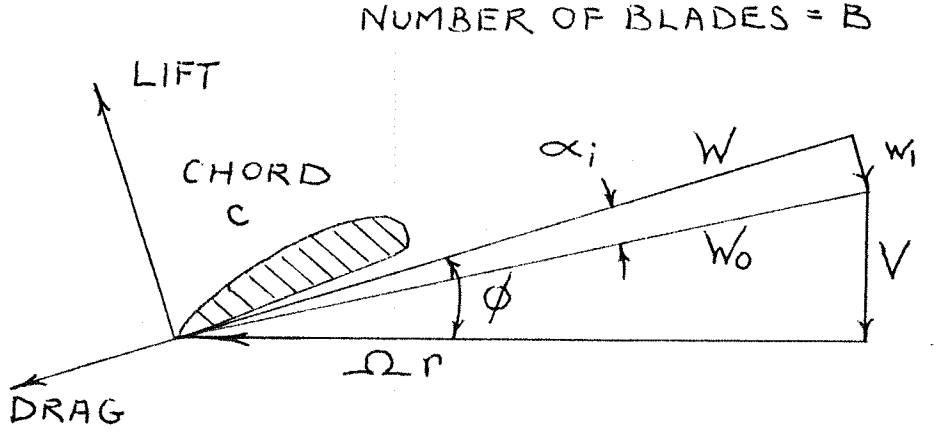

FIGURE No.5

SHAPE AND DIMENSIONS OF GAUZE SHIELDS FOR CAR MODEL CONFIGURATIONS

ALL SHIELDS HELD 39mm AHEAD OF LEADING EDGE OF CAR

ALL DIMENSIONS IN mm MODEL SIZE. SCALE 1:24

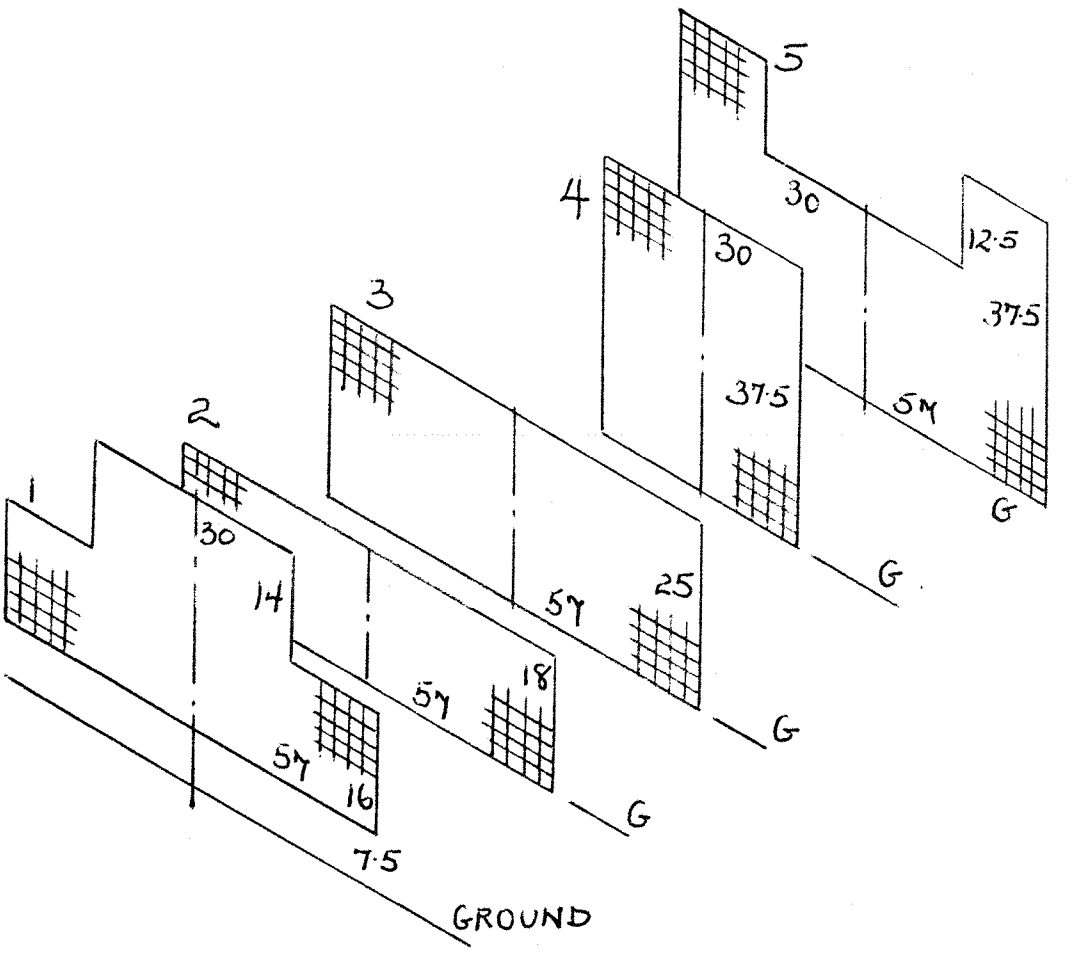

ISOMETRIC VIEWS

FIGURE No. 5

SHAPE AND DIMENSIONS OF GAUZE SHIELDS FOR CAR MODEL CONFIGURATIONS

ALL DIMENSIONS IN mm MODEL SIZE. SCALE 1:24

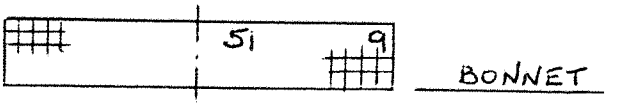

7TH CONFIGURATION BONNET SHIELD

HELD 30mm AHEAD OF LEADING EDGE OF CAB ROOF

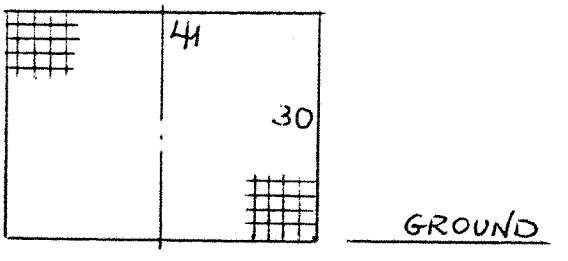

8TH CONFIGURATION

HELD 203mm AHEAD OF LEADING EDGE OF CAB ROOF

FIGURE No. 6

GAUZE AND SOLID DISCS IN TANDEM. $D_1/D_2 = 0.555$

$g/D_2 = 1.79$. VARIATION OF TURBULENCE WITH RADIUS (r) AND DISTANCE FROM SOLID DISC

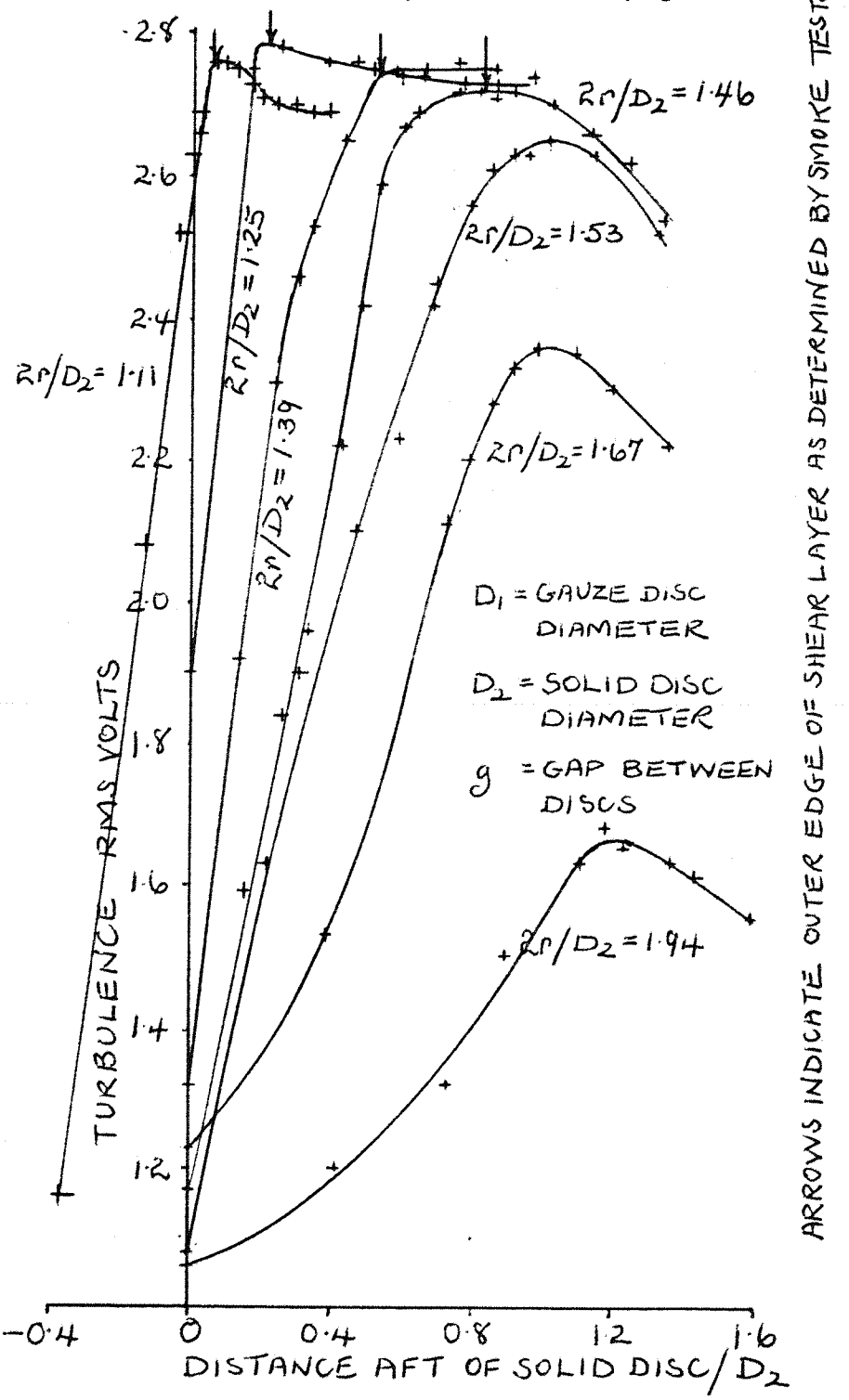

FIGURE No. 7

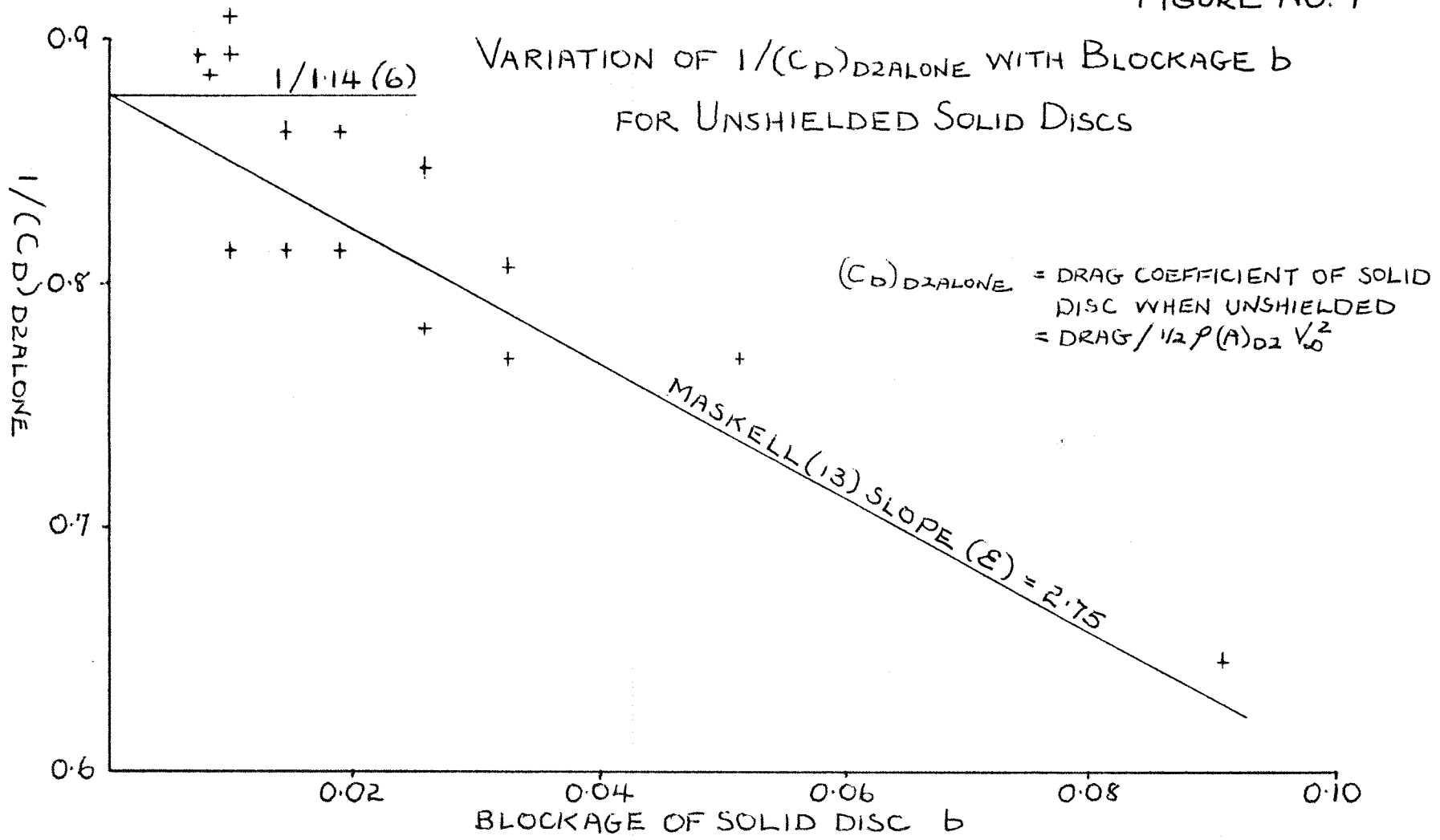
VARIATION OF 1/(C_D)_D2ALONE WITH BLOCKAGE b
FOR UNSHIELDED SOLID DISCS
1/1·14 (6)
MASKELL (13) SLOPE (ε) = 2·75
(C_D)_D2ALONE = DRAG COEFFICIENT OF SOLID DISC WHEN UNSHIELDED
= DRAG / ½ ρ (A)_D2 V_∞²
1/(C_D)_D2ALONE
0·9
0·8
0·7
0·6
0·02
0·04
0·06
0·08
0·10
BLOCKAGE OF SOLID DISC b

FIGURE No. 8

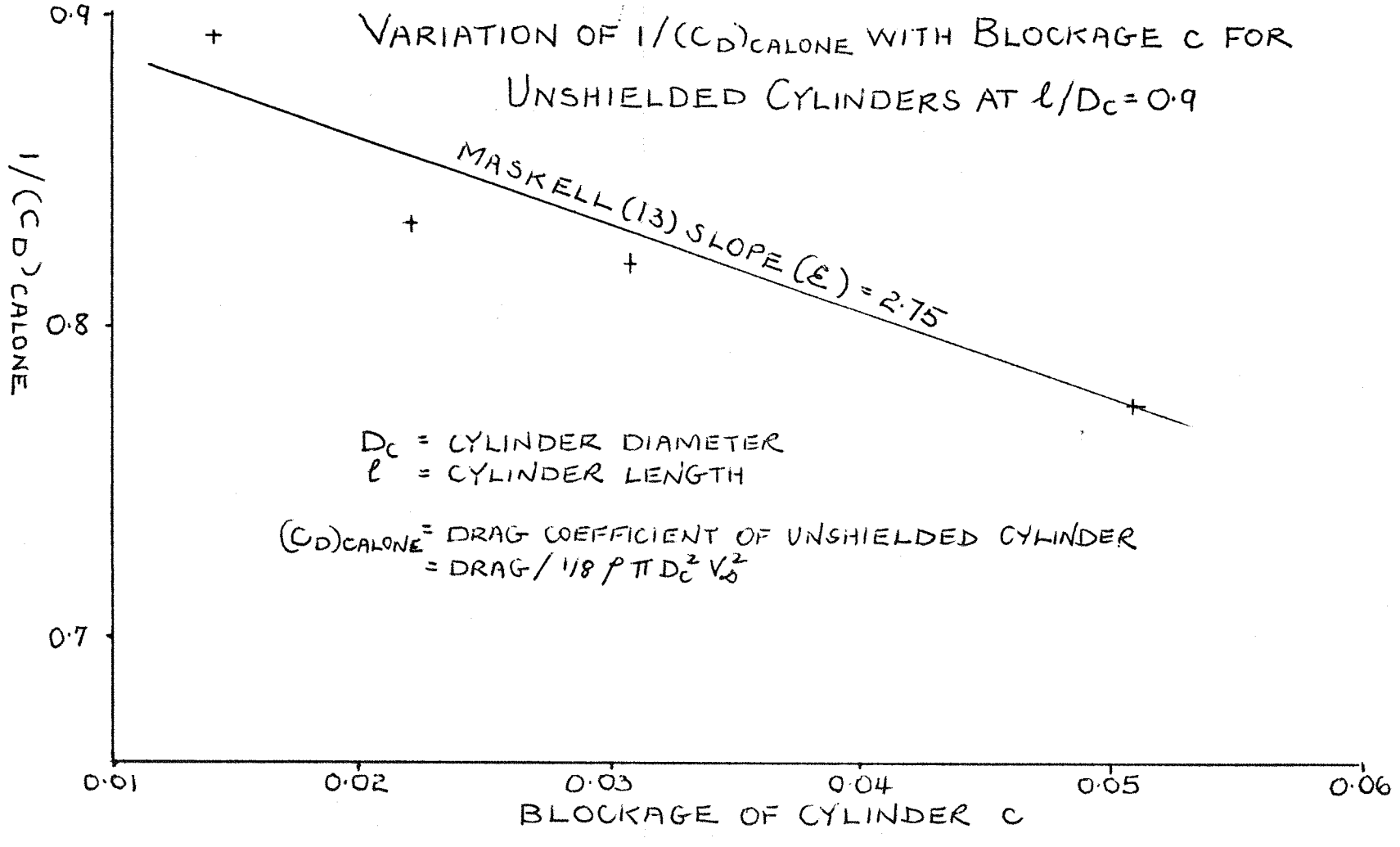
VARIATION OF $1/(C_D)_{CALONE}$ WITH BLOCKAGE c FOR UNSHIELDED CYLINDERS AT $\ell/D_C = 0.9$
MASKELL (13) SLOPE (ε) = 2.75
$1/(C_D)_{CALONE}$
0.9
0.8
0.7
0.01
0.02
0.03
0.04
0.05
0.06
BLOCKAGE OF CYLINDER c
D_C = CYLINDER DIAMETER
ℓ = CYLINDER LENGTH
$(C_D)_{CALONE}$ = DRAG COEFFICIENT OF UNSHIELDED CYLINDER
= DRAG / $1/8\ \rho\ \pi\ D_C^2\ V_0^2$

FIGURE No. 9

FLOW LINES FOR GAUZE AND SOLID DISCS IN TANDEM
$D_1/D_2 = 0.6 \quad g/D_2 = 2.0$

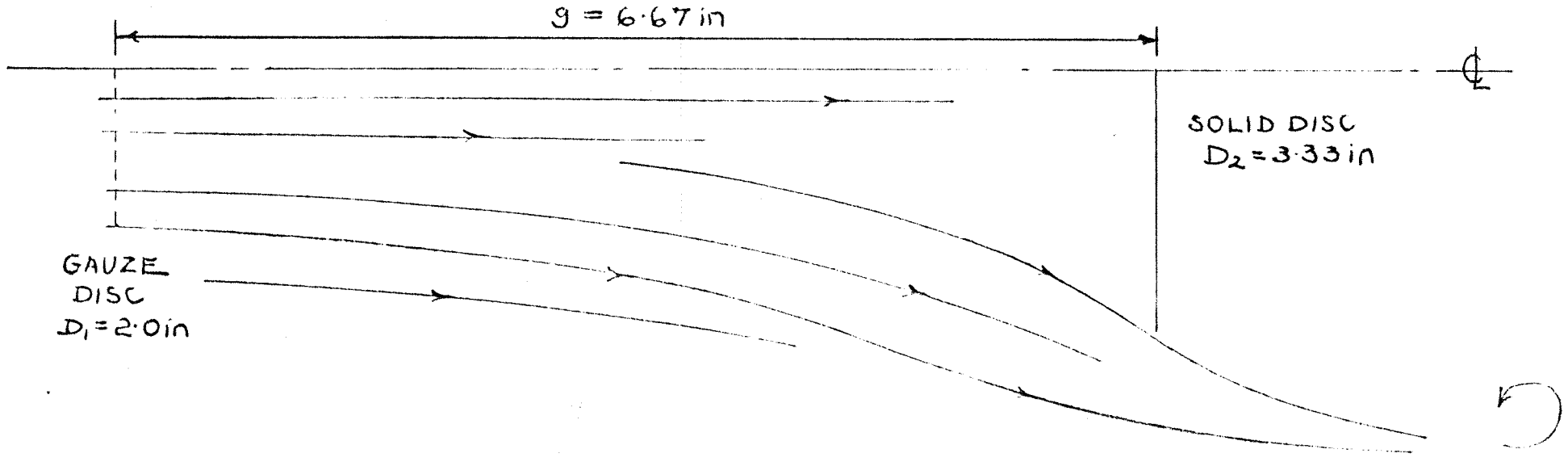

FIGURE No.10

FLOW LINE ANGLES (θ) FOR GAUZE AND SOLID DISCS IN TANDEM

$D_1/D_2 = 0.555$ $g/D_2 = 1.79$

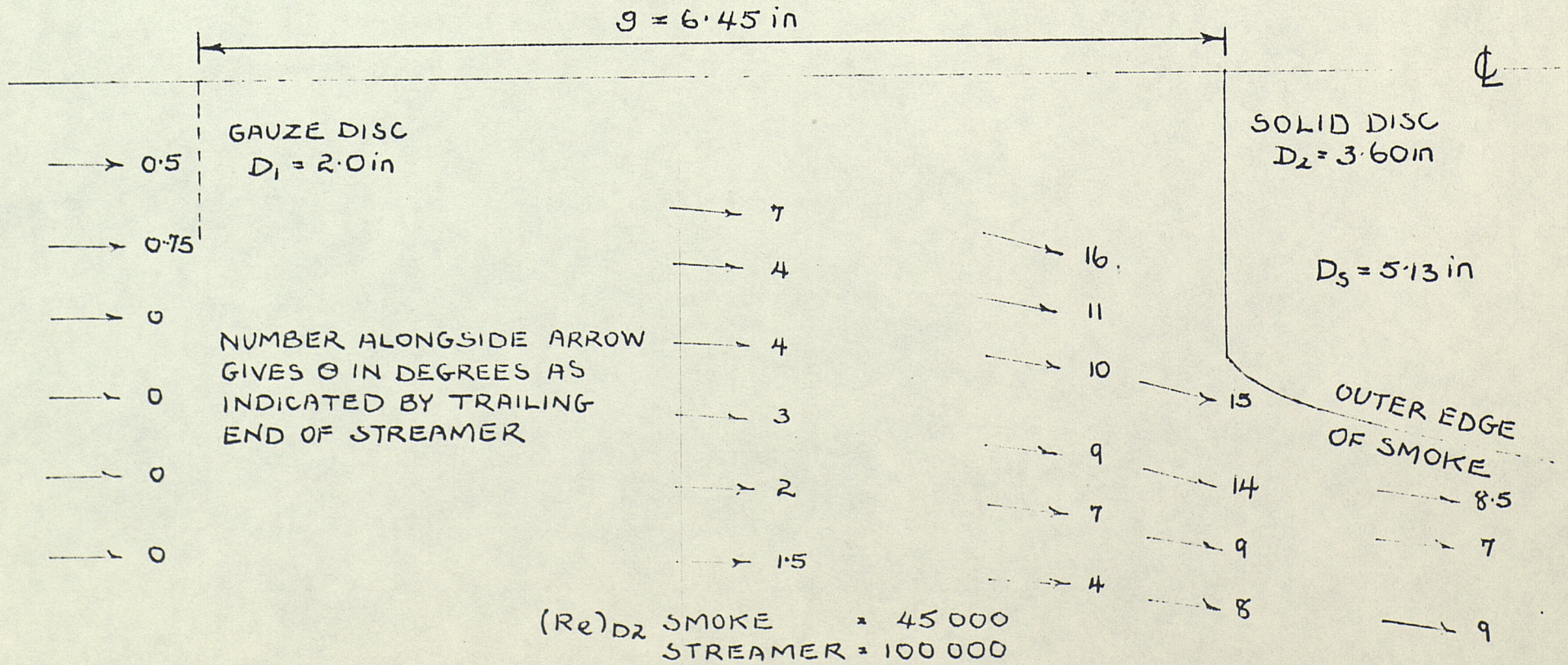

FIGURE No.11

FLOW LINE ANGLES (θ) FOR GAUZE AND SOLID DISCS IN TANDEM

$D_1/D_2 = 0.726$ $g/D_2 = 2.34$

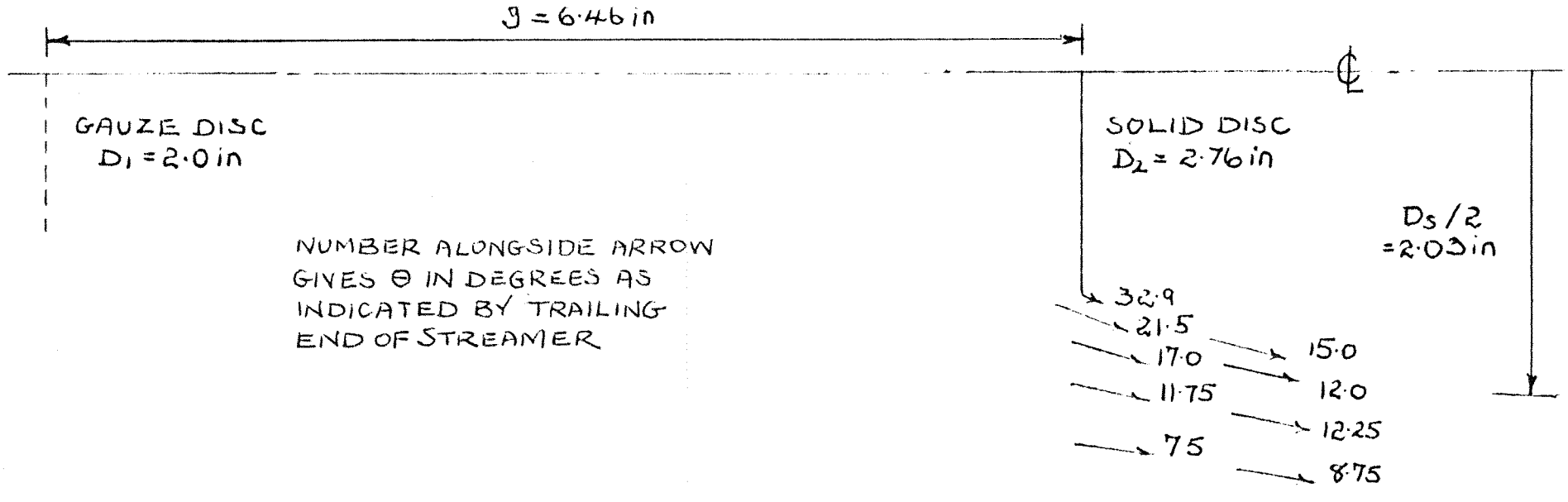

FIGURE No. 12

FLOW LINE ANGLES (θ) FOR GAUZE AND SOLID DISCS IN TANDEM

$D_1/D_2 = 0.726 \quad g/D_2 = 1.80$

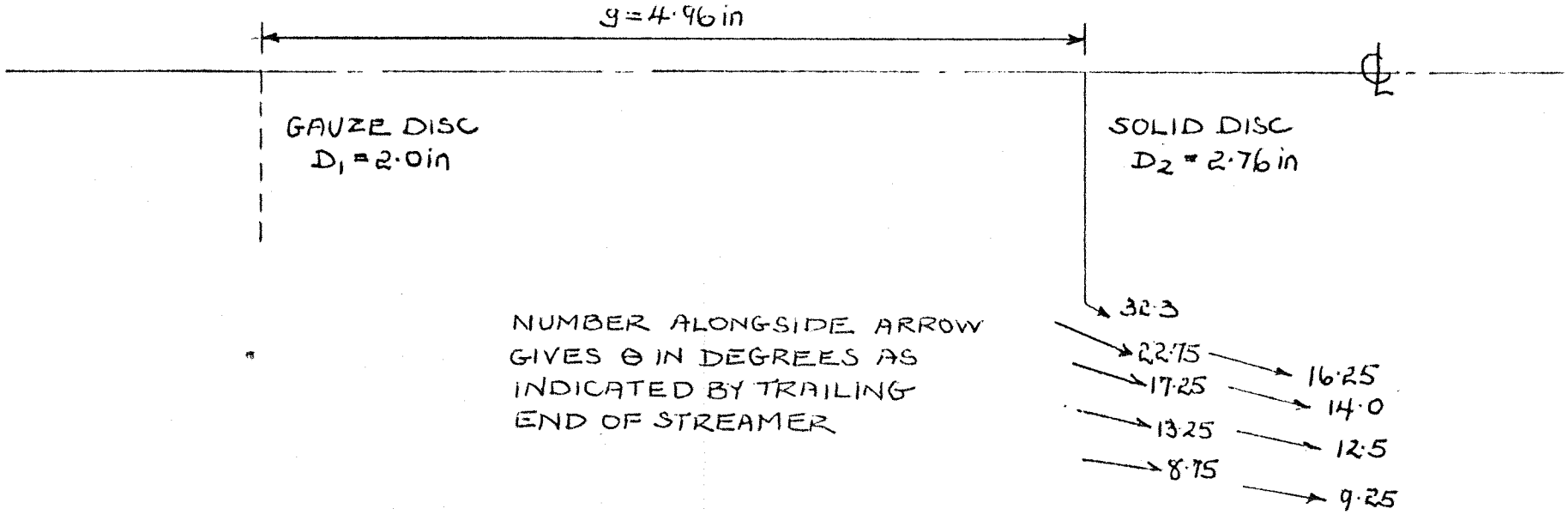

FIGURE No.13

FLOW LINE ANGLES (θ) FOR GAUZE AND SOLID DISCS IN TANDEM

$D_1/D_2 = 0.726 \quad g/D_2 = 1.27$

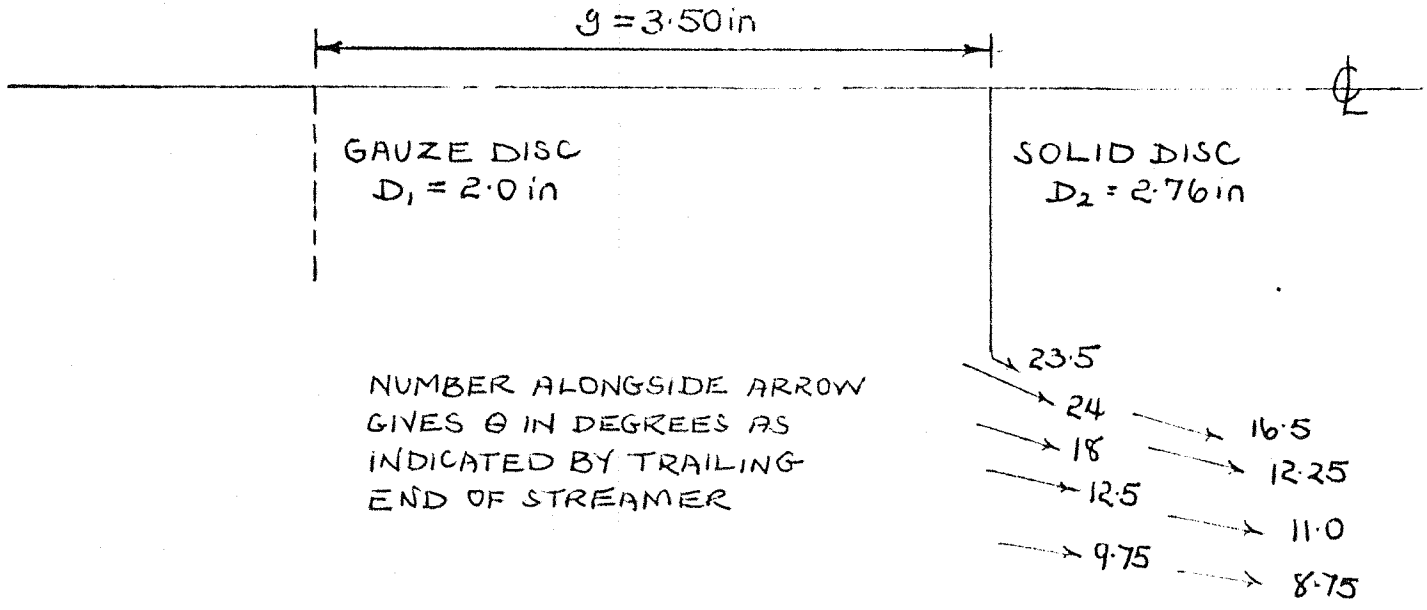

FIGURE No.14

POLAR COORDINATES OF PRESSURE TAPPINGS ON FACE OF SOLID DISC. D_2 = 3·601 in

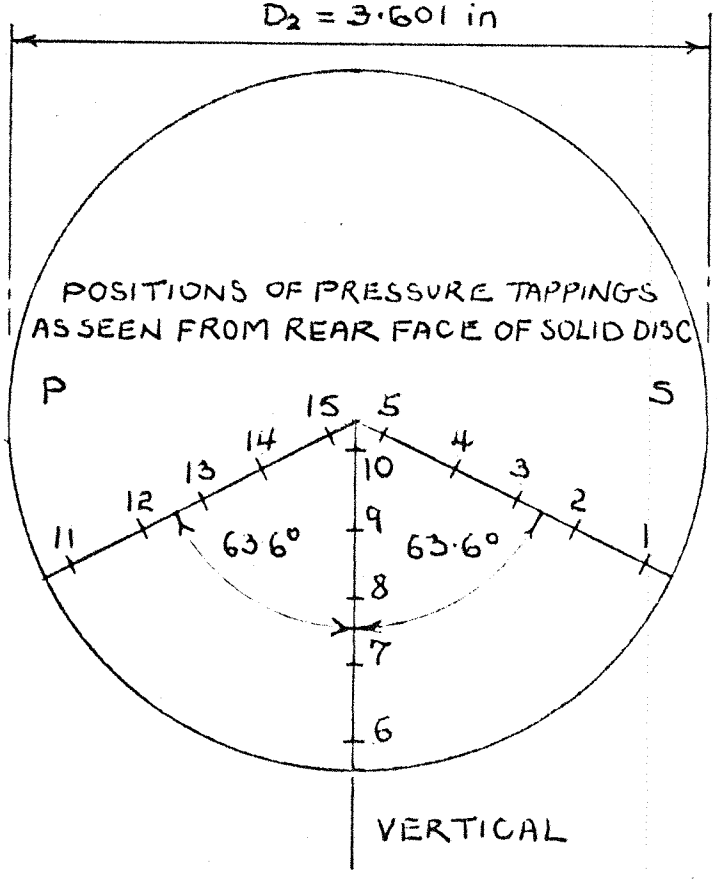

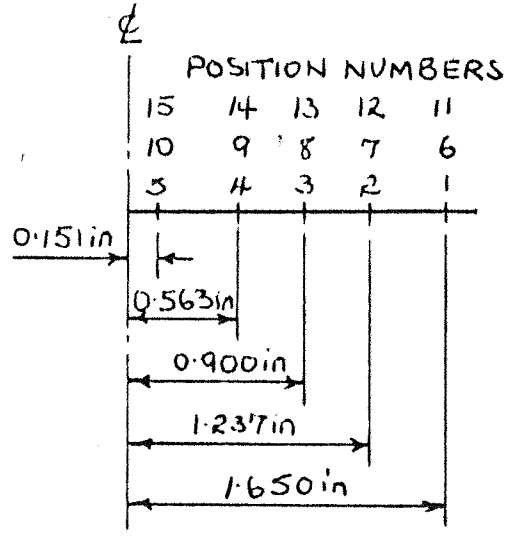

RADIAL DISTANCES

FIGURE No.15

DOUBLE TUBE VELOCITY MEASURING DEVICE

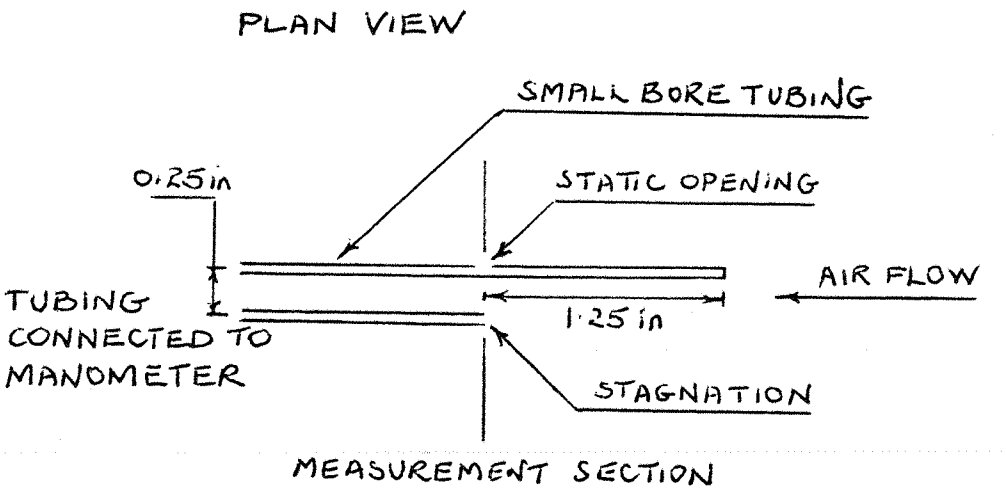

FIGURE No.16.

DIAGRAMMATIC SKETCH OF MUTUAL INTERFERENCE FORCE APPARATUS

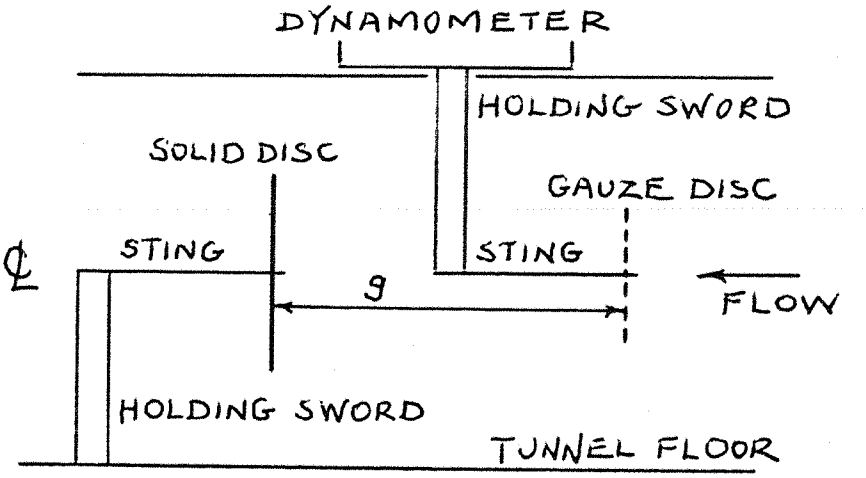

FIGURE No. 17

DIAGRAMMATIC SKETCH OF SMOKE APPARATUS

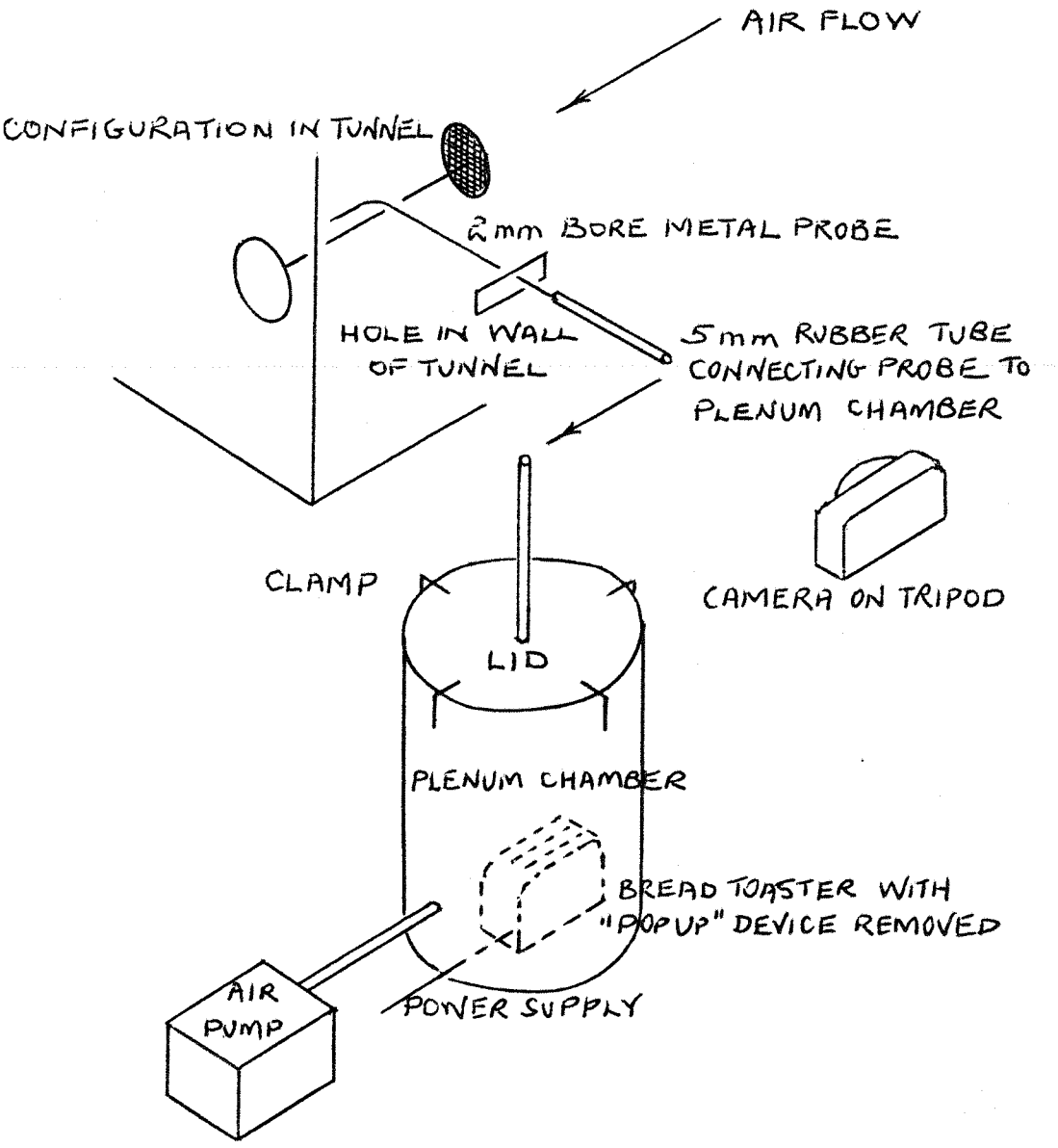

FIGURE No. 18

POSITIONING OF PRESSURE TUBE TO GIVE A SINGLE REPRESENTATIVE READING OF BACK PRESSURE ON SOLID DISC

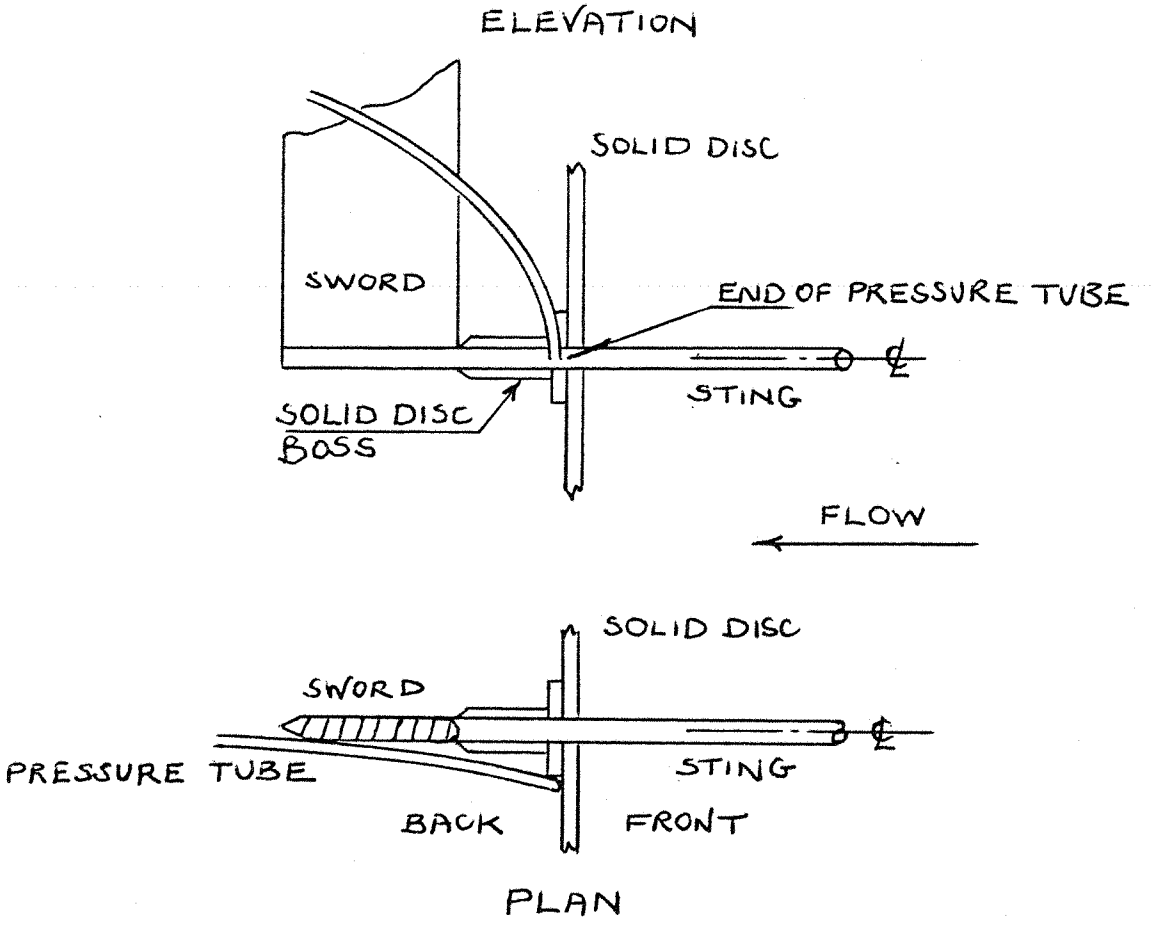

FIGURE NO. 19

VARIATION OF MINIMUM DRAG COEFFICIENT WITH DIAMETER RATIO FOR GAUZE AND SOLID DISCS IN TANDEM. COMPARISON WITH SIMPLE SHIELDING THEORY

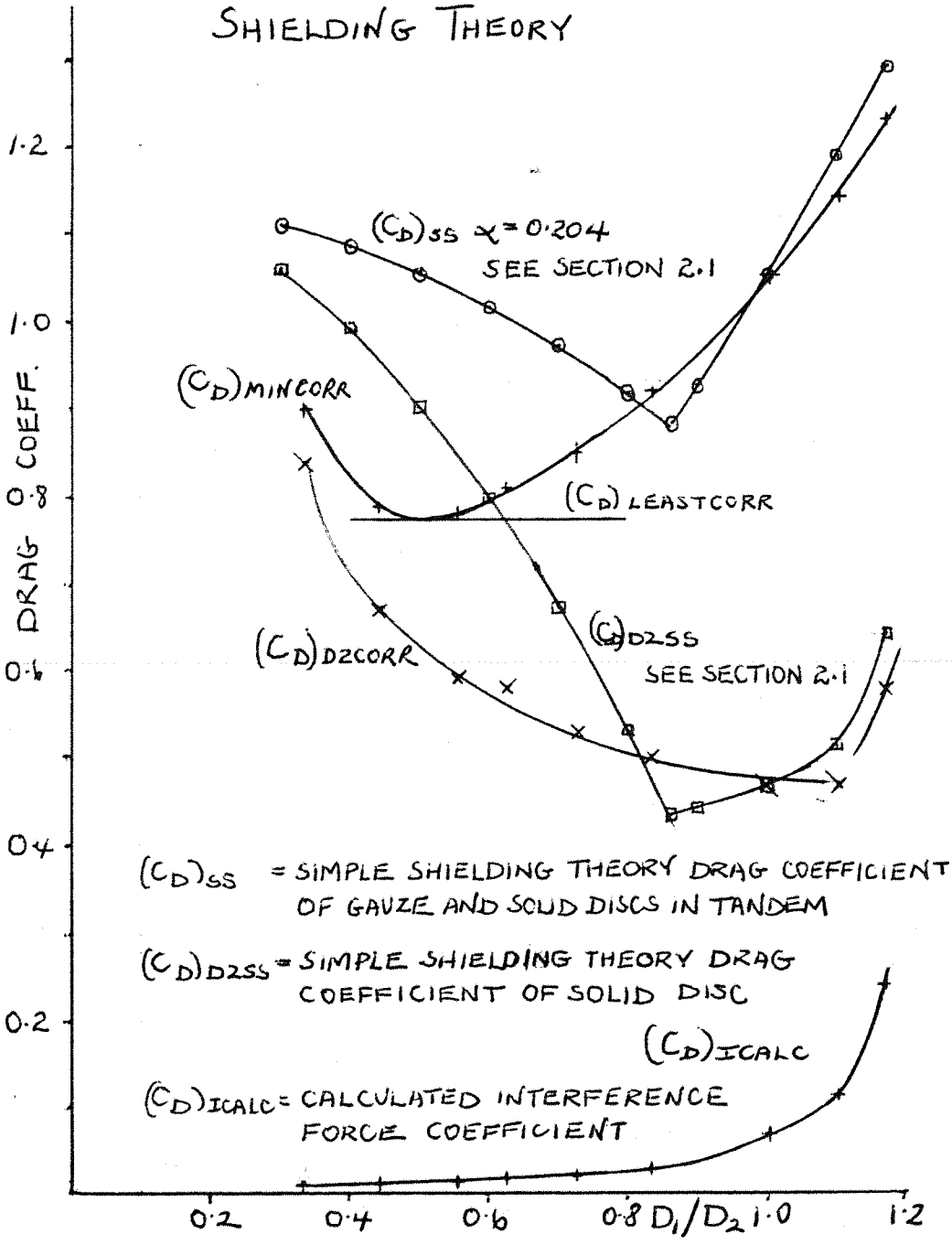

$(C_D)_{SS}$ = SIMPLE SHIELDING THEORY DRAG COEFFICIENT OF GAUZE AND SOLID DISCS IN TANDEM

$(C_D)_{D2SS}$ = SIMPLE SHIELDING THEORY DRAG COEFFICIENT OF SOLID DISC

$(C_D)_{ICALC}$ = CALCULATED INTERFERENCE FORCE COEFFICIENT

$(C_D)_{MINCORR}$ = EXPERIMENTALLY DERIVED MINIMUM DRAG COEFFICIENT CORRECTED FOR BLOCKAGE

$(C_D)_{D2CORR}$ = EXPERIMENTALLY DERIVED DRAG COEFFICIENT OF SOLID DISC CORRECTED FOR BLOCKAGE WHEN IN TANDEM WITH GAUZE DISC

FIGURE NO. 20

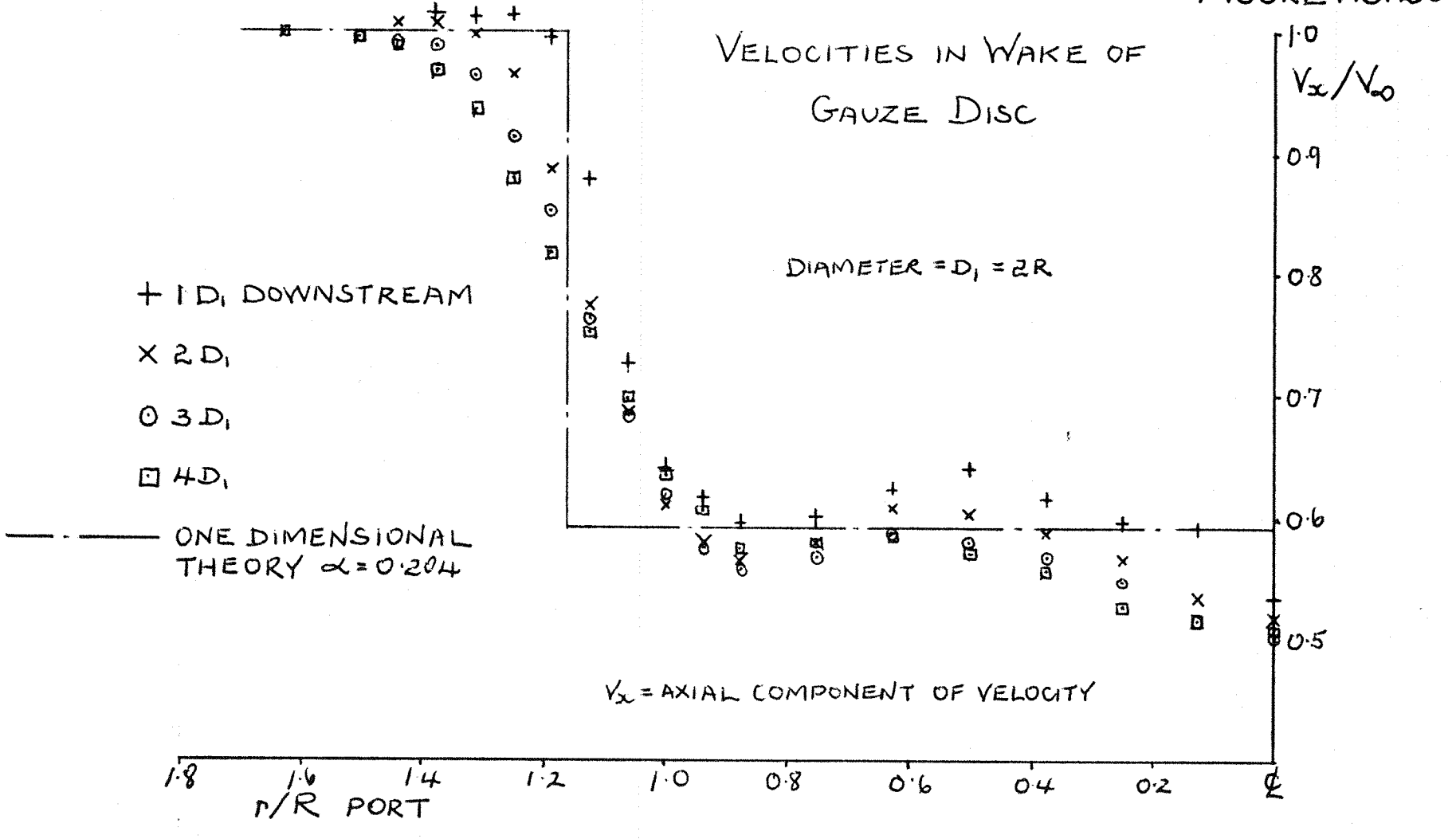
VELOCITIES IN WAKE OF GAUZE DISC
DIAMETER = D_1 = 2R
+ 1 D_1 DOWNSTREAM
× 2 D_1
⊙ 3 D_1
⊡ 4 D_1
ONE DIMENSIONAL THEORY α = 0·204
V_x = AXIAL COMPONENT OF VELOCITY
V_x/V_∞
1·0
0·9
0·8
0·7
0·6
0·5
1·8
1·6
1·4
1·2
1·0
0·8
0·6
0·4
0·2
℄
r/R PORT

FIGURE No. 20

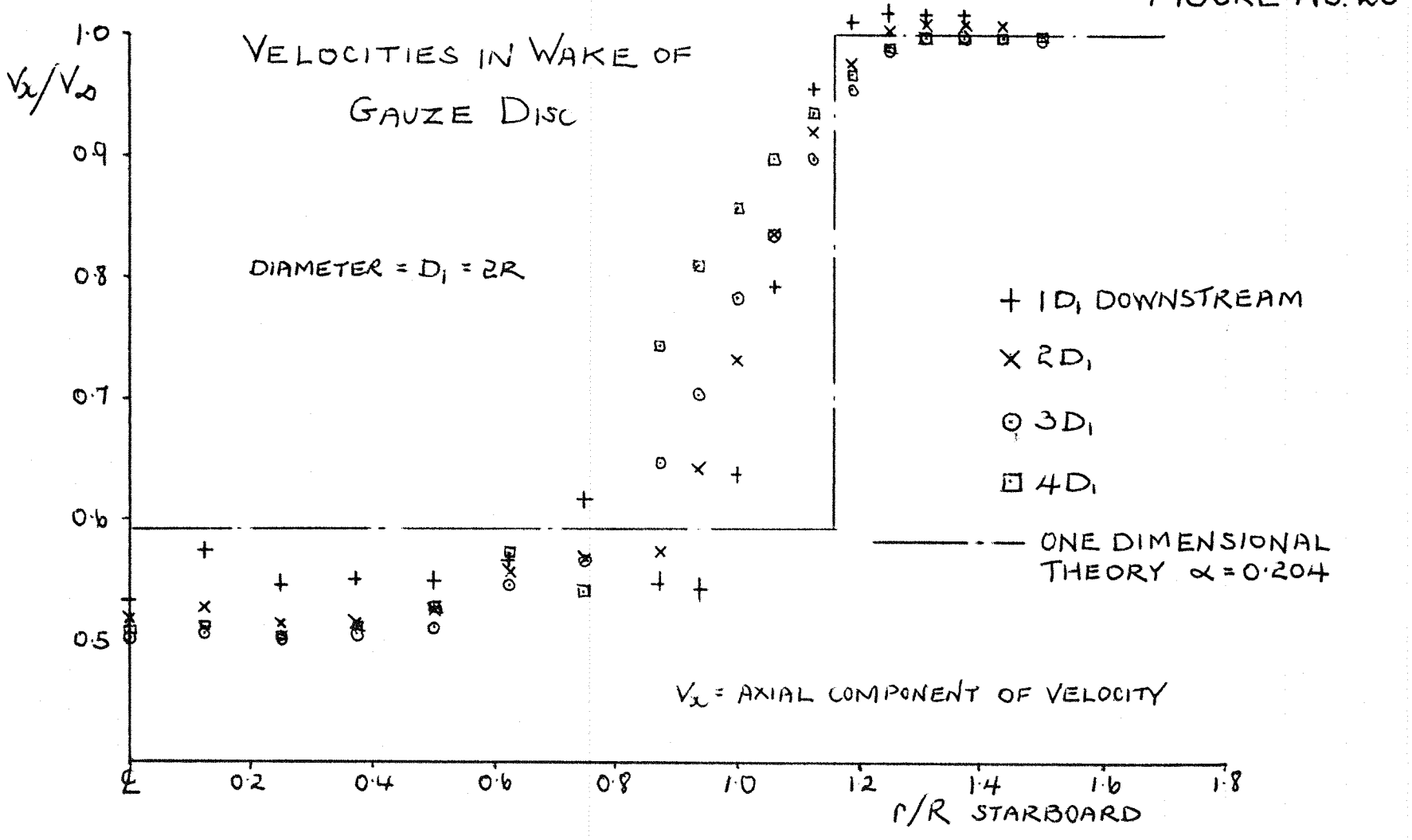
VELOCITIES IN WAKE OF GAUZE DISC
DIAMETER = D_1 = 2R
V_x/V_∞
1·0
0·9
0·8
0·7
0·6
0·5
+ $1D_1$ DOWNSTREAM
× $2D_1$
⊙ $3D_1$
⊡ $4D_1$
ONE DIMENSIONAL THEORY $\alpha = 0.204$
V_x = AXIAL COMPONENT OF VELOCITY
℄
0·2
0·4
0·6
0·8
1·0
1·2
1·4
1·6
1·8
r/R STARBOARD

FIGURE No.21

SIMPLIFIED REPRESENTATION OF THE VELOCITY DISTRIBUTION IN THE WAKE OF THE GAUZE DISC AT $x/D_1 = 4$

D_1 = DIAMETER OF GAUZE DISC
x = DISTANCE DOWNSTREAM OF GAUZE DISC
V_∞ = FREE STREAM VELOCITY
V_x = AXIAL COMPONENT OF VELOCITY IN WAKE

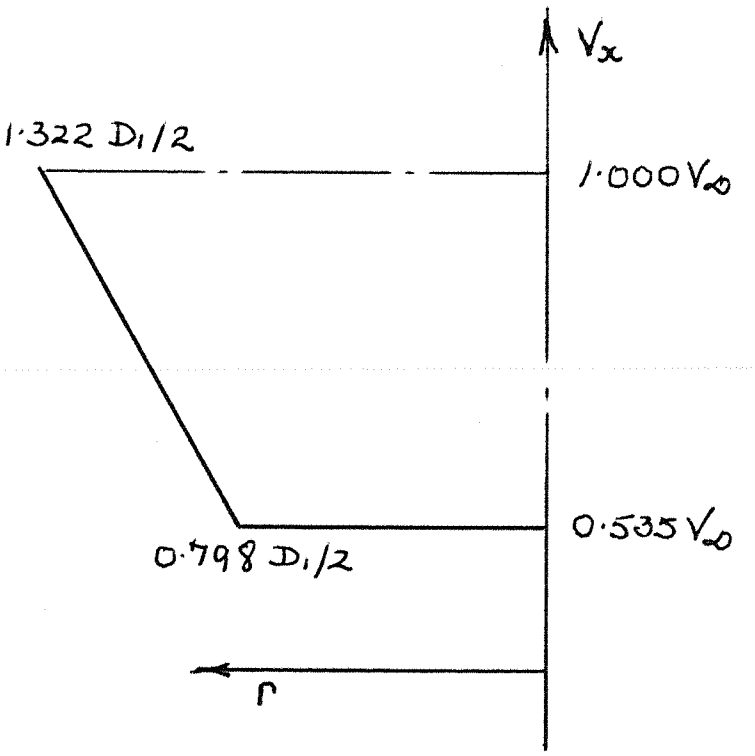

FIGURE No.22

RANKINE OVOID USED IN CALCULATION OF MUTUAL INTERFERENCE

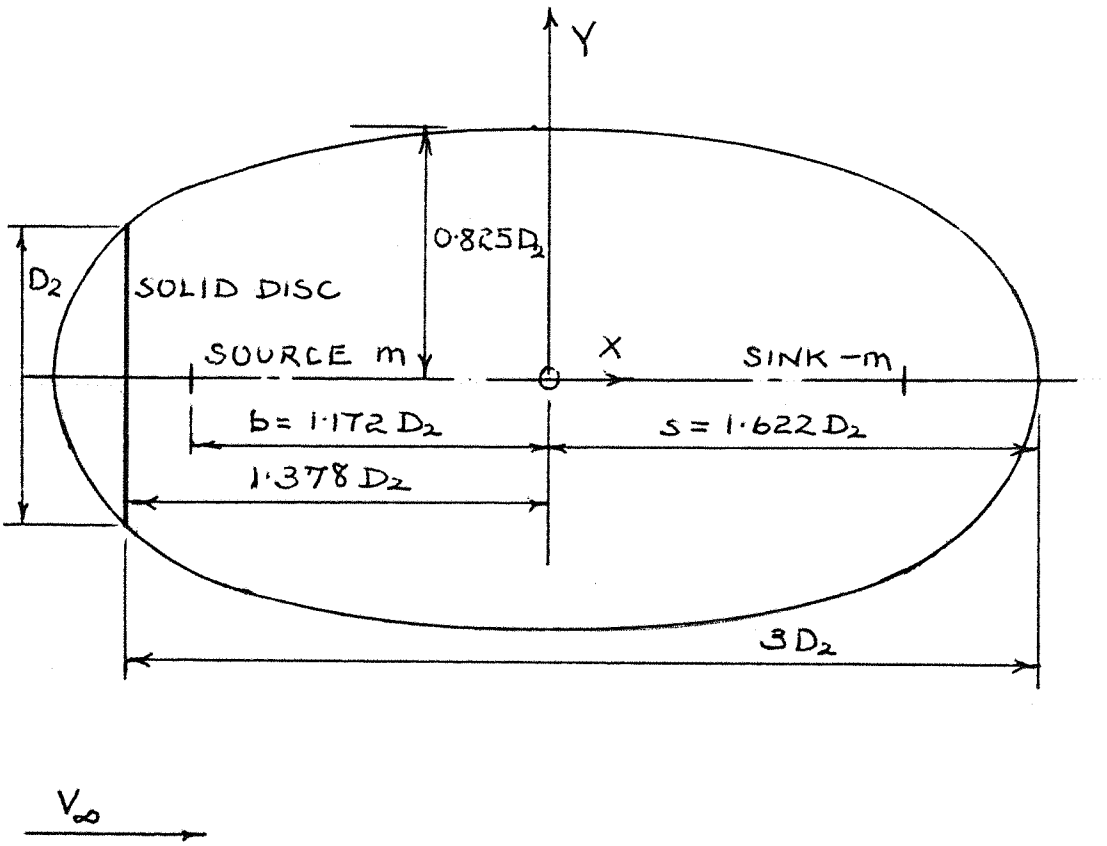

FIGURE No. 23

IWASAKI DATA FOR 3 BLADED WINDMILLS

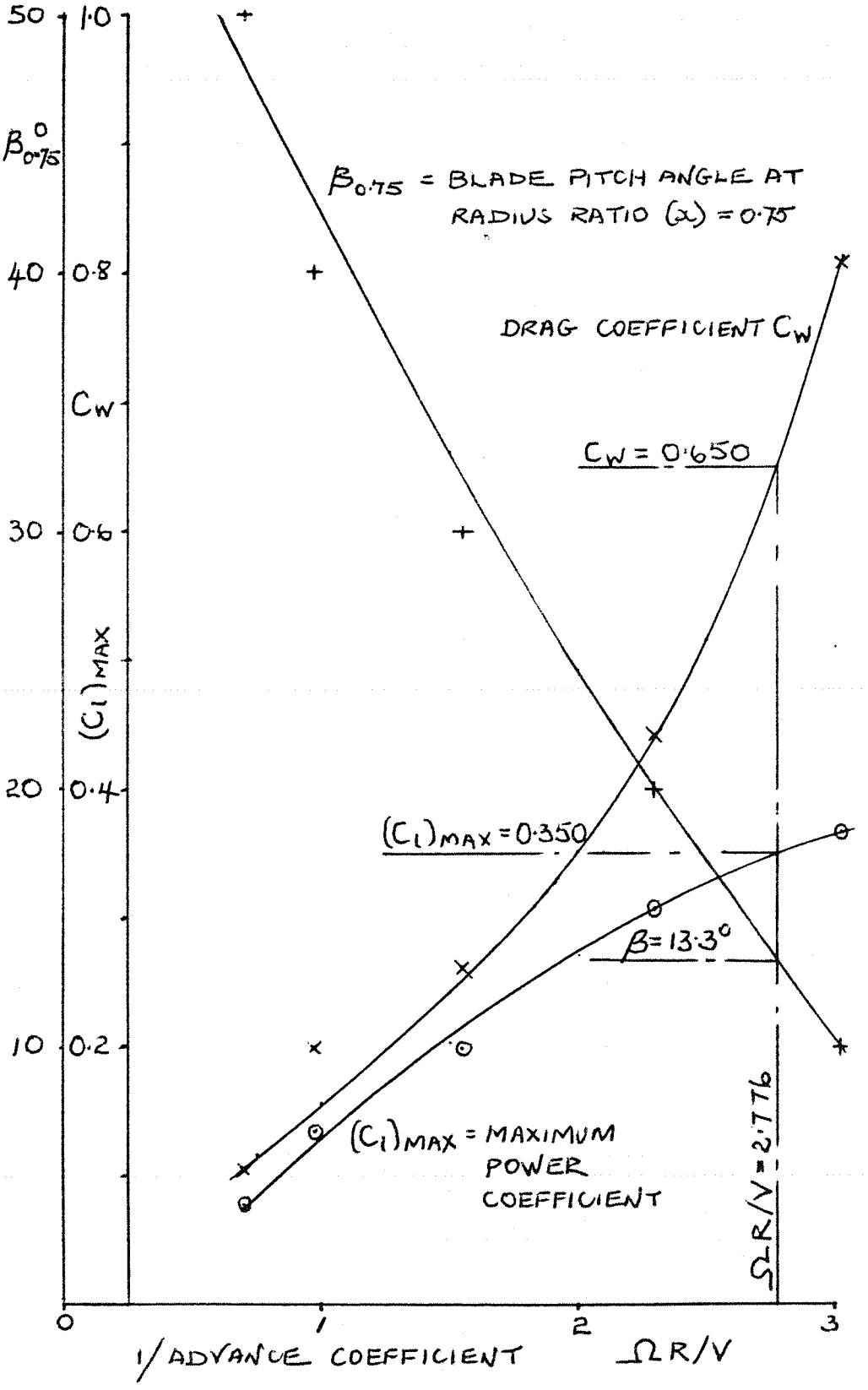

FIGURE No. 24

CHARACTERISTICS OF GÖTTINGEN 623 SECTION

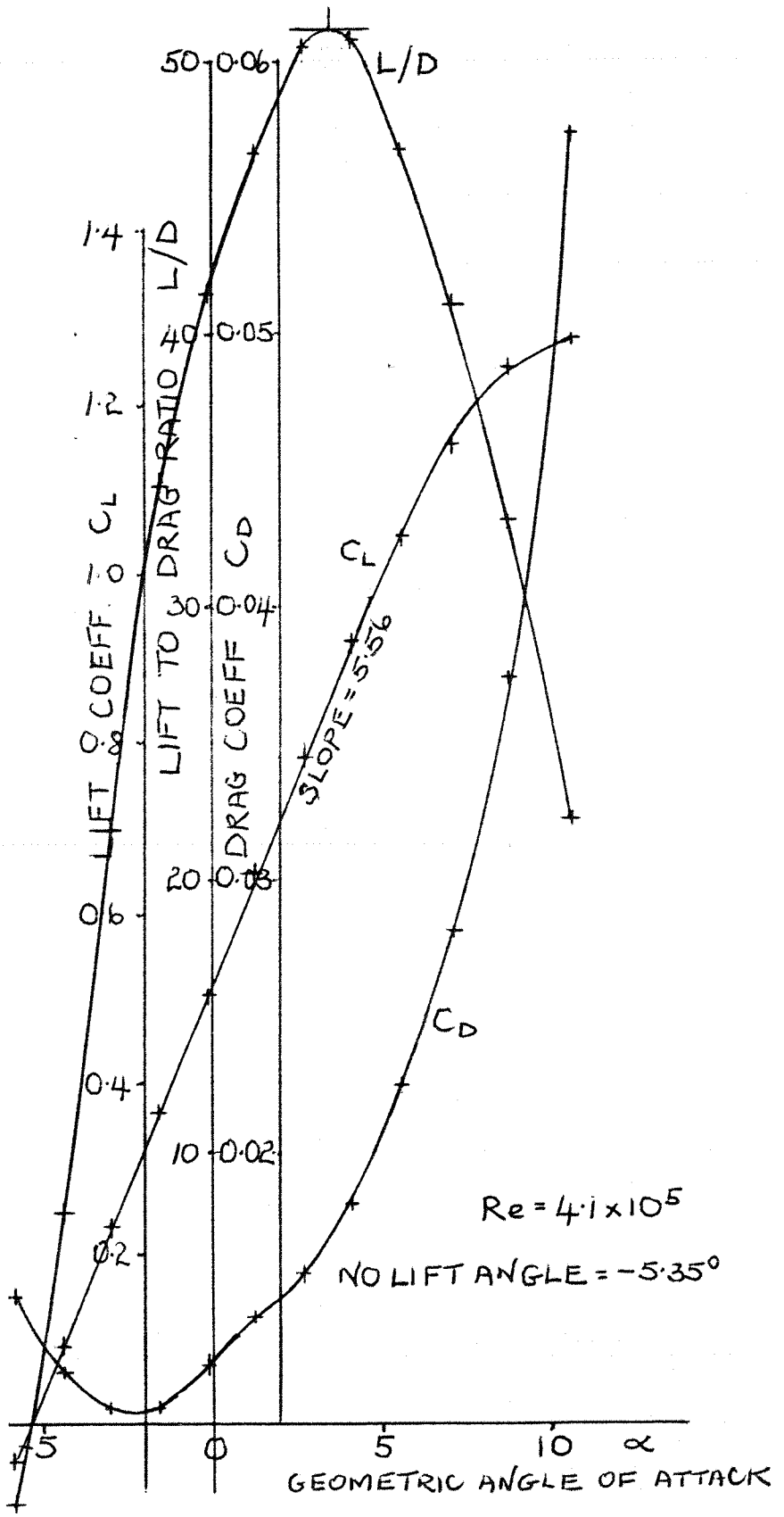

FIGURE No. 25

GEOMETRIC DETAILS OF EQUIVALENT WINDMILL

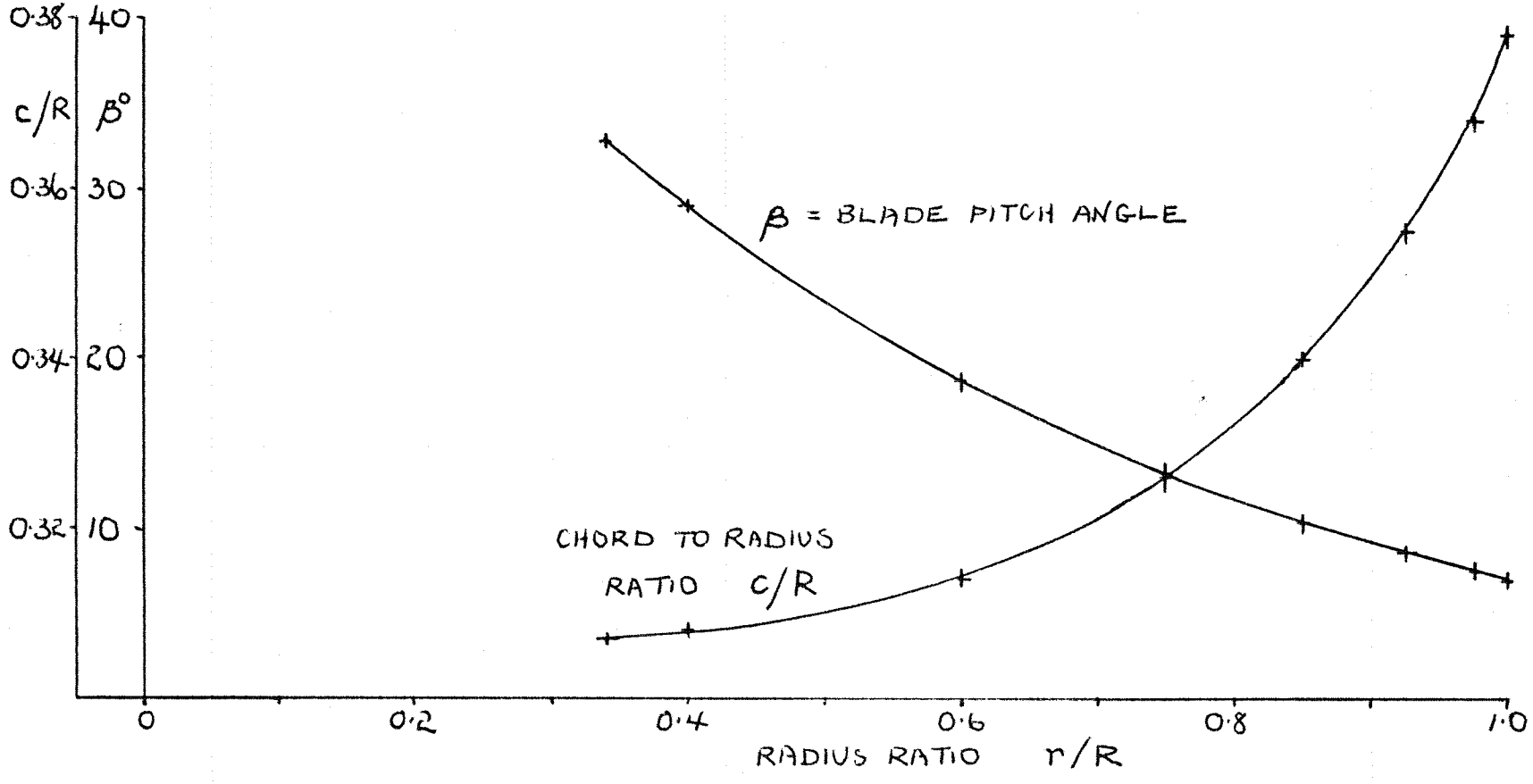

FIGURE No. 26

VARIATION OF C_D WITH g/D_2 FOR $D_1/D_2 = 1.003$ & 0.833

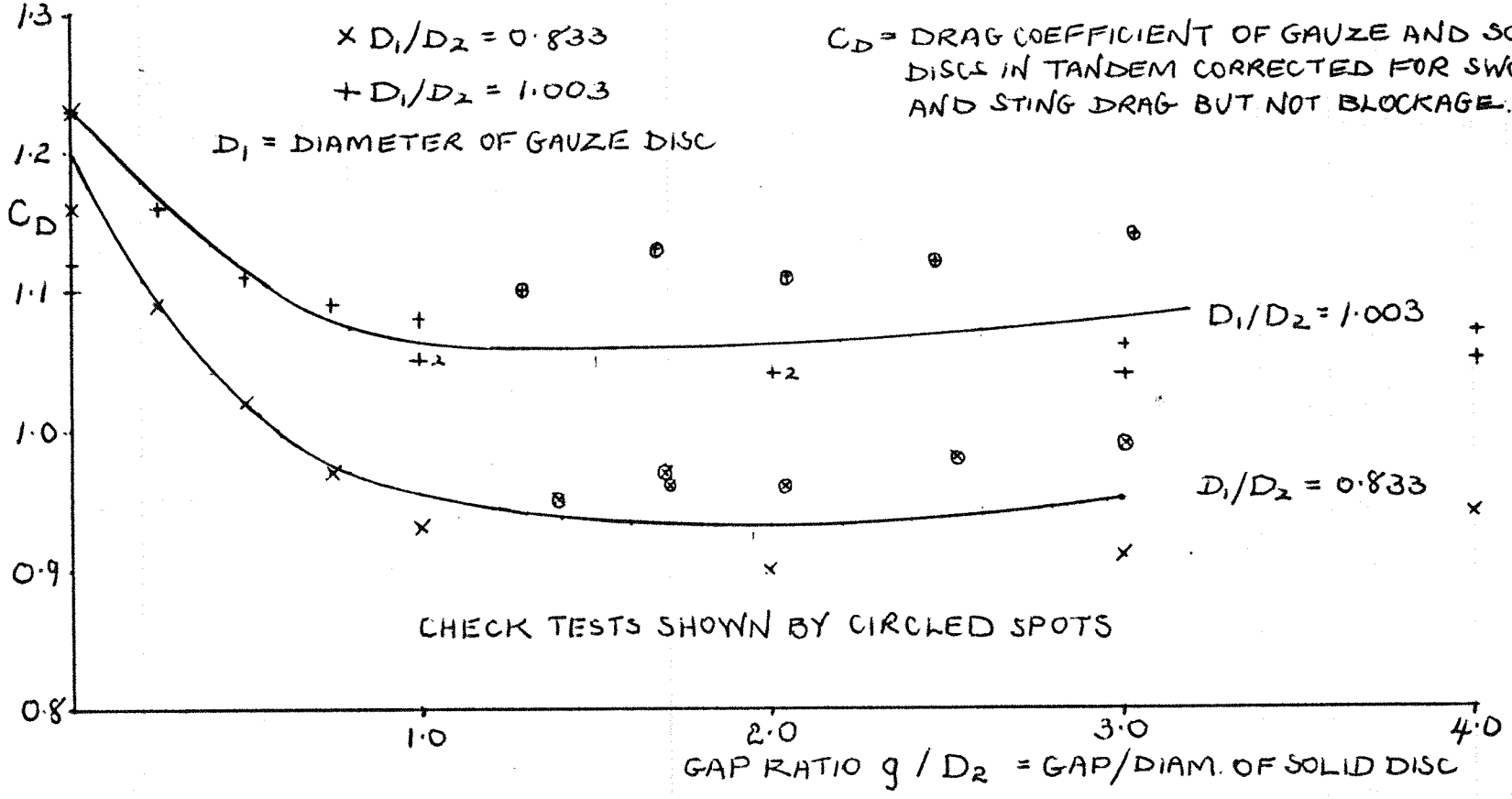

g = GAP BETWEEN GAUZE AND SOLID DISCS IN TANDEM

FIGURE No. 27

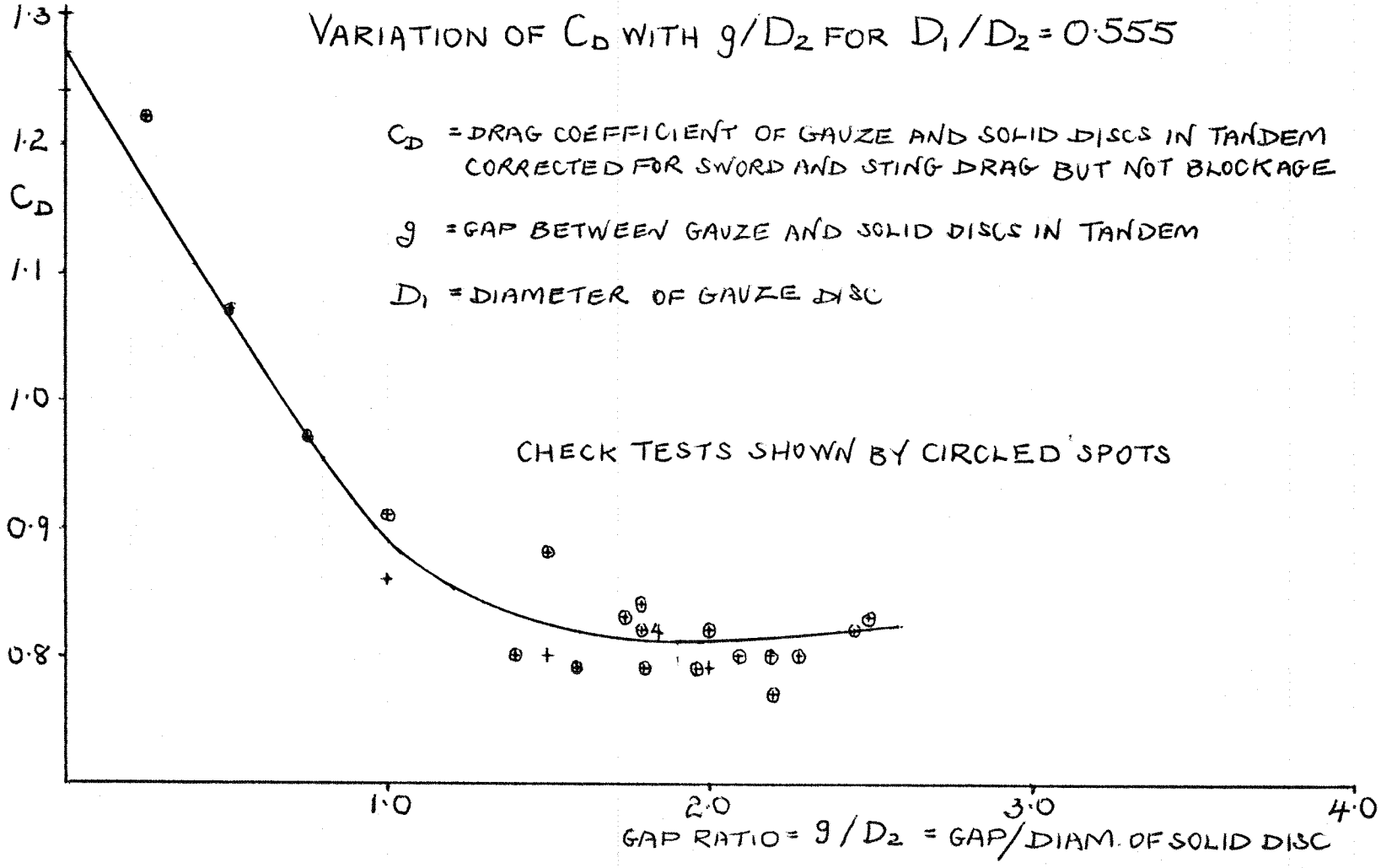
VARIATION OF C_D WITH g/D_2 FOR $D_1/D_2 = 0.555$
C_D = DRAG COEFFICIENT OF GAUZE AND SOLID DISCS IN TANDEM CORRECTED FOR SWORD AND STING DRAG BUT NOT BLOCKAGE
g = GAP BETWEEN GAUZE AND SOLID DISCS IN TANDEM
D_1 = DIAMETER OF GAUZE DISC
CHECK TESTS SHOWN BY CIRCLED SPOTS
1·3
1·2
C_D
1·1
1·0
0·9
0·8
1·0
2·0
3·0
4·0
GAP RATIO = g/D_2 = GAP/DIAM. OF SOLID DISC

FIGURE No. 28

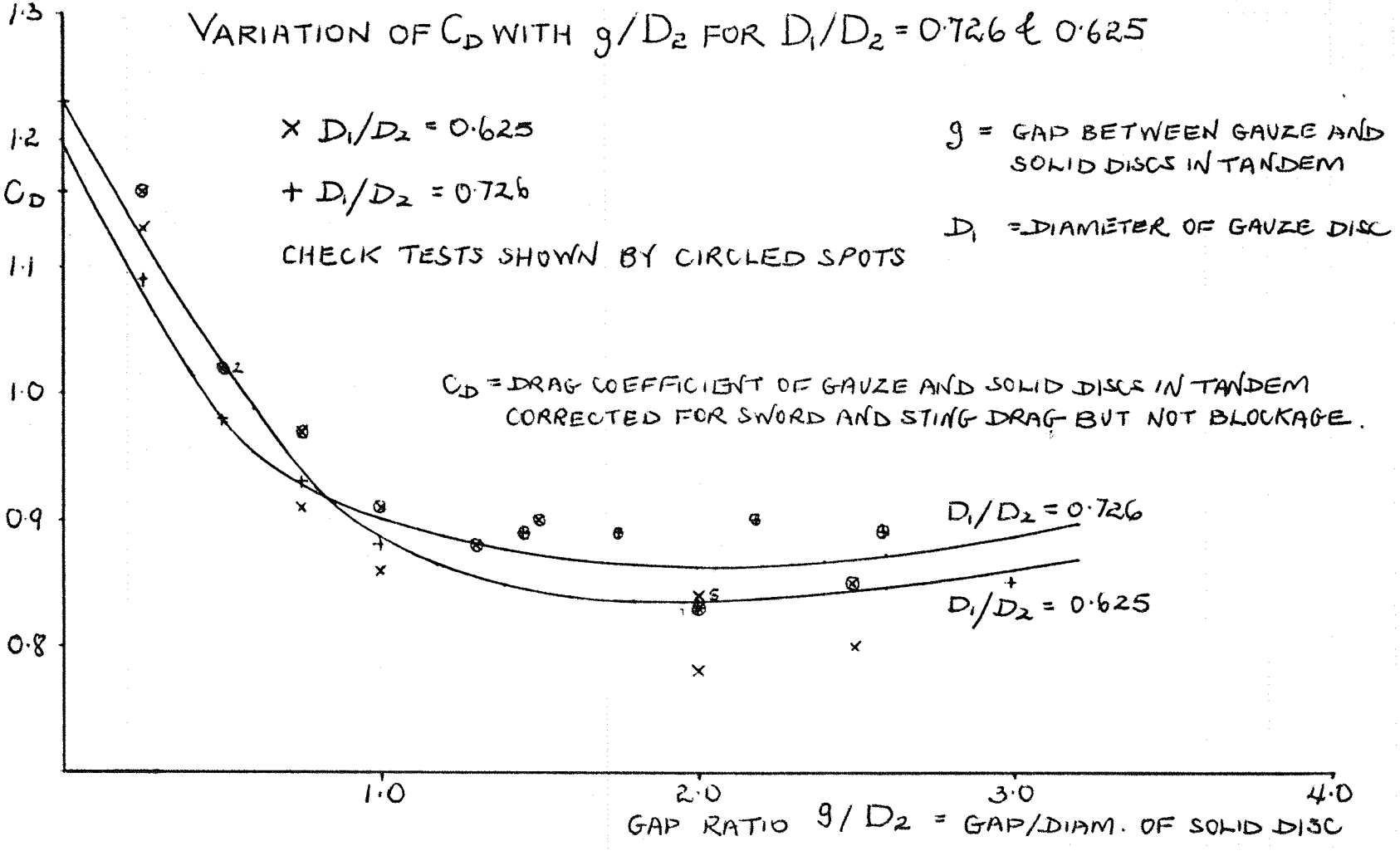
VARIATION OF C_D WITH g/D_2 FOR $D_1/D_2 = 0.726$ & 0.625
× $D_1/D_2 = 0.625$
+ $D_1/D_2 = 0.726$
CHECK TESTS SHOWN BY CIRCLED SPOTS
g = GAP BETWEEN GAUZE AND SOLID DISCS IN TANDEM
D_1 = DIAMETER OF GAUZE DISC
C_D = DRAG COEFFICIENT OF GAUZE AND SOLID DISCS IN TANDEM CORRECTED FOR SWORD AND STING DRAG BUT NOT BLOCKAGE.
$D_1/D_2 = 0.726$
$D_1/D_2 = 0.625$
1·3
1·2
C_D
1·1
1·0
0·9
0·8
1·0
2·0
3·0
4·0
GAP RATIO g/D_2 = GAP/DIAM. OF SOLID DISC

FIGURE No. 29

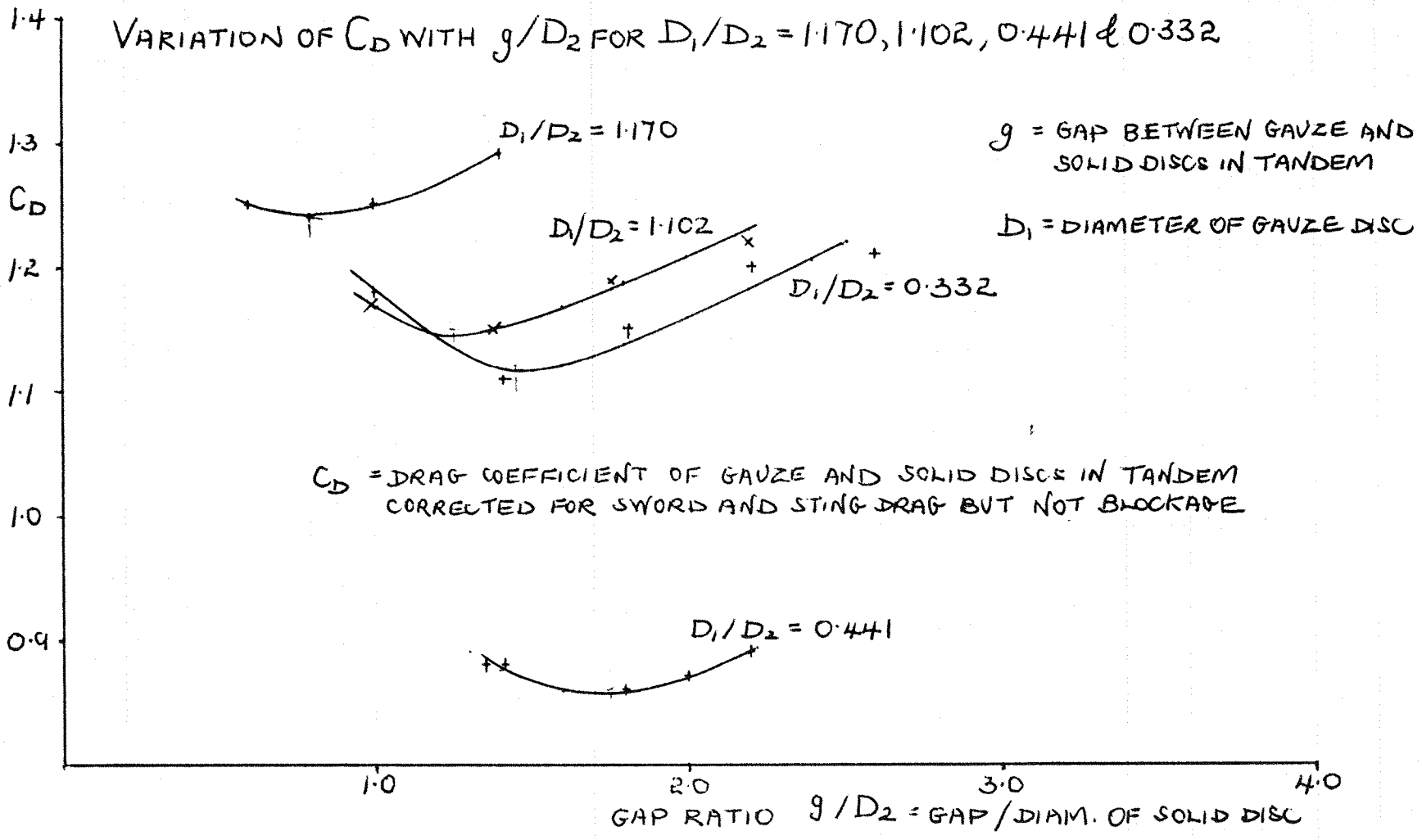
VARIATION OF C_D WITH g/D_2 FOR $D_1/D_2 = 1.170, 1.102, 0.441$ & 0.332
$D_1/D_2 = 1.170$
$D_1/D_2 = 1.102$
$D_1/D_2 = 0.332$
$D_1/D_2 = 0.441$
g = GAP BETWEEN GAUZE AND SOLID DISCS IN TANDEM
D_1 = DIAMETER OF GAUZE DISC
C_D = DRAG COEFFICIENT OF GAUZE AND SOLID DISCS IN TANDEM CORRECTED FOR SWORD AND STING DRAG BUT NOT BLOCKAGE
C_D
1·4
1·3
1·2
1·1
1·0
0·9
1·0
2·0
3·0
4·0
GAP RATIO g/D_2 = GAP / DIAM. OF SOLID DISC

FIGURE No. 30

VARIATION OF g/D_1 AT $(C_D)_{MIN}$ WITH D_1/D_2

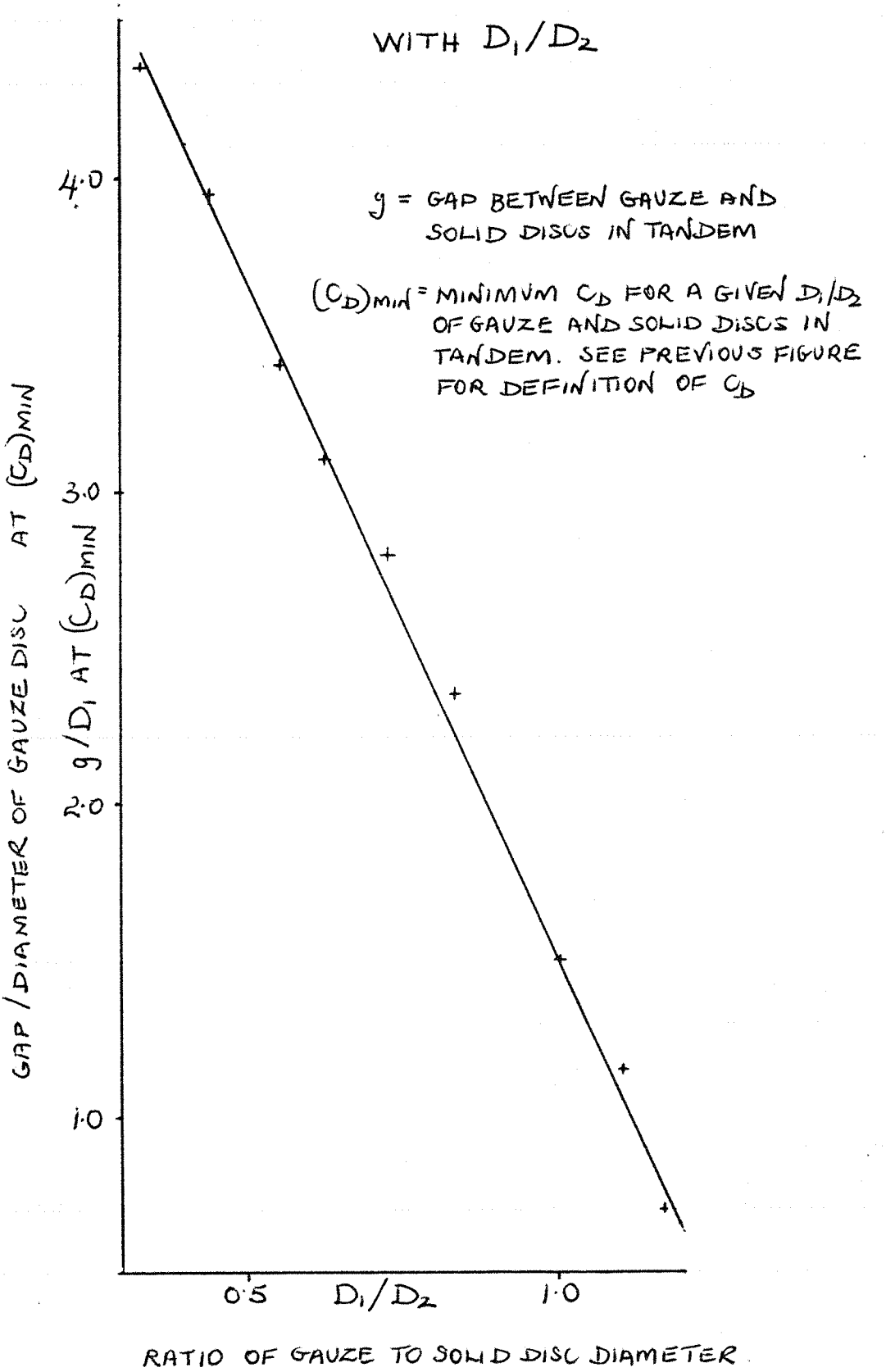

FIGURE NO. 31

VARIATION OF $(C_D)_{MIN}$ WITH D_1/D_2

$(C_D)_{MIN}$ = MINIMUM C_D FOR A GIVEN D_1/D_2 OF GAUZE AND SOLID DISCS IN TANDEM. SEE FIGURE 29 FOR DEFINITION OF C_D.

D_{10} = DIAMETER OF GAUZE DISC AT WHICH COMPLETE SHIELDING EFFECTIVELY OCCURS

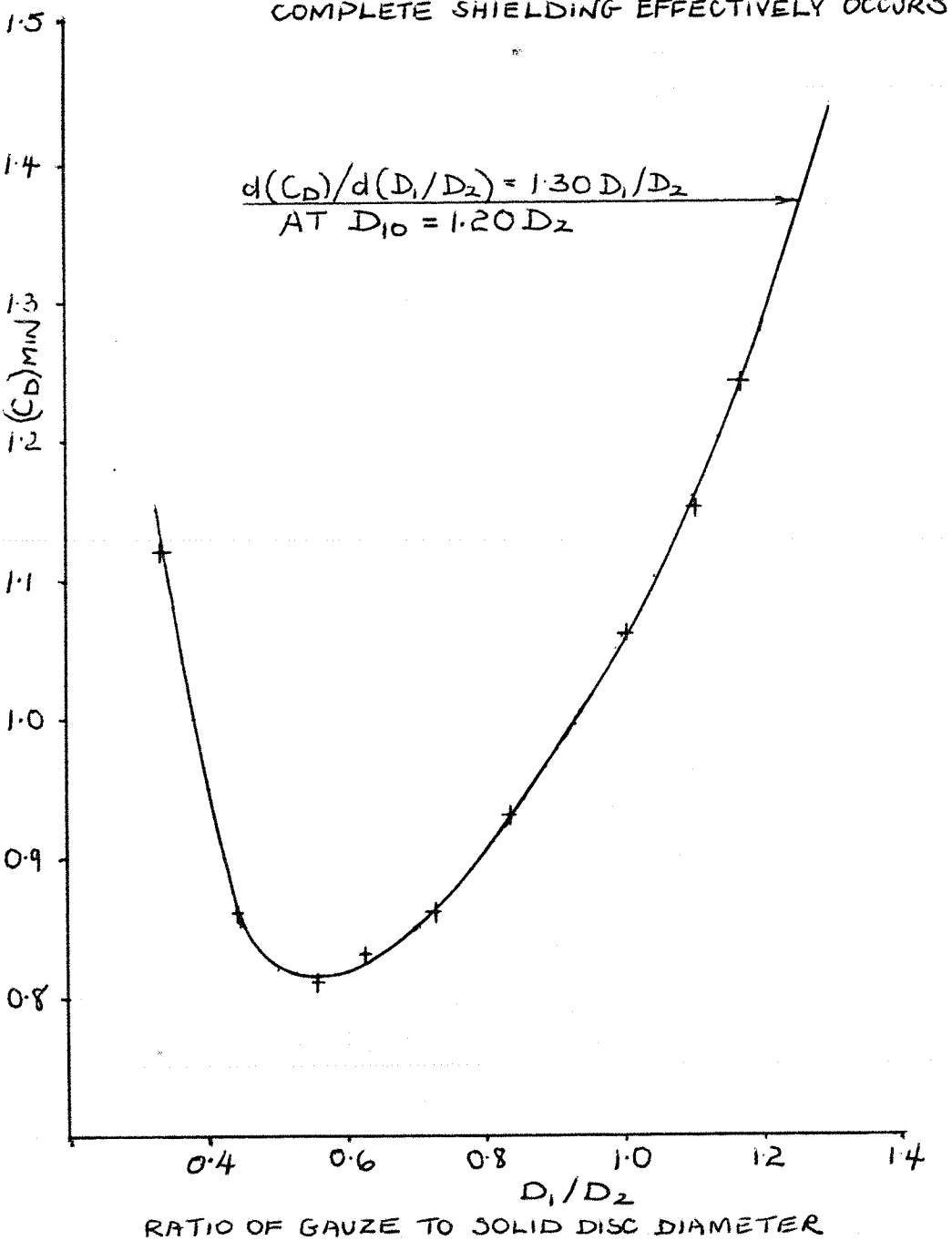

FIGURE No. 32

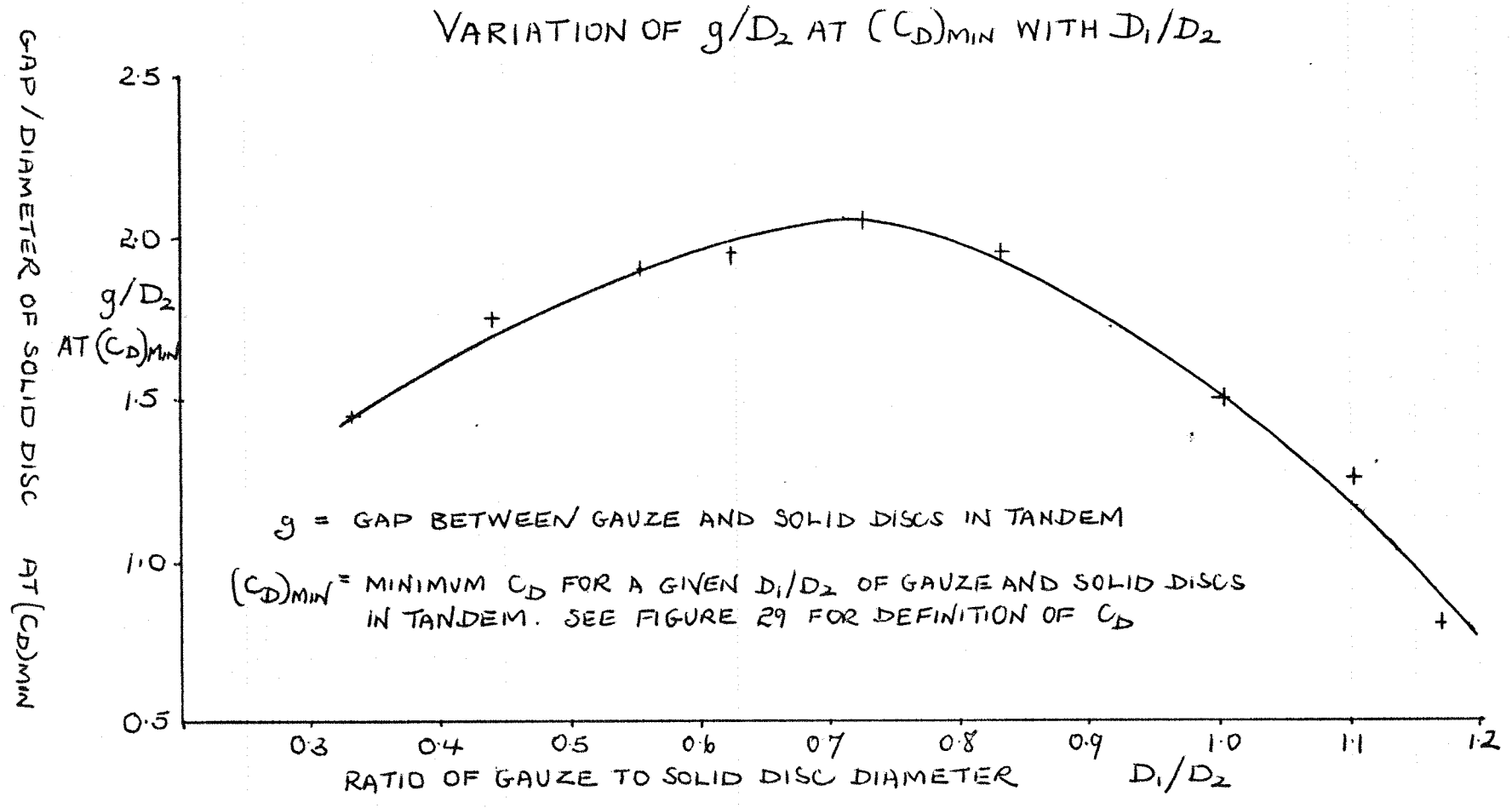
VARIATION OF g/D₂ AT (C_D)MIN WITH D₁/D₂
GAP / DIAMETER OF SOLID DISC AT (C_D)MIN
g/D₂ AT (C_D)MIN
2·5
2·0
1·5
1·0
0·5
g = GAP BETWEEN GAUZE AND SOLID DISCS IN TANDEM
(C_D)MIN = MINIMUM C_D FOR A GIVEN D₁/D₂ OF GAUZE AND SOLID DISCS IN TANDEM. SEE FIGURE 29 FOR DEFINITION OF C_D
0·3
0·4
0·5
0·6
0·7
0·8
0·9
1·0
1·1
1·2
RATIO OF GAUZE TO SOLID DISC DIAMETER D₁/D₂

FIGURE NO. 33

VARIATION OF $A_S/(A)_{D2}$, $(\overline{C_P})_F$, $(\overline{C_P})_S$, $(\Theta)_{D2}$ AND V_{EFF}/V_∞ WITH D_1/D_2 AT $g = 6.46$ IN

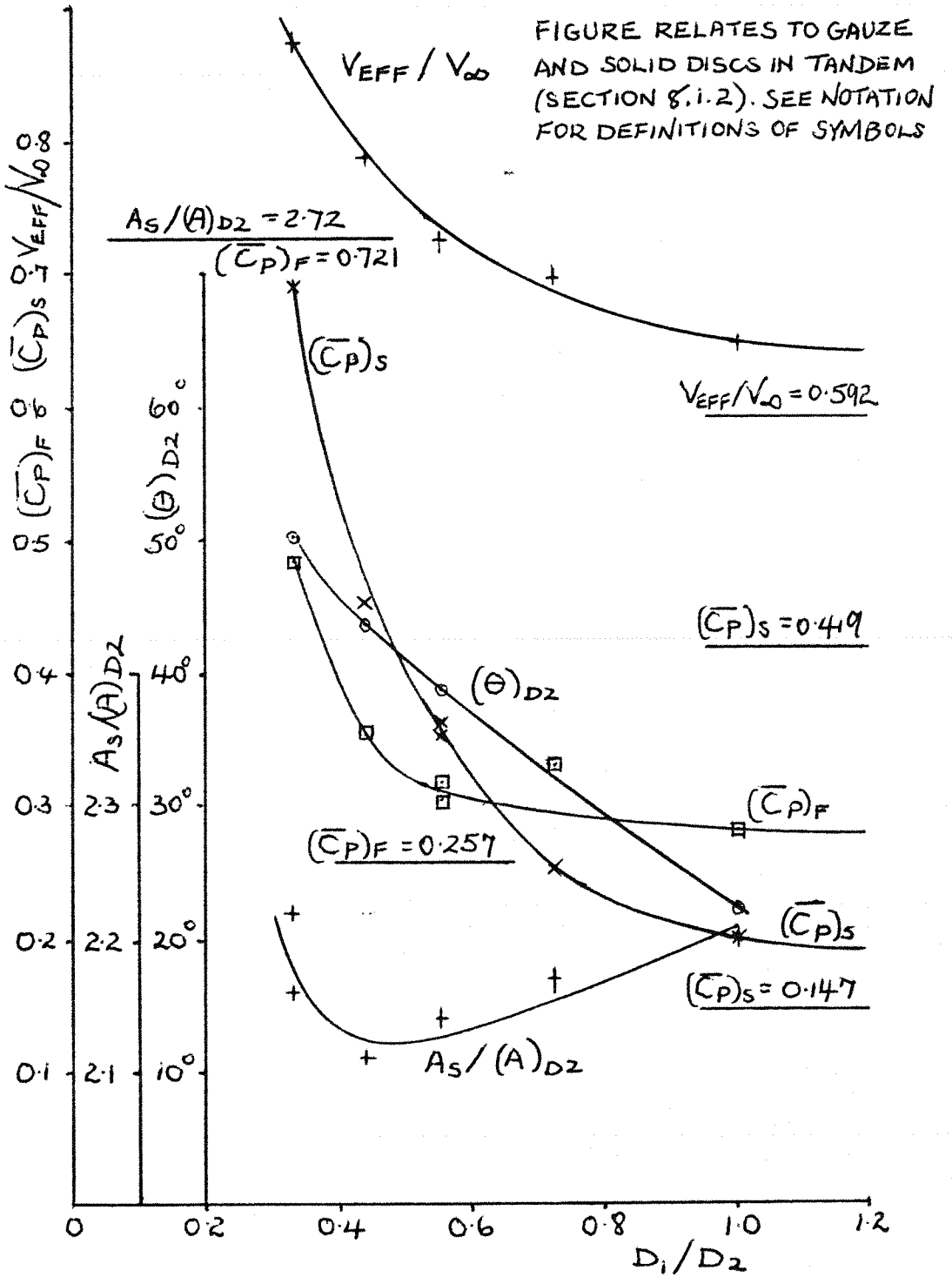

FIGURE No. 34

VARIATION OF $A_S/(A)_{D2}$, $(\overline{C_P})_{F,CALC}$, $(\overline{C_P})_S$, $(C_D)_{FBCALC}$ AND V_{EFF}/V_∞ WITH g/D_2 AT

$D_1/D_2 = 0.555$

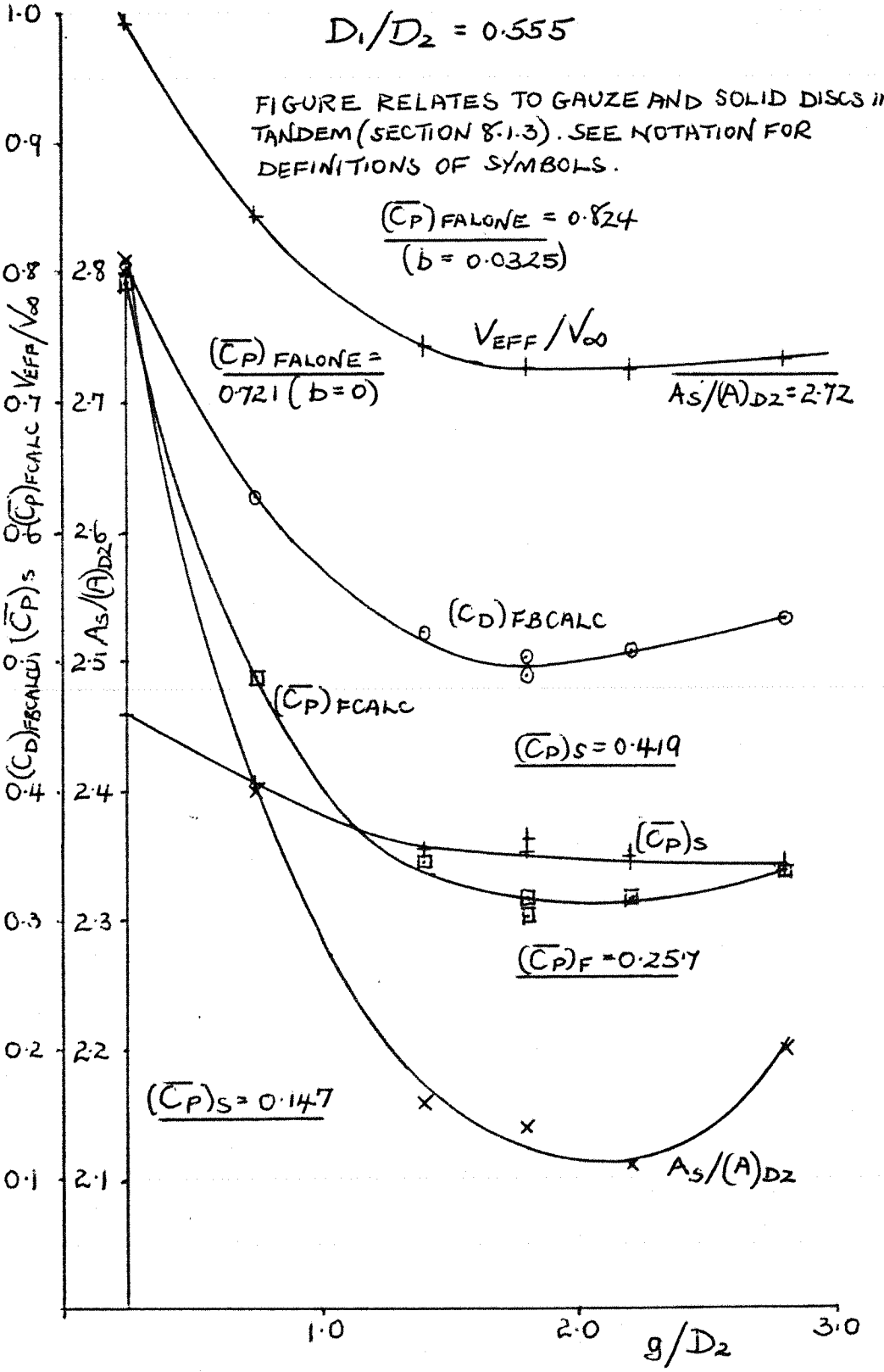

FIGURE No. 35

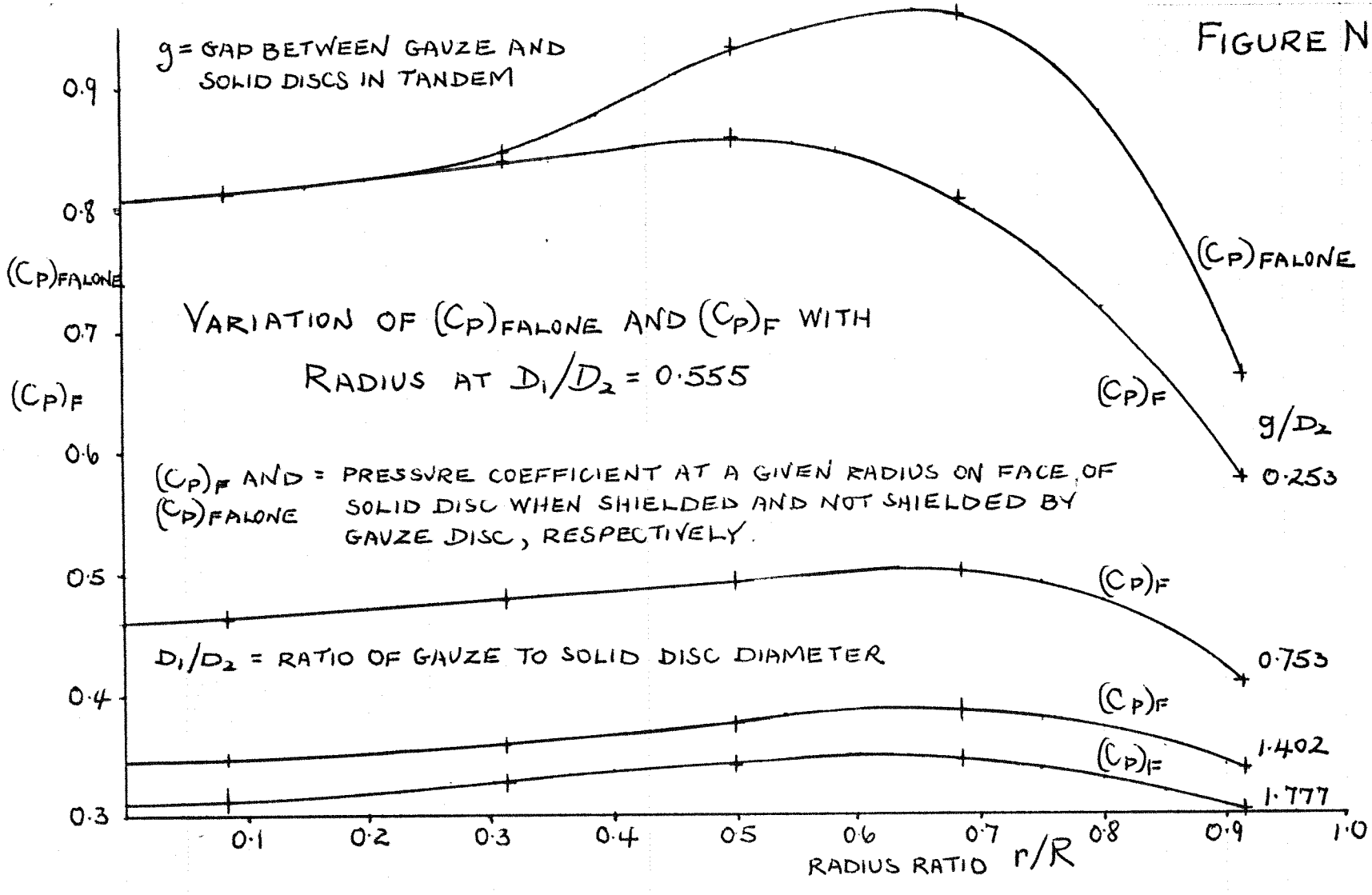
g = GAP BETWEEN GAUZE AND SOLID DISCS IN TANDEM
VARIATION OF $(C_P)_{FALONE}$ AND $(C_P)_F$ WITH RADIUS AT $D_1/D_2 = 0.555$
$(C_P)_F$ AND $(C_P)_{FALONE}$ = PRESSURE COEFFICIENT AT A GIVEN RADIUS ON FACE OF SOLID DISC WHEN SHIELDED AND NOT SHIELDED BY GAUZE DISC, RESPECTIVELY.
D_1/D_2 = RATIO OF GAUZE TO SOLID DISC DIAMETER
$(C_P)_{FALONE}$
$(C_P)_F$
g/D_2
0.253
0.753
1.402
1.777
0.9
0.8
0.7
0.6
0.5
0.4
0.3
0.1
0.2
0.3
0.4
0.5
0.6
0.7
0.8
0.9
1.0
RADIUS RATIO r/R

FIGURE No. 36

VARIATION OF $1+\{(\overline{C_P})_{FCALC}/(\overline{C_P})_S\}$ WITH $A_S/(A)_{D2}$

FIGURE USED TO CHECK APPLICABILITY OF ROSHKO AND KOENIG SEMI-INFINITE HALF BODY THEORY TO GAUZE AND SOLID DISCS IN TANDEM (SECTION 8.1.4)

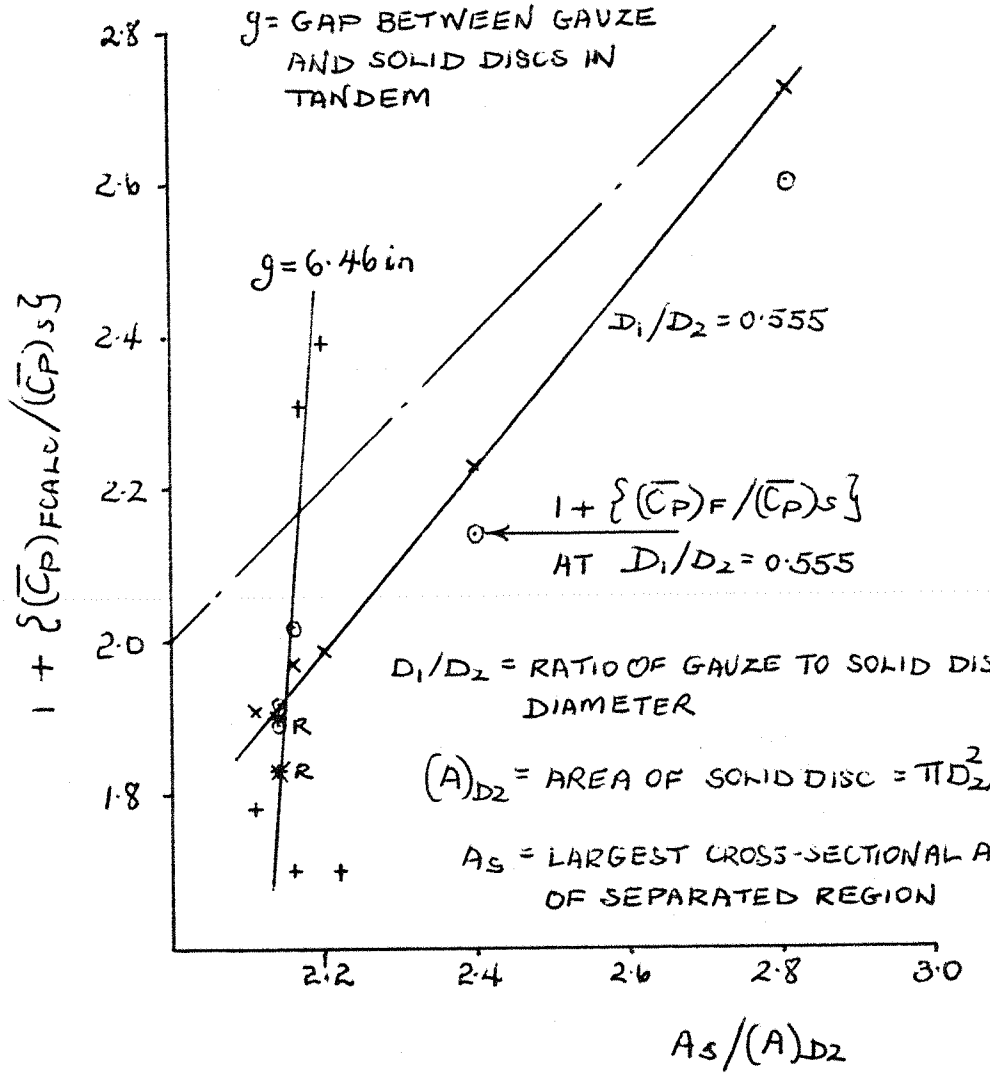

$(\overline{C_P})_{FCALC}$ = CALCULATED MEAN PRESSURE COEFFICIENT ON FACE OF SOLID DISC WHEN SHIELDED BY GAUZE DISC

$(\overline{C_P})_F$ = MEASURED MEAN PRESSURE COEFFICIENT ON FACE OF SOLID DISC WHEN SHIELDED BY GAUZE DISC

$(\overline{C_P})_S$ = MEASURED MEAN PRESSURE COEFFICIENT ON BACK OF SOLID DISC WHEN SHIELDED BY GAUZE DISC

FIGURE No 37

VARIATION OF $(C_D)_{D2}$ AND $(C_D)_{D2CALC}$ WITH g/D_2 AT $D_1/D_2 = 0.555$

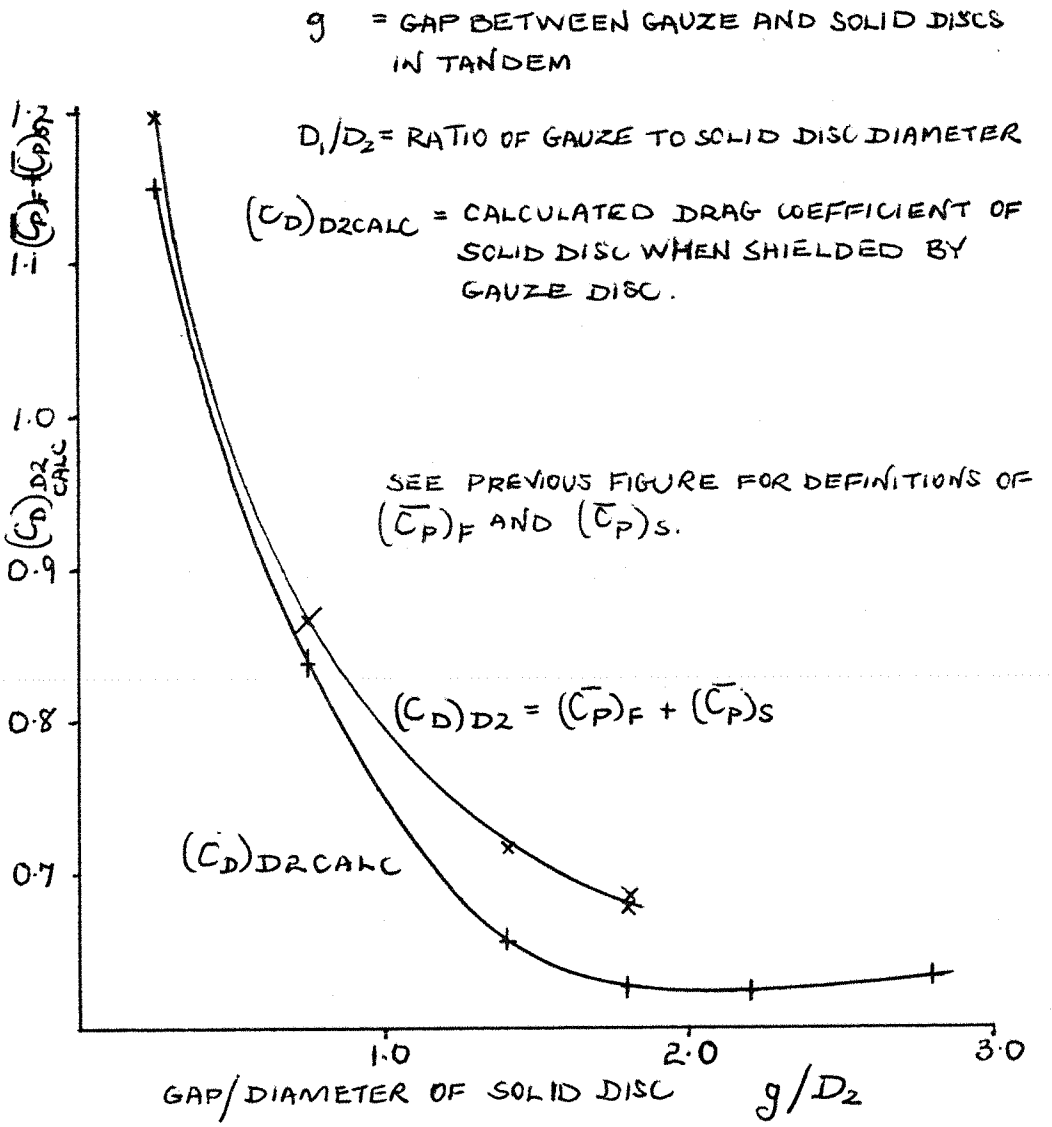

FIGURE No 38

VELOCITIES IN WAKE OF GAUZE AND SOLID DISCS IN TANDEM

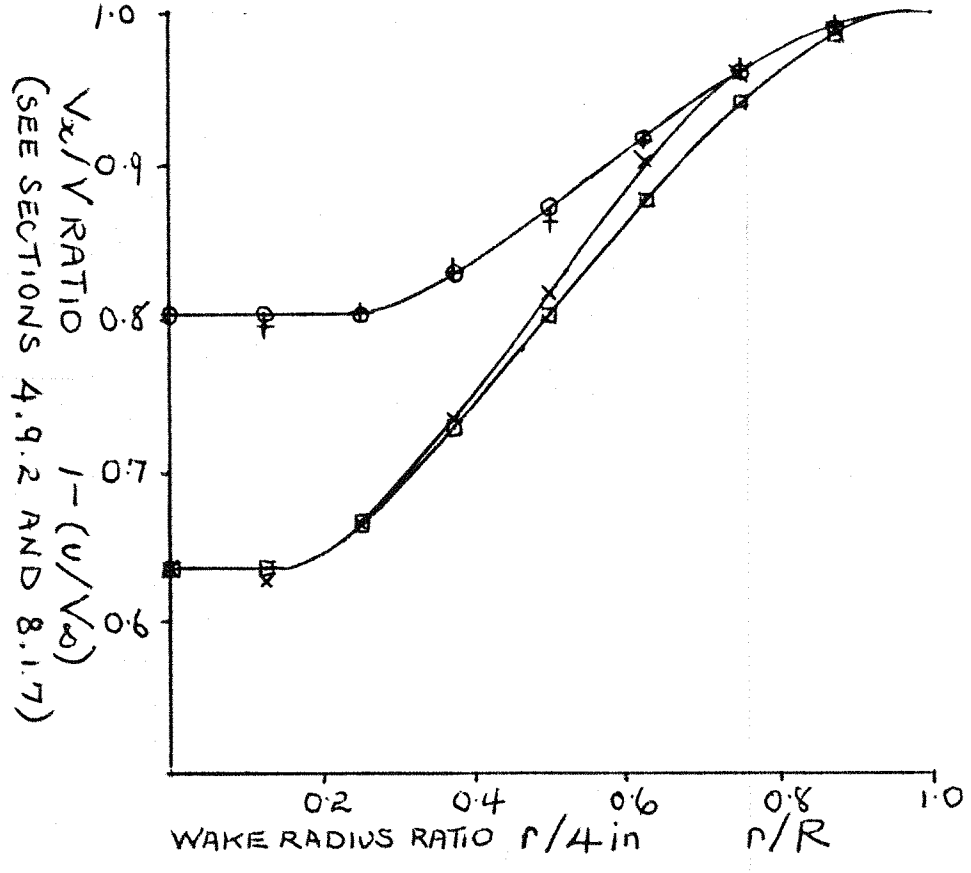

D_2 = DIAMETER OF SOLID DISC

$4D_2$ DOWNSTREAM OF SOLID DISC

+ V_x/V RATIO FOR APPROX. OPT. CONFIG.

⊙ $1-(U/V_\infty)$

$3D_2$ DOWNSTREAM OF SOLID DISC

× V_x/V RATIO FOR APPROX. OPT. CONFIG.

⊡ $1-(U/V_\infty)$

U/V_∞ = VELOCITY DEFECT RATIO

SEE SECTION 7.1.23 FOR DEFINITION OF V_x/V RATIO

FIGURE No. 39

VARIATION OF VOLUMETRIC FLOW RATE WITH RADIUS FOR THE APPROX. OPT. CONFIG. OF GAUZE AND SOLID DISCS IN TANDEM

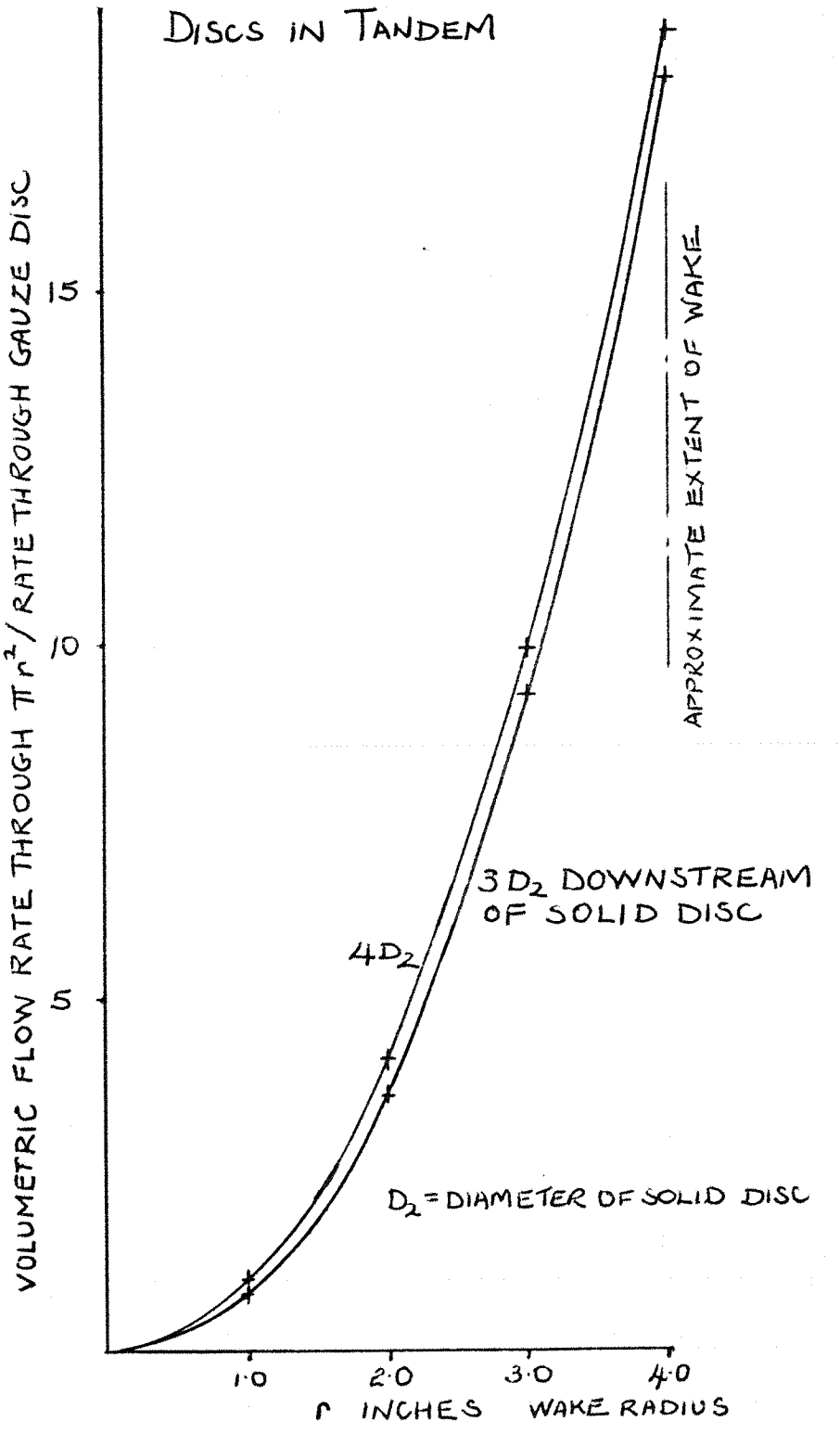

FIGURE No. 40

VARIATION OF $(C_D)_I$ AND $(C_D)_{ICALC}$ WITH g/D_2 AND D_1/D_2

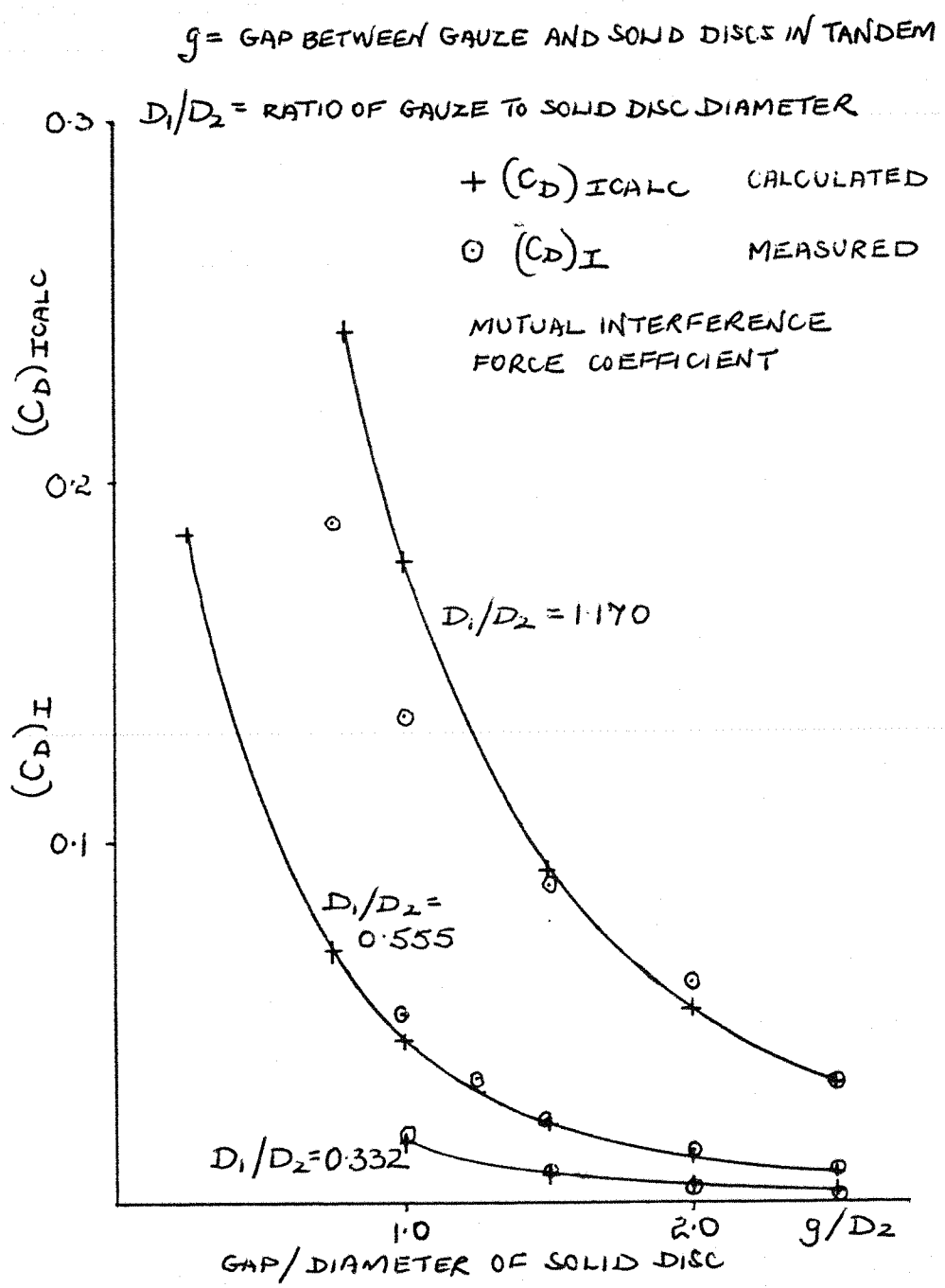

FIGURE No. 41

VARIATION OF $(C_D)_{CMINCORR}$ WITH l/D_C AND D_1/D_C

$(C_D)_{CMINCORR}$ = MINIMUM MEASURED DRAG COEFFICIENT OF GAUZE DISC AND SOLID CYLINDER IN TANDEM OBTAINED BY VARYING THE GAP BETWEEN GAUZE DISC AND FRONT FACE OF CYLINDER CORRECTED FOR SWORD AND STING DRAG AND FOR BLOCKAGE

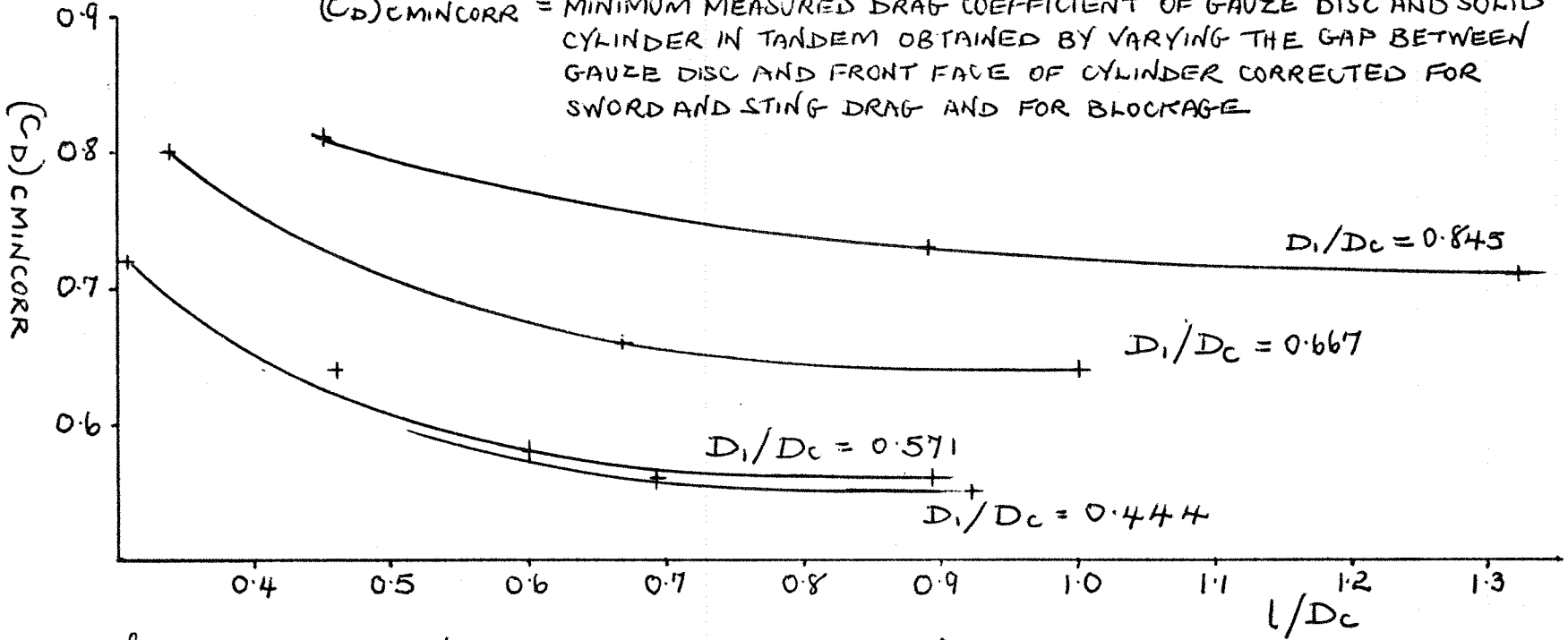

l = LENGTH OF CYLINDER D_C = DIAMETER OF CYLINDER D_1 = DIAMETER OF GAUZE DISC

FIGURE No. 42

VARIATION OF $(C_D)_{CLEAST}$ WITH D_i/D_c

$(C_D)_{CLEAST}$ = LEAST $(C_D)_{CMINCORR}$ FOR A GIVEN D_i/D_c

SEE PREVIOUS FIGURE FOR DEFINITION OF $(C_D)_{CMINCORR}$

D_i = DIAMETER OF GAUZE DISC

D_c = DIAMETER OF CYLINDER

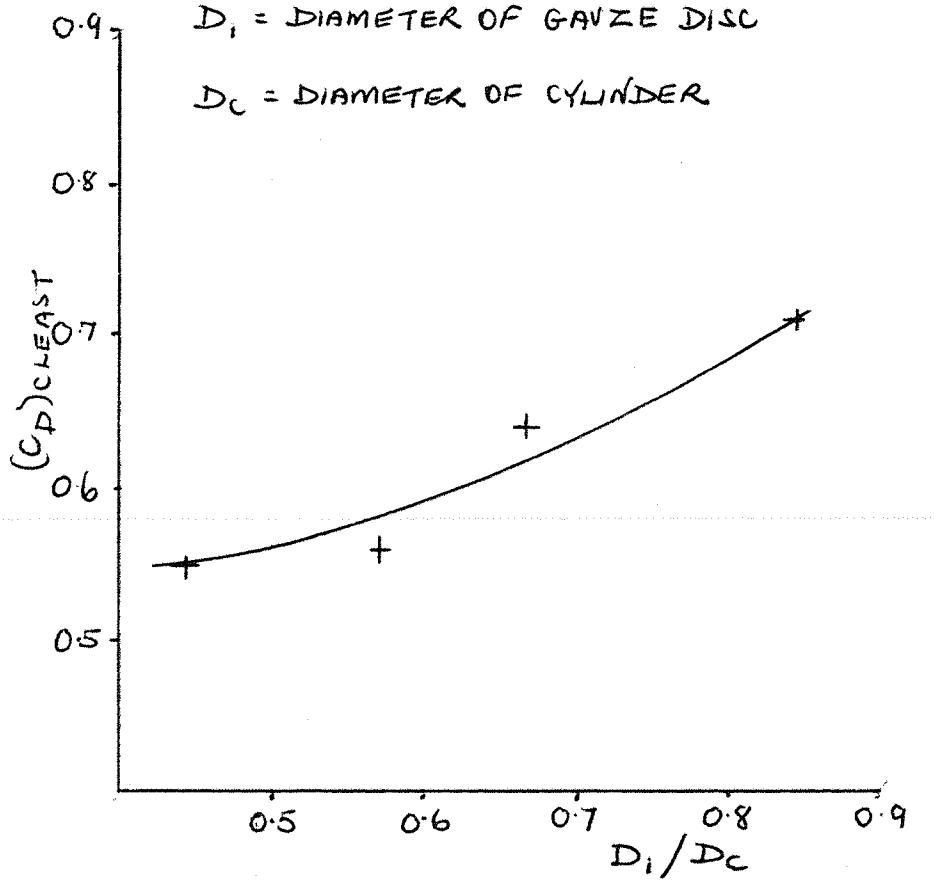

PHOTOGRAPH No 1

SIXTH CONFIGURATION OF CAR MODEL TESTED

PHOTOGRAPH No.2

SLIDING UNIPOD AND BASE WITH
METRE RULE GUIDE

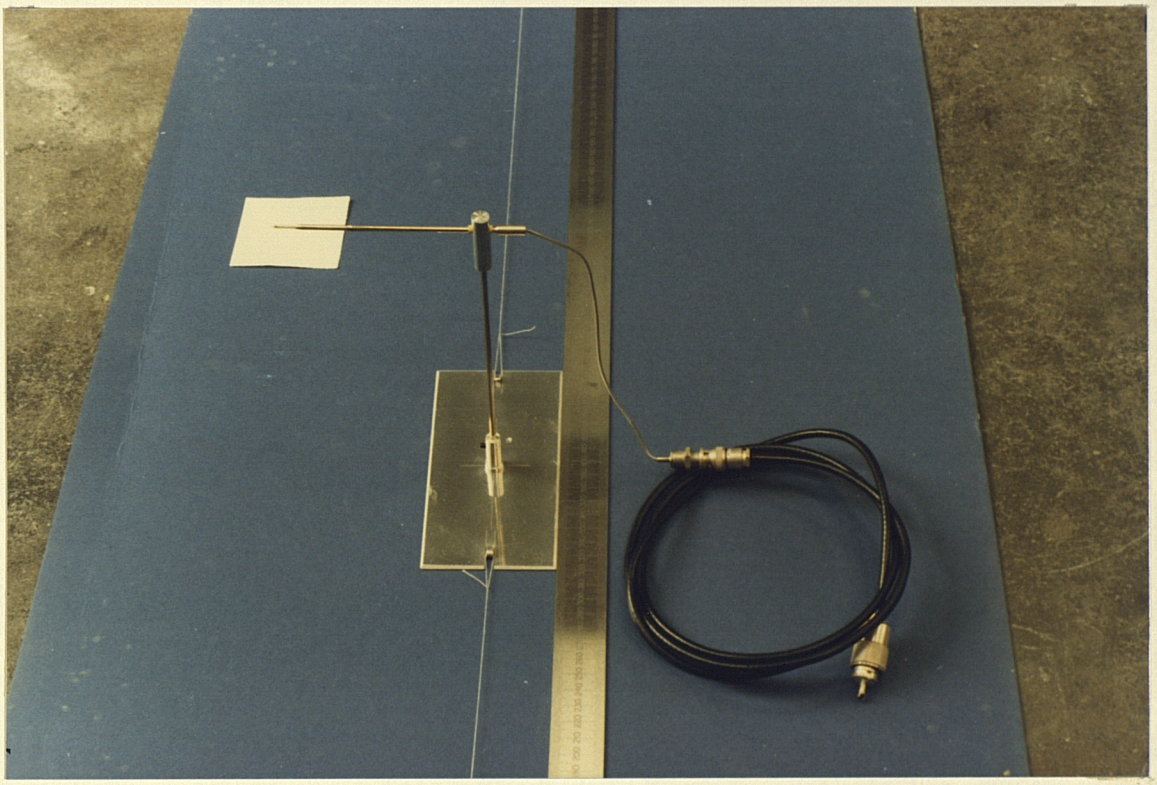

PHOTOGRAPH No. 3

MANOMETER BANK

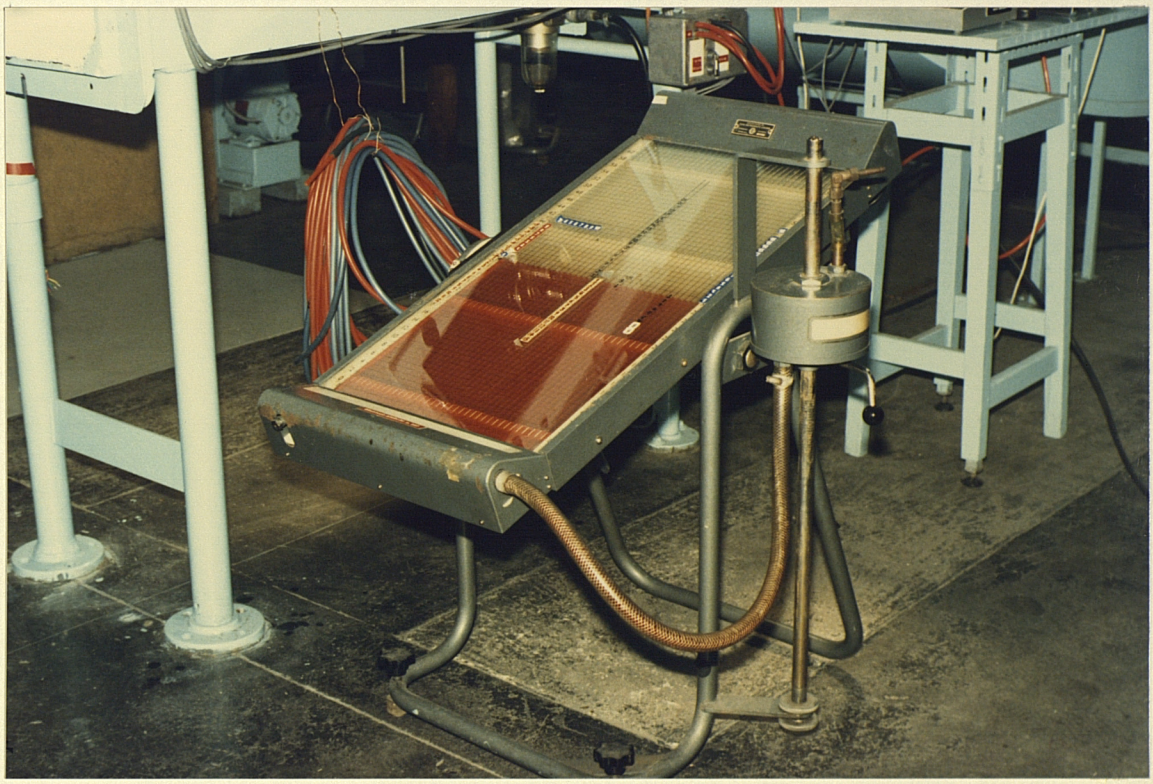

PHOTOGRAPH NO. 4

SMOKE GENERATOR AND PROBE

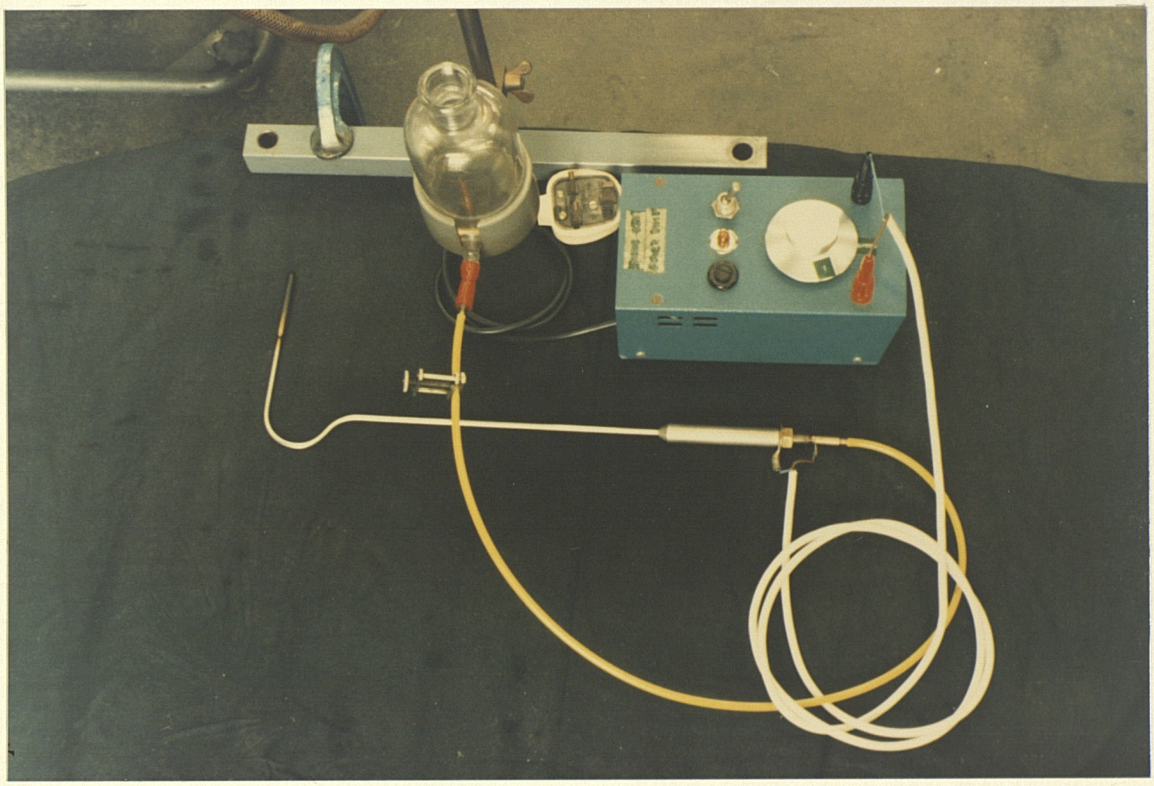

PHOTOGRAPH NO. 5

CONSTANT TEMPERATURE ANEMOMETER

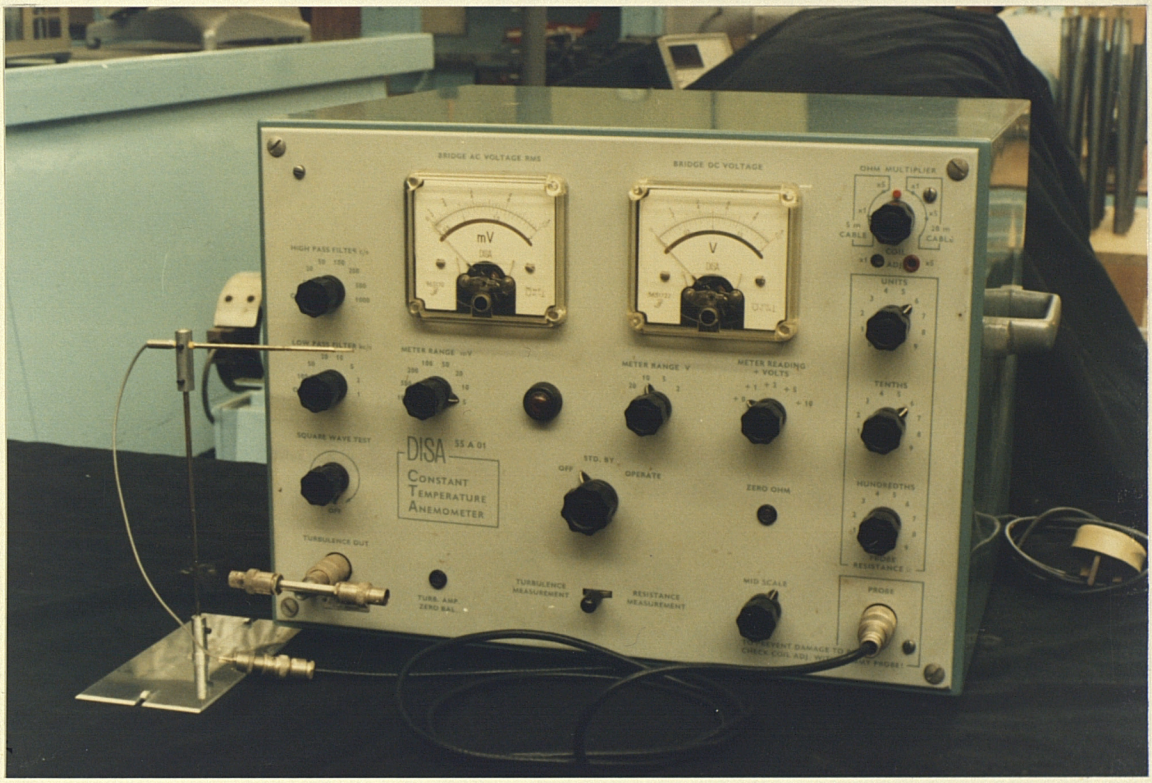

PHOTOGRAPH NO. 6

PITOT-STATIC TUBE RAKE

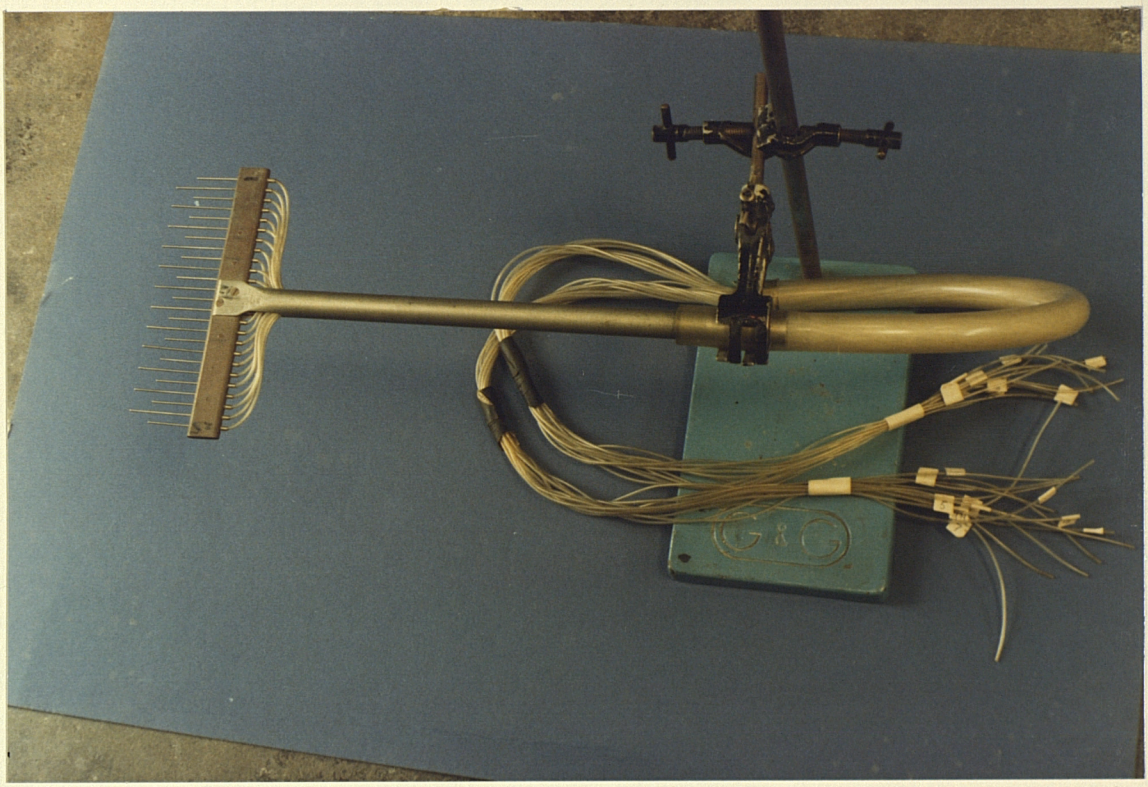

PHOTOGRAPH No. 7

MICROMANOMETER

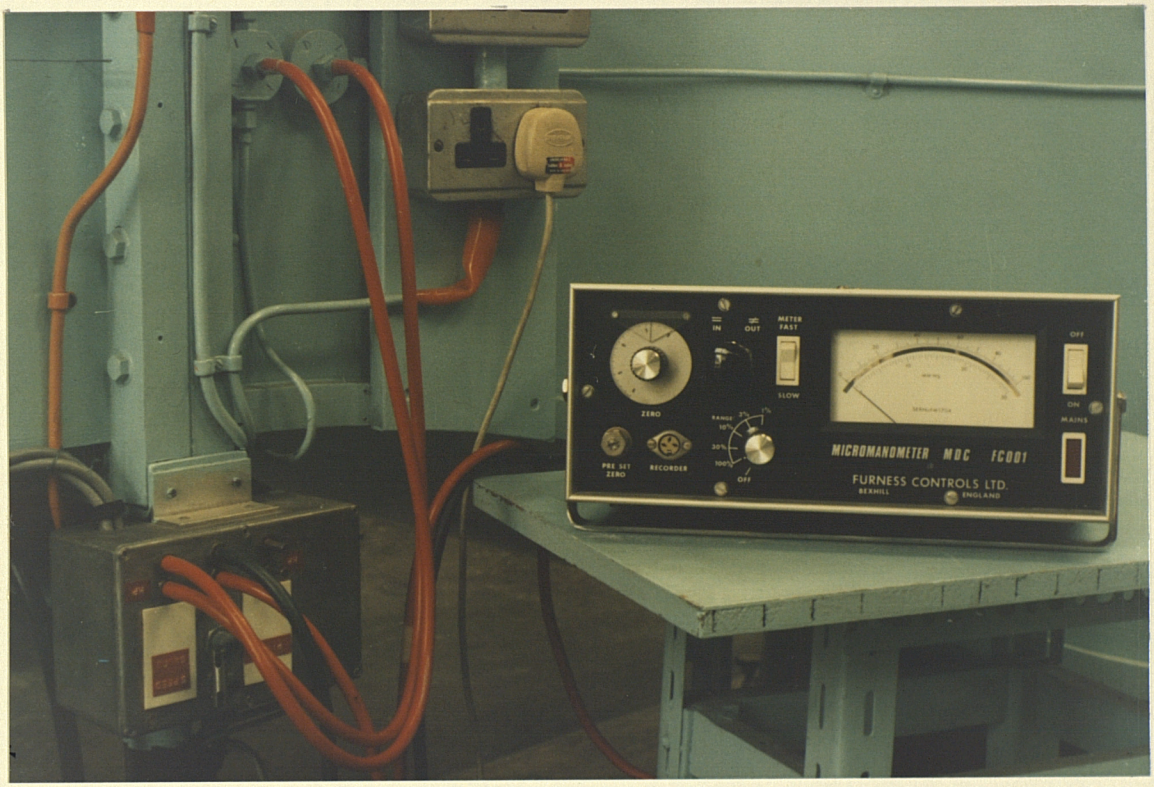

PHOTOGRAPH No. 8

WIND TUNNEL (1)

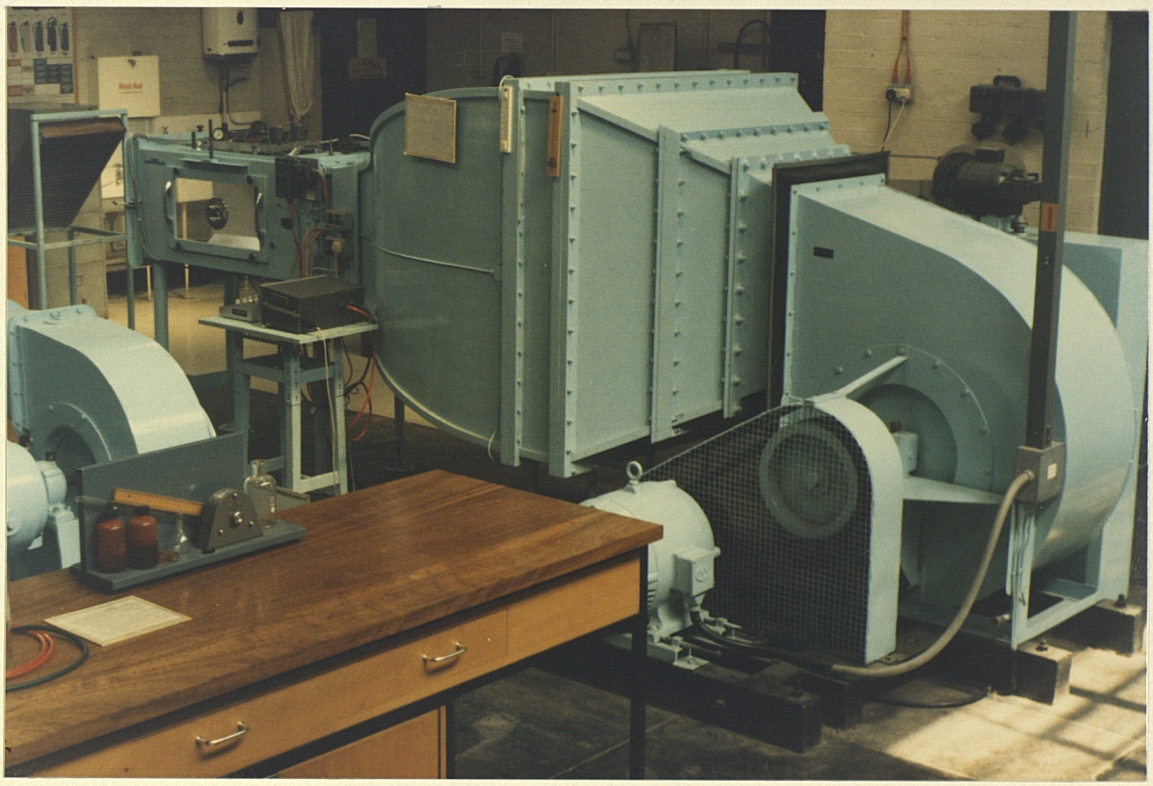

PHOTOGRAPH No.9

WIND TUNNEL (2)

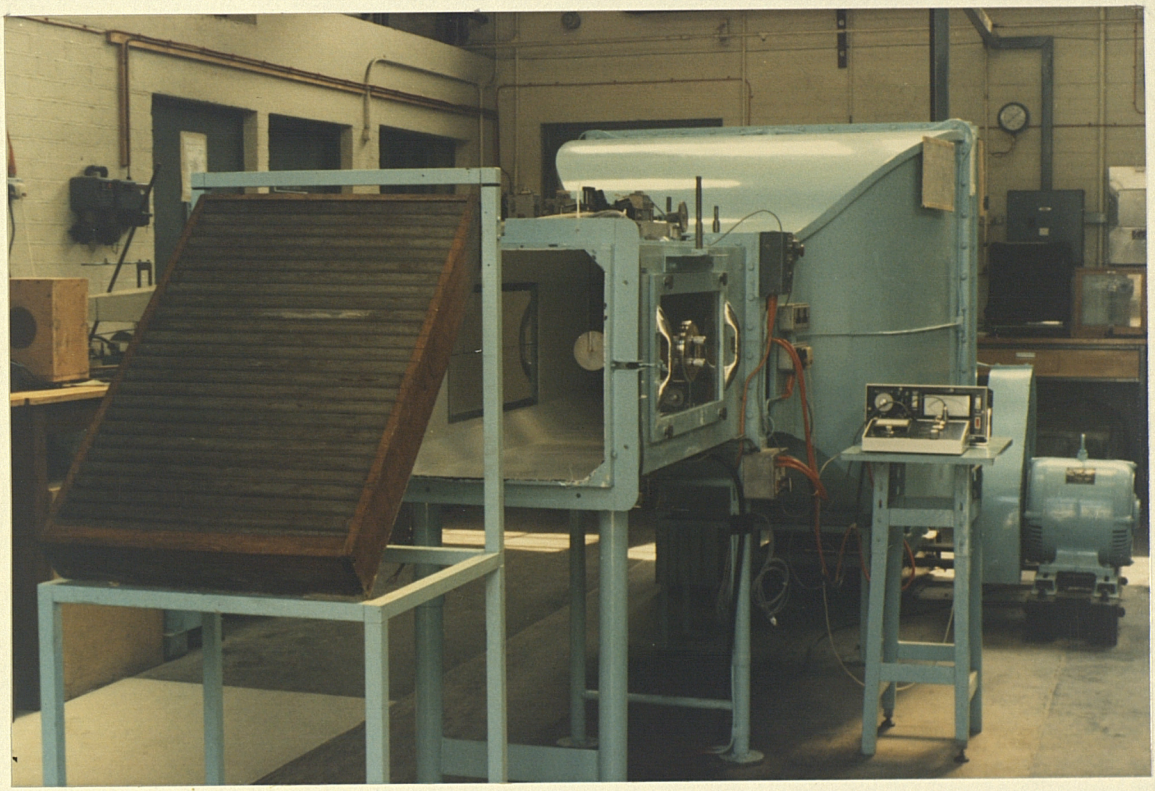

PHOTOGRAPH NO. 10

WIND TUNNEL (3)

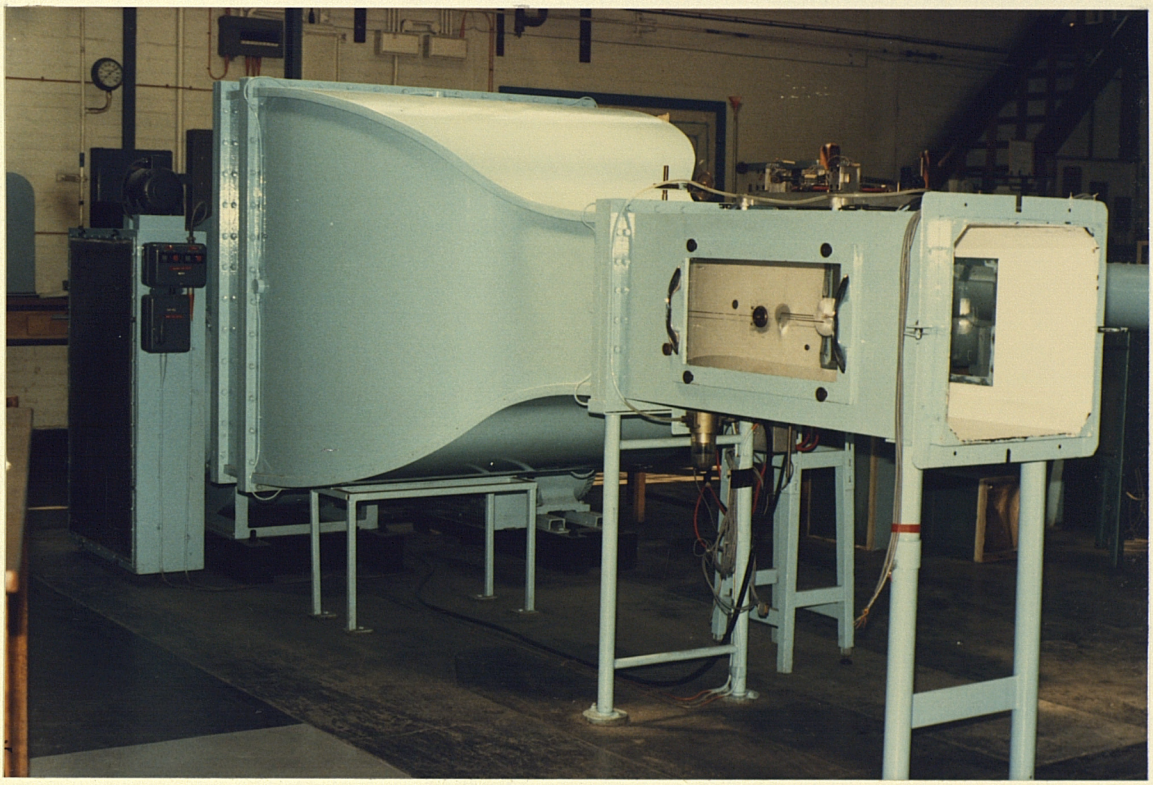

PHOTOGRAPH No.11

WIND TUNNEL (4)

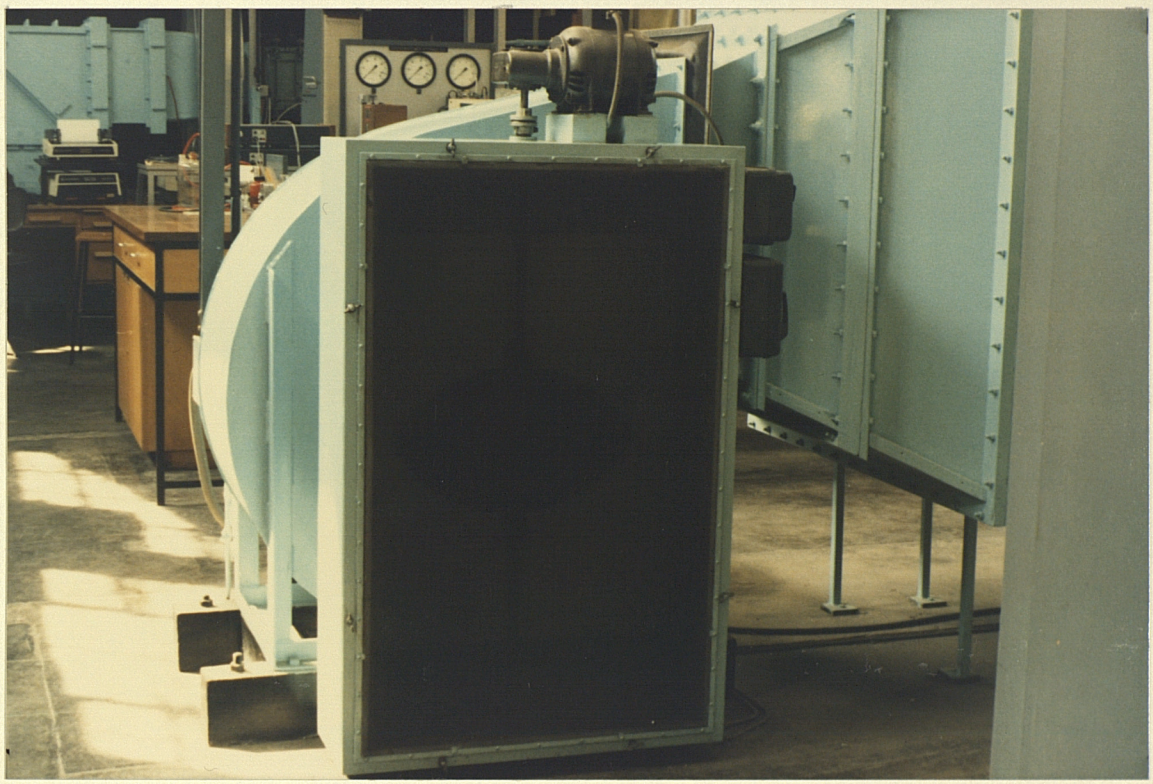

PHOTOGRAPH No.12

WIND TUNNEL (5)

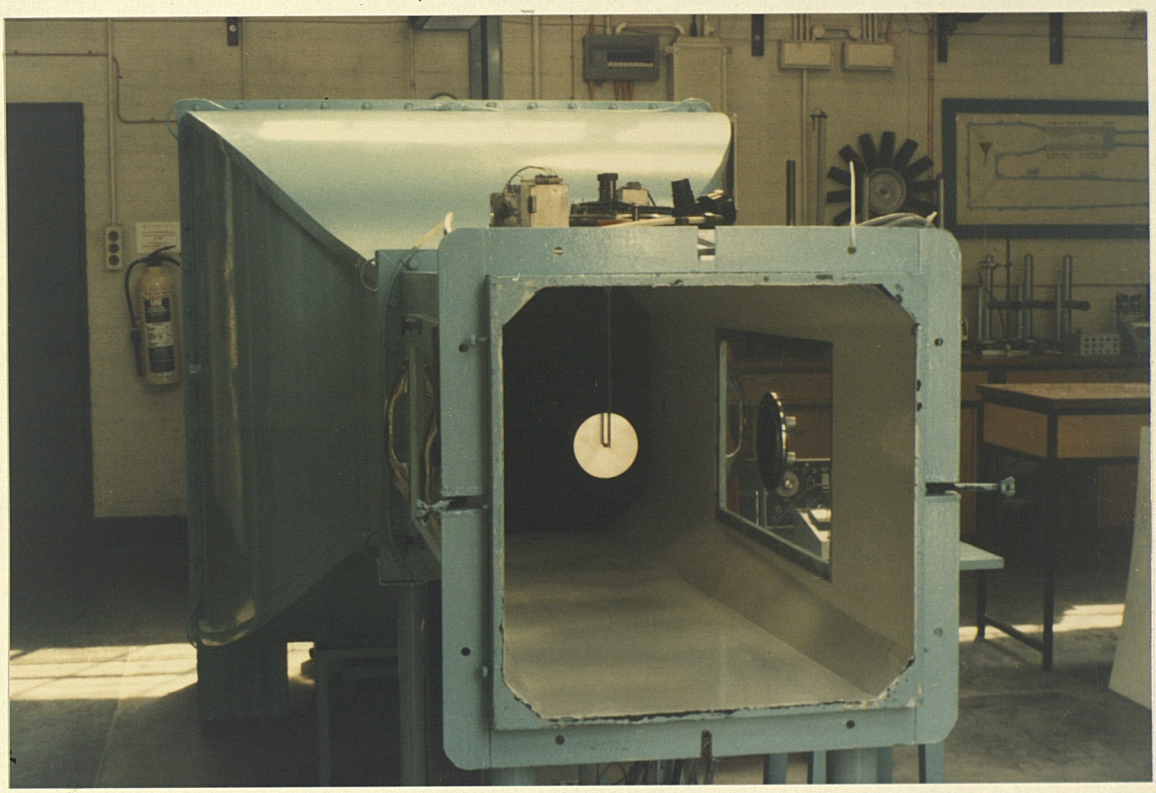

PHOTOGRAPH NO. 13

BAROMETER

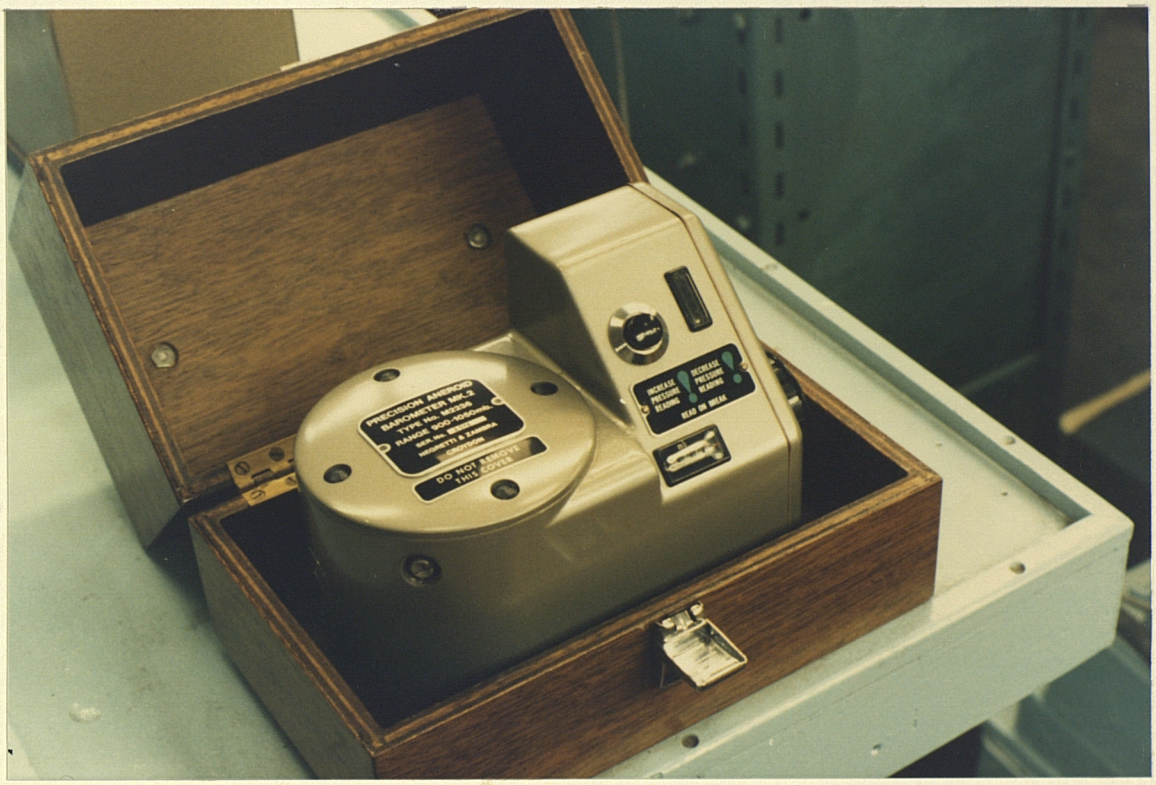

PHOTOGRAPH No.14

DRAG DYNAMOMETER (1)

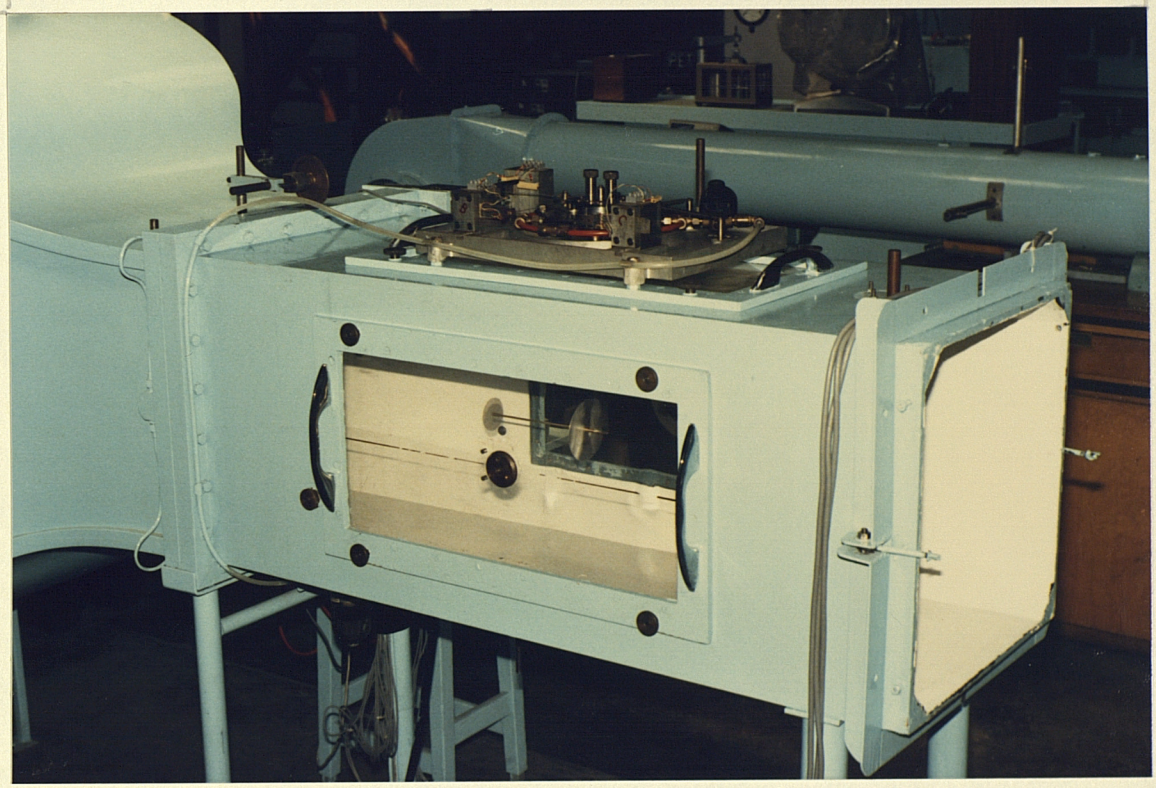

PHOTOGRAPH NO. 15

DRAG DYNAMOMETER (2)

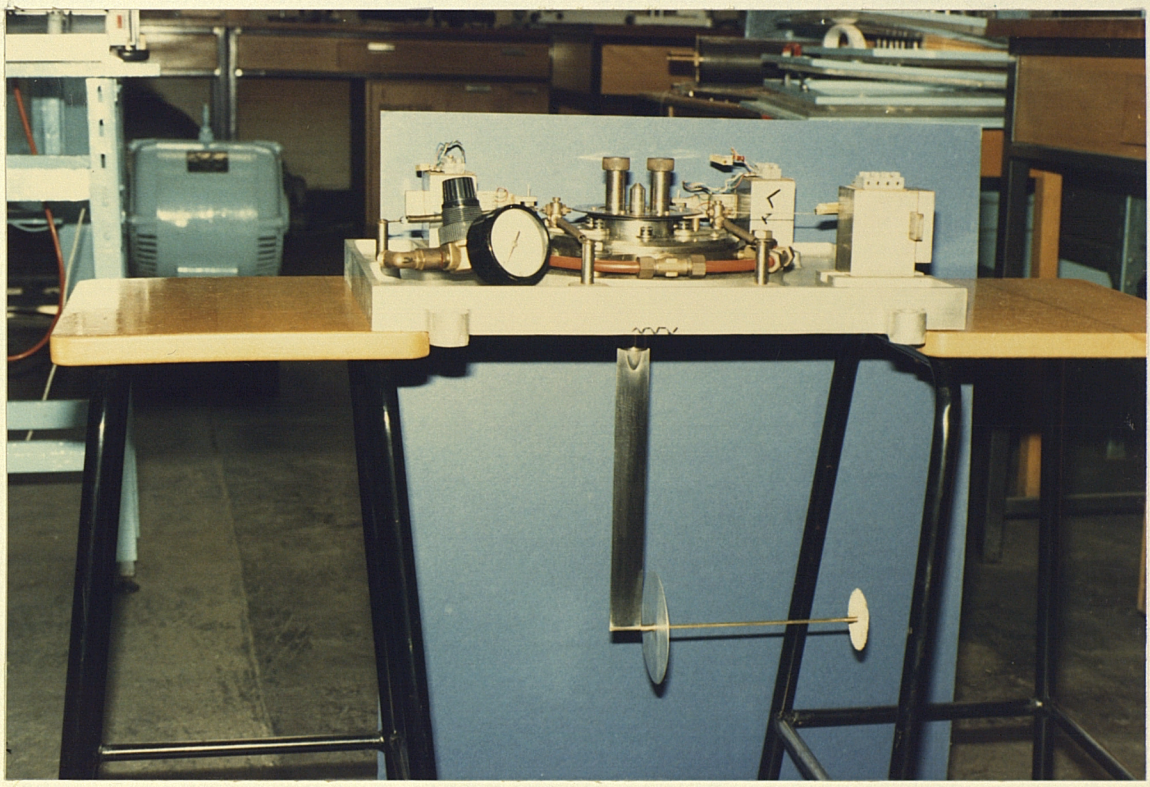

PHOTOGRAPH No.16

DRAG DYNAMOMETER (3)

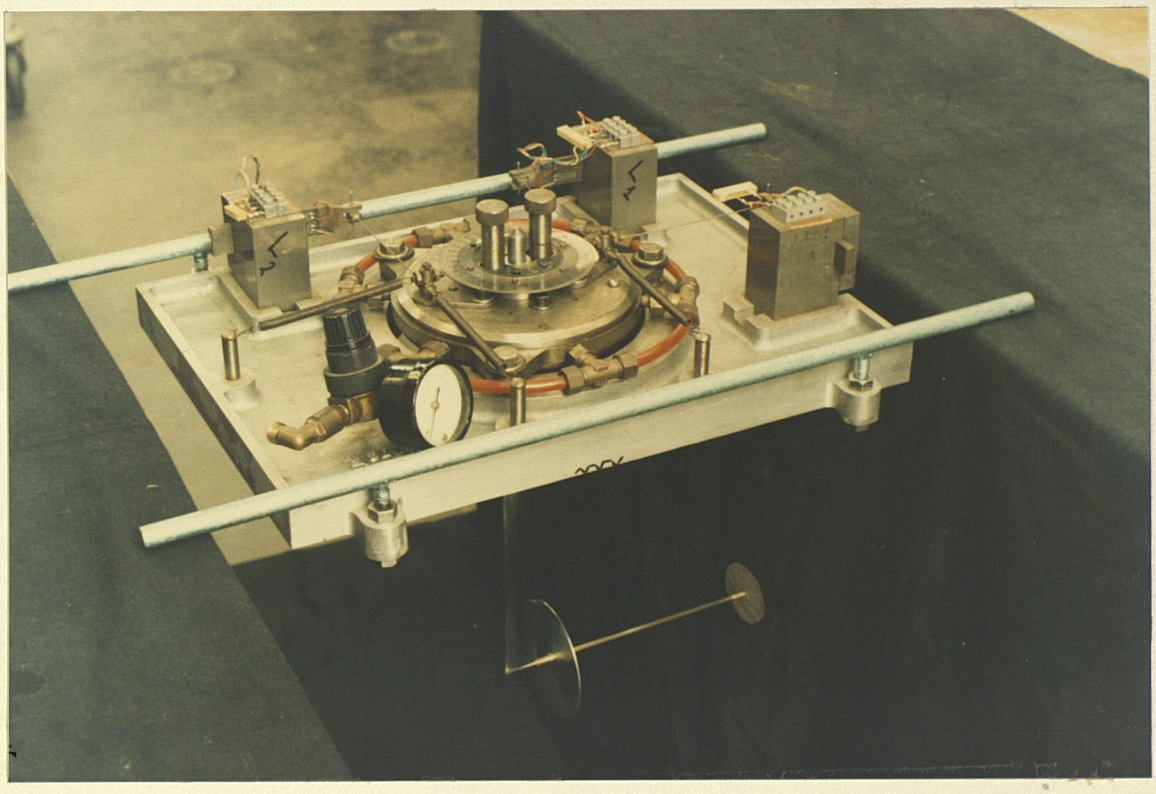

PHOTOGRAPH No. 17

DRAG DYNAMOMETER (4)

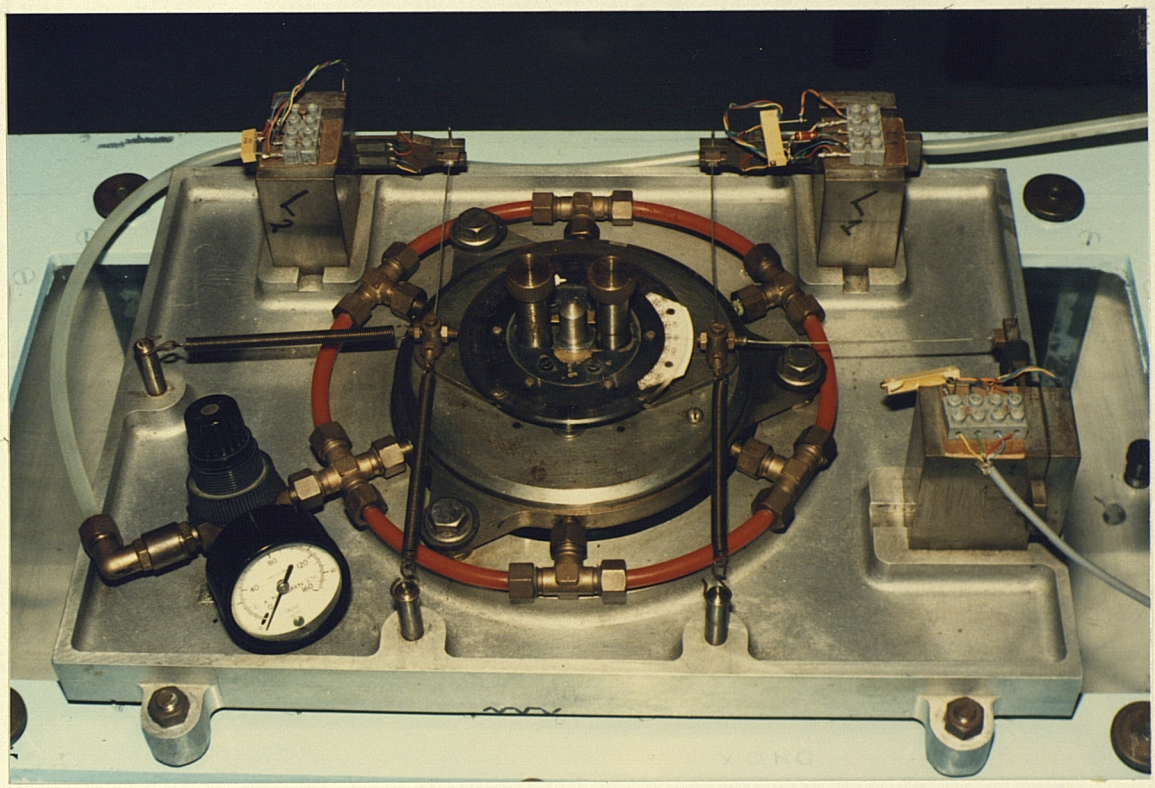

PHOTOGRAPH No. 18

TRANSDUCER EXCITATION & MEASURING UNIT

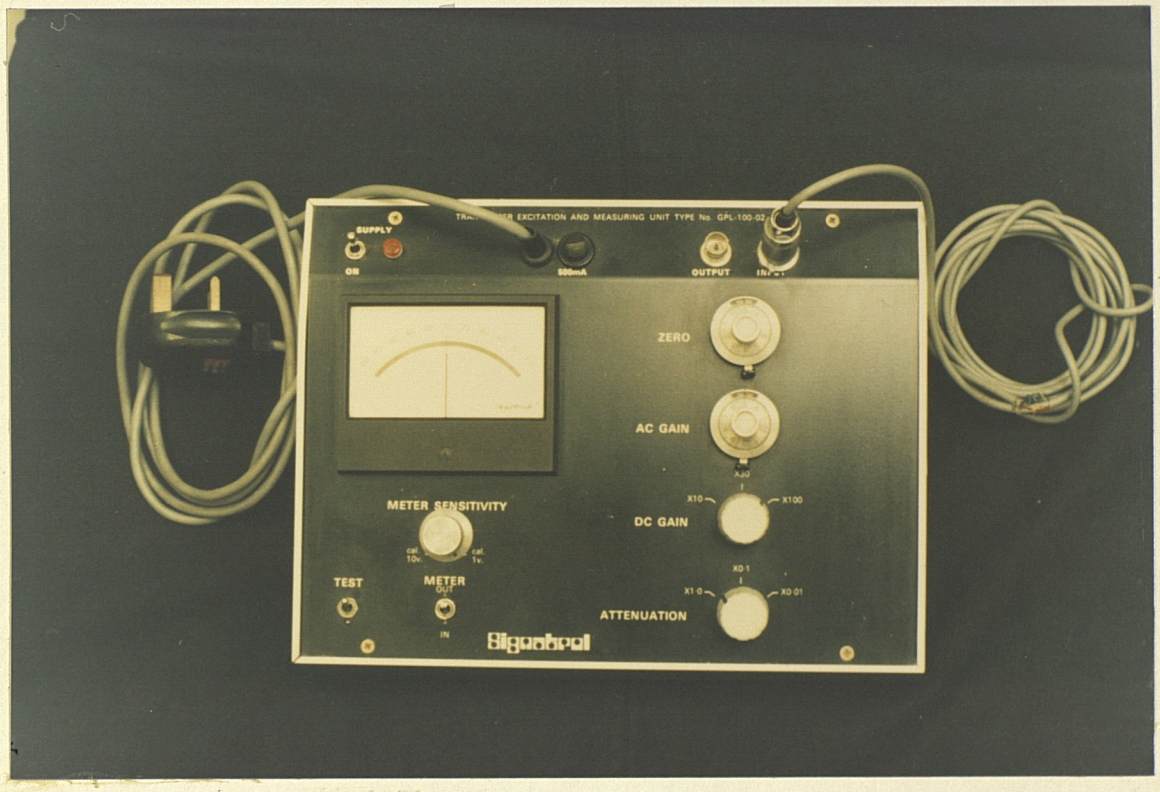

PHOTOGRAPH No.19

GAUZE AND SOLID DISCS

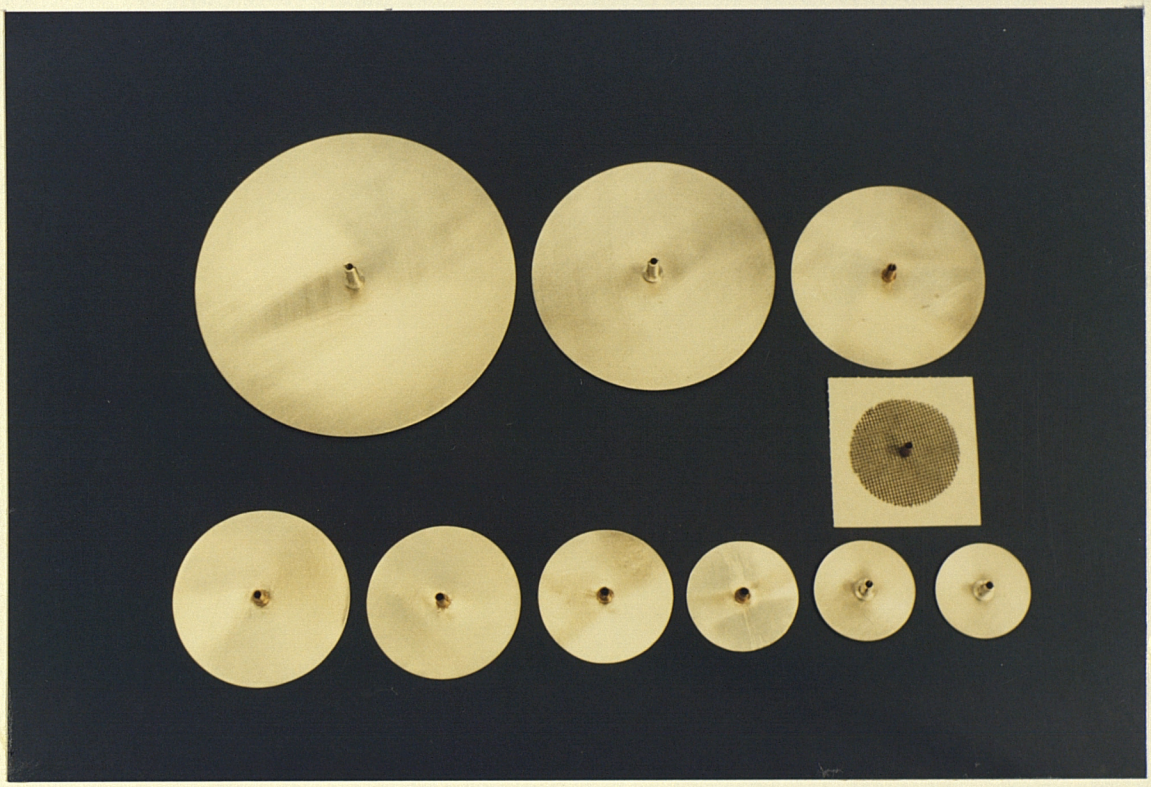

PHOTOGRAPH NO. 20

APPROXIMATELY OPTIMUM CONFIGURATION OF GAUZE AND SOLID DISCS IN TANDEM

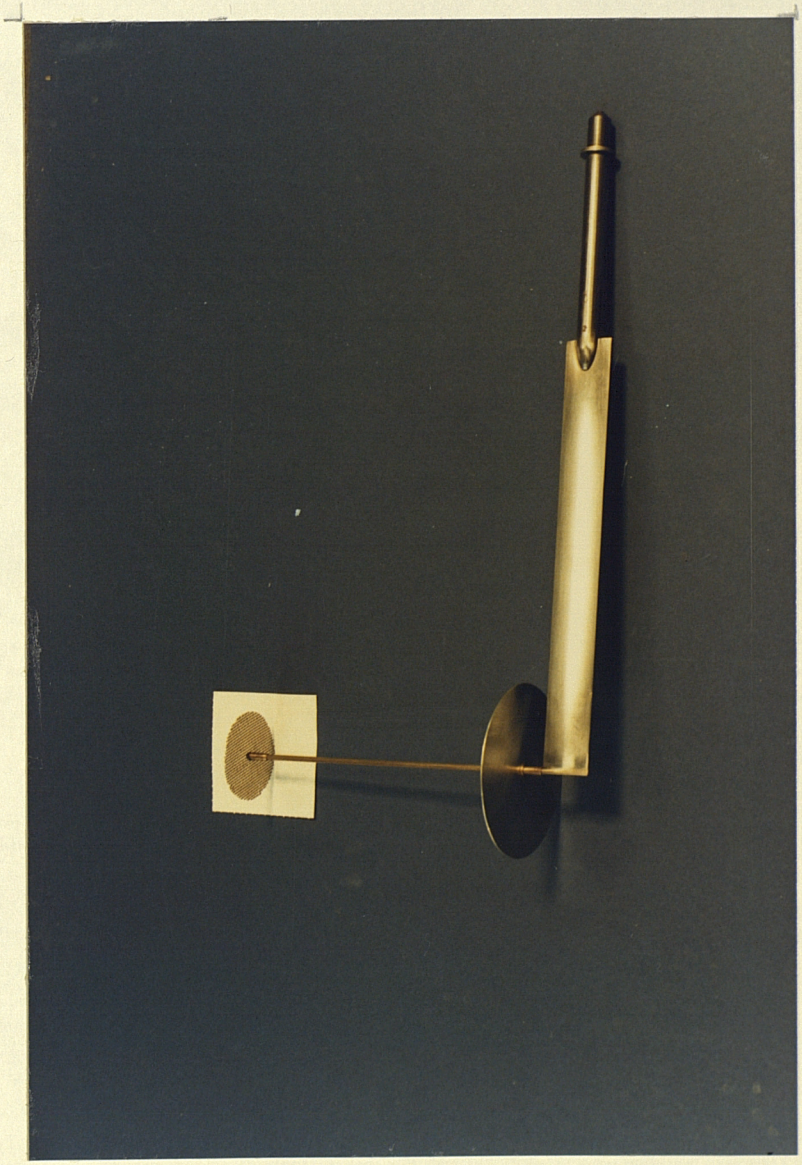

PHOTOGRAPH No.21

CAR MODEL IN WIND TUNNEL

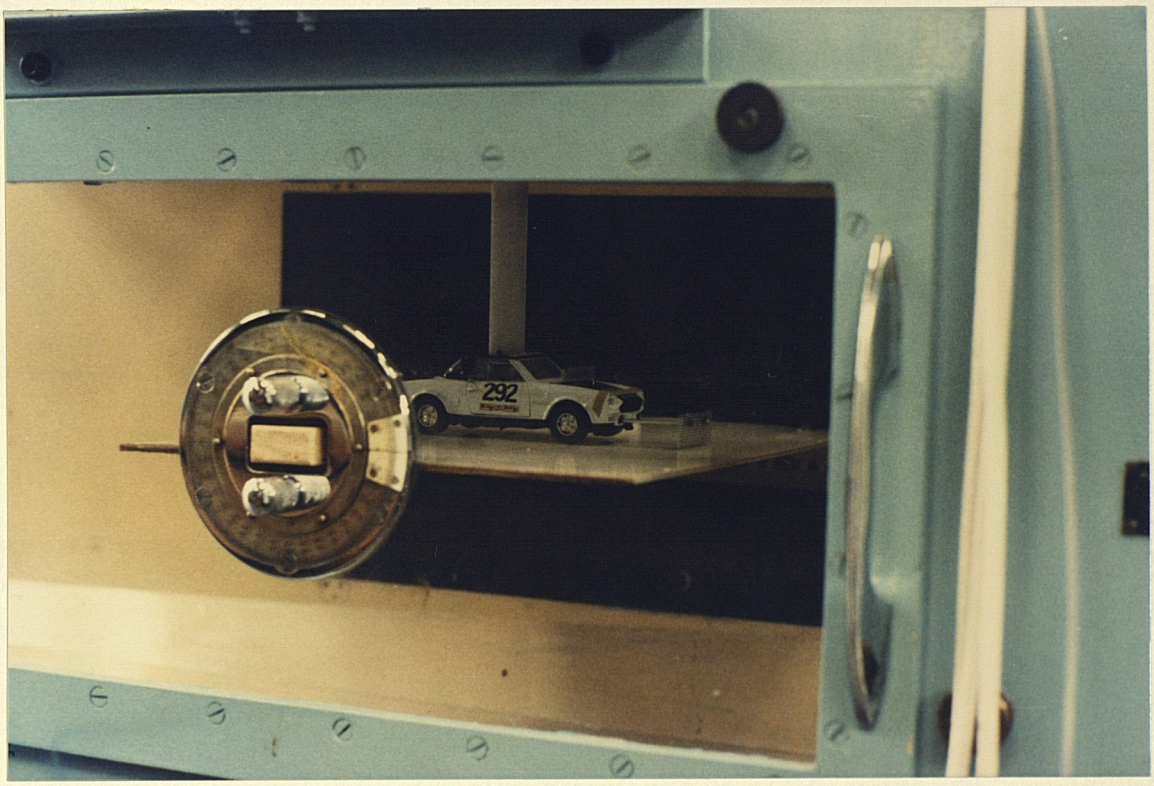

PHOTOGRAPH No. 22

SOLID CYLINDERS

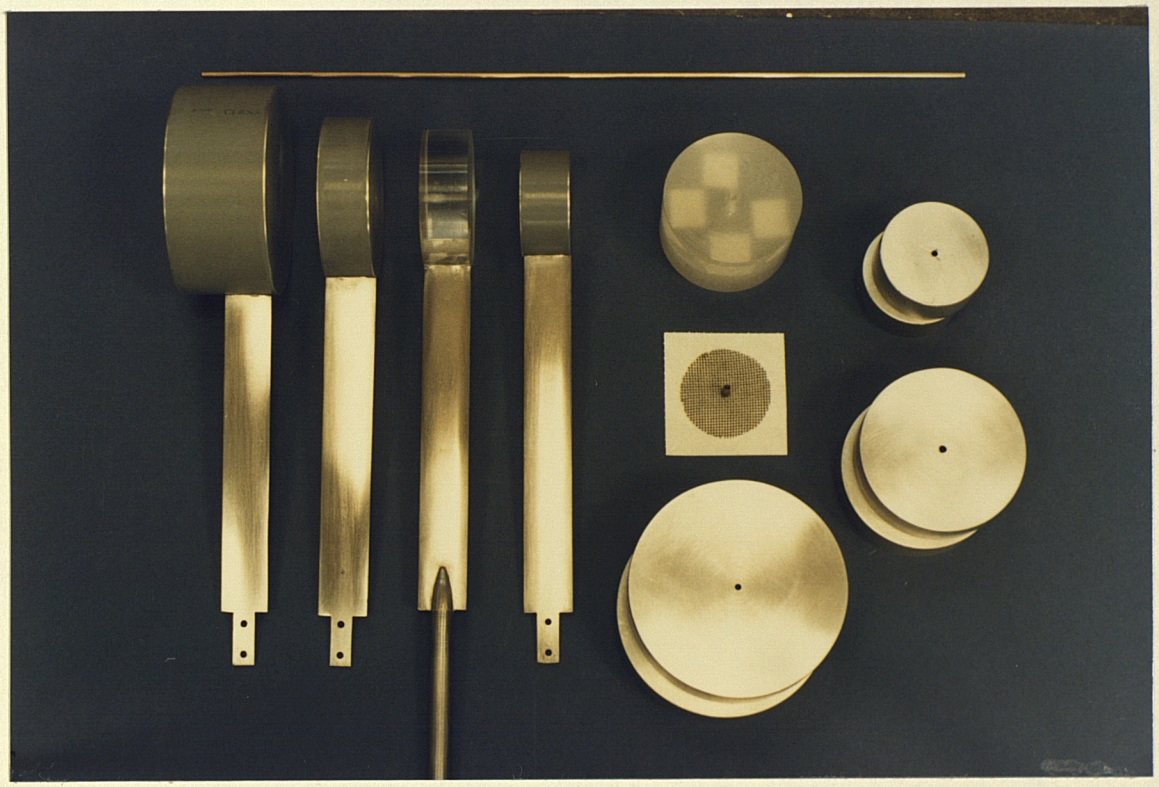

PHOTOGRAPH No. 23

APPROXIMATELY OPTIMUM CONFIGURATION OF GAUZE DISC AND SOLID CYLINDERS IN TANDEM

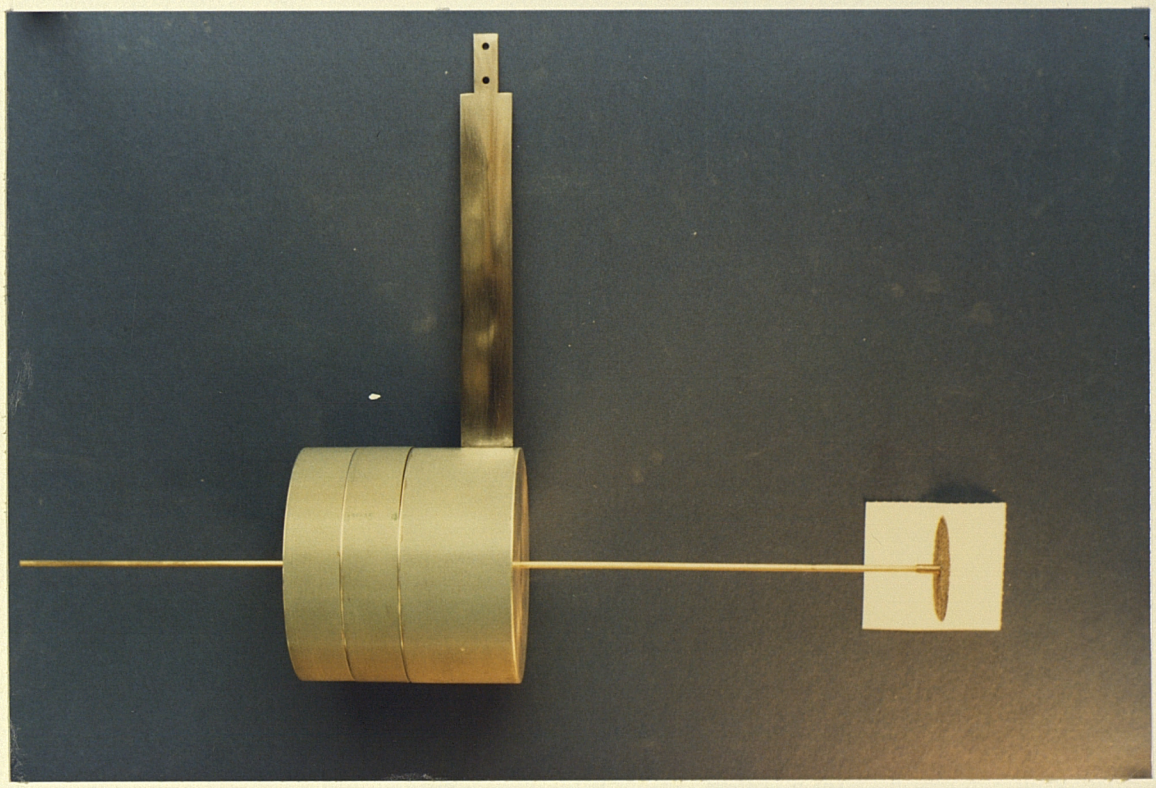

PHOTOGRAPH No. 24

PRESSURE TAPPINGS ON FACE OF SOLID DISC